UNIVERSIDADE DO ALGARVE

Faculdade de Ciências e Tecnologia

Bio-synthesis of nanosized semiconductors using mine wastes as material sources

João Miguel Martins Novaes Pinto da Costa

Doutoramento em Ciências do Mar, Terra e Ambiente

Ramo Ciências e Tecnologia do Ambiente

Área de Especialização: Química Ambiental

Faro

2013

"**Bio-synthesis of nanosized semiconductors using mine wastes as material sources**"

Declaração de Autoria do Trabalho

Declaro ser o autor deste trabalho, que é original e inédito. Autores e trabalhos consultados estão devidamente citados no texto e constam da listagem de referências incluída.

João Miguel Martins Novaes Pinto da Costa

FCT Fundação para a Ciência e a Tecnologia
MINISTÉRIO DA EDUCAÇÃO E CIÊNCIA

The present thesis was supported by Fundação para a Ciência e a Tecnologia through a PhD grant (SFRH/BD/43784/2008) and, partially, through project PTDC/AAG-TEC/2721/2012.

Acknowledgements

One of the inherent joys of completion is to look back over this past journey and remember all those whose help and support were invaluable along this fulfilling path.

First, I would like to thank my supervisors, Professor Maria Clara Costa and Professor Tito Trindade. Their knowledge was invaluable, as well as their ideas, suggestions and valuable time. I would also like to thank Professor João Lourenço and Professor Olinda Monteiro, who were kind enough to help navigate what were uncharted waters for me.

To Dr. Violeta Girão, I would like to express my most heartfelt gratitude. Not only for her breadth of knowledge, but, mostly, for her kindness and friendship. It is no exaggeration to state that, without her, this would have not been possible.

To my friends and colleagues at the Microbiology, Virology and Leukemia Molecular Biology Laboratories of the University of the Algarve, I wish to express my gratitude for sharing so many good times and for lending their ears when expressing my frustrations.

For the same reasons, I would like to thank my friends in and outside the academic circle.

To my family, thank you.

Thank you to the colleagues at the Nano Laboratory, at the University of Aveiro, and at the Faculty of Sciences and Technology, in Lisbon, who made me feel welcome and never hesitated in helping me whenever necessary.

To the anonymous and not-so-unknown reviewers who, throughout this process, helped in shaping and guiding this work with their instructive comments, thank you.

Last, but most definitely not least, to Virgínia. Thank you. For being you.

Abstract

This work describes the synthesis of nanosized metal sulfides and respective SiO_2 and/or TiO_2 composites in high yield via a straightforward process, under ambient conditions (temperature and pressure), by adding to aqueous metals a nutrient solution containing biologically generated sulfide from sulfate-reducing bacteria (SRB). The nanoparticles' (NPs) morphological properties were shown not to be markedly altered by the SRB growth media composition neither by the presence of bacterial cells.

We further extended the work carried out, using the effluent of a bioremediation system previously established. The process results in the synthesis of added value products obtained from metal rich effluents, such as Acid Mine Drainage (AMD), when associated with the bioremediation process.

Precipitation of metals using sulfide allows for the possibility of selective recovery, as different metal sulfides possess different solubilities. We have evaluated the selective precipitation of CuS, ZnS and FeS as nanosized metal sulfides. Again, we have also tested the precipitation of these metal sulfides in the presence of support structures, such as SiO_2. Studies were carried out using both artificial and real solutions in a continuous bioremediation system. We found that this method allowed for a highly selective precipitation of copper and a lower selectivity in the precipitation of zinc and iron, though all metals were efficiently removed (>93% removal).

This research has also demonstrated the potential of ZnS-TiO_2 nanocomposites as catalysts in the photodegradation of organic pollutants using the cationic dye, Safranin-T, as a model contaminant. The influence of the catalyst amount, initial pH and dye concentration were also evaluated. Finally, the efficiency of the precipitates as catalysts in sunlight mediated photodegradation was investigated, using different volumes of dye-contaminated water (150 mL and 10 L). This work demonstrates that all tested composites have the potential to be used as photocatalysts for the degradation of Safranin-T.

Keywords: Bioremediation, metal sulfides, nanocomposites, photocatalysis.

Resumo

O presente trabalho teve como principal objetivo a síntese de nano-materiais utilizando subprodutos de um processo de biorremediação para, seguidamente, testar a sua eficiência em aplicações ambientais, tais como a fotocatálise de poluentes orgânicos. Mais concretamente, procedeu-se à síntese de nanopartículas de sulfuretos metálicos (*e.g.,* CuS, ZnS) e compósitos de TiO_2 ou SiO_2, utilizando o sulfureto produzido em excesso pelas bactérias sulfato-redutoras (SRB) num processo de biorremediação desenvolvido para o tratamento das águas ácidas de mina (AMD ou ARD) Portuguesas. Subsequentemente, a eficiência destas partículas enquanto catalisadores para a fotodegração de poluentes orgânicos (Safranina-T, um corante) foi testada em ambientes simulados e reais.

As AMD são um problema ambiental particularmente relevante, sendo que estas se formam, sobretudo, em minas abandonadas, nas quais os minérios explorados incluem sulfuretos. A exposição desses sulfuretos à água e oxigénio, bem como à atividade microbiana, resulta na formação de águas acídicas (pH<3) que, usualmente, são caracterizadas por elevadas concentrações de sulfato (>2g.L^{-1}) e metais, nomeadamente, os comummente designados como "metais pesados", entre os quais se destacam o ferro, o cobre e o zinco. O tratamento destas águas, com vista à minimização do seu efeito adverso no meio ambiente, consiste, habitualmente, na adição de agentes neutralizantes, como óxido de cálcio (cal), culminando na precipitação dos metais presentes como óxidos. No entanto, estes tratamentos geram grandes volumes de lamas, que, por sua vez, têm de ser devidamente acondicionados. De notar, igualmente, que estes métodos pouco ou nada fazem para eliminar o sulfato presente, não constituindo, assim, uma forma eficiente no tratamentos destas águas residuais.

As SRB utilizam o sulfato como aceitador final de eletrões durante o metabolismo da matéria orgânica, resultando na produção de sulfureto (H_2S). Consequentemente, na presença de iões metálicos, este sulfureto biogerado pode ser utilizado na precipitação dos metais presentes na AMD. Assim, o tratamento biológico recorrendo a bactérias sulfato redutoras tem sido amplamente estudado, com inúmeros sistemas propostos ao longo de anos recentes. É de salientar, no entanto, que estes sistemas requerem, em geral, que as estirpes ou consórcios de bactérias utilizadas sejam resistentes aos metais presentes na AMD a tratar. Neste trabalho, utilizou-se um consórcio anteriormente descrito como resistente à AMD com elevadas concentrações de Fe, Cu e Zn e cuja

análise filogenética (determinada em estudos anteriores) revelou consistir, essencialmente, em SRB afiliadas ao género *Desulfovibrio*.

A síntese de nano-sulfuretos metálicos tem sido descrita utilizando uma numerosa variedade de técnicas, incluindo irradiação por micro-ondas, processos hidrotermais, reações sólido-líquido e síntese mediada por agentes quelantes, entre outras.

Tendo como base as considerações anteriores, reveste-se de particular importância a síntese de nano-sulfuretos metálicos recorrendo ao sulfureto gerado pelo crescimento das SRB num sistema de biorremediação, evitando, assim, a utilização de químicos adicionais, elevadas temperaturas e/ou pressões.

Apesar dos fenómenos físicos da formação de cristais estarem bem determinados, os processos moleculares e químicos envolvidos na transformação de espécies dissolvidas em materiais sólidos não é ainda percebido na sua totalidade. Consequentemente, após a otimização do processo de síntese, procederam-se a estudos com vista a esclarecer a potencial influência da composição do meio e da presença de partículas em suspensão nas características morfológicas das partículas sintetizadas. Utilizando meios de diferente composição para o crescimento das bactérias, bem como procedendo à síntese das nanopartículas utilizando meio filtrado e não filtrado, determinou-se que os semicondutores produzidos não apresentavam diferenças morfológicas significativas, nomeadamente, no que concerne à forma, tamanho e deposição nos suportes utilizados (TiO_2 e SiO_2).

Tendo demonstrado a exequibilidade do processo para a obtenção de nanopartículas e compósitos de CuS e ZnS, e considerando as diferentes solubilidades dos sulfuretos metálicos estudados, avaliou-se o potencial para recuperar seletivamente estes mesmos sulfuretos metálicos partindo de soluções artificiais e reais contaminadas com diversos metais. Apesar do procedimento estabelecido ter resultado numa recuperação que se pode considerar apenas parcialmente seletiva para zinco e ferro, o método desenvolvido revelou ser bastante seletivo na recuperação de cobre enquanto CuS. Mais, as partículas obtidas em todos os passos mostraram ser monodispersas e de tamanho idêntico ao obtido aquando da precipitação utilizando soluções contendo apenas um metal dissolvido. Estes resultados foram idênticos aos obtidos quando AMD real, proveniente da Mina de S. Domingos (Mértola), foi utilizada. É de realçar, no entanto, que, apesar da fraca seletividade do processo para a precipitação de ferro e zinco separadamente enquanto sulfuretos metálicos, o método desenvolvido permitiu a quase total remoção

(>93%) de todos os metais estudados presentes e as partículas obtidas, mesmo aquando da utilização de TiO_2 enquanto suporte, nunca excederam os 30 nm.

Os corantes orgânicos estão entre os agentes poluidores mais persistentes no meio ambiente. Quando utilizados na indústria têxtil, estes corantes devem ser altamente estáveis e resistentes, não só à lavagem, mas também ao Sol e à atividade microbiana. Consequentemente, estes agentes não são facilmente removidos de efluentes por tratamentos químicos convencionais. Recentemente, os denominados processos avançados de oxidação (AOP) têm-se revelado como uma alternativa interessante em que não ocorre a formação de produtos policíclicos intermediários, igualmente perigosos. Nos AOP, um semicondutor – não tóxico – torna-se num poderoso agente oxidante, catalisando a formação de radicais livres, quando exposto a um comprimento de onda adequado, resultando habitualmente na conversão do poluente em água e dióxido de carbono. Ou seja, o semicondutor catalisa um processo que resulta na completa mineralização do poluente. Uma vez que o grau de modificação à superfície dos catalisadores pode afetar a eficiência do processo, os compósitos de $ZnS\text{-}TiO_2$ foram preparados com diferentes razões entre o suporte e o sulfureto metálico. Após identificar o compósito com o melhor desempenho procedeu-se à realização de estudos em condições laboratoriais controladas, com vista a estudar os efeitos de diversos parâmetros, nomeadamente, quantidade do catalisador, concentração do corante e influência do pH. Nestas condições laboratoriais controladas, as partículas utilizadas mostraram ser altamente eficientes na degradação da Safranina-T. Mais, estas foram caracterizadas antes e após a sua utilização, sendo que os resultados mostraram que não se verificaram quaisquer alterações durante o processo de fotocatálise, demonstrando, assim, o seu elevado potencial de reutilização.

Depois de identificadas as condições mais favoráveis à fotodegradação do corante estudado, e tirando proveito das condições climatéricas privilegiadas da região Algarvia, procedeu-se, em seguida, à degradação da Safranina-T utilizando a luz solar. Após demonstrada, uma vez mais, a elevada eficiência dos compósitos quando aplicados em volumes pequenos (150 mL), estudou-se o comportamento destas partículas em volumes maiores (10 L), demonstrando, assim, a viabilidade do processo em escalas superiores.

Em suma, este trabalho demonstrou que é possível sintetizar produtos com valor e interesse comercial utilizando subprodutos de um processo de biorremediação. Numa altura em que a utilização racional da água é uma preocupação cada vez mais premente,

o resultado final é um processo integrado no qual, a partir de águas contaminadas, é possível obter água adequada à irrigação e nano-sulfuretos metálicos e compósitos com atividade fotocatalítica demonstrada e que estes, por sua vez, podem ser utilizados na descontaminação de águas poluídas com contaminantes orgânicos, como corantes.

Os resultados alcançados não constituem, em si, o final do trabalho a desenvolver. Estabelecem, sim, um ponto de partida para trabalhos futuros, como o estudo da eficiência destes catalisadores na degradação de poluentes emergentes, como, por exemplo, antibióticos. Igualmente, os resultados obtidos oferecem uma ponte para a multidisciplinaridade, integrando nanotecnologia, tecnologias ambientais e biotecnologia com as subsequentes potencialidades que tal integração oferece.

Poderão ser utilizados organismos geneticamente modificados com vista à sua utilização na recuperação seletiva de metais, com grupos diferentes de microrganismos responsáveis pela recuperação de diferentes metais?

Poderá o processo de biorremediação sofrer alterações que permitam a sua aplicação noutro tipo de efluentes que não a AMD?

Será possível estabelecer processos que permitam um elevado controlo sobre as características morfológicas das partículas sintetizadas, como estrutura cristalina, dimensões e forma?

Poderão ser as partículas já obtidas utilizadas em outras aplicações, como a optoeletrónica?

Por fim, e tal como anteriormente referido, poderão ser estes catalisadores utilizados na degradação de outros compostos, como antibióticos?

Palavras-chave: Biorremediação, fotocatálise, nanocompósitos, sulfuretos metálicos.

**Texto convertido utilizando o conversor da Porto Editora, em conformidade com o Acordo Ortográfico de 1990.*

Anyone who believes in infinite
growth on a physically finite planet,
is either mad or an economist.

Kenneth E. Boulding, 1966. Economist and Environmental Adviser to the President, J. F. Kennedy.

.

Table of Contents

Chapter 1 – Introduction

1.1 Metal Mining, AMD and Metal Sulfide Precipitation

1.1.1 Metal Mining

Since ancient times, mining has been the form by which metals were extracted from nature (Gosar, 2004). In fact, the oldest mine dates from nearly 43,000 years ago and this was the place in which Paleolithic humans gathered hematite for the production of a red pigment ochre (N.T.C., 2012). However, mining and the processing of metal ores are important factors in environmental pollution, and the primarily concern in mining areas are related to the damage of the landscape and the formation of acid mine drainage (AMD) (Dudka and Adriano, 1997).

The current paucity of metals can be considered, to some extent, a paradox. Though metals constitute most of the Earth's crust (Gadd, 2010), they have become increasingly scarce, due to their extensive use in numerous industries and insufficient or inefficient recovery (Wernick and Themelis, 1998). Many have opinionated that the long-term demand will increase, pacing the global economy (Williamson, 1995), but also that their demand will decrease, due to the use of alternative materials and/or a more efficient use (Tilton, 1990; Williams *et al.*, 1987). Volatility, more than anything else, will characterize the worldwide metal market in the foreseeable future, as global demand shifts, energy costs rise and economic instability persists (KPMG, 2012). Consensus exists, however, in the opinion that emerging markets will outperform the industrialized, as depicted for steel in Figures 1.1A and 1.1B.

Either way, this is a limited resource and should be managed as such (Cui and Forssberg, 2003; Sibley *et al.*, 1995; Tuncuk *et al.*, 2012).

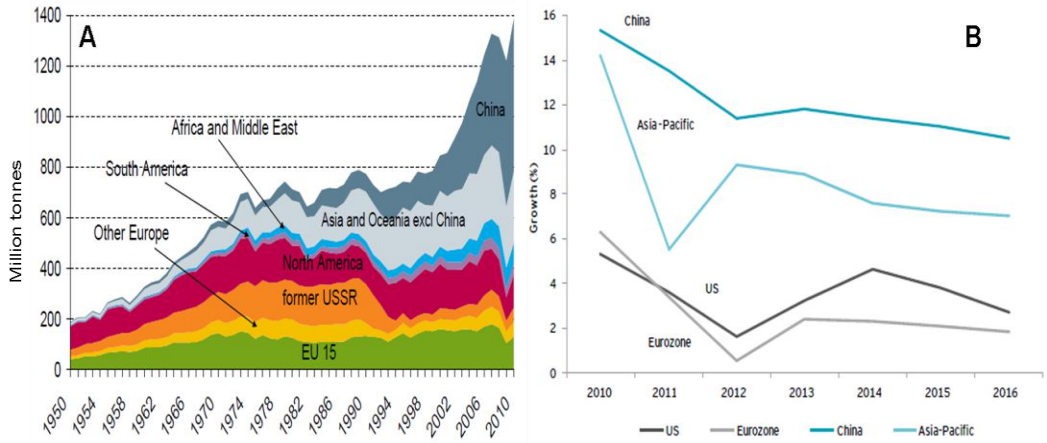

Figure 1.1 – In A, the use of steel worldwide, divided by region (adapted from (Askerov, 2012)). In B, the industrial estimated production of steel for the different world regions (adapted from (Ernst and Young, 2012)).

1.1.2 Acid Mine Drainage – Contamination, Prevention and Treatment

AMD, also sometimes referred to as ARD (Acid Rock Drainage) forms when mining wastes contain sulfide ores. The dissolution of such ores, when exposed to water, oxygen and microbial activity, results in the formation of acidic waters that contain high concentrations of metals and sulfates (Elliott *et al.*, 1998; Evangelou and Zhang, 1995; Johnson and Hallberg, 2005; Natarajan, 2008; Sheoran and Sheoran, 2006). In the US alone, over 19,300 km of streams and rivers and approximately 73,000 hectares (approximately 180,500 acres) of lakes and reservoirs have been contaminated by AMD (Johnson and Hallberg, 2005; Kleinmann, 1989; Sheoran and Sheoran, 2006). The oxidative dissolution process of sulfide minerals, namely, the role of microorganisms, has been the subject of some debate (Fowler *et al.*, 2001; Schippers and Sand, 1999), though there is an agreement on the process leading to the acidification of these waters. Sulfides may be divided into two groups: acid-soluble and acid-insoluble (Johnson, 2003). The former can be solubilized by bacteria that oxidize sulfur whilst producing hydrogen sulfide, as is the case of ZnS, as described in Equation 1.1. The hydrogen sulfide formed is oxidized by sulfur-oxidizing bacteria, thus regenerating the protons (Equation 1.2). In turn, acid-insoluble sulfides can be oxidized by ferric iron with subsequent solubilization (Equation 1.3) (Johnson, 2003).

$$ZnS + 2H^+ \rightarrow Zn^{2+} + H_2S \quad (1.1)$$

$$H_2S + 2O_2 \rightarrow 2H^+ + SO_4^{2-} \quad (1.2)$$

$$FeS_2 + 6Fe^{3+} + 3H_2O \rightarrow 7Fe^{2+} + S_2O_3^{2-} + 6H^+ \quad (1.3)$$

Ferrous iron can then be oxidized by iron-oxidizing bacteria, leading to the regeneration of ferric iron, the chemical oxidant. Particularly in the presence of this ion, thiosulfate is unstable, oxidizing to tetrathionate, which is then decomposed into, among other polythionates, sulfur and sulfate (Johnson, 2003; Schippers and Sand, 1999). These polythionates, commonly referred to as "reduced inorganic sulfur compounds", or RISC, support the growth of other sulfur bacteria rather than iron-oxidizing.

1.1.2.1 Prevention and Remediation

Due to the high environmental risk that AMD waters present, numerous strategies have been evaluated for their minimization and/or prevention. Figure 1.2 schematizes such approaches.

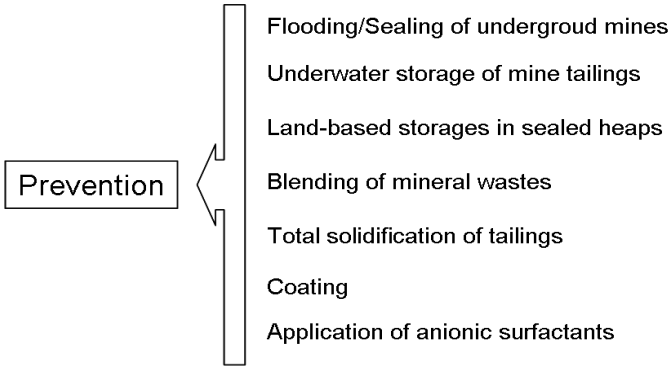

Figure 1.2 – Strategies for the prevention or minimization of the generation of acid mine waters (adapted from (Johnson and Hallberg, 2005)).

Because the formation of AMD requires oxygen and water, by excluding either one or both of these, it will be possible to reduce or completely inhibit the formation of such contaminated waters. This is the rationale behind the flooding of underground mines and underwater storage of mine tailings. The former consists in flooding and sealing of deep mines, in which the dissolved oxygen is consumed by microorganisms present and its replenishment is blocked due to the sealing of the mine (Johnson and Hallberg, 2005). The latter process – underwater storage of mine tailings – is achieved by

covering the tailings with a layer of organic material or sediment. This will not only limit oxygen diffusion, but will also prevent the scattering of the mine tailings, due to rain and wind. Clay is a common material used for this purpose (Li *et al.*, 1997). Land-based storages usually resort to clay as the sealing material, but it should be noted that in non-tempered zones, the use of such material may pose a risk, as high temperature amplitudes may result in the cracking of the clay (Swanson *et al.*, 1997). The blending of acid-generating and acid-consuming materials, which culminate in the formation of inert compounds, has also been suggested for preventing the generation of acid mine waters (Mehling *et al.*, 1997). Solidification of tailings is a variation of the previously described method. In this process, solid phosphates are added to pyrite containing wastes, precipitating ferric ion as ferric phosphate, diminishing its potential to act as an oxidizing agent (Evangelou, 1998; Johnson and Hallberg, 2005). Alternatively, soluble phosphates can be added, and, in the presence of hydrogen peroxide, pyrite is oxidized, producing ferric ion. This then reacts with the added phosphate, producing a surface "coating" of ferric phosphate (Evangelou, 1998). Finally, because sulfur and iron-oxidizing bacteria play a pivotal role in the generation of acid mine drainage, the addition of biocides, such as anionic surfactants (namely, sodium dodecyl sulfate, or SDS) has been studied (Loos *et al.*, 1989). However, this has proven to be a method with highly variable results, which, at best, only solve this problem in the short-term (Johnson and Hallberg, 2005).

Considering the difficulties in the prevention of the formation of AMD and the consequent contamination of the environment, but also the fact that many of these mines have been abandoned for many years (Costa and Duarte, 2005; Guo *et al.*, 2009; Navarro *et al.*, 2008; Tian *et al.*, 2009), it is often feasible only to minimize the impact of these waters in the surrounding environment.

Remediation processes can be divided into abiotic and biological (Johnson and Hallberg, 2005). In turn, these can be either active or passive systems, as depicted in Figure 1.3. The latter refers to the use of ecosystems based on natural or constructed wetlands; the former commonly refers to systems that require the continuous addition of alkaline materials for the precipitation of metals and neutralization of the acidic mine water.

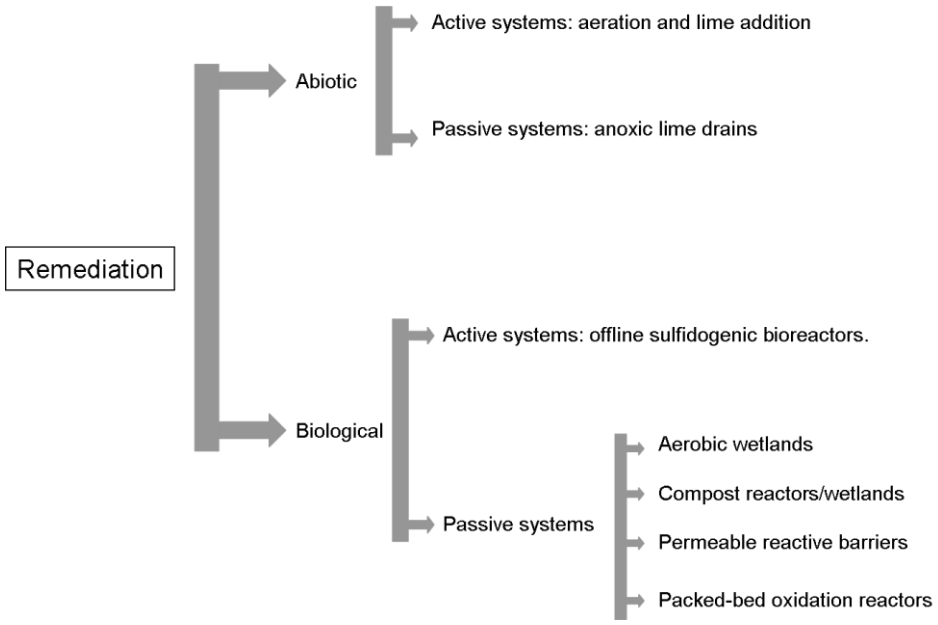

Figure 1.3 – Abiotic and biological strategies for the treatment of AMD.

The most frequently used remediation strategy for minimizing the effects of the acidic waters is the active addition of a chemical neutralizing agent, such as lime (Costa and Duarte, 2005; Coulton *et al.*, 2003). This will result in an increase of the pH, causing many of the metals present to precipitate as carbonates and hydroxides (Johnson and Hallberg, 2005). The sludge obtained by this process is iron-rich, but it will also contain other metals. The composition of the sludge will vary, according to the unique chemistry of the water treated. Diverse neutralizing agents have been used, including lime (Labastida *et al.*, 2012), calcium carbonate (Lee *et al.*, 2007), cement dust (Mackie and Walsh, 2012) and magnesium oxide (Herrera *et al.*, 2007). However, such treatments require high operating costs (Madzivire *et al.*, 2011), do little to remove the sulfate present (Johnson and Hallberg, 2005) and generate high volumes of sludge, which, in turn, need to be disposed off (da Costa *et al.*, 2012).

Anoxic limestone drains (ALD) are passive systems, in which the addition of alkalinity to the AMD is coupled to the maintenance of iron in its reduced form, avoiding the oxidation of ferrous iron and, thus, preventing the precipitation of ferric oxide on the limestone, a process known as armoring (Kleinmann, 1989). Within the drain, the partial pressure of carbon dioxide rises, which accelerates the dissolution of the limestone with subsequent increase in alkalinity (Matthies *et al.*, 2010). Because such systems require minimum maintenance, they are referred to as passive (Johnson and Hallberg, 2005). There are, nevertheless, many limitations in these systems. If the AMD

contains high amounts of iron or aluminum, the long-term efficiency decreases significantly, as the hydroxides formed tend to clog the drains (Matthies *et al.*, 2010). Also, because this process relies on the low partial pressure of oxygen, it is not adequate for the treatment of aerated waters, requiring these to pass through an anoxic pond prior to the ALD (Johnson and Hallberg, 2005). Finally, ferrous and manganese carbonate gels can form, causing an inadequate dissolution of the limestone (Evangelou, 1998).

Most microbiological processes are reductive in nature. These include sulfate reduction (Hashim *et al.*, 2011), methanogenesis (Koschorreck *et al.*, 2008), denitrification (Shao *et al.*, 2009) and iron (Stemmler *et al.*, 2004) or manganese reduction (Cerrato *et al.*, 2010). The activity of bacteria catalyzing the dissimilatory reduction of sulfate to sulfide results in an increase in alkalinity by transforming sulfuric acid (strong acid) into hydrogen sulfide (weak acid), as depicted in Equation 1.4. Also, because many metals form insoluble sulfides (such as zinc and copper), reduction of sulfate is an important system for removing metals from contaminated waters (Equation 1.5) (Johnson and Hallberg, 2005).

$$SO_4^{2-} + 2CH_2O + 2H^+ \rightarrow H_2S + 2H_2CO_3 \quad (1.4)$$

$$Zn^{2+} + H_2S \rightarrow ZnS + 2H^+ \quad (1.5)$$

Figure 1.3 highlights the point that most biological methods for the remediation of AMD consist of passive systems. Of these methods, only a few have been used, to this date, as full-scale systems (Battaglia-Brunet *et al.*, 2002; Hallberg and Johnson, 2005; Macías *et al.*, 2012; Whitehead and Prior, 2005). Passive remediation systems result in the accumulation of the solid products in the wetland sediments and have relatively low maintenance costs. Nonetheless, they often require a considerable initial investment (Cohen, 2006; Sheoran and Sheoran, 2006). In addition, they also require large areas and the performance is less predictable than that of chemical treatments (Johnson and Hallberg, 2002; Mitsch and Wise, 1998).

Offline sulfidogenic reactors are active, engineered systems that, despite their high maintenance costs, present three potential advantages when compared to passive treatments. These are i) predictability and performance control; ii) potential for selective recovery of the metals present in the AMD; and iii) significant decrease of the sulfate content (Amils, 1999; Lens *et al.*, 2000). Like in compost bioreactors and permeable

reactive barriers (passive systems), offline sulfidogenic reactors rely on the production of sulfide for the precipitation of metals as sulfides. It should be noted that, however, such systems are optimized for the production of hydrogen sulfide (Johnson and Hallberg, 2005). These systems usually consist of two stages, one chemical and one biological or both biological, which operate independently. Two methods that make use of such systems have been described to this date: the Biosulfide® (Bratty *et al.*, 2006; Johnson, 2012; Ňancucheo and Johnson, 2012) and Sulfateq® (AMOC, 2003; Boonstra *et al.*, 1999; Elkanzi, 2009) technologies. By carefully manipulating the pH and the sulfide concentration, these systems present the possibility of achieving a selective separation of the metal sulfides. Also, sludge volumes obtained are smaller and easier to separate, as metal sulfides have lower solubilities than their oxide counterparts (Costa and Duarte, 2005).

1.1.3 Metal Sulfide Precipitation

Despite the previously described advantages of sulfide precipitation, hydroxide precipitation is still the preferred method for metal removal (Lewis, 2010). This is because dosing of the sulfide is considered difficult to control, due to the very low solubility of the metal sulfides and, consequently, the dosing sensitivity of the process. Also, there are concerns regarding the corrosiveness and toxicity of the excess sulfide (Veeken *et al.*, 2003b). The thermodynamic equilibria of metal (M) sulfide precipitation can be expressed by Equations 1.6 – 1.9 (in 0.01 – 0.1 M, at 18ºC) (Lewis, 2010).

$$H_2S \xleftrightarrow{Kp_1} HS^- + H^+, Kp_1 = \frac{[HS^-].[H^+]}{[H_2S]}, pK_1 = 6.99 \quad (1.6)$$

$$HS^- \xleftrightarrow{Kp_2} S^{2-} + H^+, Kp_2 = \frac{[H^+].[S^{2-}]}{[HS^-]}, pK_2 = 17.4 \quad (1.7)$$

$$S^{2-} + M^{2+} \leftrightarrow MS(\downarrow) \quad (1.8)$$

$$HS^- + M^{2+} \leftrightarrow MS(\downarrow) + H^+ \quad (1.9)$$

Sulfur speciation strongly depends on pH, as depicted in Figure 1.4. In Figure 1.5, the solubilities of various metal sulfides as a function of pH are illustrated.

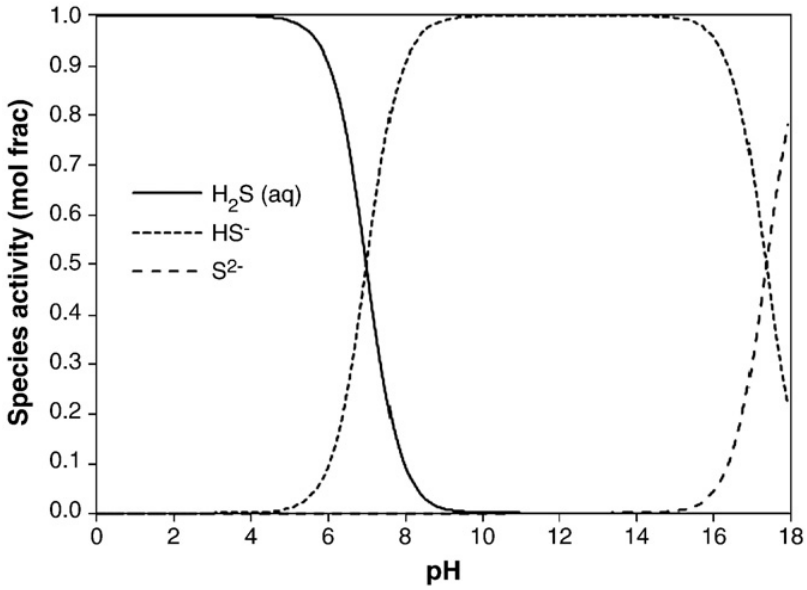

Figure 1.4 – Concentration of sulfur species as a function of pH (adapted from (Lewis, 2010; Migdisov *et al.*, 2002)).

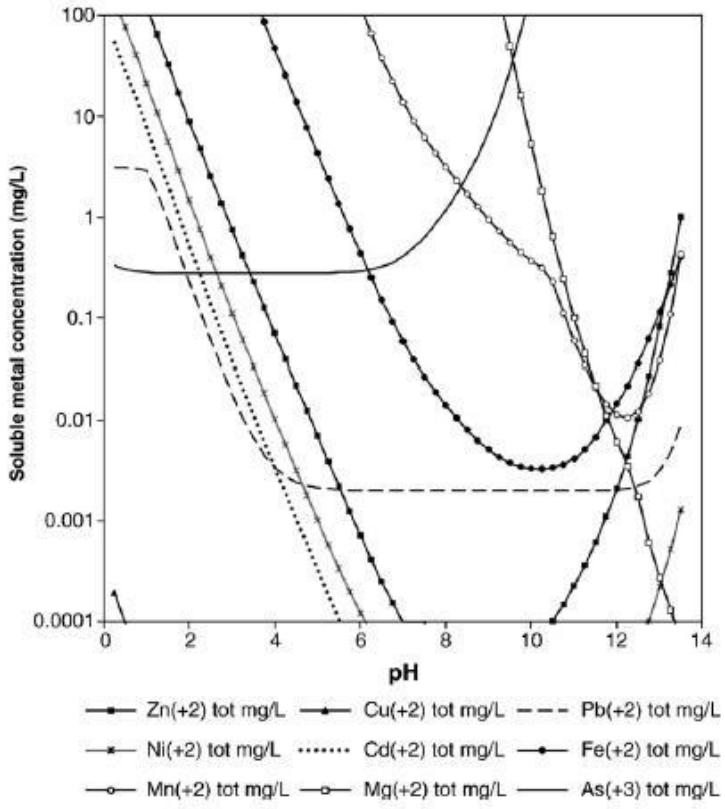

Figure 1.5 – Solubilities of metal sulfides as a function of pH (adapted from (Lewis, 2010)).

Metal sulfide species can occur as i) nanoclusters, with a size ranging between 2 – 10 nm, exhibiting bulk-like crystal structure, but too small to show bulk-like electronic

wave functions; ii) colloids ranging between 1 nm – 1 μm, formed from supersaturated solutions; and iii) metal sulfide complexes, which are truly dissolved species (Lewis, 2010; Sukola *et al.*, 2005). Metal sulfides are of particular interest as nanocrystals due to their size dependent behavior (Liu *et al*., 2003; Patel *et al*., 2012), as well as surface coatings (Abdel Rafea *et al.*, 2012; Wei *et al.*, 2005), nano-switches (Canary *et al.*, 2010; Xi *et al.*, 2009), solar cell components (Bube, 2001; Maier *et al.*, 2011), radiation absorbers (Akman *et al.*, 2013; Su *et al.*, 2011) and photocatalysts (da Costa *et al*., 2012; Franco *et al*., 2009). Other applications include gas sensors (Sagade and Sharma, 2008) and dielectric filters (Pawaskar *et al.*, 2002).

Hence, considering the vast interest in metal sulfides in numerous applications, especially at the nanoscale, as well as the beneficial nature of metal sulfide precipitation in the removal of metals from contaminated effluents, there is a potential for integrating synthesis processes in well-established bioremediation systems, though this is an idea that only recently has been suggested (Castillo *et al.*, 2012; da Costa *et al.*, 2012).

1.2 Synthesis of Nanosized Metal Sulfides

1.2.1 General Considerations

The term "nano", from the Greek *νάνος* (*naa-nosh*), means "dwarf", and, when used as a prefix, denotes a factor of 10^{-9}. For example, a flu virus particle is 100 nm and a DNA molecule is 2.5 nm wide (Thakkar *et al.*, 2010). Particles are considered as nanoparticles when at least one dimension is less than 100 nm. Such particles are of great interest, as they "bridge the gap" between atomic or molecular structures and bulk materials. The latter presents constant physical properties regardless of its size, which is not often the case for nano-sized materials. As particles get smaller, size-dependant properties change, such as surface plasmon resonance in some metallic particles or quantum confinement in semiconductors (Thakkar *et al.*, 2010). These interesting and sometimes surprising properties are not always desirable. For example, ferroelectric nanoparticles smaller than 10 nm can invert their magnetization direction at room temperatures, rendering them useless for memory usage (Mehta, 2011). On the other hand, at approximately 50 nm, copper nanoparticles begin to exhibit super-hard features, loosing the bulk material's characteristic ductility and malleability (Mehta, 2011). It is also possible to create suspensions of nanoparticles because, unlike their

bulk material counterparts, these particles do not float or sink, due to the fact that they interact strongly enough with the solvent to overcome differences in density (Kokate *et al.*, 2012). Consequently, studies on the activity of such particles while in suspensions can be performed and many have versed on the photocatalytic activity of nano-semiconductors (Chiou *et al.*, 2008; da Costa *et al.*, 2012; Franco *et al.*, 2009; Gupta *et al.*, 2012b).

The synthesis of nanoparticles uses one of two approaches: the "bottom-up" and the "top-down" alternatives (Thakkar *et al.*, 2010). The former concerns the construction of a structure atom-by-atom, molecule-by-molecule or cluster-by-cluster (Shimoda *et al.*, 2012). Initially, the blocks are formed and, after, they self-assemble into the final product via biological or chemical procedures. The "top-down" approach consists of reducing the size of a given material, either through physical or chemical means (Lin and Samia, 2006). Relative to the "bottom-up" approach, the "top-down" system results in uneven end-materials, often with surface imperfections, which may result in significant impacts in surface chemistry and physical properties (Lin and Samia, 2006; Thakkar *et al.*, 2010).

Though the physics of nucleation and crystal growth have long been known (Markov, 2003; Pimpinelli and Villain, 1998; Wunderlich, 1976), the molecular or chemical processes that lead to the formation of solid products from simple dissolved species is not fully understood (Luther *et al.*, 1999). Consequently, the focus of most fundamental studies on the precipitation of metal sulfides lies on the identification of the reduced sulfur species in aqueous solutions (Lewis, 2010).

Because zinc is commonly found in natural environments, but also because it has only one oxidation state (II), which facilitates the study of its chemistry, this metal is often chosen as a model for metal sulfide precipitation. A step-wise process for the formation of ZnS phases has been proposed (Luther *et al.*, 1999), in which, initially, zinc (II) is present in solution as a hexaaquo ion ($Zn(H_2O)_6^{2+}$). Then, zinc forms soluble complexes that, in turn, aggregate into soluble rings and clusters, such as Zn_3S_3 and $Zn_4S_6^{4-}$. The neutral clusters can undergo condensation reactions with other neutral or anionic clusters, which, ultimately, lead to the formation of the stable ZnS phases. The precipitation kinetics of zinc sulfide has also been studied using a Mixed Suspension Mixed Product Removal reactor (MSMPR) (Peters *et al.*, 1984). It was found that the process of nucleation and growth could be expressed by Equation 1.10.

$$n = n^0 . e^{(\frac{-L}{G\tau})} \quad (1.10)$$

Where n is the population density distribution (number.m^{-3}), a function of n^0, the population density nuclei (number.m^{-3}), the linear growth rate (G, m.s^{-1}), crystal size (L, m) and residence time (τ). This analysis, however, assumes that nucleation and growth are the only processes taking place and that phenomena such as attrition and aggregation are negligible (Lewis, 2010). Using the same type of reactor (MSMPR), other authors (Al-Tarazi *et al.*, 2004) have considered not only nucleation and growth processes, but also aggregation. Nonetheless, this system holds the drawback that it is not suitable for studying precipitation reactions that occur rapidly, as the assumption of perfect mixing does not stand. Other studies have been carried out, either using different systems, such as a Continuously Stirred Tank Reactor (CSTR) (Veeken *et al.*, 2003a) or bubble reactors (Al-Tarazi *et al.*, 2005), which showed that aggregation is, in fact, an important process that takes place during zinc sulfide precipitation. The same conclusions were drawn when using additional controlling mechanisms, such as the use of a sulfide electrode (Veeken *et al.*, 2003b), for close monitoring of the added sulfide.

On the other hand, copper is difficult to study, due to the fact that, in sulfidic conditions, it has the ability to reduce. Hence, it may form a wide range of sulfide, bi-sulfide and polysulfide complexes (Luther and Rickard, 2005). By measuring the solubility of *covellite* (CuS) in bi-sulfide solutions, the formation of the following complexes has been suggested (Shea and Helz, 1988): $CuS(HS)_2^{2-}$, $CuS(HS)_3^{3-}$, $CuS(S_5)_2^{3-}$, $Cu(S_4)(S_5)_2^{3-}$ and $CuS(S_5)^{2-}$, with the following equilibria (Equation 1.11):

$$CuS + nHS^- \leftrightarrow CuS(HS)_n^{-n}, n = 2 or 3 \quad (1.11)$$

It has also been shown that, in solution, sulfide reduces Cu(II) to Cu(I) before precipitation (Luther *et al.*, 2002; Theberge *et al.*, 2000). It was inferred that Cu_3S_3 rings are formed in the solution and that these are the basis for the formation of aqueous CuS clusters. These complexes were also shown to be kinetically inert to dissociation and thermodynamically strong. This means that the structural elements of the CuS precipitate are pre-formed in solution and are determinant in the development of the solid (Lewis, 2010). The kinetics of precipitation of copper sulfide have been studied using bubble reactors (Al-Tarazi *et al.*, 2005; Mokone *et al.*, 2012) and fluidized bed

reactors (van Hille *et al.*, 2005). Considering the lower solubility of CuS, when compared to that of ZnS, it would have been expected that Al-Tarazi and co-workers (Al-Tarazi *et al.*, 2005) would have obtained smaller particles for CuS. However, the copper particles were found to be active at their surface and, consequently, formed aggregates between 10 – 15 μm. Others, though not being able to successfully describe the nucleation and growth kinetics of copper sulfide, considered that supersaturation was the most influential factor (Mokone *et al.*, 2012; Sampaio *et al.*, 2009; van Hille *et al.*, 2005). Different authors, however, have proposed that the nucleation derivation period (time necessary for nucleation from the component ions) can be correlated to the concentration of the precipitate-forming ions (Choi *et al.*, 2006), as expressed in Equation 1.12.

$$t_f = K.C_0^{-(p-1)} \tag{1.12}$$

In Equation 1.12, t_f is the nucleation derivation period (min), C_o is the initial concentration of the precipitate-forming ion (mol.L^{-1}), K is a constant and p is the nucleation reaction order. Crystal growth can then be expressed according to Equation 1.13:

$$\frac{d(C_0 - C)}{dt} = K_G S.(C - C_S)^n \tag{1.13}$$

Here, C_0, C and C_S are the initial concentration, the concentration at time t and the saturation concentration of the limiting ion, respectively (mol.L^{-1}). The overall coefficient of crystal growth is expressed by K_G (L.min-1), S is the available surface area for precipitation of a given particle and n is the crystal growth order.

1.2.1.1 The Use of TiO_2 and SiO_2

Titanium dioxide (CAS N. 13463-67-7, 79.87 g.mol^{-1}) is the naturally occurring oxide of titanium. Commonly used as a pigment, it is sometimes referred to as “titanium white” or “pigment white 6” (Khataee and Kasiri, 2010). Most of this compound in industry is obtained from titanium mineral concentrates and is mainly in the anatase and rutile form (Kirk and Othmer, 1963). These are usually in the ratio of 3:1 and show an

average size of 25 nm (Ohno *et al.*, 2001). The characteristics of these TiO_2 crystal forms are shown in Figure 1.6 and Table 1.1. Besides being largely available, it's a non-toxic, cheap and chemically stable material (Gude *et al.*, 2008). The photocatalytic properties of TiO_2 were first described by Fujishima and Honda in 1972 (Fujishima and Honda, 1972). However, the photoefficiency, activity and response of TiO_2 make this material inappropriate for direct use in environmental processes (Franco *et al.*, 2009). This is because TiO_2 absorbs mainly in the UV (Robert and Malato, 2002), due to the large band gap (*ca.* 3.2 eV) (Yawalkar *et al.*, 2001). Hence, numerous efforts have been developed to overcome these limitations, such as the use of metal and non-metal dopants (Ji *et al.*, 2010; Liu *et al.*, 2009a; Zhang *et al.*, 2008), co-catalyst loading (Arifin *et al.*, 2013; Mizukoshi *et al.*, 2010) and combinations with semiconductors, such as metal sulfides (Baker and Kamat, 2009; Balis *et al.*, 2013; Tran. T *et al.*, 2012).

Table 1.1 – Crystallographic properties of the anatase and rutile form of TiO_2 (adapted from (Diebold, 2003)).

Crystal structure	*Density ($g.cm^{-3}$)*	*System*	*Space group*	*Cell parameters*		
				a	*b*	*c*
Anatase	3.830	Tetragonal	$D_{4a}^{19} - I4_1/amd$	0.3758	-	0.9514
Rutile	4.240	Tetragonal	$D_{4h}^{14} - P4_2/mnm$	0.4584	-	0.2953

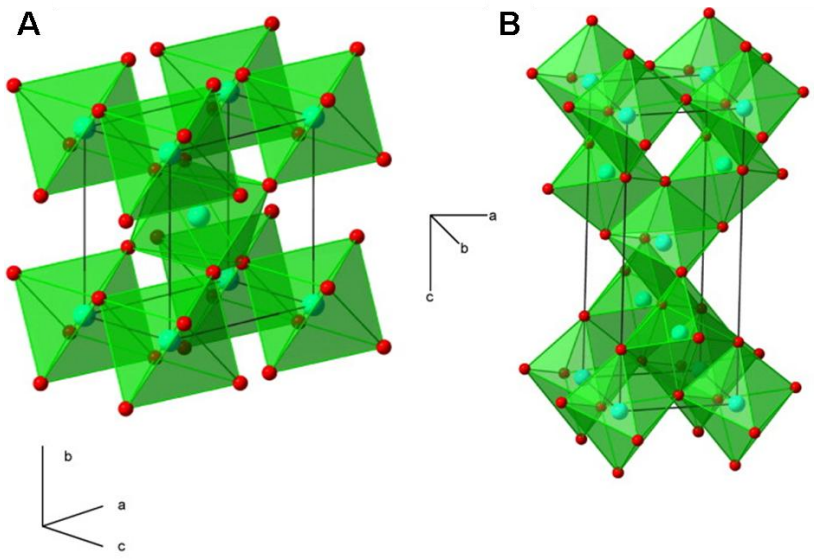

Figure 1.6 – The crystal structure of anatase (A) and rutile (B). Light blue represents Titanium and red represents Oxygen (adapted from (Yang *et al.*, 2009)).

Silicon dioxide, also known as silica (CAS N. 7631-86-9, 60.08 $g.mol^{-1}$) is an oxide most commonly found in nature as quartz and sand, but also on the cell walls of diatoms (Iler, 1979). Industrially, silica is mostly used in the production of glass materials, such as windows, bottles and glasses. It is also used in the manufacture of optical fibers (Veronese *et al.*, *in press*) and is the main component of diatomaceous earth, commonly used in filtration (Du *et al.*, 2011), insect control (Kljajić *et al.*, 2010) and in lithium ion batteries (Shen *et al.*, 2012). Other applications of silica include DNA purification (Chiang *et al.*, 2006) and microelectronics (Riordan, 2007). In most cases, the crystal structure of SiO_2 shows tetrahedral coordination (Fig. 1.7A). Silica exhibits many crystalline forms (polymorphs) and most involve the tetrahedral basic unit shown in Fig. 1.7A (Wiberg, 2001). In amorphous silica, used in the experimental works herein described, it should be noted that, although there is a local order regarding the tetrahedral organization of the oxygen atoms around the silicon atom, no long range order exists (Fig. 1.7B).

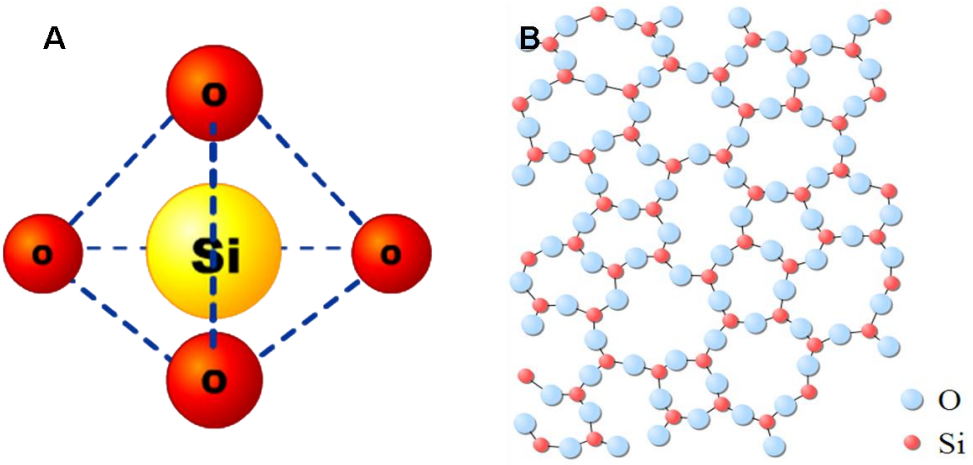

Figure 1.7 – In A, the tetrahedral coordination of silica, basic unit of the vast majority of silicates, is shown. The lack of long-range order in amorphous silica is shown in B. Note that this is a 2D representation and that a forth oxygen atom is bonded to each Si atom in front or behind of the plane represented (adapted from (Wiberg, 2001)).

Silica exhibits insulating properties and is transparent when subjected to radiations within the 300 – 800 nm range (Jankiewicz *et al.*, 2012). Moreover, this material is resistant to coagulation (Liz-Marzan *et al.*, 2001). Because the surface of unmodified SiO_2 particles is covered with silanol groups (-Si-OH), it becomes negatively charged. Hence, to facilitate the interaction of these particles, modification of the SiO_2 surface is

a strategy commonly used (Jankiewicz *et al.*, 2012). Such structures are of special interest in colloidal stability and band structure engineering (Kim *et al.*, 2003), biosensing (Kalele *et al.*, 2006b), photovoltaic solar cells (Jankiewicz *et al.*, 2012) and drug delivery (West and Halas, 2003), among others. Silica particles are, hence, used for the synthesis of many core-shell particles (Fig. 1.8), and, broadly, these can be fabricated by combining numerous types of dielectric materials, metals and semiconductors (Gutiérrez *et al.*, 2011; Kalele *et al.*, 2006a; Navarro *et al.*, 1996; Okamoto *et al.*, 2009; Yermakov *et al.*, 1984).

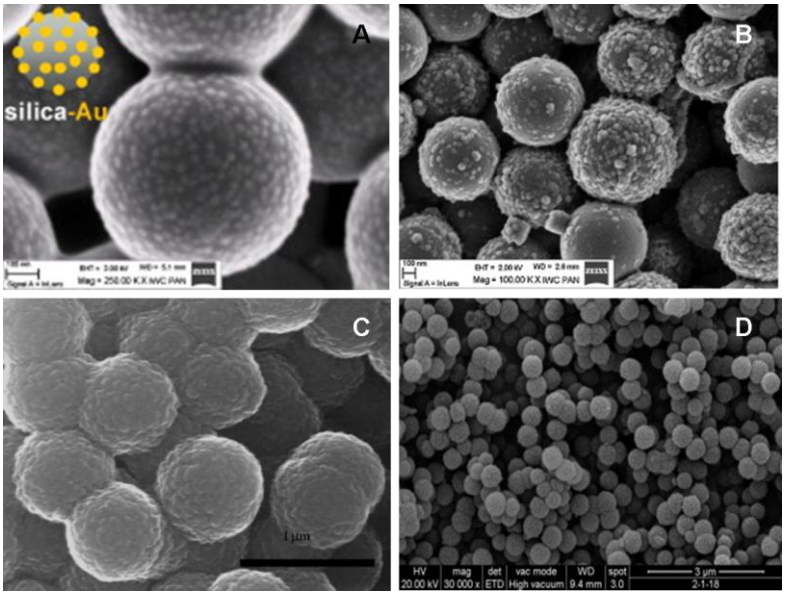

Figure 1.8 – SEM images of SiO_2 core-shell composites. In A, Au-SiO_2 particles (adapted from (Choma *et al.*, 2011)). In B, silver-silica spheres (adapted from (Choma *et al.*, 2012)). In C, the deposition of ZnS on the surface of SiO_2 (adapted from (Franco *et al.*, 2009)). Finally, in D, TiO_2-SiO_2 composites (adapted from (Di Virgilio *et al.*, 2013)).

1.2.2 Chemical Synthesis

The synthesis of both CuS and ZnS nanocrystals has been reported using a variety of methodologies and techniques. In the particular case of zinc, such techniques included high gravity (Chen *et al.*, 2004), microwave irradiation (Vaidhyanathan *et al.*, 1995), reverse micelles (Qi *et al.*, 1996), chemical vapor deposition (Bessergenev *et al.*, 1995), hydrothermal processes (Liu *et al.*, 2009b), solid-liquid chemical reactions (She *et al.*, 2010), single-molecule precursor decomposition (Monteiro *et al.*, 2004) and in the

presence of chelating agents (Xin *et al.*, 2008), amongst others. CuS nanoparticles have been synthesized using solvothermal methods (Li *et al.*, 2010), sonochemistry (Wang *et al.*, 2002), pyrolosis (Nascu *et al.*, 1997) or solid-state reactions (Parkin, 1996). Also, methods relying on the decomposition of organometallic precursors have been used (Talapin *et al.*, 2001) which include surfactant-assisted routes (Wang and Yang, 2000) and microemulsions (Dong *et al.*, 2002). A description of the synthesis methods for multiple nanosized metal sulfides is summarized in Table 1.2 and examples of the different end-products obtained are shown in Figure 1.9.

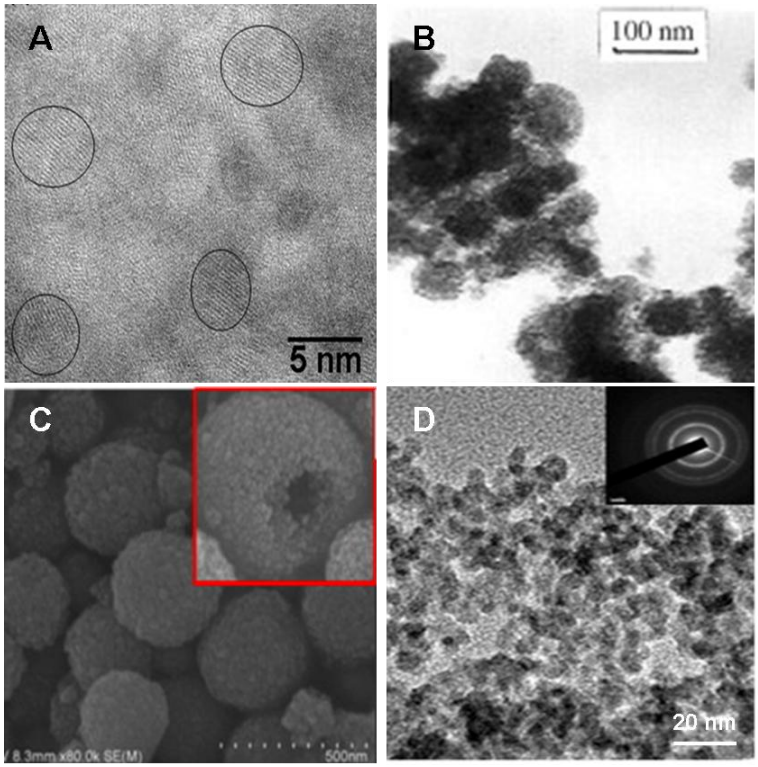

Figure 1.9 – Nanosized metal sulfides chemically synthesized. In A, TEM image of ZnS:Mn thin film obtained at 60ºC by a chemical deposition method (adapted from (Sahraei *et al*., 2013)). In B, TEM image showing CdS spheroid particles prepared by γ-radiation (adapted from (Ge *et al*., 2002)). The SEM image of 10 – 20 nm CdS spheres prepared by thermolysis (inset) that constitute the building blocks of larger hollow spheres is shown in C (adapted from (Luo *et al*., 2012)). Finally, in D, HRTEM image of CdS nanoparticles synthesized by microemulsion (adapted from (Upadhyay *et al*., 2012)).

Table 1.2 – Synthesis methods for obtaining different metal sulfides at the nano and/or near-nano scale. References are shown, as well as major findings.

Synthesis Method	**Type of nanoparticle**	**Size and morphology**	**Reference**
High gravity	ZnS	15 – 30 nm, spheroid	(Chen *et al.*, 2004)
Chemical bath	ZnS:Mn	2 nm, thin films	(Sahraei *et al.*, 2013)
Irradiation – precipitation	CdS	40 – 90 nm, spheroid and 40 – 100 nm (length) nanorods	(Ge *et al.*, 2002)
Spray pyrolysis	CuS	14 – 46 nm, spheroid	(Isac *et al.*, 2007)
Thermolysis	CuS, ZnS and Bi_2S_3	10 – 20 nm, spheroid	(Luo *et al.*, 2012)
Hydrothermal	Sb_2S_3	100 – 400 nm (length), nanorods	(Sheikhiabadi *et al.*, 2012)
Alkaline hydrolysis	Bi_2S_3	20 nm (length), nanofibers	(Neves *et al.*, 2003)
Surfactant/sulfurization	CdS, ZnS and PbS	4 – 12 nm, spheroid	(Patel *et al.*, 2012)
Micro-emulsion	CdS	4 – 14 nm, spheroid	(Upadhyay *et al.*, 2012)
Pulsing electrolysis	CuS	110 nm, spheroid	(Nekouie *et al.*, 2013)
Thermal decomposition	ZnS, CdS and PbS	4 – 18 nm, spheroid and cubic	(Yu *et al.*, 2011)
Solvent-mediated	$AgInS_2$	5 nm, spheroid (dots)	(Cheng *et al.*, 2011)
Bubble template	CuS	4 – 10 nm, spheroid	(Zhao *et al.*, 2012)
Organic phase transfer	Ag_2S	15 – 21 nm, spheroid	(Yeo *et al.*, 2010)
Micelle-template	CdS	5 nm, nanowires and nanotubes	(Xiong *et al.*, 2002)
Heat/Precipitation	ZnS, CdS and HgS	5 – 18 nm, spheroid and nanorods	(Onwudiwe and Ajibade, 2011)
Electrophoretic deposition	ZnS	20 nm, spheroid	(Vázquez *et al.*, 2011)
Single source (Langmuir-Blodgett deposition)	CdS	4 nm, quantum dots	(Ferreira *et al.*, 2001)
Metal organic chemical vapor deposition	Cu_2ZnSnS_4	10 nm, spheroid	(Edler *et al.*, 2012)

These methods, however, are mostly based on high-temperature and/or high pressure and on the use of toxic chemicals. Therefore, the production of functional nanomaterials using bacterial growth media solutions containing biologically produced sulfide, at room temperature and atmospheric pressure, avoiding the use of toxic and expensive chemicals, is an interesting alternative synthesis route. Their use presents obvious economic advantages and safety, as the sulfide is naturally produced in the growth media by sulfate-reducing bacteria enriched from environmental samples. Thus, the use of this excess sulfide – which, otherwise, would require treatment – to produce nanocrystalline materials is an important contribution not only for minimizing its impact on the environment, but also for the production of added value materials, such as nanocrystalline semiconductors. As semiconductors, the cristallinity of the nanosized metal sulfides is of the utmost importance, particularly when used in high precision industries, such as the construction of solar panels, as spatial separation of charges is of crucial importance in the design of efficient donor-acceptor heterojunctions (Bansal *et al.*, 2013; Friend *et al.*, 2012). Though it is tempting to postulate that the biological and biologically-mediated synthesis of nanosized semiconductors may not yield comparable nanostructures, regarding the cristallinity and size-dependent functionalities, some authors have already proven that this is not the case and that highly crystalline, monodisperse particles can be obtained and that there is the possibility to exert some control over size and, consequently, size-dependant functions (Bai *et al.*, 2009a; Dameron *et al.*, 1989; Gaware *et al.*, 2012; Shankar *et al.*, 2004; Song *et al.*, 2010). Some of these biological and biologically-mediated synthesis processes are described in the following section.

1.2.3 Biological Synthesis

1.2.3.1 General Outline

Metal sulfide nanoparticles of different shapes and sizes have been obtained resorting to numerous organisms, such as *Rhodopseudomonas palustris* (Bai *et al.*, 2009b), *Escherichia coli* (Shen *et al.*, 2010), *Clostridium thermoaceticum* (Cunningham and Lundie, 1993), Tobacco mosaic virus (Shenton *et al.*, 1999) and *Phaeodactylum tricornutum* (Scarano and Morelli, 2003), among others. Table 1.3 provides a summary of the biological systems used for the synthesis of different metal sulfide nanoparticles

and their respective characteristics, in terms of morphology and size. Considering the vast work carried out in this area of research, the summaries presented in Tables 1.2 and 1.3 could not but be invidious. Although extensive work has been carried out using certain methods in both biological and chemical syntheses (*e.g.*, *E. coli*-mediated synthesis of nanosized metal sulfides (Jaiganesh *et al.*, 2012; Kang *et al.*, 2008; Mi *et al.*, 2011; Shen *et al.*, 2010; Sweeney *et al.*, 2004)), herein we have tried to give a broad overview of the variety of systems that can be used for obtaining such nanostructures. In Figure 1.10, examples of the different nanostructures obtained using different organisms and biologically-mediated systems are shown.

The biosynthesis of metal sulfide nanoparticles presents numerous advantages. Such processes are characterized by occurring at neutral pH, atmospheric pressure and in a temperature range close to ambient temperature (Bai *et al*., 2009a; Castillo *et al*., 2012; da Costa *et al*., 2012; Thakkar *et al*., 2010).

1.2.3.2 Fungi and Yeasts

Fungi and yeasts are very efficient secretors of extracellular enzymes (Amore and Faraco, 2012; Kroukamp *et al*., 2013). These microorganisms have the potential to be used in large-scale production of enzymes that mediate the precipitation of metals in the media as metal sulfides (Sastry *et al.*, 2003). Genetic manipulation of these organisms – aiming at the overexpression of the desired enzymes – presents additional challenges when compared to the genetic engineering of simpler organisms, such as bacteria, as post-translational modifications are sometimes required (Su *et al.*, 2012). Fungi also show high tolerance to metals (Rajapaksha, 2011) and bioaccumulation abilities (Mishra and Malik, 2012). Consequently, syntheses using these microorganisms can be more easily scaled-up (Mukherjee *et al.*, 2001). However, some of these organisms (such as *Fusarium oxysporum*) are pathogenic to humans (O'Donnell *et al*., 2004) and plants (Edel-Hermann *et al.*, 2012), which would imply severe restrictions and the enforcement of strict control systems whenever used.

Seshadri and co-workers were able to synthesize PbS nanoparticles in the range of 2 – 5 nm using a lead-resistant yeast, *Rhodosporidium diobovatum* (Seshadri *et al.*, 2011). The authors also found that these nanoparticles were capped by a sulfur-rich peptide. In the late 80's, Dameron and collaborators have described the synthesis of CdS quantum dots (2 nm) using the yeasts *Candida glabrata* and *Schizosaccharomyces pombe*

(Dameron *et al.*, 1989), noting that the obtained nanoparticles were more monodisperse than those chemically produced. Identically, Ahmad *et al*. (Ahmad *et al.*, 2002) have produced CdS nanocrystals (5 – 20 nm) using the ascomycete fungus *Fusarium oxysporum*. The authors mentioned that this method can be extended to other systems such as PbS, ZnS and MoS_2 nanocrystals.

1.2.3.3 Virus, Plants and Algae

Protein engineering of viral cages for the synthesis of constrained nanomaterials has been the subject of several studies. Douglas and respective team (Douglas *et al.*, 2002) have used the protein cage of the cowpea chlorotic mottle virus (CCMV) for the synthesis of iron oxide nanoparticles and Rong has reported the use of the protein cages of different viruses – namely, the M13 bacteriophage and the CCMV – in the synthesis of iron oxide nanoparticles of diverse architectures (Rong *et al.*, 2011). Only a limited amount of work has been developed in the synthesis of metal sulfide nanoparticles using viruses. Shenton and co-workers (Shenton *et al.*, 1999) used Tobacco mosaic virus to produce CdS nanotubes. Resorting to the viral capsid of the bacteriophage M13, Flynn and respective team (Flynn *et al.*, 2003) were able to successfully synthesize ZnS and CdS nanoparticles. Moreover these authors have shown that the phage constructs were able to control the crystal size of the nanoparticles obtained. Using a similar approach, Iwahori and collaborators (Iwahori *et al.*, 2011) have used the protein cage apoferritin to synthesize CuS nanocrystals.

Identically, few studies have been carried out using plants (or plant extracts) and algae in the synthesis of metal sulfides, though a few have reported the successful precipitation of elemental gold and silver. Armendariz and co-workers, for example, have used *Avena sativa* (oat) biomass to recover Au(III) from aqueous solutions as elemental gold nanoparticles (Armendariz *et al.*, 2004) and Singaravelu and co-workers have used a type of brown algae (*Sargassum wightii*) to obtain monodisperse gold nanoparticles (Singaravelu *et al.*, 2007). The precipitation of metal sulfides resorting to plants and/or algae has been feebly studied and, consequently, the synthesis of nanosized metal sulfides resorting to plants and algae is at this point poorly understood. However, 20 – 30 nm nanoparticles of FeS have been precipitated using *Apium* sp. (Rickard *et al.*, 2007). There are intrinsic limitations to such processes because the synthesis takes place extracellularly. This is because the space between the cellulose

fibrils is approximately 5 nm wide (Thimm *et al.*, 2000), and therefore there are physical constraints for the precipitation of the metal sulfides within the plant cell walls. Nonetheless, Mata and collaborators were able to use brown algae, *Fucus vesiculosus*, to precipitate PbS nanocrystals with an average size of 9 nm (Mata *et al.*, 2007), while simultaneously removing Au(III).

1.2.3.4 Bacteria

The most investigated microorganisms for the precipitation of nanosized metal sulfides have been bacteria. These organisms are easier to manipulate and also show extreme resistance and bioaccumulation capabilities for heavy metals (Choudhary *et al.*, 2012; Poirier *et al.*, 2013; Zhang *et al.*, 2012). Figure 1.10 and Table 1.3 contain some examples of the work carried out using numerous bacteria in the synthesis of metal sulfide nanoparticles.

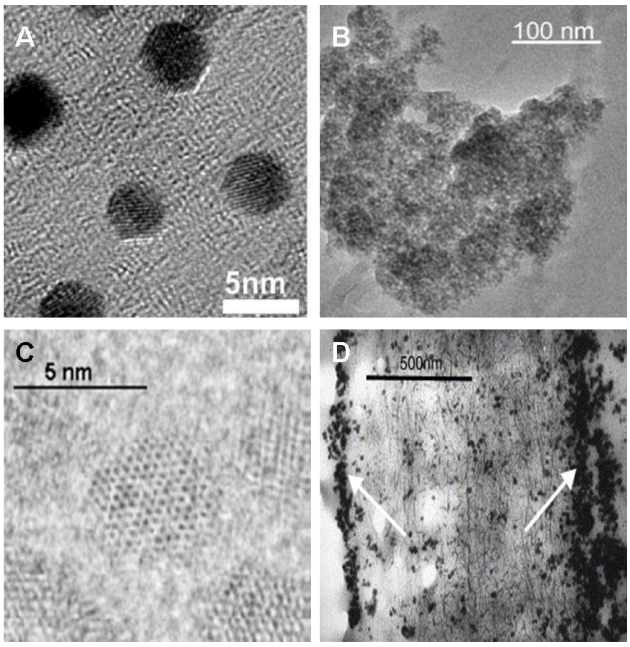

Figure 1.10 – Nanosized metal sulfides synthesized using biological systems. In A, HRTEM images of ZnS crystals obtained using viral capsids (adapted from (Flynn *et al.*, 2003)). In B, ZnS spheroid particles (20 – 30 nm) synthesized using biologically produced sulfide (adapted from (da Costa *et al.*, 2012)). HRTEM of PbS nanocrystallites prepared using the yeast *Torulopsis* sp. is shown in C. In D, TEM image of a section of *Apium* sp. parenchyma cell, showing the direction of diffusion (arrows) of the produced FeS particles (adapted from (Rickard *et al.*, 2007)).

Table 1.3 – Biological systems used for the synthesis of different nanosized metal sulfides. References are shown, as well as major findings.

Biological system		**Type of nanoparticle**	**Size and morphology**	**Reference**
Virus	Tobacco mosaic virus	CdS and PbS	16 – 50 nm, nanotubes	(Shenton *et al.*, 1999)
	M13 Bacteriophage	ZnS and CdS	2 – 5 nm, spheroid	(Flynn *et al.*, 2003)
Bacteria	*Actinobacter* sp.	Fe_3S_4 and FeS_2	7 – 20 nm, spheroid	(Bharde *et al.*, 2008)
	Clostridium thermoaceticum	CdS	n.d.	(Cunningham and Lundie, 1993)
	Escherichia coli	CdS	<2.5 nm, spheroid (dots)	(Shen *et al.*, 2010)
	Klebsiella aerogenes	CdS	20 – 200 nm, spheroid	(Holmes *et al.*, 1995)
	Klebsiella planticola	CdS	n.d.	(Sharma *et al.*, 2000)
	Klebsiella pneumoniae	CdS	4 nm, spheroid	(Holmes *et al.*, 1997)
	Magnetotactic bacteria	Fe_3S_4 and FeS_2	n.d.	(Mann *et al.*, 1990)
	Pseudomonas stutzeri	Ag_2S	25 – 45 nm, spheroid	(Slawson *et al.*, 1992)
	Rhodopseudomonas palustris	CdS	8 nm, spheroid	(Bai *et al.*, 2009b)
	Shewanella oneidensis	Ag_2S	6 – 12 nm, spheroid	(Suresh *et al.*, 2011)
	Sulfate-reducing bacteria	ZnS	20 – 30 nm, spheroid	(da Costa *et al.*, 2012)
Fungi and Yeast	*Candida glabrata*	CdS	2 nm, n.d.	(Dameron *et al.*, 1989)
	Fusarium oxysporum	CdS	5 – 20 nm, spheroid	(Ahmad *et al.*, 2002)
	Schizosaccharomyces pombe	CdS	2 nm, n.d.	(Dameron *et al.*, 1989)
	Torulopsis sp.	PbS	2 – 5 nm, spheroid	(Kowshik *et al.*, 2002)
	Rhodosporidium diobovatum	PbS	2 – 5 nm, spheroid	(Seshadri *et al.*, 2011)
Plant and Algae	*Phaeodactylum tricornutum*	CdS	<2 nm, spheroid (dots)	(Scarano and Morelli, 2003)
	Fucus vesiculosus	PbS	9 nm, spheroid	(Mata *et al.*, 2007)
	Apium sp.	FeS	20 – 30 nm, spheroid	(Rickard *et al.*, 2007)
Other	Egg membrane	CdS	<100 nm, n.d.	(Pattabi and Uchil, 2000)
	Aminoacid (L-cysteine)	Bi_2S_3	50 nm, nanorods	(Zhang *et al.*, 2006)

1.3 The Case for Sulfate-Reducing Bacteria (SRB)

Consisting of a group of diverse morphology, dissimilatory sulfate- or sulfur-reducing bacteria (SRB) includes fourteen (14) gram-negative bacteria (Barton and Hamilton, 2007; Bergey and Breed, 1957). SRB are amongst the oldest forms of life and can be traced back to 3.5 billion years ago (Barton and Fauque, 2009; Hohmann-Marriott and Blankenship, 2011; Tice and Lowe, 2004). The sulfate reduction process can occur by two distinct pathways: assimilatory and dissimilatory (Grein *et al.*, 2012). In the assimilatory pathway, small amounts of sulfate are reduced for the synthesis of sulfur-containing cell components, such as proteins (Leustek *et al.*, 2000). In contrast, in the dissimilatory pathway, large amounts of sulfate are reduced for obtaining energy and the excess sulfide is expelled (Barton, 1995; Muyzer and Stams, 2008). Both pathways are described in Figure 1.11. As an energy-yielding process, the dissimilatory metabolism is probably one of the earliest pathways sustaining life (Canfield and Raiswell, 1999; Canfield *et al.*, 2006). Between the Promethean Period of the Hadean (4,000 million years ago) and the Archean (2,500 million years ago) Eons (Goldblatt *et al.*, 2010), Earth's anoxic atmosphere was rich in H_2S and SO_2, due to volcanic and hydrothermal sources (Grein *et al.*, 2012). In turn, these compounds could undergo photolysis, generating elemental sulfur and sulfate (Farquhar *et al.*, 2001; Pavlov and Kasting, 2002). These could then serve as an electron acceptor in the oxidation of H_2. An alternative biological strategy could be the disproportionation of elemental sulfur and sulfur compounds of intermediate oxidation states, such as sulfite or thiosulfate (Grein *et al.*, 2012). Such strategies have been reported in studies of sulfur isotopes and microfossil records (Philippot *et al.*, 2007; Shen *et al.*, 2001; Wacey *et al.*, 2011).

These organisms range between 0.4 – 3.0 μm in diameter and are strictly anaerobic (Bergey and Breed, 1957). Based on ribosomal RNA, they have been categorized in four sub-groups: gram-negative mesophilic SRB, gram-positive spore forming SRB, thermophilic bacterial SRB and thermophilic archaeal SRB (Castro *et al.*, 2000).

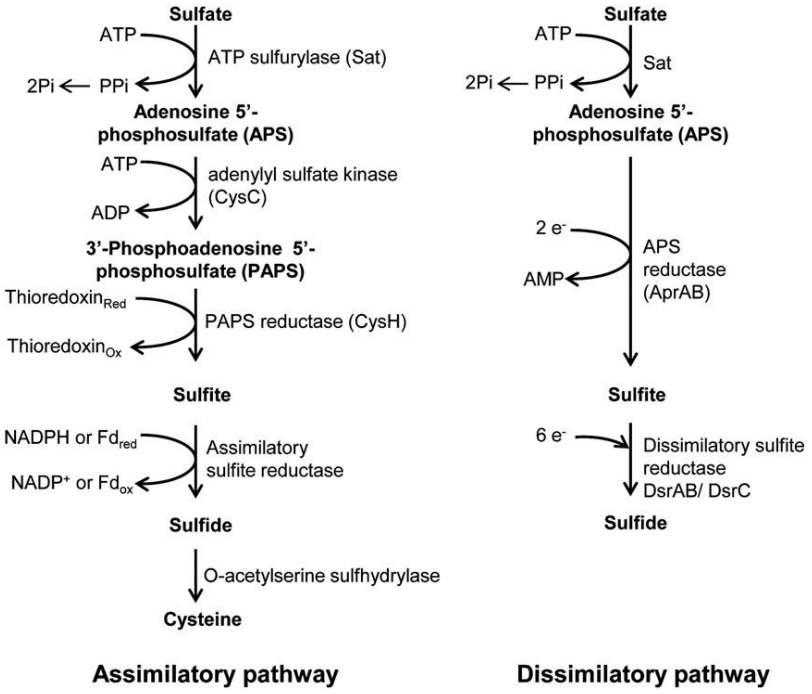

Figure 1.11 – Assimilatory and dissimilatory pathways of sulfate reduction (adapted from (Grein *et al.*, 2012)).

Sulfate-reducing bacteria have long proven to possess a high potential in bioremediation processes (Hard *et al.*, 1997; Pagnanelli *et al.*, 2012; Summers, 1992). Interestingly, it has been reported that the use of bacteria is more efficient in bioremediation systems whenever used as a consortium, as opposed to pure cultures (Cheung and Gu, 2003; Cheung and Gu, 2007; Sheoran *et al.*, 2010). Such synergistic effect may be due to the numerous metabolic capabilities of the present member bacteria. These, however, can be highly complex and may include the removal of metabolites by a species produced by another. If not removed, such metabolites could hinder microbial activity (Cerqueira *et al.*, 2011). Co-metabolism processes, in which a species is capable of degrade compounds only partially degraded by a first species, is also a possibility (Sieburth, 1988; Vaiopoulou and Gikas, 2012).

1.4 A Brief Note on "Heavy Metals"

In recent years, the term "heavy metals" has been used in an increasing number of legislative initiatives and publications (e.g. (91/271/EEC, 1991; Barakat, 2011b)). These often relate to the chemical hazards, toxicity and contamination of a group of elements that include both metals and metalloids (semi-metals) (Duffus, 2002). Generally, the

elements considered have an atomic weight between 63.5 and 200.6 and their specific gravity is greater than 5.0 (Fu and Wang, 2011; Srivastava and Majumder, 2008). However, in both the scientific literature and in legal regulations, the term "heavy metals" has been inconsistently used, which has led to a general vagueness regarding the significance of the expression. The term is often related to toxicity and pollution and, although "heavy" connotes high density, the knowledge of such parameter does little for the prediction of the biological effects of metal (Duffus, 2002). Over the years, many have raised questions regarding the use of the term "heavy metals" (Nieboer and Richardson, 1980; Phipps, 1981; vanLoon and Duffy, 2000) but attempts in providing a chemically sound definition have so far failed (Duffus, 2002). Metals are described as "elements which conduct electricity, have a metallic luster, are malleable and ductile, form cations and have basic oxides" (Atkins and Jones, 1997). However, such definition would include many elements, and, therefore, more subtle divisions have been attempted when defining the "heavy metals" group. Such divisions (Duffus, 2002) are based on:

- **Density** – metals having a density greater than 4 $g.cm^{-3}$, 5 $g.cm^{-3}$, 6 $g.cm^{-3}$ and 7 $g.cm^{-3}$ (Bjerrum, 1936; Davies, 1987; Grant and Grant, 1987; Scott and Brewer, 1983)
- **Atomic weight** – metals with a high atomic number, with an atomic weight greater than sodium or an atomic weight greater than 40 (Hodgson *et al.*, 1988; Holister, 1976; Rand *et al.*, 1995).
- **Atomic number** – metal of moderate atomic number, with an atomic number greater than 20, with an atomic number greater than calcium or with an atomic number between 21 and 92 (Hale, 1988; Luckey, 1975; Lyman, 1995; Walker, 1988).
- **Other chemical properties** – metals which readily react with dithizone (C_6H_5N) or which react with fatty acids forming soaps (Bates, 1995; Hampel, 1976).
- **Toxicity** – metals toxic to animals and aerobic and anaerobic processes; elements or compounds that are toxic in nature (Hodgson *et al.*, 1988; Scott, 1981).

Based on the Lewis acidity, the metal ions are currently classified as Class A, Class B or Borderline (Figure 1.12), a categorization that depends on their affinity for different

ligands (Ahrland *et al.*, 1958). An also common description for Class A and Class B ions is "hard acids" and "soft acids", respectively (Pearson, 1968a; Pearson, 1968b). Class A metal ions, or "hard acids", tend to form complexes with non-polarizable ligands, such as oxygen donors. The bonds formed are, in most cases, ionic, though the formation of π (pi) bonds also occurs. Class B metal ions, or "soft acids", usually form covalent bonds with polarizable ligands (Duffus, 2002).

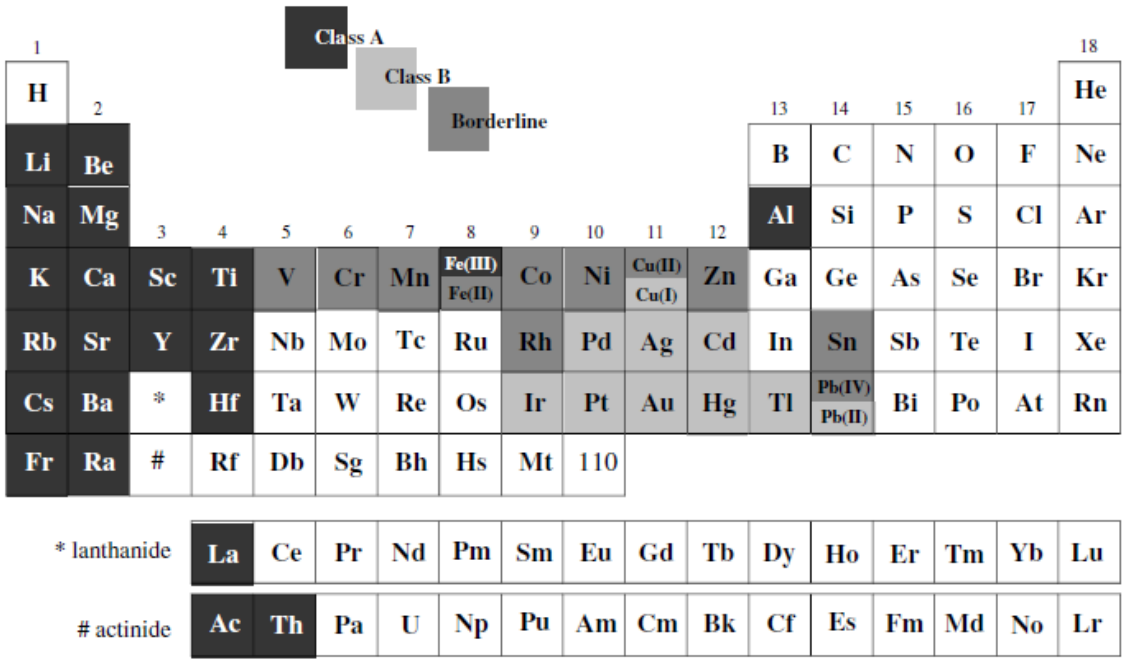

Figure 1.12 – Classification of the metal ions of the Periodic Table as Class A, Class B or Borderline. Note that copper may be either Class B or Borderline, depending whether it is Cu (I) or Cu (II), respectively. Identically, iron may be Class A (Fe(III)) or Borderline (Fe(II)). Adapted from (Duffus, 2002).

Although it seems clear that the terminology "heavy metals" has no real sound or scientific basis, its use is widely disseminated in both scientific and legislative literatures.

Nonetheless, due to its ubiquity, the term will sometimes be used in the present work, and, whenever mentioned, this will refer to the three most commonly found metals in sites contaminated as a result of mining activities in the Iberian pyritic belt (Zn, Cu and Fe) (Costa and Duarte, 2005; Garcia *et al.*, 2001). Such metals are Borderline metal ions, as based on their Lewis acidity (Duffus, 2002).

1.5 Photocatalysis

1.5.1 The Dye Safranin-T

Safranin-T (CAS N. 477-73-6, 350.85 $g.mol^{-1}$) is a reddish brown water soluble phenazine dye, belonging to the quinine imine class (Rauf *et al.*, 2011; Vinu *et al.*, 2010). Safranin-T (Figure 1.13) is mainly used in the dyeing processes of tannin, cotton, wool, leather and silk (Gupta *et al.*, 2007), but it is also present as a food dye in candies and cookies (Zaghbani *et al.*, 2008). This dye has been reported as a potential carcinogen (Saha *et al.*, 2013) and shown to interact with DNA (Sarkar *et al.*, 2008). As a dye, Safranin-T is subjected to regulations (40.CFR-§148.261, 2005; 1907/2006/EEC, 2006). Due to its wide application in numerous industries, the development of a practical treatment system for its elimination is of particular interest and many studies have been carried out investigating the photodegradation of Safranin (Dong *et al.*, 2012; El-Kemary *et al.*, 2011; El-Kemary and El-Shamy, 2009; Gupta *et al.*, 2007; Hamity *et al.*, 2008; Hayat *et al.*, 2011; Kernazhitsky *et al.*, 2013; Pouretedal *et al.*, 2009; Rauf *et al.*, 2007).

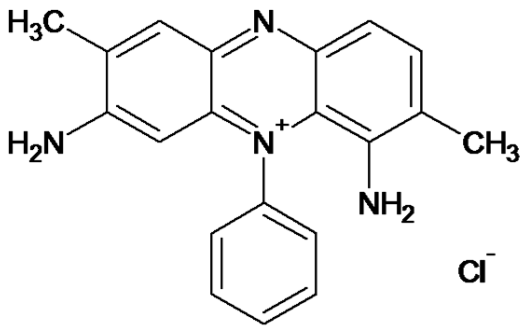

Figure 1.13 – Chemical structure of Safranin-T (adapted from (Zaghbani *et al.*, 2008)).

1.5.2 Photocatalysis of Dyes

Dyes are used in numerous industries, such as cosmetic, textile, leather and pharmaceutical, among others. Worldwide, there are over 100,000 commercially available dyes and the annual estimated production exceeds 80,000 tons (Sanroman *et al.*, 2010). Of these, 15-20% is estimated to be lost during the dyeing process, making their way into the industries effluents (Konstantinou and Albanis, 2004; Weber and

Stickney, 1993). The discharge of these contaminated wastewaters constitutes a source of environmental contamination, eutrophication and may result in the formation of harmful byproducts, through chemical reactions, such as oxidation and hydrolysis (Neppolian *et al.*, 2002).

The decontamination of industrial wastewaters – namely, for the removal of dyes – relies on the use of non-destructive techniques, such as adsorption of activated carbon (Meshko *et al.*, 2001), reverse osmosis (Nataraj *et al.*, 2009), coagulation mediated by chemical agents (Moghaddam *et al.*, 2010) or ultrafiltration (deLara *et al.*, 2012). Nonetheless, such treatments merely result in a transfer of the contaminants, and, consequently, cause a secondary pollution. Furthermore, the materials used in these procedures require regeneration, which is often expensive (Konstantinou and Albanis, 2004). Oxidation processes, such as ozonation, have been used in the treatment of wastewaters (Silva *et al.*, 2009), but these have high operational costs and show low efficiency in the removal of carbon content, often requiring combined treatment operations (de Souza *et al.*, 2010). This lead to the development of Advanced Oxidation Processes (AOP's) which are becoming increasingly researched for the treatment of numerous wastes (Chu *et al.*, 2012; Guimarães *et al.*, 2012; Souza *et al.*, 2012). AOP's are based on the generation of highly reactive species, such as hydroxyl radicals ($^{\bullet}OH$). These are then capable of readily and non-selectively oxidizing a wide range of compounds. The generation of these radicals can be achieved through Fenton reactions (Sun *et al.*, 2008), H_2O_2-UV processes (Dixit *et al.*, 2011) or by using semiconductors, such as TiO_2 (Choi *et al.*, 2010). Among these, TiO_2-mediated photocatalysis appears to show the most promise due to its inherent destructive nature (Konstantinou and Albanis, 2004). As atmospheric oxygen can be used as oxidant, no mass transfer is required, and it has been shown to lead to a complete mineralization of organic carbon (Janaki *et al.*, 2012; Vinu *et al.*, 2010).

The TiO_2-mediated photocatalytic mechanism for the degradation of dyes has been thoroughly described in the literature (Bandara *et al.*, 1999; Bianco-Prevot *et al.*, 2001; Galindo *et al.*, 2000; Houas *et al.*, 2001) and is summarized in Equations 1.14 – 1.21. When an aqueous suspension of TiO_2 is irradiated with an energy exceeding its band gap energy, conduction band electrons (e^-) and valence band holes (h^+) are generated (Equation 1.14). The latter can oxidize the organic molecule to form R^+, or it can react with OH^- and H_2O, resulting in the formation of $OH^{\bullet}$ radicals (Equations 1.15 and 1.16). In turn, the photogenerated electrons can either reduce the dye (Equation 1.21) or

react with electron acceptors, such as O_2, which can be adsorbed on the surface of the catalyst or dissolved in the water, resulting in the formation of the superoxide radical $O_2^{\bullet -}$ (Equation 1.17). The radical $OH^{\bullet}$ is a very strong oxidizing agent, with a standard redox potential of 2.8V (Konstantinou and Albanis, 2004), thus being able to oxidize most dyes.

$$TiO_2 + h\nu(UV) \rightarrow TiO_2(e_{CB}^- + h_{VB}^+) \quad (1.14)$$

$$TiO_2(h_{VB}^+) + H_2O \rightarrow TiO_2 + H^+ + OH^{\bullet} \quad (1.15)$$

$$TiO_2(h_{VB}^+) + HO^- \rightarrow TiO_2 + HO^{\bullet} \quad (1.16)$$

$$TiO_2(e_{CB}^-) + O_2 \rightarrow TiO_2 + O_2^{\bullet -} \quad (1.17)$$

$$O_2^{\bullet -} + H^+ \rightarrow HO_2^{\bullet} \quad (1.18)$$

$$Dye + HO^{\bullet} \rightarrow Degradation\ Products \quad (1.19)$$

$$Dye + h_{VB}^+ \rightarrow Oxidation\ Products \quad (1.20)$$

$$Dye + e_{CB}^- \rightarrow Reduction\ Products \quad (1.21)$$

It should be noted, however, that the photocatalytic oxidation mechanism (Equations 1.14 – 1.21) differs from that of photosensitized oxidation. The mechanism of photosensitized oxidation by visible radiation (>420 nm), namely in the case of dyes, involves the excitation of the adsorbed compounds, resulting in the formation of singlet or triplet states, followed by the injection of electrons of the excited molecule onto the conduction band of the TiO_2 particles. The molecule is then converted to its cationic radical, and, finally, undergoes degradation (Daneshvar *et al.*, 2003; Epling and Lin, 2002; Vinodgopal *et al.*, 1994). This mechanism is summarized in Equations 1.22 through 1.25.

$$Dye + h\nu(vis) \rightarrow {}^1Dye^* / {}^3Dye^* \quad (1.22)$$

$${}^1Dye^* / {}^3Dye^* + TiO_2 \rightarrow Dye^{\bullet +} + TiO_2(e_{CB}^-) \quad (1.23)$$

$$TiO_2(e_{CB}^-) + O_2 \rightarrow O_2^{\bullet -} + TiO_2 \quad (1.24)$$

$$Dye^{\bullet +} \rightarrow Degradation\ products \quad (1.25)$$

The cationic dye radicals can then undergo oxidation (Equations 1.26 and 1.27) or interact with the $O_2^{\bullet-}$, $HO_2^{\bullet}$ or $HO^{\bullet-}$ radicals, generating intermediaries that, eventually, lead to the formation of CO_2 (Janaki *et al.*, 2012; Konstantinou and Albanis, 2004; Vinu *et al.*, 2010).

$$Dye^{\bullet+} + HO^{-} \rightarrow Dye + HO^{\bullet} \quad (1.26)$$

$$Dye + 2HO^{\bullet} \rightarrow H_2O + \text{Oxidation products} \quad (1.27)$$

$$2HO^{\bullet} + H^{+} + TiO_2(e_{CB}^{-}) \rightarrow H_2O_2 + TiO_2 \quad (1.28)$$

$$H_2O_2 + TiO\ (e_{CB}^{-}) \rightarrow HO^{\bullet} + HO^{-} + TiO_2 \quad (1.29)$$

$$Dye^{\bullet+} + O_2^{\bullet-} \rightarrow DO_2 \rightarrow Degradation\ products \quad (1.30)$$

$$Dye^{\bullet+} + HO_2^{\bullet}(or HO^{\bullet}) \rightarrow Degradation\ products \quad (1.31)$$

Both photo-oxidation and photosensitization mechanisms take place during irradiation, but, to this date, it has not been unequivocally shown whether – if any – of these mechanisms are prevalent during the photocatalytic process (Bettoni *et al.*, 2011; Epling and Lin, 2002; Galindo *et al.*, 2001; Konstantinou and Albanis, 2004).

The general mechanism of the photocatalysis of pollutants on TiO_2 nanomaterials is summarized in Figure 1.14.

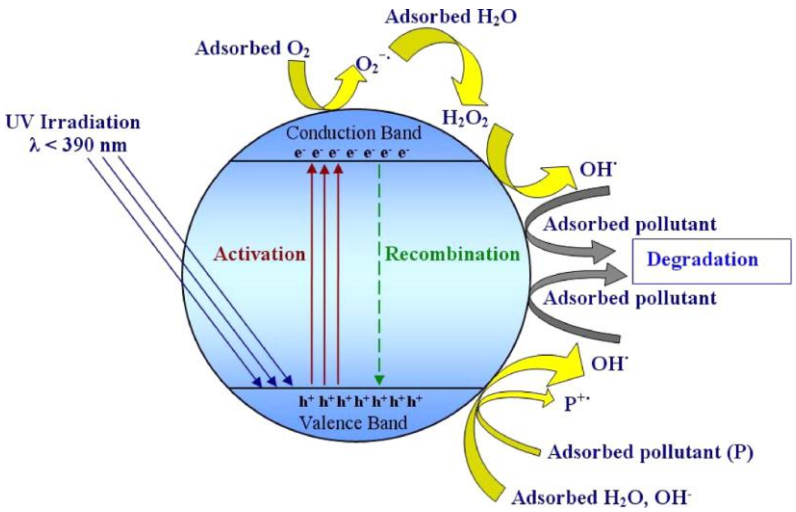

Figure 1.14 – The general mechanism proposed for the degradation of pollutants on TiO_2 (adapted from (Khataee and Kasiri, 2010)).

1.5.3 Kinetics and Factors Affecting the Photocatalytic Degradation Process

1.5.3.1 Kinetics

Many authors have shown that the TiO_2-mediated photocatalytic oxidation of numerous dyes fits the Langmuir-Hinshelwood (L-H) kinetics model (Galindo *et al.*, 2001; Gupta *et al.*, 2012a; Gupta *et al.*, 2012b; Houas *et al.*, 2001; Tang and Huren, 1995; Toor *et al.*, 2006). This model, when the initial concentration is small (Rauf *et al.*, 2011), can be expressed by Equation 1.32.

$$\ln\left(\frac{C_0}{C_i}\right) = K_{app}.t \qquad (1.32)$$

For Eq. 1.32, C_0 is the initial dye concentration, C_i is the concentration at time t and K_{app} is the apparent reaction rate constant. When representing the $\ln(C_0\text{-}C_i)$ versus time, the slope will equal the apparent first-order rate constant, K_{app}. Plotting $1/K_{app}$ against $1/C_i$ allows for the determination of the Langmuir adsorption constant (slope, expressed as M^{-1}) (Chong *et al.*, 2010). The L-H model, which has been established to correlate the dependence of the reaction rate on the initial concentrations of the solute, may fit the rate of TiO_2-mediated photocatalysis of dyes because the reaction takes place between (Khataee and Kasiri, 2010):

- Two adsorbed substances
- A radical linked to the surface and a substrate molecule in solution
- Two species in solution
- A radical in solution and an adsorbed substrate molecule.

Nonetheless, it has not been possible, so far, to determine whether the process occurs on the surface, in solution or at the interface (Bianco Prevot *et al.*, 2001).

1.5.3.2 Factors Influencing the Photocatalytic Degradation Process

1.5.3.2.1 Effect of the Initial Concentration of Dye

It has been reported that, generally, an increase in dye concentration results in higher degradation rates (Franco *et al.*, 2009; Sakthivel *et al.*, 2003; Saquib and Muneer, 2003). This is to be expected, as the degradation rate merely relates to the probability of the formation of radicals and subsequent reaction of these radicals with the dye molecules. Hence, as the amount of dye molecules available increase, so does the reaction rate. However, at a given point, an increase in the dye concentration will result in a decrease of the degradation rate. This occurs because, when the concentration of the dye is high enough, there is a decrease in the formation of radicals at the surface of the catalyst, as the active sites are covered by the dye molecules (Khataee and Kasiri, 2010). Another reason for this phenomenon is that, when the dye is sufficiently concentrated, there will be a decrease in the amount of radiation that reaches the catalyst's surface, and, consequently, there is a decrease in the formation of the $^{\bullet}OH$ and $O_2^{\bullet-}$ radicals (Franco *et al.*, 2009).

1.5.3.2.2 Effect of the pH

Titanium dioxide has the tendency to adsorb water at its surface, resulting in the formation of titanium-hydroxide groups (Kasuga *et al.*, 2002). Changes in the pH values will, hence, affect the state of ionization of the surface, as described in Equations 1.33 and 1.34, but also to that of the reactant dyes and products (Konstantinou and Albanis, 2004).

$$TiOH + H^+ \leftrightarrow TiOH_2^+ \quad (1.33)$$

$$TiOH + HO^- \leftrightarrow TiO^- + H_2O \quad (1.34)$$

Thus, the pH can actively influence the adsorption of the dye molecules onto the surface of the catalyst, affecting the photodegradation efficiency (Fox and Dulay, 1993). Considering that the point of zero charge (pzc) of TiO_2 (P25) varies between 6.3 and 6.8 (Barakat, 2011a; Bouanimba *et al.*, 2011), then the surface charge of this catalyst should be polarized as described by Equation 1.35 (Baran *et al.*, 2008).

$$TiOH_2^+ \xleftarrow{pH<pH_{pzc}} TiOH \xleftarrow{pH>pH_{pzc}} TiO^- \quad (1.35)$$

The reaction between hydroxide ions and positive holes can lead to the formation of hydroxyl radicals. At low pH values, positive holes are considered the major oxidation species. Contrarily, at high pH values, the predominant oxidation species are the hydroxyl radicals (Konstantinou and Albanis, 2004; Tang and Huang, 1995). Consequently, the $HO^{\bullet}$ radicals can be more easily generated in alkaline media, through oxidation of hydroxide ions available at the TiO_2 surface. However, in these conditions, there is a Coulombic repulsion between the negatively charged surface of the photocatalyst and the hydroxide anions (Konstantinou and Albanis, 2004), which could result in a decrease in the formation of the $HO^{\bullet}$ radicals and, consequently, in a lower photodegradation efficiency. Interestingly, it has been reported that, in the case of cationic dyes, the use of a pH value between 6 – 7, as opposed to values noticeably alkaline or acidic, enhances the photodegradation activity, with a more pronounced effect at pH values between 11 and 13 (Bouanimba *et al.*, 2011; Poulios and Aetopoulou, 1999; Tang *et al.*, 1997). This may be because, at such "extreme" pH levels, the hydroxyl radicals are quickly scavenged, having no opportunity to react with the dye molecules (Davis and Huang, 1989). Ultimately, considering that the influence of the pH ultimately depends on the characteristics of both the catalyst and the dye, the effect of this parameter must always be determined on a case-by-case basis.

1.5.3.2.3 Effect of Catalyst Loading

Commonly, it was found that an increase of the amount of catalyst resulted in an increase of the degradation rates, whether in static (Franco *et al.*, 2009; Sakthivel *et al.*, 2003), dynamic flow (Li *et al.*, 2010b; Subramanian and Kannan, 2010) or slurry reactors (Akyol and Bayramoglu, 2008; Chong *et al.*, 2009). However, after a certain level is reached, the reaction rate decreases and becomes independent of the catalyst concentration. This is because, as it stands to reason, an increase in the amount of catalyst will result in a larger availability of active sites. When the suspended catalyst reaches a certain amount, however, light penetration decreases and, consequently, the degradation rate of the photocatalytic process also decreases. When the amount of catalyst is higher, sedimentation and agglomeration of the particles may occur, which may culminate in a decrease of the degradation rate, as part of the catalyst's surface

becomes unavailable (Konstantinou and Albanis, 2004). Moreover, higher catalyst loading may result in the inactivation of the activated molecules by collision with ground state molecules, thus decreasing the photocatalytic degradation rate (Neppolian *et al.*, 2002). In the end, the optimal amount of catalyst (TiO_2) will depend on the working conditions of the photoreactor and on the dye itself, namely, on its initial concentration (Herrmann, 1999).

1.5.3.2.4 Effects of Dopants

Because of its wide band gap and, consequently, of the fact that TiO_2 becomes photoactive under ultraviolet excitation, only about 3 – 5% of the solar energy reaching the Earth's surface can be utilized, making the use of this catalyst impractical for the treatment of wastewaters (Chiou *et al.*, 2008; Huang *et al.*, 2009). Additionally, the activity of titanium dioxide is further limited by the low interfacial charge-transfer rates but also by its high electron-hole pair recombination (Liu *et al.*, 2006). Hence, several strategies for *sensitizing* TiO_2 to visible light and decreasing the high recombination rate have been developed, mostly focusing on doping TiO_2 with metal ions (Hoffmann *et al.*, 1995). Such ions include rare earth metals (Shi *et al.*, 2012), noble metals (Todorova *et al.*, 2008) and transition metals (Gurkan *et al.*, 2013). Doping of the titanium dioxide with metals has been demonstrated to improve the photocatalytic activity of the catalyst by widening the light absorption range, enhancing the quantum efficiency, by reducing the electron-hole pair recombination and improving the redox potential of the radicals photogenerated (Teh and Mohamed, 2011). Although most studies verse on metal-doped TiO_2, there have been investigations on the effect of doping titanium dioxide with non-metals and their impact on the photoefficiency of the catalyst. Positive outcomes have been observed using carbon (Mai *et al.*, 2009), fluorine (Kim *et al.*, 2012), sulfur (Han *et al.*, 2011) and nitrogen (Devi *et al.*, 2012). For the latter, the incorporation into TiO_2 causes changes in the electrical conductivity, refraction index and photocatalytic activity towards visible light absorption, by narrowing of the band gap (Ao *et al.*, 2009; Teh and Mohamed, 2011). The carbon-doped TiO_2 particles have been asserted to possess the theoretical advantage of introducing new states (C 2p) close to the valence band of the TiO_2 (O 2p), thus shifting the edge of the valence band towards higher energy and, consequently, a narrower band gap (Mai *et al.*, 2009; Ren *et al.*, 2007). When using sulfur-doped TiO_2, it was observed not only that a significant

shift of the optical absorption edge towards the visible region takes place (Liu *et al.*, 2009c), but also that there is an increase in the Brunauer-Emmet-Teller (or BET) area (Brunauer *et al.*, 1938), thus improving the photocatalytic activity of TiO_2 (Han *et al.*, 2011). Finally, doping of the titanium dioxide with fluoride results in a higher generation of hydroxyl radicals, due to the elevated availability of holes at the catalyst's surface (Vijayabalan *et al.*, 2009) and in a shift of the absorption towards the visible region of the light spectrum (Khoa Le *et al.*, 2012), thus resulting in an enhancement of the photodegradation reaction. Having considered the undeniable beneficial effects of TiO_2 doping on its photocatalytic activity, it should be noted, however, that there are several drawbacks to using such techniques, particularly in the case of metal doping. Doped titanium dioxide has been demonstrated to be thermally unstable (Freiman *et al.*, 2007; Wong *et al.*, 2006; Zaitsev *et al.*, 2000) and the metal ions that dope TiO_2 have been identified as the prevalent cause of blockage of the active sites at the surface of the catalyst (Teh and Mohamed, 2011; Xiao *et al.*, 2006). Moreover, metal centers in doped materials tend to act as electron traps, which results in the improvement of the recombination electron-hole pairs, therefore reducing the photocatalytic activity (Matos *et al.*, 2007). Last, at large scale, metal doping would require the installation of expensive ion-implantation facilities with subsequent environmental dangers (Teh and Mohamed, 2011). Although problems may be avoided by using non-metal dopants, such materials have also shown some disadvantages, such as reduction of the visible light photoactivity due to decrease on the non-metal component during the annealing process (Chen *et al.*, 2009).

1.5.3.2.5 Effects of Other Variables and Parameters

Light intensity and irradiation time are also important factors that should be taken into consideration when evaluating the kinetics of the photocatalytic process. It has been reported that, at low light intensities (0 – 20 $mW.cm^{-2}$), there is a linear variation between the reaction rate and the light intensity (Ollis *et al.*, 1991). At intermediate light intensities, the reaction kinetics becomes half-order: the reaction rate depends on the square root of the light intensity (Herrmann, 1999). At higher light intensities, the reaction rate becomes independent (Konstantinou and Albanis, 2004). This is probably due to the fact that, at low intensities, reactions involving the formation of electron-hole

pairs are predominant and reactions of electron-hole recombination are negligible. The prevalence of the latter reaction, however, increases with light intensity, resulting in the lower rate of photodegradation (Sauer *et al.*, 2002). The degree of degradation increases with irradiation time, as is to be expected. Nonetheless, the reaction rate decreases with time, namely, in reactions that follow first-order kinetics. This slowing of the reaction kinetics is due to the decrease of the molecules of dye, but may also be due to the competition between the reactant molecules and the molecules of the degradation products for the reactive sites (Rauf *et al.*, 2011). The active sites at the surface of the catalyst may also be deactivated due to the deposition of strong by-products, such as carbon. Additionally, in the case of dyes with nitrogen groups, the slow kinetics after a certain amount of time may be caused by the difficulty of converting the nitrogen atoms of the dye into oxidized nitrogen compounds (Bandara *et al.*, 1999).

The use of oxidizing agents for the enhancement of the photodegradation has been extensively studied, and, mainly, concerns the use of either hydrogen peroxide (H_2O_2) or peroxodissulfate ($S_2O_8^{2-}$) (Kumar *et al.*, 2008; Kuriechen *et al.*, 2011; Riga *et al.*, 2007; Wen *et al.*, 2011; Zhang *et al.*, 2013). The reactive radicals intermediates ($SO_4^{\bullet-}$ and $HO^{\bullet}$) (Shinde *et al.*, 2011) formed play a double role as both a strong oxidant, but also as an electron scavenger, inhibiting the recombination of the electron-hole pair at the surface of the catalyst (Gaya and Abdullah, 2008; Grätzel *et al.*, 1990). This leads, ultimately, to an increase in the degradation rate of the photocatalytic reaction. Some, however, have noted that H_2O_2, particularly, can be adsorbed onto TiO_2 particles and modify its surface, with concomitant decrease in the activity of the catalyst (Konstantinou and Albanis, 2004). Others have questioned the use of such oxidizing agents, as their activity seems to sometimes depend not only on the type of substrate, but also on numerous experimental conditions (Akpan and Hameed, 2009; Balcioğlu and İnel, 1996). Hence, the beneficial effects of adding such agents should be carefully addressed and weighed before their use.

Naturally occurring ions, humic acids and the presence of solvents are also parameters that may affect the efficiency of the photodegradation reaction. The presence of all these compounds is not unusual in industrial wastewaters containing dyes (Chang and Juang, 2004; Sharma *et al.*, 2007; Zhao *et al.*, 2005) and they may compete for the active sites or deactivate the photocatalyst, thus affecting the rate of the photocatalytic reaction. Generally, the presence of these compounds has shown to result in a decrease of the rate of degradation. In the case of humic acids, this may be the combined result of light

attenuation, surface deactivation and competition for the active sites (Epling and Lin, 2002; Wiszniowski *et al.*, 2002). Even at low concentrations, solvents have also been shown to have a considerable negative effect on the photocatalytic degradation of dyes (Daneshvar *et al.*, 2003; Renzi *et al.*, 1997). This may stem from the fact that, for example, ethanol is able to quench the hydroxyl radicals and it is often used with that purpose (Daneshvar *et al.*, 2003; Khodja *et al.*, 2001). Thus, the presence of these substances will culminate in a decrease of the efficiency of the photocatalytic process. Regarding the effect of inorganic ions, it has been shown that anionic species, such as HCl or H_3PO_4, exert an inhibitory effect (Daneshvar *et al.*, 2003; Epling and Lin, 2002), which may be explained by the reaction of these ions with the positively charged holes (h^+) and the hydroxyl radicals ($HO^\bullet$). Also, the anions may compete for the active sites at the surface of the catalyst, thus suppressing the photocatalytic degradation of the dye (Guillard *et al.*, 2003; Helz *et al.*, 1994; Sökmen and Özkan, 2002). The effects of several cations, namely, Cd^{2+}, Zn^{2+}, Cu^{2+}, Al^{3+} and Fe^{3+}, have also been investigated (Chen *et al.*, 2001). Results have shown that the cations Cd^{2+}, Zn^{2+} and Al^{3+} have only residual effects, explained by the alteration in the adsorption of the dye. On the other hand, both copper and iron cations have a strong inhibitory effect on the degradation reaction. These ions were demonstrated to decrease the conduction electrons-mediated reduction of oxygen, thus blocking the formation of the reactive oxygen species (ROS). The case of Fe^{3+} is, however, especially interesting, as the rate of the photodegradation is expected to increase, due to the enhanced formation of the hydroxyl radical in the presence of this ion (Feng and Nansheng, 2000) and, in fact, such improvement has been observed (Mrowetz and Selli, 2004; Zhang *et al.*, 2011). This enhancement has been attributed to the increase in adsorbed dye molecules at the surface of the iron-modified TiO_2 and this was confirmed by demonstrating the lack of kinetic effects of the non-adsorbed iron species. This apparent contradiction was resolved by showing that iron (III) cations have a positive effect on the discoloration of anionic dyes, but a negative effect for cationic dyes (Baran *et al.*, 2003). This may be explained by the fact the cations may react with the negatively charged dye molecules, resulting in the formation of non-colored substances; on the other hand, for cationic dyes, a competition for the active sites at the surface of the catalyst may occur, thus decreasing the rate of degradation. Thus, the treatment efficiency in the presence of inorganic ions must be carefully addressed, depending on the type of dye subject to photodegradation (Akpan and Hameed, 2009).

Hence, photocatalytic degradation of organic pollutants can be an important contribution for the effective treatment of wastewaters, thus having a positive effect over the environment.

References

40.CFR-§148.261, F., 2005. Hazardous Waste—Nonwastewaters From Productions of Dyes, Pigments, and Food, Drug, and Cosmetic Colorants; Mass Loadings-Based Listing; Final Rule. In: FDA (Ed.), 40 CFR Parts 148, 261, 268, 271, and 302, US, pp. 44.

91/271/EEC, E.-L., 1991. Commission Directive concerning urban waste water treatment In: E. Union (Ed.), 91/271/EEC, Brussels, pp. 12.

1907/2006/EEC, E.-L., 2006. Registration, Evaluation, Authorisation and Restriction of Chemicals (REACH). In: E. Union (Ed.), 1907/2006, Brussels, pp. 849.

Abdel Rafea, M., Farag, A.A.M., Gad, S. and Roushdy, N., 2012. Heterojunction performance of dip coated n-Cd0.5Zn0.5S thin films on different metal sulfide substrates. Materials Science in Semiconductor Processing 16(1): 89-98.

Ahmad, A., Mukherjee, P., Mandal, D., Senapati, S., Khan, M.I., Kumar, R. and Sastry, M., 2002. Enzyme Mediated Extracellular Synthesis of CdS Nanoparticles by the Fungus, Fusarium oxysporum. Journal of the American Chemical Society, 124(41): 12108-12109.

Ahrland, S., Chatt, J. and Davies, N.R., 1958. The relative affinities of ligand atoms for acceptor molecules and ions. Quarterly Reviews, Chemical Society, 12(3): 265-276.

Akman, O., Kavas, H., Baykal, A., Toprak, M.S., Çoruh, A. and Aktaş, B., 2013. Magnetic metal nanoparticles coated polyacrylonitrile textiles as microwave absorber. J Magn Magn Mater, 327(0): 151-158.

Akpan, U.G. and Hameed, B.H., 2009. Parameters affecting the photocatalytic degradation of dyes using TiO2-based photocatalysts: A review. Journal of Hazardous Materials, 170(2-3): 520-529.

Akyol, A. and Bayramoglu, M., 2008. The degradation of an azo dye in a batch slurry photocatalytic reactor. Chemical Engineering and Processing: Process Intensification, 47(12): 2150-2156.

Al-Tarazi, M., Heesink, A.B.M., Azzam, M.O.J., Abu Yahya, S. and Versteeg, G.F., 2004. Crystallization kinetics of ZnS precipitation; an experimental study using the mixed-suspension-mixed-product-removaI (MSMPR) method. Cryst Res Technol, 39(8): 675-685.

Al-Tarazi, M., Heesink, A.B.M., Versteeg, G.F., Azzam, M.O.J. and Azzam, K., 2005. Precipitation of CuS and ZnS in a bubble column reactor. Aiche J, 51(1): 235-246.

Amils, R., 1999. Biohydrometallurgy and the Environment Toward the Mining of the 21st Century: Proceedings of the International Biohydrometallurgy Symposium IBS'99 Held in San Lorenzo de El Escorial, Madrid, Spain, June 20-23, 1999. Elsevier.

AMOC, 2003. Egypt: contract awarded for gas treatment plant using new technology. Focus on Catalysts, 2003(2): 5-6.

Ao, Y., Xu, J., Fu, D. and Yuan, C., 2009. A simple method to prepare N-doped titania hollow spheres with high photocatalytic activity under visible light. Journal of Hazardous Materials, 167(1–3): 413-417.

Arifin, K., Daud, W.R.W. and Kassim, M.B., 2013. Optical and photoelectrochemical properties of a TiO_2 thin film doped with a ruthenium–tungsten bimetallic complex. Ceram Int, 39(3): 2699-2707.

Armendariz, V., Herrera, I., Peralta-Videa, J.R., Jose-Yacaman, M., Troiani, H., Santiago, P. and Gardea-Torresdey, J.L., 2004. Size controlled gold nanoparticle formation by Avena sativa biomass: use of plants in nanobiotechnology. J Nanopart Res, 6(4): 377-382.

Askerov, E., 2012. Global economic outlook and steel demand trends.

Atkins, P. and Jones, L., 1997. Chemistry - Molecules, Matter and Change, New York.

Bai, H., Zhang, Z., Guo, Y. and Jia, W., 2009a. Biological Synthesis of Size-Controlled Cadmium Sulfide Nanoparticles Using ImmobilizedRhodobacter sphaeroides. Nanoscale Res Lett, 4(7): 717 - 723.

Bai, H.J., Zhang, Z.M., Guo, Y. and Yang, G.E., 2009b. Biosynthesis of cadmium sulfide nanoparticles by photosynthetic bacteria Rhodopseudomonas palustris. Colloids and Surfaces B: Biointerfaces, 70(1): 142-146.

Baker, D.R. and Kamat, P.V., 2009. Photosensitization of TiO2 Nanostructures with CdS Quantum Dots: Particulate versus Tubular Support Architectures. Adv Funct Mater, 19(5): 805-811.

Balcioğlu, I. and İnel, Y., 1996. Photocatalytic degradation of organic contaminants in semiconductor suspensions with added H_2O_2. Journal of Environmental Science and Health . Part A: Environmental Science and Engineering and Toxicology, 31(1): 123-138.

Balis, N., Dracopoulos, V., Bourikas, K. and Lianos, P., 2013. Quantum dot sensitized solar cells based on an optimized combination of ZnS, CdS and CdSe with CoS and CuS counter electrodes. Electrochim Acta, 91(0): 246-252.

Bandara, J., Mielczarski, J.A. and Kiwi, J., 1999. 2. Photosensitized Degradation of Azo Dyes on Fe, Ti, and Al Oxides. Mechanism of Charge Transfer during the Degradation. Langmuir, 15(22): 7680-7687.

Bansal, N., Reynolds, L.X., MacLachlan, A., Lutz, T., Ashraf, R.S., Zhang, W., Nielsen, C.B., McCulloch, I., Rebois, D.G., Kirchartz, T., Hill, M.S., Molloy, K.C., Nelson, J. and Haque, S.A., 2013. Influence of crystallinity and energetics on charge separation in polymer-inorganic nanocomposite films for solar cells. Scientific reports, 3: 1531.

Barakat, M.A., 2011a. Adsorption and photodegradation of Procion yellow H-EXL dye in textile wastewater over TiO_2 suspension. Journal of Hydro-environment Research, 5(2): 137-142.

Barakat, M.A., 2011b. New trends in removing heavy metals from industrial wastewater. Arabian Journal of Chemistry, 4(4): 361-377.

Baran, W., Adamek, E. and Makowski, A., 2008. The influence of selected parameters on the photocatalytic degradation of azo-dyes in the presence of TiO_2 aqueous suspension. Chemical Engineering Journal, 145(2): 242-248.

Baran, W., Makowski, A. and Wardas, W., 2003. The influence of $FeCl_3$ on the photocatalytic degradation of dissolved azo dyes in aqueous TiO_2 suspensions. Chemosphere, 53(1): 87-95.

Barton, L. and Hamilton, W.A., 2007. Sulphate-reducing bacteria : environmental and engineered systems. Cambridge University Press, Cambridge ;.

Barton, L.L. and Fauque, G.D., 2009. Biochemistry, Physiology and Biotechnology of Sulfate-Reducing Bacteria. Adv Appl Microbiol, 68: 41-98.

Bates, R.L., 1995. Glossary of geology. American Geological Society, Alexandria, VA.

Bergey, D.H. and Breed, R.S., 1957. Bergey's manual of determinative bacteriology. Williams & Wilkins Co., Baltimore.

Bessergenev, V., Ivanova, E.N., Kovalevskaya, Y.A., Gromilov, S.A., Kirichenko, V.N., Zemskova, S.M., Vasilieva, I.G., Ayupov, B.M. and Shwarz, N.L., 1995.

Optical and Structural Proper Ties of Zns and Zns-Mn Films Prepared by Cvd Method. Mater Res Bull, 30(11): 1393-1400.

Bettoni, M., Meniconi, S., Rol, C. and Sebastiani, G.V., 2011. Selective photocatalytic oxidation at TiO2/Ti anodes of 4-methoxybenzyl alcohol to the corresponding benzaldehyde in "green" conditions. Journal of Photochemistry and Photobiology A: Chemistry, 222(1): 180-184.

Bharde, A.A., Parikh, R.Y., Baidakova, M., Jouen, S., Hannoyer, B., Enoki, T., Prasad, B.L.V., Shouche, Y.S., Ogale, S. and Sastry, M., 2008. Bacteria-Mediated Precursor-Dependent Biosynthesis of Superparamagnetic Iron Oxide and Iron Sulfide Nanoparticles. Langmuir, 24(11): 5787-5794.

Bianco Prevot, A., Baiocchi, C., Brussino, M.C., Pramauro, E., Savarino, P., Augugliaro, V., Marcì, G. and Palmisano, L., 2001. Photocatalytic Degradation of Acid Blue 80 in Aqueous Solutions Containing TiO2 Suspensions. Environ Sci Technol, 35(5): 971-976.

Bjerrum, N.J., 1936. Inorganic chemistry. W. Heinemann, London.

Boonstra, J., van Lier, R., Janssen, G., Dijkman, H. and Buisman, C.J.N., 1999. Biological treatment of acid mine drainage. In: R. Amils and A. Ballester (Eds.), Process Metallurgy. Elsevier, pp. 559-567.

Bouanimba, N., Zouaghi, R., Laid, N. and Sehili, T., 2011. Factors influencing the photocatalytic decolorization of Bromophenol blue in aqueous solution with different types of TiO_2 as photocatalysts. Desalination, 275(1–3): 224-230.

Bratty, M., Lawrence, R.W., Kratochvil, D. and Marchant, P.B., 2006. Applications of biological H_2S production from elemental sulfur in the treatment of heavy metal pollution including acid rock drainage, International Symposium of Acid Rock Drainage (ICARD), pp. 271-281.

Brunauer, S., Emmett, P.H. and Teller, E., 1938. Adsorption of Gases in Multimolecular Layers. Journal of the American Chemical Society, 60(2): 309-319.

Bube, R.H., 2001. Cadmium Sulfide and Telluride. In: K.H.J.B. Editors-in-Chief: *et al.* (Eds.), Encyclopedia of Materials: Science and Technology (Second Edition). Elsevier, Oxford, pp. 873-879.

Canary, J.W., Mortezaei, S. and Liang, J., 2010. Transition metal-based chiroptical switches for nanoscale electronics and sensors. Coordin Chem Rev, 254(19–20): 2249-2266.

Canfield, D.E. and Raiswell, R., 1999. The evolution of the sulfur cycle. Am J Sci, 299(7-9): 697-723.

Canfield, D.E., Rosing, M.T. and Bjerrum, C., 2006. Early anaerobic metabolisms. Philos T R Soc B, 361(1474): 1819-1834.

Castillo, J., Pérez-López, R., Caraballo, M.A., Nieto, J.M., Martins, M., Costa, M.C., Olías, M., Cerón, J.C. and Tucoulou, R., 2012. Biologically-induced precipitation of sphalerite–wurtzite nanoparticles by sulfate-reducing bacteria: Implications for acid mine drainage treatment. Sci Total Environ, 423(0): 176-184.

Castro, H.F., Williams, N.H. and Ogram, A., 2000. Phylogeny of sulfate-reducing bacteria. FEMS Microbiology Ecology, 31(1): 1-9.

Cerqueira, V.S., Hollenbach, E.B., Maboni, F., Vainstein, M.H., Camargo, F.A.O., Peralba, M.d.C.R. and Bento, F.M., 2011. Biodegradation potential of oily sludge by pure and mixed bacterial cultures. Bioresource Technol, 102(23): 11003-11010.

Cerrato, J.M., Falkinham Iii, J.O., Dietrich, A.M., Knocke, W.R., McKinney, C.W. and Pruden, A., 2010. Manganese-oxidizing and -reducing microorganisms isolated

from biofilms in chlorinated drinking water systems. Water Res, 44(13): 3935-3945.

Chang, M.-Y. and Juang, R.-S., 2004. Adsorption of tannic acid, humic acid, and dyes from water using the composite of chitosan and activated clay. J Colloid Interf Sci, 278(1): 18-25.

Chen, C., Li, X., Ma, W., Zhao, J., Hidaka, H. and Serpone, N., 2001. Effect of Transition Metal Ions on the TiO_2-Assisted Photodegradation of Dyes under Visible Irradiation: A Probe for the Interfacial Electron Transfer Process and Reaction Mechanism. The Journal of Physical Chemistry B, 106(2): 318-324.

Chen, Q., Jiang, D., Shi, W., Wu, D. and Xu, Y., 2009. Visible-light-activated Ce–Si co-doped TiO_2 photocatalyst. Appl Surf Sci, 255(18): 7918-7924.

Cheng, K.-C., Law, W.-C., Yong, K.-T., Nevins, J.S., Watson, D.F., Ho, H.-P. and Prasad, P.N., 2011. Synthesis of near-infrared silver-indium-sulfide (AgInS2) quantum dots as heavy-metal free photosensitizer for solar cell applications. Chem Phys Lett, 515(4–6): 254-257.

Cheung, K.H. and Gu, J.-D., 2003. Reduction of chromate (CrO_4^{2-}) by an enrichment consortium and an isolate of marine sulfate-reducing bacteria. Chemosphere, 52(9): 1523-1529.

Cheung, K.H. and Gu, J.-D., 2007. Mechanism of hexavalent chromium detoxification by microorganisms and bioremediation application potential: A review. International Biodeterioration & Biodegradation, 59(1): 8-15.

Chiang, C.-L., Sung, C.-S. and Chen, C.-Y., 2006. Application of silica–magnetite nanocomposites to the isolation of ultrapure plasmid DNA from bacterial cells. J Magn Magn Mater, 305(2): 483-490.

Choi, H., Al-Abed, S.R., Dionysiou, D.D., Stathatos, E. and Lianos, P., 2010. Chapter 8 TiO2-Based Advanced Oxidation Nanotechnologies for Water Purification and Reuse. In: C.E. Isabel and I.S. Andrea (Eds.), Sustainability Science and Engineering. Elsevier, pp. 229-254.

Choi, J.Y., Kim, D.S. and Lim, J.Y., 2006. Fundamental features of copper ion precipitation using sulfide as a precipitant in a wastewater system. J Environ Sci Heal A, 41(6): 1155-1172.

Choma, J., Dziura, A., Jamioła, D., Nyga, P. and Jaroniec, M., 2011. Preparation and properties of silica–gold core–shell particles. Colloids and Surfaces A: Physicochemical and Engineering Aspects, 373(1–3): 167-171.

Choma, J., Jamioła, D., Ludwinowicz, J. and Jaroniec, M., 2012. Deposition of silver nanoparticles on silica spheres and rods. Colloids and Surfaces A: Physicochemical and Engineering Aspects, 411(0): 74-79.

Chong, M.N., Jin, B., Chow, C.W.K. and Saint, C.P., 2009. A new approach to optimise an annular slurry photoreactor system for the degradation of Congo Red: Statistical analysis and modelling. Chemical Engineering Journal, 152(1): 158-166.

Choudhary, S., Islam, E., Kazy, S.K. and Sar, P., 2012. Uranium and other heavy metal resistance and accumulation in bacteria isolated from uranium mine wastes. Journal of Environmental Science and Health, Part A, 47(4): 622-637.

Cohen, R.R.H., 2006. Use of microbes for cost reduction of metal removal from metals and mining industry waste streams. J Clean Prod, 14(12–13): 1146-1157.

Costa, M.C. and Duarte, J.C., 2005. Bioremediation of acid mine drainage using acidic soil and organic wastes for promoting sulphate-reducing bacteria activity on a column reactor. Water Air Soil Poll, 165(1-4): 325-345.

Coulton, R.H., Bullen, C. and Hallet, C., 2003. The design and optimization of active mine water treatment plants. Land Contam Reclam(11): 6.

Cui, J. and Forssberg, E., 2003. Mechanical recycling of waste electric and electronic equipment: a review. Journal of Hazardous Materials, 99(3): 243-263.

Cunningham, D.P. and Lundie, L.L., 1993. Precipitation of Cadmium by Clostridium-Thermoaceticum. Appl Environ Microb, 59(1): 7-14.

da Costa, J.P., Girao, A.V., Lourenco, J.P., Monteiro, O.C., Trindade, T. and Costa, M.C., 2012. Synthesis of nanocrystalline ZnS using biologically generated sulfide. Hydrometallurgy, 117: 57-63.

Dameron, C.T., Reese, R.N., Mehra, R.K., Kortan, A.R., Carroll, P.J., Steigerwald, M.L., Brus, L.E. and Winge, D.R., 1989. Biosynthesis of cadmium sulphide quantum semiconductor crystallites. Nature, 338(6216): 596-597.

Daneshvar, N., Salari, D. and Khataee, A.R., 2003. Photocatalytic degradation of azo dye acid red 14 in water: investigation of the effect of operational parameters. Journal of Photochemistry and Photobiology A: Chemistry, 157(1): 111-116.

Davies, B.E., 1987. Consequences of environmental contamination by lead mining in Wales. Hydrobiologia, 149(1): 213-220.

Davis, A.P. and Huang, C.P., 1989. Removal of Phenols from Water by a Photocatalytic Oxidation Process. Water Science and Technology, 21(6-7): 455-464.

de Souza, S.M.d.A.G.U., Bonilla, K.A.S. and de Souza, A.A.U., 2010. Removal of COD and color from hydrolyzed textile azo dye by combined ozonation and biological treatment. Journal of Hazardous Materials, 179(1–3): 35-42.

deLara, E., Barredo-Damas, S., Alcaina-Miranda, M.I. and Iborra-Clar, M.I., 2012. Ultrafiltration technology with a ceramic membrane for reactive dye removal: Optimization of membrane performance. Journal of Hazardous Materials, 209–210(0): 492-500.

Devi, L.G., Nagaraj, B. and Rajashekhar, K.E., 2012. Synergistic effect of Ag deposition and nitrogen doping in TiO_2 for the degradation of phenol under solar irradiation in presence of electron acceptor. Chemical Engineering Journal, 181–182(0): 259-266.

Di Virgilio, A.L., Maisuls, I., Kleitz, F. and Arnal, P.M., 2013. A new synthesis pathway for colloidal silica spheres coated with crystalline titanium oxide and its comparative cyto- and genotoxic study with titanium oxide nanoparticles in rat osteosarcoma (UMR106) cells. J Colloid Interf Sci, 394(0): 147-156.

Diebold, U., 2003. The surface science of titanium dioxide. Surface Science Reports, 48(5–8): 53-229.

Dixit, A., Tirpude, A.J., Mungray, A.K. and Chakraborty, M., 2011. Degradation of 2, 4 DCP by sequential biological–advanced oxidation process using UASB and UV/TiO2/H2O2. Desalination, 272(1–3): 265-269.

Dong, W., Sun, Y., Ma, Q., Zhu, L., Hua, W., Lu, X., Zhuang, G., Zhang, S., Guo, Z. and Zhao, D., 2012. Excellent photocatalytic degradation activities of ordered mesoporous anatase TiO_2–SiO_2 nanocomposites to various organic contaminants. Journal of Hazardous Materials, 229–230(0): 307-320.

Dong, X., Potter, D. and Erkey, C., 2002. Synthesis of CuS nanoparticles in water-in-carbon dioxide microemulsions. Ind Eng Chem Res, 41(18): 4489-4493.

Douglas, T., Strable, E., Willits, D., Aitouchen, A., Libera, M. and Young, M., 2002. Protein Engineering of a Viral Cage for Constrained Nanomaterials Synthesis. Adv Mater, 14(6): 415-418.

Du, L., Chen, X., Li, W. and Zhu, Q., 2011. A Study on Enhancement of Filtration Process with Filter Aids Diatomaceous Earth and Wood Pulp Cellulose. Chinese J Chem Eng, 19(5): 792-798.

Dudka, S. and Adriano, D.C., 1997. Environmental impacts of metal ore mining and processing: A review. J Environ Qual, 26(3): 590-602.

Duffus, J.H., 2002. "Heavy metals" - A meaningless term? (IUPAC technical report). Pure Appl Chem, 74(5): 793-807.

Edel-Hermann, V., Gautheron, N. and Steinberg, C., 2012. Genetic diversity of Fusarium oxysporum and related species pathogenic on tomato in Algeria and other Mediterranean countries. Plant Pathology, 61(4): 787-800.

Edler, M., Rath, T., Schenk, A., Fischereder, A., Haas, W., Edler, M., Chernev, B., Kunert, B., Hofer, F., Resel, R. and Trimmel, G., 2012. Copper zinc tin sulfide layers prepared from solution processable metal dithiocarbamate precursors. Mater Chem Phys, 136(2–3): 582-588.

El-Kemary, M., Abdel-Moneam, Y., Madkour, M. and El-Mehasseb, I., 2011. Enhanced photocatalytic degradation of Safranin-O by heterogeneous nanoparticles for environmental applications. J Lumin, 131(4): 570-576.

El-Kemary, M. and El-Shamy, H., 2009. Fluorescence modulation and photodegradation characteristics of safranin O dye in the presence of ZnS nanoparticles. Journal of Photochemistry and Photobiology A: Chemistry, 205(2–3): 151-155.

Elkanzi, E.M., 2009. Simulation of the Process of Biological Removal of Hydrogen Sulfide from Gas. In: E.A. Hassan, G.V.R. Reklaitis, G.V.R.R. Mahmoud M. El-HalwagiA2 - Hassan E. Alfadala and M.E.-H. Mahmoud (Eds.), Proceedings of the 1st Annual Gas Processing Symposium. Elsevier, Amsterdam, pp. 266-275.

Epling, G.A. and Lin, C., 2002. Photoassisted bleaching of dyes utilizing TiO2 and visible light. Chemosphere, 46(4): 561-570.

Ernst and Young, 2012. Global steel — 2011 trends, 2012 outlook. 1112-1316449, Ersnt & Young

Evangelou, V.P., 1998. Pyrite chemistry: The key for abatement of acid mine drainage. Environm Sci: 197-222.

Feng, W. and Nansheng, D., 2000. Photochemistry of hydrolytic iron (III) species and photoinduced degradation of organic compounds. A minireview. Chemosphere, 41(8): 1137-1147.

Ferreira, P.M.S., Barros Timmons, A., Neves, M.C., Dynarowicz, P. and Trindade, T., 2001. Langmuir–Blodgett manipulation of capped cadmium sulfide quantum dots. Thin Solid Films, 389(1–2): 272-277.

Flynn, C.E., Mao, C., Hayhurst, A., Williams, J.L., Georgiou, G., Iverson, B. and Belcher, A.M., 2003. Synthesis and organization of nanoscale II-VI semiconductor materials using evolved peptide specificity and viral capsid assembly. J Mater Chem, 13(10): 2414-2421.

Fowler, T.A., Holmes, P.R. and Crundwell, F.K., 2001. On the kinetics and mechanism of the dissolution of pyrite in the presence of Thiobacillus ferrooxidans. Hydrometallurgy, 59(2-3): 257-270.

Fox, M.A. and Dulay, M.T., 1993. Heterogeneous photocatalysis. Chemical Reviews, 93(1): 341-357.

Franco, A., Neves, M.C., Carrott, M.M.L.R., Mendonca, M.H., Pereira, M.I. and Monteiro, O.C., 2009. Photocatalytic decolorization of methylene blue in the presence of TiO_2/ZnS nanocomposites. Journal of Hazardous Materials, 161(1): 545-550.

Freiman, S., Singh, M., Fischman, G.S., Hellmann, J., Logan, K., Coyle, T., Hobbs, L., Smith, J., Sideridis, C. and Green, M., 2007. Global Roadmap for Ceramic and Glass Technology with CD-ROM. Wiley.

Friend, R.F., Phillips, M.F., Rao, A.F., Wilson, M., Li, Z.F. and McNeill, C.R., 2012. Excitons and charges at organic semiconductor heterojunctions. Faraday Discuss, 155(1359-6640 (Print)).

Fujishima, A. and Honda, K., 1972. Electrochemical Photolysis of Water at a Semiconductor Electrode. Nature, 238(5358): 37-38.

Gadd, G.M., 2010. Metals, minerals and microbes: geomicrobiology and bioremediation. Microbiol-Sgm, 156: 609-643.

Galindo, C., Jacques, P. and Kalt, A., 2001. Photooxidation of the phenylazonaphthol AO20 on TiO_2: kinetic and mechanistic investigations. Chemosphere, 45(6-7): 997-1005.

Garcia, C., Moreno, D.A., Ballester, A., Blazquez, M.L. and Gonzalez, F., 2001. Bioremediation of an industrial acid mine water by metal-tolerant sulphate-reducing bacteria. Minerals Engineering, 14(9): 997-1008.

Gaware, U., Kamble, V. and Ankamwar, B., 2012. Ecofriendly Synthesis of Anisotropic Gold Nanoparticles: A Potential Candidate of SERS Studies. International Journal of Electrochemistry, 2012: 6.

Ge, X., Ni, Y. and Zhang, Z., 2002. A novel route to prepare cadmium sulfide nano-rods. Radiat Phys Chem, 64(3): 223-227.

Goldblatt, C., Zahnle, K.J., Sleep, N.H. and Nisbet, E.G., 2010. The Eons of Chaos and Hades. Solid Earth, 1(1): 1-3.

Gosar, M., 2004. Environmental impacts of metal mining. Materials and Geoenvironment, 51(4): 10.

Grant, R. and Grant, C., 1987. Grant and Hackh's Chemical Dictionary. McGraw-Hill, New York, 641 pp.

Grein, F., Ramos, A.R., Venceslau, S.S. and Pereira, I.A.C., 2012. Unifying concepts in anaerobic respiration: Insights from dissimilatory sulfur metabolism. Biochimica et Biophysica Acta (BBA) - Bioenergetics(0).

Guillard, C., Lachheb, H., Houas, A., Ksibi, M., Elaloui, E. and Herrmann, J.M., 2003. Influence of chemical structure of dyes, of pH and of inorganic salts on their photocatalytic degradation by TiO_2 comparison of the efficiency of powder and supported TiO_2. Journal of Photochemistry and Photobiology A: Chemistry, 158(1): 27-36.

Gupta, V.K., Jain, R., Mittal, A., Mathur, M. and Sikarwar, S., 2007. Photochemical degradation of the hazardous dye Safranin-T using TiO_2 catalyst. J Colloid Interf Sci, 309(2): 464-469.

Gurkan, Y.Y., Kasapbasi, E. and Cinar, Z., 2013. Enhanced solar photocatalytic activity of TiO2 by selenium(IV) ion-doping: Characterization and DFT modeling of the surface. Chemical Engineering Journal, 214(0): 34-44.

Gutiérrez, O.Y., Kaufmann, C., Hrabar, A., Zhu, Y. and Lercher, J.A., 2011. Synthesis of methyl mercaptan from carbonyl sulfide over sulfide K_2MoO_4/SiO_2. J Catal, 280(2): 264-273.

Hale, W.G., 1988. Collins Dictionary of Biology, HARPER COLLINS PUBLISHER.

Hamity, M., Lema, R.H., Suchetti, C.A. and Gsponer, H.E., 2008. UV–vis photodegradation of dyes in the presence of colloidal Q-CdS. Journal of Photochemistry and Photobiology A: Chemistry, 200(2–3): 445-450.

Hampel, C.A., 1976. Glossary of chemical terms. Van Nostrand Reinhold, New York :.

Han, C., Pelaez, M., Likodimos, V., Kontos, A.G., Falaras, P., O'Shea, K. and Dionysiou, D.D., 2011. Innovative visible light-activated sulfur doped TiO2 films for water treatment. Applied Catalysis B: Environmental, 107(1–2): 77-87.

Hashim, M.A., Mukhopadhyay, S., Sahu, J.N. and Sengupta, B., 2011. Remediation technologies for heavy metal contaminated groundwater. J Environ Manage, 92(10): 2355-2388.

Hayat, K., Gondal, M.A., Khaled, M.M., Yamani, Z.H. and Ahmed, S., 2011. Laser induced photocatalytic degradation of hazardous dye (Safranin-O) using self synthesized nanocrystalline WO3. Journal of Hazardous Materials, 186(2–3): 1226-1233.

Helz, G.R., Zepp, R.G. and Crosby, D.G., 1994. Aquatic and surface photochemistry. Lewis Publishers.

Herrera, P., Uchiyama, H., Igarashi, T., Asakura, K., Ochi, Y., Ishizuka, F. and Kawada, S., 2007. Acid mine drainage treatment through a two-step neutralization ferrite-formation process in northern Japan: Physical and chemical characterization of the sludge. Minerals Engineering, 20(14): 1309-1314.

Herrmann, J.M., 1999. Heterogeneous photocatalysis: fundamentals and applications to the removal of various types of aqueous pollutants. Catal Today, 53(1): 115-129.

Hodgson, E., Mailman, R.B. and Chambers, J.E., 1988. Macmillan dictionary of toxicology. Macmillan, London :.

Hoffmann, M.R., Martin, S.T., Choi, W. and Bahnemann, D.W., 1995. Environmental Applications of Semiconductor Photocatalysis. Chemical Reviews, 95(1): 69-96.

Hohmann-Marriott, M.F. and Blankenship, R.E., 2011. Evolution of Photosynthesis. Annu Rev Plant Biol, 62: 515-548.

Holister, G.S., 1976. The environment : a dictionary of the world around us / Geoffrey Holister and Andrew Porteous. Arrow reference series. Arrow Books, London :.

Holmes, J.D., Richardson, D.J., Saed, S., Evans-Gowing, R., Russell, D.A. and Sodeau, J.R., 1997. Cadmium-specific formation of metal sulfide 'Q-particles' by Klebsiella pneumoniae. Microbiology+, 143(8): 2521-2530.

Holmes, J.D., Smith, P.R., Evansgowing, R., Richardson, D.J., Russell, D.A. and Sodeau, J.R., 1995. Energy-Dispersive X-Ray-Analysis of the Extracellular Cadmium-Sulfide Crystallites of Klebsiella-Aerogenes. Arch Microbiol, 163(2): 143-147.

Iler, R.K., 1979. The chemistry of silica : solubility, polymerization, colloid and surface properties, and biochemistry. Wiley, New York :.

Isac, L.A., Duta, A., Kriza, A., Enesca, I.A. and Nanu, M., 2007. The growth of CuS thin films by Spray Pyrolysis. Proceedings of the International Conference on Nanoscience and Technology, 61: 477-481.

Iwahori, K., Takagi, R., Kishimoto, N. and Yamashita, I., 2011. A size controlled synthesis of CuS nano-particles in the protein cage, apoferritin. Mater Lett, 65(21–22): 3245-3247.

Jaiganesh, T., Daisy Vimala Rani, J. and Girigoswami, A., 2012. Spectroscopically characterized cadmium sulfide quantum dots lengthening the lag phase of Escherichia coli growth. Spectrochimica Acta Part A: Molecular and Biomolecular Spectroscopy, 92(0): 29-32.

Janaki, V., Oh, B.-T., Shanthi, K., Lee, K.-J., Ramasamy, A.K. and Kamala-Kannan, S., 2012. Efficiency of various semiconductor catalysts for photodegradation of Safranin-T. Research on Chemical Intermediates.

Jankiewicz, B.J., Jamiola, D., Choma, J. and Jaroniec, M., 2012. Silica–metal core–shell nanostructures. Advances in Colloid and Interface Science, 170(1–2): 28-47.

Ji, P.F., Takeuchi, M., Cuong, T.M., Zhang, J.L., Matsuoka, M. and Anpo, M., 2010. Recent advances in visible light-responsive titanium oxide-based photocatalysts. Research on Chemical Intermediates, 36(4): 327-347.

Johnson, D.B., 2003. Chemical and Microbiological Characteristics of Mineral Spoils and Drainage Waters at Abandoned Coal and Metal Mines. Water, Air, & Soil Pollution: Focus, 3(1): 47-66.

Johnson, D.B., 2012. Reductive dissolution of minerals and selective recovery of metals using acidophilic iron- and sulfate-reducing acidophiles. Hydrometallurgy, 127–128(0): 172-177.

Johnson, D.B. and Hallberg, K.B., 2002. Pitfalls of passive mine water treatment. Reviews in Environmental Science and Biotechnology, 1(4): 335-343.

Johnson, D.B. and Hallberg, K.B., 2005. Acid mine drainage remediation options: a review. Sci Total Environ, 338(1-2): 3-14.

Kalele, S., Gosavi, S.W., Urban, J. and Kulkarni, S.K., 2006a. Nanoshell particles: synthesis, properties and applications. Curr Sci India, 91(8): 1038-1052.

Kalele, S.A., Kundu, A.A., Gosavi, S.W., Deobagkar, D.N., Deobagkar, D.D. and Kulkarni, S.K., 2006b. Rapid detection of Escherichia coli by using anti body-conjugated silver nanoshells. Small, 2(3): 335-338.

Kang, S.H., Bozhilov, K.N., Myung, N.V., Mulchandani, A. and Chen, W., 2008. Microbial Synthesis of CdS Nanocrystals in Genetically Engineered E. coli. Angewandte Chemie, 120(28): 5264-5267.

Kasuga, T., Kondo, H. and Nogami, M., 2002. Apatite formation on TiO2 in simulated body fluid. J Cryst Growth, 235(1-4): 235-240.

Kernazhitsky, L., Shymanovska, V., Gavrilko, T., Naumov, V., Kshnyakin, V. and Khalyavka, T., 2013. A comparative study of optical absorption and photocatalytic properties of nanocrystalline single-phase anatase and rutile tio2 doped with transition metal cations. J Solid State Chem(0).

Khataee, A.R. and Kasiri, M.B., 2010. Photocatalytic degradation of organic dyes in the presence of nanostructured titanium dioxide: Influence of the chemical structure of dyes. J Mol Catal a-Chem, 328(1-2): 8-26.

Khoa Le, T., Flahaut, D., Foix, D., Blanc, S., Hung Nguyen, H.K., Xuan Huynh, T.K. and Martinez, H., 2012. Study of surface fluorination of photocatalytic TiO2 by thermal shock method. J Solid State Chem, 187(0): 300-308.

Khodja, A.A., Sehili, T., Pilichowski, J.-F. and Boule, P., 2001. Photocatalytic degradation of 2-phenylphenol on TiO_2 and ZnO in aqueous suspensions. Journal of Photochemistry and Photobiology A: Chemistry, 141(2–3): 231-239.

Kim, J.-H., Nishimura, F., Yonezawa, S. and Takashima, M., 2012. Enhanced dispersion stability and photocatalytic activity of TiO_2 particles fluorinated by fluorine gas. Journal of Fluorine Chemistry, 144(0): 165-170.

Kim, S., Fisher, B., Eisler, H.J. and Bawendi, M., 2003. Type-II quantum dots: CdTe/CdSe(core/shell) and CdSe/ZinTe(core/shell) heterostructures. Journal of the American Chemical Society, 125(38): 11466-11467.

Kirk, R.E. and Othmer, D.F., 1963. Encyclopedia of chemical technology. Interscience Publishers, New York :.

Kleinmann, R.L.P., 1989. Research and Developments, control methods for both coal and metal mines, U.S. Bureau of Mines.

Kljajić, P., Andrić, G., Adamović, M., Bodroža-Solarov, M., Marković, M. and Perić, I., 2010. Laboratory assessment of insecticidal effectiveness of natural zeolite and diatomaceous earth formulations against three stored-product beetle pests. Journal of Stored Products Research, 46(1): 1-6.

Kokate, C., J, P.H. and Jalalpure, S., 2012. Textbook of Pharmaceutical Biotechnology. Elsevier Health Sciences APAC.

Konstantinou, I.K. and Albanis, T.A., 2004. TiO2-assisted photocatalytic degradation of azo dyes in aqueous solution: kinetic and mechanistic investigations - A review. Appl Catal B-Environ, 49(1): 1-14.

Koschorreck, M., Wendt-Potthoff, K., Scharf, B. and Richnow, H.H., 2008. Methanogenesis in the sediment of the acidic Lake Caviahue in Argentina. Journal of Volcanology and Geothermal Research, 178(2): 197-204.

Kowshik, M., Vogel, W., Urban, J., Kulkarni, S.K. and Paknikar, K.M., 2002. Microbial Synthesis of Semiconductor PbS Nanocrystallites. Adv Mater, 14(11): 815-818.

KPMG, I., 2012. Global Metals Outlook: Manufacturing Resilience, KPMG International Cooperative, Bern.

Kumar, P.S., Sivakumar, R., Anandan, S., Madhavan, J., Maruthamuthu, P. and Ashokkumar, M., 2008. Photocatalytic degradation of Acid Red 88 using Au–TiO2 nanoparticles in aqueous solutions. Water Res, 42(19): 4878-4884.

Kuriechen, S.K., Murugesan, S., Raj, S.P. and Maruthamuthu, P., 2011. Visible light assisted photocatalytic mineralization of Reactive Red 180 using colloidal TiO2 and oxone. Chemical Engineering Journal, 174(2–3): 530-538.

Labastida, I., Armienta, M.A., Lara-Castro, R.H., Aguayo, A., Cruz, O. and Ceniceros, N., 2012. Treatment of mining acidic leachates with indigenous limestone, Zimapan Mexico. Journal of Hazardous Materials(0).

Lee, M., Paik, I.S., Kim, I., Kang, H. and Lee, S., 2007. Remediation of heavy metal contaminated groundwater originated from abandoned mine using lime and calcium carbonate. Journal of Hazardous Materials, 144(1–2): 208-214.

Lens, L.H.P., Lens, P.N.L. and Pol, L.W.H., 2000. Environmental Technologies to Treat Sulfur Pollution: Principles and Engineering. Iwa Publishing.

Lewis, A.E., 2010. Review of metal sulphide precipitation. Hydrometallurgy, 104(2): 222-234.

Li, F., Wu, J.F., Qin, Q.H., Li, Z. and Huang, X.T., 2010. Controllable synthesis, optical and photocatalytic properties of CuS nanomaterials with hierarchical structures. Powder Technol, 198(2): 267-274.

Li, M.G., Aube, B.C. and St. Arnaud, L.C., 1997. Considerations in the use of shallow water covers for decommissioning reactive tailings, International Conference on Acid Rock Drainage, Vancouver, pp. 115-130.

Lin, X.-M. and Samia, A.C.S., 2006. Synthesis, assembly and physical properties of magnetic nanoparticles. J Magn Magn Mater, 305(1): 100-109.

Liu, G., Sun, C.H., Yan, X.X., Cheng, L., Chen, Z.G., Wang, X.W., Wang, L.Z., Smith, S.C., Lu, G.Q. and Cheng, H.M., 2009a. Iodine doped anatase TiO2 photocatalyst with ultra-long visible light response: correlation between geometric/electronic structures and mechanisms. J Mater Chem, 19(18): 2822-2829.

Liu, J., Ma, J.F., Liu, Y., Song, Z.W., Sun, Y., Fang, J.R. and Liu, Z.S., 2009b. Synthesis of ZnS nanoparticles via hydrothermal process assisted by microemulsion technique. J Alloy Compd, 486(1-2): L40-L43.

Liu, Y., Liu, J., Lin, Y., Zhang, Y. and Wei, Y., 2009c. Simple fabrication and photocatalytic activity of S-doped TiO_2 under low power LED visible light irradiation. Ceram Int, 35(8): 3061-3065.

Liu, Z., Sun, D.D., Guo, P. and Leckie, J.O., 2006. An Efficient Bicomponent TiO_2/SnO_2 Nanofiber Photocatalyst Fabricated by Electrospinning with a Side-by-Side Dual Spinneret Method. Nano Lett, 7(4): 1081-1085.

Liz-Marzan, Correa-Duarte, M.A., Pastoriza-Santos, I., Ung, T., Kotov, K. and Giersig, M., 2001. Core-shell nanoparticles and assemblies thereof. In: H.S. Nalwa (Ed.), Handbook of surfaces and interfaces of materials. Academic Press, pp. 189-237.

Loos, M.A., Bosch, C., Maré, J., Immelman, E. and Sanderson, R.D., 1989. Evaluation of sodium lauryl sulfate, sodium benzoate and sorbic acid as inhibitors of acidification of South African coal waste, Biennial Symposium of the Groundwater Division of the Geological Survey of South Africa. Geological Society of South Africa, Pretoria, pp. 193-200.

Luckey, T.D., 1975. Heavy metal toxicity, safety, and hormology, Stuttgart, G. Thieme; New York, Academic Press.

Luo, M., Liu, Y., Hu, J., Li, J., Liu, J. and Richards, R.M., 2012. General strategy for one-pot synthesis of metal sulfide hollow spheres with enhanced photocatalytic activity. Applied Catalysis B: Environmental, 125(0): 180-188.

Luther, G., III and Rickard, D., 2005. Metal Sulfide Cluster Complexes and their Biogeochemical Importance in the Environment. J Nanopart Res, 7(4-5): 389-407.

Luther, G.W., Theberge, S.M. and Rickard, D.T., 1999. Evidence for aqueous clusters as intermediates during zinc sulfide formation. Geochim Cosmochim Ac, 63(19-20): 3159-3169.

Luther, G.W., Theberge, S.M., Rozan, T.F., Rickard, D., Rowlands, C.C. and Oldroyd, A., 2002. Aqueous copper sulfide clusters as intermediates during copper sulfide formation. Environ Sci Technol, 36(3): 394-402.

Lyman, W.J., 1995. Transport and transformation processes. Fundamentals of Aquatic Toxicology. Taylor & Francis, Washington D. C., 1125 pp.

Mackie, A.L. and Walsh, M.E., 2012. Bench-scale study of active mine water treatment using cement kiln dust (CKD) as a neutralization agent. Water Res, 46(2): 327-334.

Madzivire, G., Gitari, W.M., Vadapalli, V.R.K., Ojumu, T.V. and Petrik, L.F., 2011. Fate of sulphate removed during the treatment of circumneutral mine water and acid mine drainage with coal fly ash: Modelling and experimental approach. Minerals Engineering, 24(13): 1467-1477.

Mai, L., Huang, C., Wang, D., Zhang, Z. and Wang, Y., 2009. Effect of C doping on the structural and optical properties of sol–gel TiO2 thin films. Appl Surf Sci, 255(22): 9285-9289.

Maier, E., Fischereder, A., Haas, W., Mauthner, G., Albering, J., Rath, T., Hofer, F., List, E.J.W. and Trimmel, G., 2011. Metal sulfide–polymer nanocomposite thin films prepared by a direct formation route for photovoltaic applications. Thin Solid Films, 519(13): 4201-4206.

Mann, S., Sparks, N.H.C., Frankel, R.B., Bazylinski, D.A. and Jannasch, H.W., 1990. Biomineralization of ferrimagnetic greigite (Fe_3S_4) and iron pyrite (FeS_2) in a magnetotactic bacterium. Nature, 343(6255): 258-261.

Mata, Y.N., Torres, E., Blazquez, M., Ballester, A., Gonzalez, F. and Munoz, J.A., 2007. Lead and gold removal using sugar-beet pectin gels with and without immobilized fucus vesiculosus. Adv Mat Res, 20-21: 599-602.

Matos, J., Laine, J., Herrmann, J.M., Uzcategui, D. and Brito, J.L., 2007. Influence of activated carbon upon titania on aqueous photocatalytic consecutive runs of phenol photodegradation. Applied Catalysis B: Environmental, 70(1–4): 461-469.

Matthies, R., Aplin, A.C. and Jarvis, A.P., 2010. Performance of a passive treatment system for net-acidic coal mine drainage over five years of operation. Sci Total Environ, 408(20): 4877-4885.

Mehling, P.E., Day, S.J. and Sexsmith, K.S., 1997. Blending and layering waste rock to delay, mitigate or prevent acid generation: a case review study., International Conference on Acid Rock Drainage, Vancouver, pp. 953-970.

Mehta, N., 2011. Applied Physics for Engineers. PHI Learning Pvt. Ltd.

Meshko, V., Markovska, L., Mincheva, M. and Rodrigues, A.E., 2001. Adsorption of basic dyes on granular acivated carbon and natural zeolite. Water Res, 35(14): 3357-3366.

Mi, C., Wang, Y., Zhang, J., Huang, H., Xu, L., Wang, S., Fang, X., Fang, J., Mao, C. and Xu, S., 2011. Biosynthesis and characterization of CdS quantum dots in genetically engineered Escherichia coli. J Biotechnol, 153(3–4): 125-132.

Mishra, A. and Malik, A., 2012. Simultaneous bioaccumulation of multiple metals from electroplating effluent using Aspergillus lentulus. Water Res, 46(16): 4991-4998.

Mitsch, W.J. and Wise, K.M., 1998. Water quality, fate of metals, and predictive model validation of a constructed wetland treating acid mine drainage. Water Res, 32(6): 1888-1900.

Mizukoshi, Y., Sato, K., Konno, T.J. and Masahashi, N., 2010. Dependence of photocatalytic activities upon the structures of Au/Pd bimetallic nanoparticles immobilized on TiO_2 surface. Applied Catalysis B: Environmental, 94(3–4): 248-253.

Moghaddam, S., Moghaddam, M.R. and Arami, M., 2010. Coagulation/flocculation process for dye removal using sludge from water treatment plant: Optimization through response surface methodology. Journal of Hazardous Materials, 175(1–3): 651-657.

Mokone, T.P., van Hille, R.P. and Lewis, A.E., 2012. Metal sulphides from wastewater: Assessing the impact of supersaturation control strategies. Water Res, 46(7): 2088-2100.

Monteiro, O.C., Neves, M.C. and Trindade, T., 2004. Zinc sulfide nanocoating of silica submicron spheres using a single-source method. J Nanosci Nanotechno, 4(1-2): 146-150.

Mrowetz, M. and Selli, E., 2004. Effects of iron species in the photocatalytic degradation of an azo dye in TiO_2 aqueous suspensions. Journal of Photochemistry and Photobiology A: Chemistry, 162(1): 89-95.

Mukherjee, P., Ahmad, A., Mandal, D., Senapati, S., Sainkar, S.R., Khan, M.I., Parishcha, R., Ajaykumar, P.V., Alam, M., Kumar, R. and Sastry, M., 2001. Fungus-Mediated Synthesis of Silver Nanoparticles and Their Immobilization in the Mycelial Matrix: A Novel Biological Approach to Nanoparticle Synthesis. Nano Lett, 1(10): 515-519.

N.T.C., 2012. Malolotja Archaeology, Lion Cavern. In: S.N.T. Commission (Ed.), Cultural Resources.

Ňancucheo, I. and Johnson, D.B., 2012. Selective removal of transition metals from acidic mine waters by novel consortia of acidophilic sulfidogenic bacteria. Microbial Biotechnology, 5(1): 34-44.

Nascu, C., Pop, I., Ionescu, V., Indrea, E. and Bratu, I., 1997. Spray pyrolysis deposition of CuS thin films. Mater Lett, 32(2-3): 73-77.

Nataraj, S.K., Hosamani, K.M. and Aminabhavi, T.M., 2009. Nanofiltration and reverse osmosis thin film composite membrane module for the removal of dye and salts from the simulated mixtures. Desalination, 249(1): 12-17.

Navarro, R., Pawelec, B., Fierro, J.L.G. and Vasudevan, P.T., 1996. Dibenzothiophene hydrodesulfurization on silica-alumina-supported transition metal sulfide catalysts. Applied Catalysis A: General, 148(1): 23-40.

Nekouie, R.K., Rashchi, F. and Joda, N.N., 2013. Effect of organic additives on synthesis of copper nano powders by pulsing electrolysis. Powder Technol(0).

Neppolian, B., Choi, H.C., Sakthivel, S., Arabindoo, B. and Murugesan, V., 2002. Solar light induced and TiO_2 assisted degradation of textile dye reactive blue 4. Chemosphere, 46(8): 1173-1181.

Neves, M.C., Liz-Marzán, L.M. and Trindade, T., 2003. Synthesis and assembly of SiO_2-coated Bi_2S_3 nanofibers. J Colloid Interf Sci, 264(2): 391-395.

Nieboer, E. and Richardson, D.H.S., 1980. The Replacement of the Non-Descript Term Heavy-Metals by a Biologically and Chemically Significant Classification of Metal-Ions. Environ Pollut B, 1(1): 3-26.

Ohno, T., Sarukawa, K., Tokieda, K. and Matsumura, M., 2001. Morphology of a TiO2 Photocatalyst (Degussa, P-25) Consisting of Anatase and Rutile Crystalline Phases. J Catal, 203(1): 82-86.

Okamoto, Y., Hioka, K., Arakawa, K., Fujikawa, T., Ebihara, T. and Kubota, T., 2009. Effect of sulfidation atmosphere on the hydrodesulfurization activity of SiO2-supported Co–Mo sulfide catalysts: Local structure and intrinsic activity of the active sites. J Catal, 268(1): 49-59.

Ollis, D.F., Pelizzetti, E. and Serpone, N., 1991. Photocatalyzed destruction of water contaminants. Environ Sci Technol, 25(9): 1522-1529.

Onwudiwe, D.C. and Ajibade, P.A., 2011. Zn(II), Cd(II) and Hg(II) complexes of N-methyl-N-phenyl dithiocarbamate as single-source precursors for the synthesis of metal sulfide nanoparticles. Mater Lett, 65(21–22): 3258-3261.

Parkin, I.P., 1996. Solid state metathesis reaction for metal borides, silicides, pnictides and chalcogenides: Ionic or elemental pathways. Chem Soc Rev, 25(3): 199-+.

Patel, J.D., Mighri, F. and Ajji, A., 2012. Generalized chemical route to develop fatty acid capped highly dispersed semiconducting metal sulphide nanocrystals. Mater Res Bull, 47(8): 2016-2021.

Pattabi, M. and Uchil, J., 2000. Synthesis of Cadmium Sulphide nanoparticles. Sol Energ Mat Sol C, 63(4): 309-314.

Pawaskar, N.R., Sathaye, S.D., Bhadbhade, M.M. and Patil, K.R., 2002. Applicability of liquid-liquid interface reaction technique for the preparation of zinc sulfide nano particulate thin films. Mater Res Bull, 37(9): 1539-1546.

Pearson, R.G., 1968a. Hard and Soft Acids and Bases Hsab .1. Fundamental Principles. J Chem Educ, 45(9): 581-&.

Pearson, R.G., 1968b. Hard and Soft Acids and Bases Hsab .2. Underlying Theories. J Chem Educ, 45(10): 643-&.

Peters, R.W., Chang, T.-K. and Ku, Y., 1984. Heavy metal crystallization kinetics in an MSMPR crystallizer employing sulfide precipitation. Journal Name: AIChE Symp. Ser.; (United States); Journal Volume: 80:240: Medium: X; Size: Pages: 55-75.

Philippot, P., Van Zuilen, M., Lepot, K., Thomazo, C., Farquhar, J. and Van Kranendonk, M.J., 2007. Early Archaean microorganisms preferred elemental sulfur, not sulfate. Science, 317(5844): 1534-1537.

Phipps, D.A., 1981. Chemistry and biochemistry of trace metals in biological systems. Effect of Heavy Metal Pollution on Plants. Applied Science Publishers.

Poirier, I., Hammann, P., Kuhn, L. and Bertrand, M., 2013. Strategies developed by the marine bacterium Pseudomonas fluorescens BA3SM1 to resist metals: A proteome analysis. Aquat Toxicol, 128–129(0): 215-232.

Pouretedal, H.R., Norozi, A., Keshavarz, M.H. and Semnani, A., 2009. Nanoparticles of zinc sulfide doped with manganese, nickel and copper as nanophotocatalyst in the degradation of organic dyes. Journal of Hazardous Materials, 162(2–3): 674-681.

Qi, L.M., Ma, J.M., Cheng, H.M. and Zhao, Z.G., 1996. Synthesis and characterization of mixed CdS-ZnS nanoparticles in reverse micelles. Colloid Surface A, 111(3): 195-202.

Rajapaksha, R.M.C.P., 2011. Heavy metal tolerance of culturable bacteria and fungi in a long-term cultivated tropical ultisol. European Journal of Soil Biology, 47(1): 9-15.

Rand, G.M., Wells, P.G. and McCarty, L.S., 1995. Introduction to aquatic toxicology",. Fundamentals of Aquatic Toxicology. Taylor & Francis, Washington D. C., 1125 pp.

Rauf, M.A., Bukallah, S.B., Hamadi, A., Sulaiman, A. and Hammadi, F., 2007. The effect of operational parameters on the photoinduced decoloration of dyes using a hybrid catalyst V_2O_5/TiO_2. Chemical Engineering Journal, 129(1–3): 167-172.

Rauf, M.A., Meetani, M.A. and Hisaindee, S., 2011. An overview on the photocatalytic degradation of azo dyes in the presence of TiO_2 doped with selective transition metals. Desalination, 276(1-3): 13-27.

Renzi, C., Guillard, C., Herrmann, J.-M., Pichat, P. and Baldi, G., 1997. Effects of methanol, formamide, acetone and acetate ions on phenol disappearance rate and aromatic products in UV-irradiated TiO_2 aqueous suspensions. Chemosphere, 35(4): 819-826.

Rickard, D., Grimes, S., Butler, I., Oldroyd, A. and Davies, K.L., 2007. Botanical constraints on pyrite formation. Chem Geol, 236(3–4): 228-246.

Riga, A., Soutsas, K., Ntampegliotis, K., Karayannis, V. and Papapolymerou, G., 2007. Effect of system parameters and of inorganic salts on the decolorization and degradation of Procion H-exl dyes. Comparison of H2O2/UV, Fenton, UV/Fenton, TiO_2/UV and TiO_2/UV/H_2O_2 processes. Desalination, 211(1–3): 72-86.

Riordan, M., 2007. The Silicon Dioxide Solution. IEEE Spectr., 44(12): 51-56.

Robert, D. and Malato, S., 2002. Solar photocatalysis: a clean process for water detoxification. Sci Total Environ, 291(1-3): 85-97.

Rong, J., Niu, Z., Lee, L.A. and Wang, Q., 2011. 2.06 - Chemistry and Materials Development of Protein-Based Nanoparticles. In: L.A. Editors-in-Chief: David, D.S. Gregory and P.W. Gary (Eds.), Comprehensive Nanoscience and Technology. Academic Press, Amsterdam, pp. 153-174.

Sagade, A.A. and Sharma, R., 2008. Copper sulphide (CuxS) as an ammonia gas sensor working at room temperature. Sensors and Actuators B: Chemical, 133(1): 135-143.

Saha, I., Bhattacharyya, J. and Kumar, G.S., 2013. Thermodynamic investigations of ligand–protein interactions: Binding of the phenazinium dyes phenosafranin and safranin O with human serum albumin. The Journal of Chemical Thermodynamics, 56(0): 114-122.

Sahraei, R., Daneshfar, A., Goudarzi, A., Abbasi, S., Ara, M.H.M. and Rahimi, F., 2013. Optical properties of nanocrystalline ZnS:Mn thin films prepared by chemical bath deposition method. J Mater Sci: Mater Electron, 24(1): 260-266.

Sakthivel, S., Neppolian, B., Shankar, M.V., Arabindoo, B., Palanichamy, M. and Murugesan, V., 2003. Solar photocatalytic degradation of azo dye: comparison of photocatalytic efficiency of ZnO and TiO_2. Sol Energ Mat Sol C, 77(1): 65-82.

Sampaio, R.M.M., Timmers, R.A., Xu, Y., Keesman, K.J. and Lens, P.N.L., 2009. Selective precipitation of Cu from Zn in a pS controlled continuously stirred tank reactor. Journal of Hazardous Materials, 165(1-3): 256-265.

Sanroman, M.A., Deive, F.J., Dominguez, A., Barrio, T. and Longo, M.A., 2010. Dye decolourization by newly isolated thermophilic microorganisms. Ibic2010: 2nd International Conference on Industrial Biotechnology, 20: 151-156.

Saquib, M. and Muneer, M., 2003. TiO2-mediated photocatalytic degradation of a triphenylmethane dye (gentian violet), in aqueous suspensions. Dyes Pigments, 56(1): 37-49.

Sarkar, D., Das, P., Basak, S. and Chattopadhyay, N., 2008. Binding Interaction of Cationic Phenazinium Dyes with Calf Thymus DNA: A Comparative Study. The Journal of Physical Chemistry B, 112(30): 9243-9249.

Sastry, M., Ahmad, A., Khan, M.I. and Kumar, R., 2003. Biosynthesis of metal nanoparticles using fungi and actinomycete. Curr Sci India, 85(2): 162-170.

Sauer, T., Cesconeto Neto, G., José, H.J. and Moreira, R.F.P.M., 2002. Kinetics of photocatalytic degradation of reactive dyes in a TiO2 slurry reactor. Journal of Photochemistry and Photobiology A: Chemistry, 149(1–3): 147-154.

Scarano, G. and Morelli, E., 2003. Properties of phytochelatin-coated CdS nanocrystallites formed in a marine phytoplanktonic alga (Phaeodactylum tricornutum, Bohlin) in response to Cd. Plant Science, 165(4): 803-810.

Schippers, A. and Sand, W., 1999. Bacterial leaching of metal sulfides proceeds by two indirect mechanisms via thiosulfate or via polysulfides and sulfur. Appl Environ Microb, 65(1): 319-321.

Scott, J.S., 1981. Dictionary of waste and water treatment. Butterworths, London ;.

Scott, T. and Brewer, M., 1983. The concise encyclopedia of biochemistry. Biochemical Education, 11(4): 147-149.

Seshadri, S., Saranya, K. and Kowshik, M., 2011. Green Synthesis of Lead Sulfide Nanoparticles by the Lead Resistant Marine Yeast, Rhodosporidium diobovatum. Biotechnol Progr, 27(5): 1464-1469.

Shankar, S.S., Rai, A., Ankamwar, B., Singh, A., Ahmad, A. and Sastry, M., 2004. Biological synthesis of triangular gold nanoprisms. Nat Mater, 3(7): 482-488.

Shao, M., Zhang, T. and Fang, H.H.P., 2009. Autotrophic denitrification and its effect on metal speciation during marine sediment remediation. Water Res, 43(12): 2961-2968.

Sharma, K.P., Sharma, S., Sharma, S., Singh, P.K., Kumar, S., Grover, R. and Sharma, P.K., 2007. A comparative study on characterization of textile wastewaters (untreated and treated) toxicity by chemical and biological tests. Chemosphere, 69(1): 48-54.

Sharma, P.K., Balkwill, D.L., Frenkel, A. and Vairavamurthy, M.A., 2000. A New Klebsiella planticola Strain (Cd-1) Grows Anaerobically at High Cadmium Concentrations and Precipitates Cadmium Sulfide. Appl Environ Microb, 66(7): 3083-3087.

She, Y.Y., Yang, J. and Qiu, K.Q., 2010. Synthesis of ZnS nanoparticles by solid-liquid chemical reaction with ZnO and Na_2S under ultrasonic. T Nonferr Metal Soc, 20: S211-S215.

Shea, D. and Helz, G.R., 1988. The Solubility of Copper in Sulfidic Waters - Sulfide and Polysulfide Complexes in Equilibrium with Covellite. Geochim Cosmochim Ac, 52(7): 1815-1825.

Sheikhiabadi, P.G., Salavati-Niasari, M. and Davar, F., 2012. Hydrothermal synthesis and optical properties of antimony sulfide micro and nano-size with different morphologies. Mater Lett, 71(0): 168-171.

Shen, L., Bao, N., Prevelige, P.E. and Gupta, A., 2010. Escherichia coli Bacteria-Templated Synthesis of Nanoporous Cadmium Sulfide Hollow Microrods for Efficient Photocatalytic Hydrogen Production. The Journal of Physical Chemistry C, 114(6): 2551-2559.

Shen, L., Guo, X., Fang, X., Wang, Z. and Chen, L., 2012. Magnesiothermically reduced diatomaceous earth as a porous silicon anode material for lithium ion batteries. Journal of Power Sources, 213(0): 229-232.

Shen, Y.A., Buick, R. and Canfield, D.E., 2001. Isotopic evidence for microbial sulphate reduction in the early Archaean era. Nature, 410(6824): 77-81.

Shenton, W., Douglas, T., Young, M., Stubbs, G. and Mann, S., 1999. Inorganic–Organic Nanotube Composites from Template Mineralization of Tobacco Mosaic Virus. Adv Mater, 11(3): 253-256.

Sheoran, A.S. and Sheoran, V., 2006. Heavy metal removal mechanism of acid mine drainage in wetlands: A critical review. Minerals Engineering, 19(2): 105-116.

Sheoran, A.S., Sheoran, V. and Choudhary, R.P., 2010. Bioremediation of acid-rock drainage by sulphate-reducing prokaryotes: A review. Minerals Engineering, 23(14): 1073-1100.

Shi, H., Zhang, T., An, T., Li, B. and Wang, X., 2012. Enhancement of photocatalytic activity of nano-scale TiO_2 particles co-doped by rare earth elements and heteropolyacids. J Colloid Interf Sci, 380(1): 121-127.

Shimoda, A., Sawada, S.-i., Kano, A., Maruyama, A., Moquin, A., Winnik, F.M. and Akiyoshi, K., 2012. Dual crosslinked hydrogel nanoparticles by nanogel bottom-up method for sustained-release delivery. Colloids and Surfaces B: Biointerfaces, 99(0): 38-44.

Shinde, S.S., Shinde, P.S., Bhosale, C.H. and Rajpure, K.Y., 2011. Zinc oxide mediated heterogeneous photocatalytic degradation of organic species under solar radiation. Journal of Photochemistry and Photobiology B: Biology, 104(3): 425-433.

Sibley, S.F., Butterman, W.C. and Staff, 1995. Metals recycling in the United States. Resources, Conservation and Recycling, 15(3–4): 259-267.

Silva, A.C., Pic, J.S., Sant'Anna Jr, G.L. and Dezotti, M., 2009. Ozonation of azo dyes (Orange II and Acid Red 27) in saline media. Journal of Hazardous Materials, 169(1–3): 965-971.

Singaravelu, G., Arockiamary, J.S., Kumar, V.G. and Govindaraju, K., 2007. A novel extracellular synthesis of monodisperse gold nanoparticles using marine alga, Sargassum wightii Greville. Colloids and Surfaces B: Biointerfaces, 57(1): 97-101.

Slawson, R.M., Vandyke, M.I., Lee, H. and Trevors, J.T., 1992. Germanium and Silver Resistance, Accumulation, and Toxicity in Microorganisms. Plasmid, 27(1): 72-79.

Sökmen, M. and Özkan, A., 2002. Decolourising textile wastewater with modified titania: the effects of inorganic anions on the photocatalysis. Journal of Photochemistry and Photobiology A: Chemistry, 147(1): 77-81.

Song, J., Kwon, E.-Y. and Kim, B., 2010. Biological synthesis of platinum nanoparticles using Diopyros kaki leaf extract. Bioprocess Biosyst Eng, 33(1): 159-164.

Stemmler, S.J., Loyaux-Lawniczak, S. and Berthelin, J., 2004. Effect of soil water content on the microbial reduction of iron oxides. Cr Geosci, 336(13): 1171-1179.

Su, Q.M., Li, J., Zhong, G., Du, G.H. and Xu, B.S., 2011. In Situ Synthesis of Iron/Nickel Sulfide Nanostructures-Filled Carbon Nanotubes and Their Electromagnetic and Microwave-Absorbing Properties. J Phys Chem C, 115(5): 1838-1842.

Su, X., Schmitz, G., Zhang, M., Mackie, R.I. and Cann, I.K.O., 2012. Chapter One - Heterologous Gene Expression in Filamentous Fungi. In: M.G. Geoffrey and S. Sima (Eds.), Advances in Applied Microbiology. Academic Press, pp. 1-61.

Sukola, K., Wang, F.Y. and Tessier, A., 2005. Metal-sulfide species in oxic waters. Anal Chim Acta, 528(2): 183-195.

Sun, J.-H., Sun, S.-P., Fan, M.-H., Guo, H.-Q., Lee, Y.-F. and Sun, R.-X., 2008. Oxidative decomposition of p-nitroaniline in water by solar photo-Fenton advanced oxidation process. Journal of Hazardous Materials, 153(1–2): 187-193.

Suresh, A.K., Doktycz, M.J., Wang, W., Moon, J.-W., Gu, B., Meyer Iii, H.M., Hensley, D.K., Allison, D.P., Phelps, T.J. and Pelletier, D.A., 2011. Monodispersed biocompatible silver sulfide nanoparticles: Facile extracellular biosynthesis using the γ-proteobacterium, Shewanella oneidensis. Acta Biomaterialia, 7(12): 4253-4258.

Swanson, D.A., Barbour, S.L. and Wilson, G.W., 1997. Dry-site versus wet-site cover design, International Conference on Acid Rock Drainage, Vancouver, pp. 1595-1610.

Sweeney, R.Y., Mao, C., Gao, X., Burt, J.L., Belcher, A.M., Georgiou, G. and Iverson, B.L., 2004. Bacterial Biosynthesis of Cadmium Sulfide Nanocrystals. Chem Biol, 11(11): 1553-1559.

Talapin, D.V., Rogach, A.L., Kornowski, A., Haase, M. and Weller, H., 2001. Highly luminescent monodisperse CdSe and CdSe/ZnS nanocrystals synthesized in a hexadecylamine-trioctylphosphine oxide-trioctylphospine mixture. Nano Lett, 1(4): 207-211.

Teh, C.M. and Mohamed, A.R., 2011. Roles of titanium dioxide and ion-doped titanium dioxide on photocatalytic degradation of organic pollutants (phenolic compounds and dyes) in aqueous solutions: A review. J Alloy Compd, 509(5): 1648-1660.

Thakkar, K.N., Mhatre, S.S. and Parikh, R.Y., 2010. Biological synthesis of metallic nanoparticles. Nanomedicine: Nanotechnology, Biology and Medicine, 6(2): 257-262.

Theberge, S.M., Luther, G.W., Rozan, T.F. and Rickard, D.T., 2000. Evidence for aqueous clusters as intermediates during copper sulfide formation. Abstr Pap Am Chem S, 220: U371-U371.

Thimm, J.C., Burritt, D.J., Ducker, W.A. and Melton, L.D., 2000. Celery (Apium graveolens L.) parenchyma cell walls examined by atomic force microscopy: effect of dehydration on cellulose microfibrils. Planta, 212(1): 25-32.

Tice, M.M. and Lowe, D.R., 2004. Photosynthetic microbial mats in the 3,416-Myr-old ocean. Nature, 431(7008): 549-552.

Tilton, J.E., 1990. World Metal Demand: Trends and Prospects. RFF Press.

Todorova, N., Giannakopoulou, T., Vaimakis, T. and Trapalis, C., 2008. Structure tailoring of fluorine-doped TiO_2 nanostructured powders. Materials Science and Engineering: B, 152(1–3): 50-54.

Tran. T, T., Sheng, P., Huang, C.a., Li, J., Chen, L., Yuan, L., Grimes, C.A. and Cai, Q., 2012. Synthesis and photocatalytic application of ternary Cu–Zn–S nanoparticle-sensitized TiO2 nanotube arrays. Chemical Engineering Journal, 210(0): 425-431.

Tuncuk, A., Stazi, V., Akcil, A., Yazici, E.Y. and Deveci, H., 2012. Aqueous metal recovery techniques from e-scrap: Hydrometallurgy in recycling. Minerals Engineering, 25(1): 28-37.

Upadhyay, R.K., Sharma, M., Singh, D.K., Amritphale, S.S. and Chandra, N., 2012. Photo degradation of synthetic dyes using cadmium sulfide nanoparticles synthesized in the presence of different capping agents. Sep Purif Technol, 88(0): 39-45.

Vaidhyanathan, B., Ganguli, M. and Rao, K.J., 1995. Fast Solid-State Synthesis of Metal Vanadates and Chalcogenides Using Microwave Irradiation. Mater Res Bull, 30(9): 1173-1177.

van Hille, R.P., A. Peterson, K. and Lewis, A.E., 2005. Copper sulphide precipitation in a fluidised bed reactor. Chem Eng Sci, 60(10): 2571-2578.

vanLoon, G.W. and Duffy, S.J., 2000. Environmental Chemistry: A Global Perspective Oxford University Press, pp. 512.

Vázquez, A., López, I. and Gómez, I., 2011. Growth of one-dimensional zinc sulfide nanostructures through electrophoretic deposition. Mater Lett, 65(15–16): 2422-2425.

Veeken, A.H.M., Akoto, L., Pol, L.W.H. and Weijma, J., 2003a. Control of the sulfide (S2-) concentration for optimal zinc removal by sulfide precipitation in a continuously stirred tank reactor. Water Res, 37(15): 3709-3717.

Veeken, A.H.M., de Vries, S., van der Mark, A. and Rulkens, W.H., 2003b. Selective precipitation of heavy metals as controlled by a sulfide-selective electrode. Separ Sci Technol, 38(1): 1-19.

Veronese, I., Cantone, M.C., Chiodini, N., Fasoli, M., Mones, E., Moretti, F. and Vedda, A., *in press*. The influence of the stem effect in Eu-doped silica optical fibres. Radiation Measurements(0).

Vijayabalan, A., Selvam, K., Velmurugan, R. and Swaminathan, M., 2009. Photocatalytic activity of surface fluorinated TiO_2-P25 in the degradation of Reactive Orange 4. Journal of Hazardous Materials, 172(2–3): 914-921.

Vinu, R., Akki, S.U. and Madras, G., 2010. Investigation of dye functional group on the photocatalytic degradation of dyes by nano-$TiO(_2)$. Journal of Hazardous Materials, 176(1-3): 765-773.

Wacey, D., Kilburn, M.R., Saunders, M., Cliff, J. and Brasier, M.D., 2011. Microfossils of sulphur-metabolizing cells in 3.4-billion-year-old rocks of Western Australia. Nat Geosci, 4(10): 698-702.

Walker, P.M., 1988. Chambers science and technology dictionary. Cambridge, Cambridge, 1088 pp.

Wang, H., Zhang, H.R., Zhao, X.N., Xu, S. and Zhu, J.J., 2002. Preparation of copper monosulfide and nickel monosulfide nanoparticles by sonochemical method. Mater Lett, 55(4): 253-258.

Wang, S.H. and Yang, S.H., 2000. Surfactant-assisted growth of crystalline copper sulphide nanowire arrays. Chem Phys Lett, 322(6): 567-571.

Wei, X.-W., Song, X.-J., Xu, J., Ni, Y.-H. and Zhang, P., 2005. Coating multi-walled carbon nanotubes with metal sulfides. Mater Chem Phys, 92(1): 159-163.

Wen, P., Yang, S., Ishikawa, Y., Itoh, H. and Feng, Q., 2011. Visible light sensitization effect of polyaminobenzoate adsorbed on TiO2 nanocrystal surface. Appl Surf Sci, 257(6): 2126-2133.

Wernick, I.K. and Themelis, N.J., 1998. Recycling metals for the environment. Annu Rev Energ Env, 23: 465-497.

West, J.L. and Halas, N.J., 2003. Engineered nanomaterials for biophotonics applications: Improving sensing, imaging, and therapeutics. Annu Rev Biomed Eng, 5: 285-292.

Wiberg, E., 2001. Inorganic chemistry. Academic Press ;, San Diego :.

Williams, R.H., Larson, E.D. and Ross, M.H., 1987. Materials, Affluence, and Industrial Energy Use. Annu Rev Energy, 12: 99-144.

Williamson, D., 1995. Into the Next Millennium: The Long Bull Market in Metals and Mineral, 11 pp.

Wong, M.-S., Pang Chou, H. and Yang, T.-S., 2006. Reactively sputtered N-doped titanium oxide films as visible-light photocatalyst. Thin Solid Films, 494(1–2): 244-249.

Xi, Y., Hu, C., Zhang, X., Zhang, Y. and Wang, Z.L., 2009. Optical switches based on nanowires synthesized by molten salt solvent method. Solid State Commun, 149(43–44): 1894-1896.

Xiao, J., Peng, T., Li, R., Peng, Z. and Yan, C., 2006. Preparation, phase transformation and photocatalytic activities of cerium-doped mesoporous titania nanoparticles. J Solid State Chem, 179(4): 1161-1170.

Xin, B.P., Huang, Q., Chen, S. and Tang, X.M., 2008. High-purity Nano Particles ZnS Production by a Simple Coupling Reaction Process of Biological Reduction and Chemical Precipitation Mediated with EDTA. Biotechnol Progr, 24(5): 1171-1177.

Xiong, Y., Xie, Y., Yang, J., Zhang, R., Wu, C. and Du, G., 2002. In situ micelle-template-interface reaction route to CdS nanotubes and nanowires. J Mater Chem, 12(12): 3712-3716.

Yang, Z., Choi, D., Kerisit, S., Rosso, K.M., Wang, D., Zhang, J., Graff, G. and Liu, J., 2009. Nanostructures and lithium electrochemical reactivity of lithium titanites and titanium oxides: A review. Journal of Power Sources, 192(2): 588-598.

Yawalkar, A.A., Bhatkhande, D.S., Pangarkar, V.G. and Beenackers, A.A.C.M., 2001. Solar-assisted photochemical and photocatalytic degradation of phenol. J Chem Technol Biot, 76(4): 363-370.

Yeo, S.Y., Tan, W.L., Abu Bakar, M. and Ismail, J., 2010. Silver sulfide/poly(3-hydroxybutyrate) nanocomposites: Thermal stability and kinetic analysis of thermal degradation. Polymer Degradation and Stability, 95(8): 1299-1304.

Yermakov, Y.I., Startsev, A.N. and Burmistrov, V.A., 1984. Sulphide catalysts on silica as a support. i. effect of the preparation technique of (ni,w)/si02 and (ni,mo)/si02 catalysts on their activity in thiophen hydrogenolysis. Appl Catal, 11(1): 1-13.

Yu, L., Lv, Y., Chen, G., Zhang, X., Zeng, Y., Huang, H. and Feng, Y., 2011. A generally synthetic route to semiconducting metal sulfide nanocrystals by using corresponding metal powder and cysteine as metallic and sulfuric sources, respectively. Inorg Chim Acta, 376(1): 659-663.

Zaghbani, N., Hafiane, A. and Dhahbi, M., 2008. Removal of Safranin T from wastewater using micellar enhanced ultrafiltration. Desalination, 222(1-3): 348-356.

Zaitsev, S.V., Moon, J., Takagi, H. and Awano, M., 2000. Preparation and characterization of nanocrystalline doped TiO_2. Advanced Powder Technology, 11(2): 211-220.

Zhang, B., Ye, X., Hou, W., Zhao, Y. and Xie, Y., 2006. Biomolecule-Assisted Synthesis and Electrochemical Hydrogen Storage of Bi_2S_3 Flowerlike Patterns with Well-Aligned Nanorods. The Journal of Physical Chemistry B, 110(18): 8978-8985.

Zhang, G.K., Ding, X.M., Hu, Y.J., Huang, B.B., Zhang, X.Y., Qin, X.Y., Zhou, J. and Xie, J.W., 2008. Photocatalytic Degradation of 4BS Dye by N,S-Codoped TiO2 Pillared Montmorillonite Photocatalysts under Visible-Light Irradiation. J Phys Chem C, 112(46): 17994-17997.

Zhang, J., Fu, D., Gao, H. and Deng, L., 2011. Mechanism of enhanced photocatalysis of TiO2 by Fe3+ in suspensions. Appl Surf Sci, 258(4): 1294-1299.

Zhang, Q., Li, C. and Li, T., 2013. Rapid photocatalytic decolorization of methylene blue using high photon flux UV/TiO2/H_2O_2 process. Chemical Engineering Journal(0).

Zhang, W.-h., Huang, Z., He, L.-y. and Sheng, X.-f., 2012. Assessment of bacterial communities and characterization of lead-resistant bacteria in the rhizosphere soils of metal-tolerant Chenopodium ambrosioides grown on lead–zinc mine tailings. Chemosphere, 87(10): 1171-1178.

Zhao, G., Li, M., Hu, Z. and Hu, H., 2005. Dissociation and removal of complex chromium ions containing in dye wastewaters. Sep Purif Technol, 43(3): 227-232.

Zhao, L., Tao, F., Quan, Z., Zhou, X., Yuan, Y. and Hu, J., 2012. Bubble template synthesis of copper sulfide hollow spheres and their applications in lithium ion battery. Mater Lett, 68(0): 28-31.

Chapter 2 – Synthesis of Nanocrystalline ZnS Using Biologically Generated Sulfide

João Pinto da Costa[1], Ana Violeta Girão[2], João P. Lourenço[3], O.C. Monteiro[4], Tito Trindade[2], Maria Clara Costa[1*]

[1]Universidade do Algarve, CCMar, Campus Gambelas, 8005-139 Faro, Portugal.
[2]Universidade de Aveiro, CICECO, 3810-193 Aveiro, Portugal.
[3]Universidade do Algarve, CIQA, FCT, Ed. 2, Campus Gambelas, 8005-139 Faro, Portugal.
[4]Universidade de Lisboa, FCUL, CQB, Campo Grande, 1749-016 Lisboa, Portugal.

*Corresponding author
Universidade do Algarve, Campus Gambelas
FCT – Edifício 8, Lab. 2.35
8005-139 Faro, Portugal
mcorada@ualg.pt, tel.: +351 289 800 900 Ext: 7245

A modified version of this chapter has been published as:
da Costa, J., Girão, A. V., Lourenço, J. P., Monteiro, O. C., Trindade, T. and Costa, M. C., (2012), Synthesis of nanocrystalline ZnS using biologically generated sulfide. Hydromet. 117:57-63.

Abstract

This work describes the synthesis of ZnS powders in high yield and via a straightforward process, under ambient conditions (temperature and pressure), by adding to aqueous zinc (II) a nutrient solution containing biologically generated sulfide from sulfate-reducing bacteria (SRB). The powders obtained as above were composed mainly of ZnS (*sphalerite*) nanoparticles (NPs) exhibiting a spheroidal morphology (20–30 nm). The NP's morphological properties and crystalline phase were not markedly altered by the SRB growth media composition neither by the presence of bacterial cells. The relevance of this method to obtain ZnS supported solid substrates has been demonstrated by performing the synthesis in the presence of TiO_2 and SiO_2 submicron particles.

Keywords: zinc sulfide, nanoparticles, sulfate-reducing bacteria, titanium dioxide, amorphous silica.

2.1. Introduction

Sulfate-reducing bacteria (SRB) use sulfate as the terminal electron acceptor during the metabolism of organic matter (CH_2O), resulting in the production of H_2S according to Reaction 2.1 (Barnes *et al*., 1992).

$$SO_4^{2-} + 2CH_2O \rightarrow H_2S_{(g)} + 2HCO_3^- \quad (2.1)$$

Hence, in the presence of metal ions, the biologically generated sulfide can be used for metal precipitation (Bhagat *et al*., 2004). SRB have been used in bioremediation processes, namely, in the reduction of high-content sulfate and metals in effluents (Costa and Duarte, 2005; Garcia *et al*., 2001). Nevertheless, the process generates an excess of sulfide and the elimination of the sulfide in excess and disposal of the metal sulfides are also problems that need to be carefully addressed.

The production of metal sulfide nanoparticles has been described using a variety of methods, including high gravity (Chen *et al*., 2004), microwave irradiation (Vaidhyanathan *et al*., 1995), reverse micelles (Qi *et al*., 1996), chemical vapor deposition (Bessergenev *et al*., 1995), hydrothermal processes (Liu *et al*., 2009), solid-liquid chemical reactions (She *et al*., 2010), single-molecular precursor decomposition (Monteiro *et al*., 2004) and in the presence of chelating agents (Xin *et al*., 2008), amongst others. Most of these methods are based on high-temperature, and/or high pressure, radiation and on the use of toxic chemicals, namely, H_2S as the sulfide source. Therefore, the production of functional nanomaterials using bacterial growth media solutions containing biologically produced sulfide, at room temperature and atmospheric pressure, avoiding the use of toxic and expensive chemicals, is an interesting alternative synthesis route. Their use presents obvious economic advantages and safety, as the sulfide is naturally produced in the growth media by sulfate-reducing bacteria enriched from environmental samples. Thus, the use of this excess sulfide to produce nanocrystalline materials is an important contribution not only to solve this problem but that simultaneously results in high value materials such as nanocrystalline semiconductors. The thermodynamic equilibria involved in metal sulfide precipitation can be generally described by the following equations:

$$H_2S \overset{Kp_1}{\leftrightarrow} HS^- + H^+, Kp_1 = \frac{[HS^-][H^+]}{[H_2S]}, pK_1 = 6.99 \quad (2.2)$$

$$HS^- \overset{Kp_2}{\leftrightarrow} S^{2-} + H^+, Kp_2 = \frac{[S^{2-}][H^+]}{[HS^-]}, pK_2 = 17.4 \quad (2.3)$$

$$M^{2+} + S^{2-} \leftrightarrow MS(s) \quad (2.4)$$

$$M^{2+} + HS^- \leftrightarrow MS(s) + H^+ \quad (2.5)$$

Although the physical process of crystal formation is well known, the molecular and chemical processes involved in the transformation of dissolved species to solid products are not well established (Lewis, 2010). Due to the fact that in aqueous systems Zn (II) is the only stable oxidation state and that it is quite frequent in sediments and natural environments, this metal has often been studied as a model for metal sulfide precipitation studies, and a stepwise process for the formation of stable ZnS phases has been proposed (Luther *et al*., 1999). Other authors have successfully precipitated zinc (II) using biogenic sulfide (Bijmans *et al*., 2009; Esposito *et al*., 2006; Mokone *et al*., 2010). However, the ZnS particles produced, under the tested conditions, have always been proven to be larger than 1 μm.

In this work, a SRB consortium previously described (Martins *et al*., 2010) and grown in different nutrient media, was used as the source of the biologically produced sulfide, for the synthesis of ZnS nanoparticles. The media used were modified versions of Sani (Sani *et al*., 2001) and Postgate B (Postgate, 1966). The main aim of the present work was the production of crystalline ZnS nanoparticles (and derived nanocomposites) in order to assess the characteristics of the powders that result from distinct growth media composition and from the presence of particulates.

2.2. Materials and Methods

2.2.1 Bacterial Consortium and Growth Conditions

A SRB consortium isolated from the wetland of the Urgeiriça mine (North of Portugal) and selected from previous studies (Martins *et al*., 2010), containing mainly species affiliated to *Desulfovibrio desulfuricans*, was used as inoculum. These cultures were grown and maintained in minimum salt medium (Sani *et al*., 2001) (MSM: 1g.L^{-1} NH_4Cl; 0.06g.L^{-1} $CaCl_2.6H_2O$; 0.05g.L^{-1} yeast extract; 1g.L^{-1} $MgSO_4.7H_2O$; 2g.L^{-1} Na_2SO_4, and 5g.L^{-1} $C_3H_5NaO_3$) and modified Postgate B medium (Postgate, 1966) (MPM: 0.5g.L^{-1} $K_3PO_4.H_2O$; 1g.L^{-1} NH_4Cl; 1g.L^{-1} $CaSO_4.2H_2O$; 1g.L^{-1} yeast extract; 2g.L^{-1} $MgSO_4.7H_2O$; 0.01g.L^{-1} resazurin; 0.5g.L^{-1} Na_2SO_3; 7.75g.L^{-1} $C_3H_5NaO_3$) in anaerobic conditions, at room temperature in 100 mL batches. This SRB culture was able to reduce more than 97% of sulfate in 7 and in 14 days of incubation in MPM (data not shown) and in MSM (Martins *et al*., 2010), respectively. Anaerobic conditions were achieved by purging the medium with nitrogen gas and by adding ~10 mL of sterile liquid paraffin. Growth parameters, such as sulfate and soluble sulfide, pH and redox potential were measured over time. The cultures were subcultured every three weeks, using 10% (v/v) of SRB inoculum. In the described experiments, only stable cultures (subcultured a minimum of three times) were used.

2.2.2 Zinc Sulfide Precipitation

Zinc (II) solution (~100 mgL^{-1}) was prepared with distilled water using zinc sulfate hepta-hydrate ($ZnSO_4.7H_2O$, >99.5%, Panreac). The pH of the solution was adjusted to 7 using a 1M NaOH aqueous solution. For the negative control, distilled water (pH = 7) with no zinc (II) was used.

TiO_2 and SiO_2 powders were used as substrates for the irregular precipitation of ZnS. Commercial P-25 TiO_2, (Degussa) with a particle size of ~25 nm was used. The SiO_2 particles were prepared using a modified version of the Stöber method (Stober *et al*., 1968) by mixing 1.12 mL of tetraethyl-orthosilicate (Merck KGaA), 24.75 mL of absolute ethanol (Panreac), and 5 mL of ammonia 20% (Panreac) to 8 mL of distilled water. This solution was stirred during 2 hours at room temperature. After filtration, the

resulting white particles were dried and submitted to a thermal treatment at 700ºC for 4 hours.

After evaluation of the growth parameters, as previously described, an aliquot of the sulfide containing growth media was added to the zinc ion solution described above. The addition was performed when over 90% of the sulfate had been converted to sulfide. The growth culture volume added was calculated based on twice the sulfide content necessary to ensure the complete precipitation of the zinc ion present in the solution. This addition, to 50 mL of the metal solution, was carried out using different methodologies: with and without filtration of the growth medium (0.2 μm filter, Macherey-Nagel); in absence or presence of TiO_2 (0.06 g) or SiO_2 (0.125 g). This operation was done drop-by-drop, using a gas tight syringe with a hypodermic needle, and the metal solution under magnetic stirring at room temperature. After ZnS precipitation, the pH of the resulting suspension was measured, as well as the zinc ion concentration.

The chemically generated ZnS was also obtained by precipitating Zn^{2+} with 8 mM aqueous Na_2S solution (Sigma-Aldrich) in similar experimental conditions. After precipitation, the suspensions were centrifuged two times (Rotofix 32A, Hettich) for 10 minutes at ~3700 RCF, washed twice with distilled water and dried under vacuum at room temperature (APT.Line VD, Binder).

The description of the samples, according to the experiments is shown in Table 2.1.

2.2.3 Analytical Methods

Periodically, SRB growth media samples were collected from each batch with a syringe *via* the top of the glass flasks. Sulfide concentration was measured immediately after sampling using a UV-Visible spectrophotometer (DR 2800, Hach-Lange) by the Methylene Blue Method (665 nm, Hach-Lange). Sulfate concentration was also measured by UV/Visible spectroscopy at 450 nm (Hach-Lange) using the sulfaVer4 method (Hach-Lange).

Redox potential and pH of the growth media were measured using a pH/Eh Meter (GLP 21, Crison). Zn (II) concentrations, before and after precipitation, were measured by flame atomic absorption spectroscopy using a Shimadzu AA-680 model spectrometer. For each sample, three aliquots were considered.

The precipitated materials were analyzed by XRD, using a PANalytical X'Pert Pro powder difractommeter operating at 45 kV and 40 mA, with CuKα radiation filtered by Ni. XRD patterns were recorded using a X'Celerator detector, with a step size (2θ) of 0.016 and a time per step of 50 seconds. The HighScore Plus software, with the ICDD PDF-2 database, was used for peak analysis and crystalline phase identification.

Morphological characterization of the precipitates was performed by Electron Mycroscopy. Scanning Electron Microscopy (SEM) coupled with an Energy-Dispersive X-ray Spectroscopy (EDX) analyzer. A FEG-SEM Hitachi S4100 microscope, operating at 25 kV and a Bruker EDX detector were used for this purpose. The samples were prepared by deposition of an aliquot of the precipitates directly onto the carbon tape and then coated by carbon evaporation (Emitech K950X). Transmission Electron Microscopy (TEM) coupled to EDX detector was carried out using a FEG-TEM Hitachi H9000 microscope operated at 300 kV and a Bruker EDX analyzer. The samples were prepared by placing a suspension drop, containing the precipitates dispersed in ultra-pure distilled water, on a copper grid coated with an amorphous carbon film.

Raman scattering spectroscopy was carried out using a RFS 100/S Bruker FT-Raman spectrometer (Bruker Optics), with a Nd:YAG laser, operating at 100 mW and a resolution of 4 cm^{-1}. Data was acquired using the OPUS software (v. 6.5, Bruker Optics).

2.3. Results and Discussion

In order to assess the influence of the growth media composition on the formation of the zinc sulfide nanoparticles, the consortium used as inoculum was grown in MSM and MPM, since both have been successfully used for the growth and activity of SRB (Martins *et al*., 2010).

Figure 2.1 illustrates the concentration of Zn^{2+} after precipitation and the corresponding percentage of zinc removal from a starting solution containing 105.4 mgL^{-1} of this metal ion. The results are shown for the supernatant solutions from which the precipitates were collected, by adding filtered MSM growth media and non-filtered MSM growth media, in the absence (samples S-F and S-NF, respectively) and presence of TiO_2 (samples S-F-T and S-NF-T) or SiO_2 (samples S-F-S and S-NF-S). Also shown are the results, under similar conditions, when the growth medium was MPM (samples P-F, P-NF, P-F-T, P-NF-T, P-F-S and P-NF-S). Table 2.2 shows the final pH of the solutions, after addition of the growth media for ZnS precipitation, using the sample description established in Table 2.1 and according to the growth media used.

Table 2.1 – Samples' abbreviations and corresponding description.

Abbreviation used	**Growth medium**	**Treatment**	**Substrate**
S-F	MSM	Filtered	-
S-NF	MSM	Non-filtered	-
S-F-T	MSM	Filtered	TiO_2
S-NF-T	MSM	Non-filtered	TiO_2
S-F-S	MSM	Filtered	SiO_2
S-NF-S	MSM	Non-filtered	SiO_2
P-F	MPM	Filtered	-
P-NF	MPM	Non-filtered	.
P-F-T	MPM	Filtered	TiO_2
P-NF-T	MPM	Non-filtered	TiO_2
P-F-S	MPM	Filtered	SiO_2
P-NF-S	MPM	Non-filtered	SiO_2
Chem	-	Non-filtered	-

Table 2.2 – The pH (25ºC) of zinc (II) solutions after precipitation, from a starting solution of Zn (II) at pH 7.00.

Sample	Growth media added	
	MSM	MPM
F	7.03	6.41
NF	7.11	6.45
F-T	7.14	6.68
NF-T	7.26	6.35
F-S	7.12	6.76
NF-S	7.09	6.37
Chem	5.20	

For the experimental conditions investigated here and as illustrated in Figure 2.1, the above method allows high zinc removal percentage (≥90%) whenever a solution containing the biological generated sulfide was added to the zinc (II) solution. Under all tested conditions, vestigial amounts of zinc species remained in solution (concentrations lower than 4 $mg.L^{-1}$), with the exception of samples P-NF-S, P-F-S and Chem. For the latter, a zinc removal percentage of approximately 87% was obtained using aqueous Na_2S as precipitating agent. The lower percentage of zinc removal, obtained by chemical synthesis of ZnS, may be due to the solution low pH after precipitation (Table 2.2). The pH value for the sample P-NF-S was also slightly lower, which may account for the lower (87.2%) percentage of zinc removal, when compared to all other samples analyzed. The high removal percentages are in accordance with reports made by other authors for zinc sulfide precipitation using biogenic sulfide (Bijmans *et al*., 2009; Esposito *et al*., 2006; Mokone *et al*., 2010). Moreover, a lower pH value may result in a lower precipitation efficiency of this metal as previously reported by Mokone and collaborators (Mokone *et al.*, 2010). Nonetheless, the lower efficiency may also be due to the lower availability of sulfide species for interacting with the metal in the solution, as lower pH values will alter the equilibrium of the dissolved sulfide species (Jimenez-Rodriguez *et al*., 2009; Kleinjan *et al*., 2005).

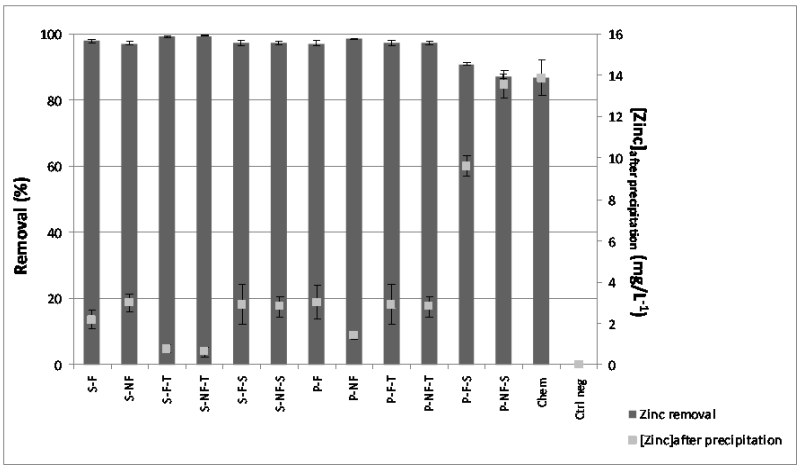

Figure 2.1 – Zinc (II) concentration in solution after precipitation and corresponding removal percentage on the different samples tested. Error bars are shown. The sample description indicates whether the growth media added was filtered (F or NF), the type of growth media used (MSM – S; MPM – P) or if a chemical agent was used (Chem) and the presence of TiO_2 (T) or SiO_2 (S) as substrates.

The XRD patterns of the obtained precipitates by adding biologically generated sulfide by the consortium grown in MSM are shown in Figure 2.2A. Figure 2.2 A1 refers to the materials prepared using filtered (S-F) growth media. Figure 2.2 A2 shows the results for materials prepared using non-filtered growth media (S-NF). The XRD results show that cubic ZnS (*sphalerite*) is the predominant crystalline phase in the analyzed samples; this phase was also observed for ZnS powders obtained when the MPM growth medium was used as the sulfate source, either filtered or non-filtered. The XRD patterns for the chemically synthesized ZnS (Chem) are also present for comparative purposes (Figure 2.2 A3). The observed peak broadening is probably due to the small size of the ZnS particles. Using the Scherrer equation (Scherrer, 1922) (Equation 2.6), the average ZnS crystallite size was estimated as 24, 22 and 11 nm for the S-F, S-NF and Chem samples, respectively.

$$Dp = \frac{K * \lambda}{\beta * \cos\theta} \qquad (2.6)$$

The diameter of the particles (*Dp*) was calculated based on the form factor (K, 0.94), the wavelength of the radiation source (λ), full width at half maximum in radians (β) and the Bragg angle (θ). Unless stated otherwise, the most intense peak observed was

considered in the determination of the diameter using Equation 2.6. However, the definite size of the different materials prepared was established by electronic microscopy.

The ZnS precipitation experiments were also performed in the presence of TiO_2 and SiO_2 as powdered substrate materials present in the reacting mixtures. As expected, the XRD patterns obtained for the TiO_2 samples showed predominantly the reflections corresponding to anatase, but also rutile, and precluded the detection of nanocrystalline ZnS by this technique. As observed in Figure 2.2B, there are no discernable differences between the spectra obtained for when adding filtered (Figure 2.2 B1) and non-filtered (Figure 2.2 B2) MSM growth media to Zn (II) solutions containing TiO_2 powders (Figure 2.2 B3). Conversely, for the experiments carried out in the presence of amorphous SiO_2 (Figure 2.2 C3) powders, the XRD patterns indicated the presence of the ZnS phase for both filtered (Figure 2.2 C1) and non-filtered samples (Figure 2.2 C2). Application of the Scherrer equation to this sample, led to average ZnS crystallite sizes about 16 nm and 17 nm, for the S-F-S and S-NF-S samples, respectively, thus resulting in dimensions comparable to those of the ZnS crystallites obtained in the absence of powdered substrates. Nonetheless, it should be noted that, unlike the previous analyses, these estimates were obtained using the second most intense XRD peak, as the most intense is masked by the broad peak due to amorphous SiO_2, observed between 15º and 32º (2θ).

Figure 2.3 shows the Raman spectra of the chemically generated ZnS (Chem., line -■-), TiO_2 (solid line) and of the precipitate obtained by the addition of non-filtered growth media (MSM) in a zinc (II) solution containing dispersed TiO_2 particles (sample S-NF-T, line -●-). The spectrum for the latter sample shows the cumulative "contribution" of TiO_2 and ZnS phases. Although the ZnS nanocrystallites were not detected by powder XRD for the TiO_2 containing samples, the Raman data (Figure 2.3) confirms the presence of such phase. Thus, the Raman data for this sample are consistent with those obtained by other authors for ZnS (Abdulkhadar and Thomas, 1995), as well as those obtained for commercial P25 TiO_2 (Choi *et al*., 2005). The spectra of the precipitates obtained using the same conditions, but with MPM growth media, are similar and, hence, are not shown.

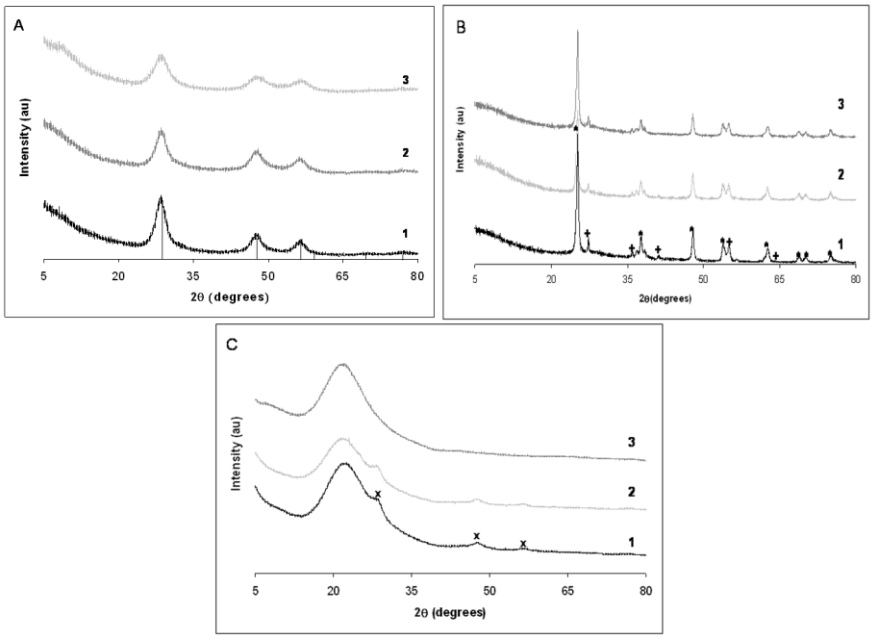

Figure 2.2 – X-Ray powder diffraction patterns for precipitates generated by addition of filtered (A1) and non-filtered (A2) MSM growth media; chemically generated (A3). Stick patterns correspond to cubic zinc sulfide phase. (JCPDS #77-2100). Figure 2.2B shows the diffraction patterns for samples obtained by adding filtered (B1) and non-filtered (B2) MSM growth media to Zn (II) solutions containing TiO_2 powders (B3). Stars (*) indicate peaks corresponding to the anatase phase and "+" indicate peaks of the rutile form. Figure 2.2C shows XRD for materials obtained by the addition of filtered (C1) and non-filtered (C2) MSM growth media in the presence of amorphous SiO_2 (C3). "x" indicates the peaks corresponding to the cubic ZnS phase (JCPDS #77-2100).

Figure 2.4 shows the SEM images and corresponding EDX analysis for the powders prepared by the addition of filtered and non-filtered MSM to the zinc (II) solution (S-F and S-NF, respectively). The particles morphology observed for these samples is predominantly spheroidal and, as expected, the EDX analysis confirmed the presence of zinc and sulfur. For the sample obtained by adding the non-filtered MSM, additional peaks for iron and silicon have been also detected. The presence of iron may be considered as an adventitious contamination. Silicon was detected because it is another trace element often present in the carbon tape used in the samples' preparation for SEM analyses.

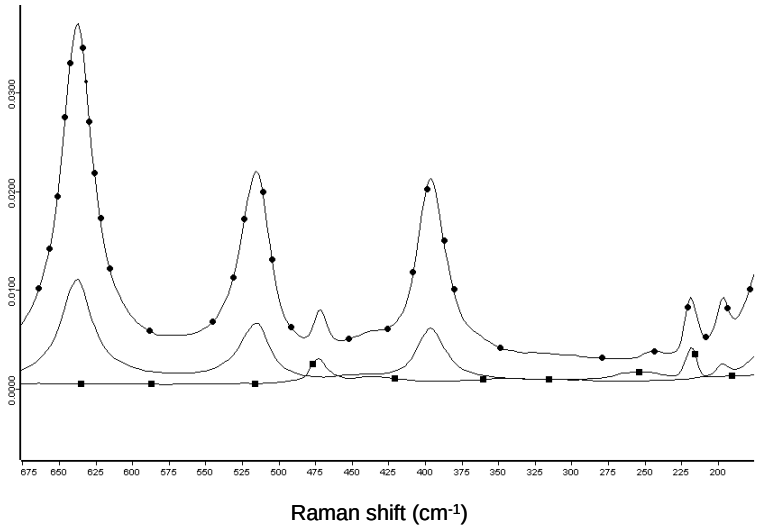

Figure 2.3 – FT-RAMAN spectra of chemically generated zinc sulfide (-■-), TiO_2 (solid line) and of the precipitate obtained by the addition of non-filtered growth media (MSM) in a zinc solution in presence of TiO_2 are shown (-•-).

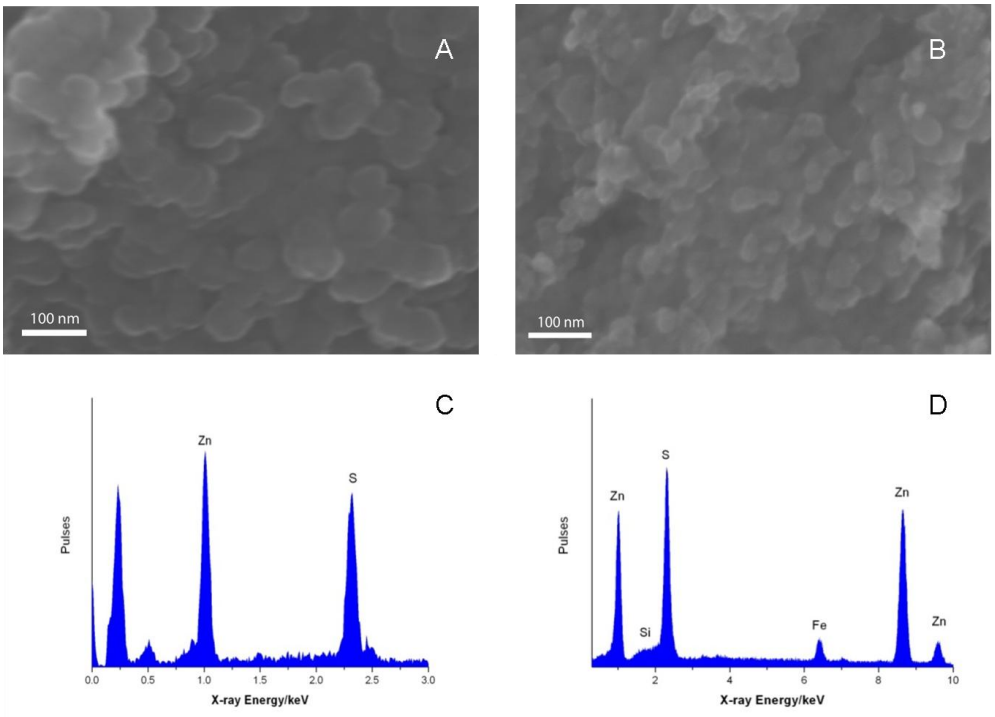

Figure 2.4 – SEM images and corresponding EDX spectra for nanosized ZnS particles obtained by adding filtered (left, A and C) and non-filtered (right, B and D) MSM growth media containing biologically generated sulfide to a Zn (II) solution

Figure 2.5 shows the SEM and EDX results for the samples obtained in the same conditions of those shown in Figure 4, but in the presence of TiO_2 (Figure 2.5A) and SiO_2 (Figure 2.5B) suspensions. The SEM images reveal that the ZnS nanocrystallites present an average diameter between 20 – 30 nm, as previously estimated by XRD using the Scherrer equation. The spheroidal morphology was observed for ZnS particles generated either in the presence or absence of the powdered substrates. Again, as earlier observed, the EDX (Figures 2.5C and 2.5D) showed the presence of zinc, sulfur and titanium, as well as silicon and, to some extent, iron and magnesium. Although the presence of the latter can be explained due to the composition of the reacting media, iron is present as adventitious contaminant.

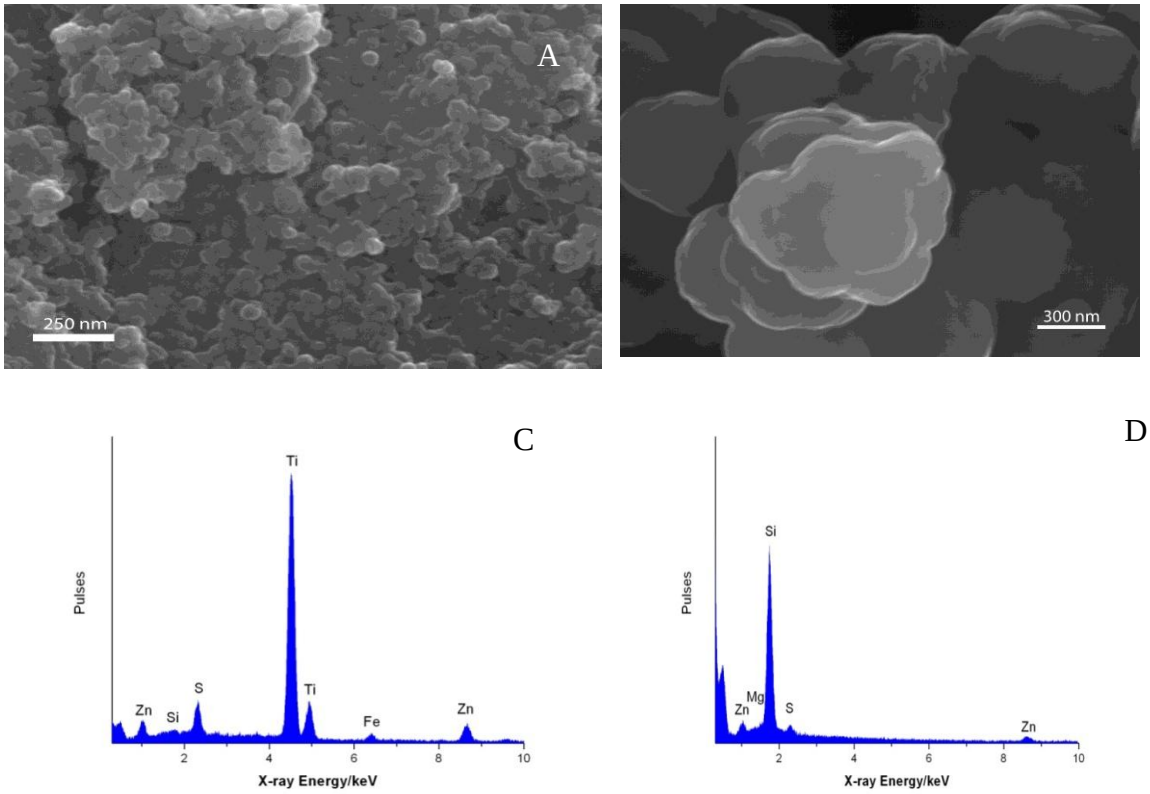

Figure 2.5 – SEM images and corresponding EDX spectra for samples prepared in the presence of TiO_2 (left, A and C) and SiO_2 (right, B and D), obtained by adding non-filtered MSM growth media containing biologically generated sulfide to a zinc (II) solution.

Other authors have reported ZnS with smaller average dimensions prepared in the absence of substrate. Liu and collaborators (Liu *et al.*, 2009) have reported particles

ranging 5 – 10 nm. ZnS nanoparticles with average diameter close to those reported in our research (ca. 27 nm) have been obtained but using high pressure methods (Chen *et al*., 2004). The particle size of the substrates, namely, SiO_2, was also in accordance (550 – 600 nm) with that described by other authors (Franco *et al*., 2009; Stober *et al*., 1968). For TiO_2, the results were consistent with the information provided by the manufacturer (25 – 30 nm).

Regarding the size of the nanocomposites particles, other authors have reported ZnS/XO_2 (X=Ti, Si) composites (Franco *et al*., 2009), ranging 20 – 30 nm for TiO_2 composites, and 600 – 750 nm for SiO_2 composites, however, using a distinct chemical method.

Figure 2.6 shows the TEM images of the ZnS nanoparticles obtained using the filtered (2.6A) and non-filtered (2.6B) MSM medium. The mean size of the spherical ZnS nanoparticles, for both cases, is within the range observed in the SEM analyses (20–30 nm) and is, again, in good agreement to those estimated by XRD. TEM analysis was also carried out, as Figure 2.6 illustrates, on the ZnS nanoparticles synthesized by the addition of the non-filtered MSM growth medium, in the presence of TiO_2 (2.6C, S-NF-T) and SiO_2 (2.6D, S-NF-S).

Noteworthy, we observed that the TiO_2 and SiO_2 particles became decorated with ZnS nanophases that result from uneven deposition of the metal sulfide at the substrates surfaces. This is in accordance with the results obtained by other authors (Franco *et al*., 2009), that did not find by electron microscopy relevant modifications on the TiO_2 morphology after ZnS deposition. However, the authors also reported that the electronic microscopy analysis of the $ZnS\text{-}SiO_2$ particles confirmed the presence of a deposited phase on the SiO_2 surface.

These results confirm the relevance of the method herein described to produce materials with potential interest as catalysts by using biogenerated sulfide as the precipitating agent in Zn (II) containing solutions. Future work should also include the study of the stability of such nanocomposites.

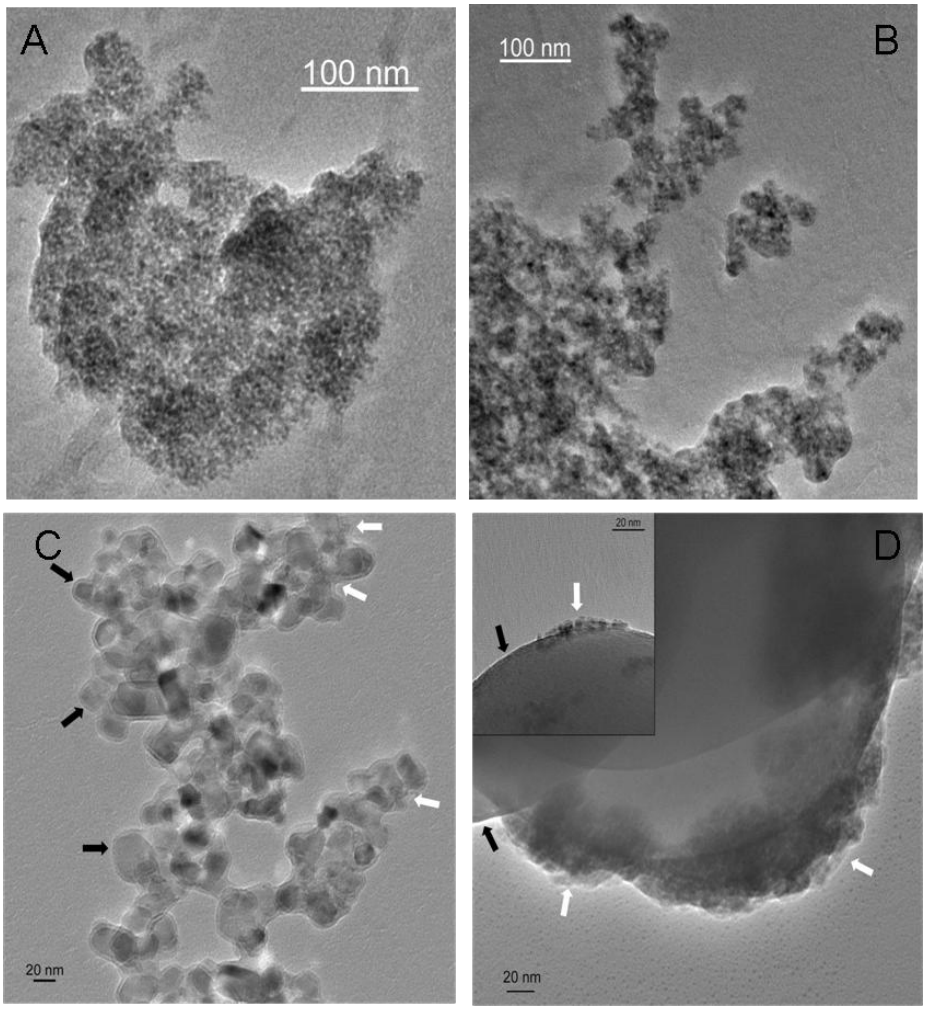

Figure 2.6 – TEM images for the nanosized particles of ZnS obtained by adding filtered (A) and non-filtered (B) MSM growth media containing biologically generated sulfide to a zinc solution. Also shown are the TEM images obtained for the nanosized particles of ZnS (white arrows) decorating TiO_2 (black arrows) (C) and SiO_2 (black arrows) particles (D), obtained by adding non-filtered MSM growth media containing biologically generated sulfide to zinc (II) suspensions containing the respective powdered substrates.

2.4. Conclusions

We have demonstrated that ZnS nanocrystals can be prepared by precipitating zinc with biologically produced sulfide. Here, sulfide species were produced by naturally occurring sulfate-reducing bacteria grown in different media. Besides the economical advantage in the use of a biological source of sulfide, the higher percentage of metal

removal means a more efficient production of nanocrystalline ZnS. It was also shown that the use of TiO_2 and SiO_2 as substrates resulted in the respective composite materials. Considering the simplicity of the process, this is a convenient route for the biological synthesis of functional materials with potential interest as photocatalysts.

Acknowledgements

Funding by Fundação para a Ciência e a Tecnologia (FCT) through a PhD grant (SFRH/BD/43784/2008) is acknowledged. A. V. Girão also thanks FCT for the Post-Doc grant (SFRH/BPD/66407/2009).

References

Abdulkhadar, M. and Thomas, B., 1995. Study of Raman-Spectra of Nanoparticles of Cds and Zns. Nanostruct Mater, 5(3): 289-298.

Barnes, L.J., Janssen, F.J., Scheeren, P.J.H., Versteegh, J.H. and Koch, R.O., 1992. Simultaneous Microbial Removal of Sulfate and Heavy-Metals from Waste-Water. T I Min Metall C, 101: C183-C189.

Bessergenev, V., Ivanova, E.N., Kovalevskaya, Y.A., Gromilov, S.A., Kirichenko, V.N., Zemskova, S.M., Vasilieva, I.G., Ayupov, B.M. and Shwarz, N.L., 1995. Optical and Structural Proper Ties of Zns and Zns-Mn Films Prepared by Cvd Method. Mater Res Bull, 30(11): 1393-1400.

Bhagat, M., Burgess, J.E., Antunes, A.P.M., Whiteley, C.G. and Duncan, J.R., 2004. Precipitation of mixed metal residues from wastewater utilising biogenic sulphide. Minerals Engineering, 17(7-8): 925-932.

Bijmans, M.F.M., van Helvoort, P.J., Buisman, C.J.N. and Lens, P.N.L., 2009. Effect of the sulfide concentration on zinc bio-precipitation in a single stage sulfidogenic bioreactor at pH 5.5. Sep Purif Technol, 69(3): 243-248.

Chen, J.F., Li, Y.L., Wang, Y.H., Yun, J. and Cao, D.P., 2004. Preparation and characterization of zinc sulfide nanoparticles under high-gravity environment. Mater Res Bull, 39(2): 185-194.

Choi, H.C., Jung, Y.M. and Kim, S.B., 2005. Size effects in the Raman spectra of TiO2 nanoparticles. Vib Spectrosc, 37(1): 33-38.

Costa, M.C. and Duarte, J.C., 2005. Bioremediation of acid mine drainage using acidic soil and organic wastes for promoting sulphate-reducing bacteria activity on a column reactor. Water Air Soil Poll, 165(1-4): 325-345.

Esposito, G., Veeken, A., Weijma, J. and Lens, P.N.L., 2006. Use of biogenic sulfide for ZnS precipitation. Sep Purif Technol, 51(1): 31-39.

Franco, A., Neves, M.C., Carrott, M.M.L.R., Mendonca, M.H., Pereira, M.I. and Monteiro, O.C., 2009. Photocatalytic decolorization of methylene blue in the presence of TiO_2/ZnS nanocomposites. Journal of Hazardous Materials, 161(1): 545-550.

Garcia, C., Moreno, D.A., Ballester, A., Blazquez, M.L. and Gonzalez, F., 2001. Bioremediation of an industrial acid mine water by metal-tolerant sulphate-reducing bacteria. Minerals Engineering, 14(9): 997-1008.

Jimenez-Rodriguez, A.M., Duran-Barrantesh, M.M., Borja, R., Sanchez, E., Colmenarejo, M.F. and Raposo, F., 2009. Heavy metals removal from acid mine drainage water using biogenic hydrogen sulphide and effluent from anaerobic treatment: Effect of pH. Journal of Hazardous Materials, 165(1-3): 759-765.

Kleinjan, W.E., de Keizer, A. and Janssen, A.J.H., 2005. Equilibrium of the reaction between dissolved sodium sulfide and biologically produced sulfur. Colloid Surface B, 43(3-4): 228-237.

Lewis, A.E., 2010. Review of metal sulphide precipitation. Hydrometallurgy, 104(2): 222-234.

Liu, J., Ma, J.F., Liu, Y., Song, Z.W., Sun, Y., Fang, J.R. and Liu, Z.S., 2009. Synthesis of ZnS nanoparticles via hydrothermal process assisted by microemulsion technique. J Alloy Compd, 486(1-2): L40-L43.

Luther, G.W., Theberge, S.M. and Rickard, D.T., 1999. Evidence for aqueous clusters as intermediates during zinc sulfide formation. Geochim Cosmochim Ac, 63(19-20): 3159-3169.

Martins, M., Faleiro, M.L., Chaves, S., Tenreiro, R. and Costa, M.C., 2010. Effect of uranium (VI) on two sulphate-reducing bacteria cultures from a uranium mine site. Sci Total Environ, 408(12): 2621-2628.

Mokone, T.P., van Hille, R.P. and Lewis, A.E., 2010. Effect of solution chemistry on particle characteristics during metal sulfide precipitation. J Colloid Interf Sci, 351(1): 10-18.

Monteiro, O.C., Neves, M.C. and Trindade, T., 2004. Zinc sulfide nanocoating of silica submicron spheres using a single-source method. J Nanosci Nanotechno, 4(1-2): 146-150.

Postgate, J.R., 1966. Media for sulphur bacteria. Lab Pract, 15(11): 1239-44.

Qi, L.M., Ma, J.M., Cheng, H.M. and Zhao, Z.G., 1996. Synthesis and characterization of mixed CdS-ZnS nanoparticles in reverse micelles. Colloid Surface A, 111(3): 195-202.

Sani, R.K., Peyton, B.M. and Brown, L.T., 2001. Copper-induced inhibition of growth of *Desulfovibrio desulfuricans* G20: assessment of its toxicity and correlation with those of zinc and lead. Appl Environ Microbiol, 67(10): 4765-72.

Scherrer, W., 1922. A theorem on lattice and volumes. Math Ann, 86: 99-107.

She, Y.Y., Yang, J. and Qiu, K.Q., 2010. Synthesis of ZnS nanoparticles by solid-liquid chemical reaction with ZnO and Na2S under ultrasonic. T Nonferr Metal Soc, 20: S211-S215.

Stober, W., Fink, A. and Bohn, E., 1968. Controlled Growth of Monodisperse Silica Spheres in Micron Size Range. J Colloid Interf Sci, 26(1): 62-&.

Vaidhyanathan, B., Ganguli, M. and Rao, K.J., 1995. Fast Solid-State Synthesis of Metal Vanadates and Chalcogenides Using Microwave Irradiation. Mater Res Bull, 30(9): 1173-1177.

Xin, B.P., Huang, Q., Chen, S. and Tang, X.M., 2008. High-purity Nano Particles ZnS Production by a Simple Coupling Reaction Process of Biological Reduction and Chemical Precipitation Mediated with EDTA. Biotechnol Progr, 24(5): 1171-1177.

Chapter 3 – Green Synthesis of *Covellite* Nanocrystals Using Biologically Generated Sulfide: Potential for Bioremediation Systems.

João Pinto da Costa[1], Ana Violeta Girão[2], João P. Lourenço[3], O.C. Monteiro[4], Tito Trindade[2], Maria Clara Costa[1*]

[1]Universidade do Algarve, CCMar, Campus Gambelas, 8005-139 Faro, Portugal.
[2]Universidade de Aveiro, CICECO, 3810-193 Aveiro, Portugal.
[3]Universidade do Algarve, CIQA, FCT, Ed. 2, Campus Gambelas, 8005-139 Faro, Portugal.
[4]Universidade de Lisboa, FCUL, CQB, Campo Grande, 1749-016 Lisboa, Portugal.

*Corresponding author
Universidade do Algarve, Campus Gambelas
FCT – Edifício 8, Lab. 2.35
8005-139 Faro, Portugal
mcorada@ualg.pt

A modified version of this chapter has been published as:
da Costa, J., Girão, A. V., Lourenço, J. P., Monteiro, O. C., Trindade, T. and Costa, M. C., (2013), Green synthesis of covellite nanocrystals using biologically generated sulfide: Potential for bioremediation systems. J. Environ. Manage. 128:226-232.

Abstract

This work describes the synthesis of CuS powders in high yield and via an environmentally friendly and straightforward process, under ambient conditions (temperature and pressure), by adding to aqueous copper (II) a nutrient solution containing biologically generated sulfide from sulfate-reducing bacteria (SRB). The powders obtained were composed of CuS (*covellite*) nanoparticles (NPs) exhibiting a spheroid morphology (<5 nm). The relevance of this method to obtain CuS supported solid substrates has been demonstrated by performing the synthesis in the presence of TiO_2 and SiO_2 submicron particles. We further extended the work carried out, which substantiates the potential of using biogenic sulfide for the production of *covellite* nanocrystals and composites, using the effluent of a bioremediation column. Hence, such process results in the synthesis of added value products obtained from metal rich effluents, such as metallurgical and industrial ones, or Acid Mine Drainage (AMD), when associated with bioremediation processes.

Keywords: CuS, nanoparticles, nanocomposites, sulfate-reducing bacteria, bioremediation.

3.1. Introduction

The hydrometallurgical treatment of ores and effluents relies heavily on metal sulfide precipitation (Lewis, 2010). Although hydroxide precipitation is a widely used method for metal removal, there are several advantages in resorting to sulfide precipitation, including the lower solubility of these precipitates and fast reaction rates, as well as better settling properties and a higher degree of metal removal (Lewis and van Hille, 2006). This method, however, is not widely used because of the toxicity and corrosiveness of excess sulfide (Veeken *et al*., 2003).

During the metabolism of organic matter (CH_2O), sulfate-reducing bacteria (SRB) use sulfate as the terminal electron acceptor, resulting in the production of H_2S.

In the presence of metal ions, biologically generated hydrogen sulfide will lead to insoluble metal sulfides, which, consequently, precipitate (Bhagat *et al*., 2004). The use of SRB in bioremediation processes is well documented, namely for the reduction of high-content sulfate and metal effluents (Costa and Duarte, 2005; Garcia *et al*., 2001). Nevertheless, the process generates sulfide in excess whose elimination and corresponding disposal of the metal sulfides are environmental issues that need to be addressed.

Research on nanoscale materials, namely, metal sulfides, has gained considerable attention in materials science due to their excellent potential in catalysis (Mallick *et al*., 2007), optical functionality (Liz-Marzan, 2006), and electronic functionalities (specificity of their surface plasmon absorption) (Kamat, 2002).

Copper sulfide nanoparticles have been synthesized using a wide variety of techniques, such as solvothermal methods (Li *et al*., 2010), sonochemistry (Wang *et al*., 2002) or pyrolosis (Nascu *et al*., 1997). Most of these methods are based on high-temperature and/or high pressure and on the use of toxic chemicals, namely, H_2S as the sulfide source. Therefore, the production of functional nanomaterials using bacterial growth media solutions, at room temperature and atmospheric pressure, avoiding the use of additional, toxic and expensive chemicals, is an interesting alternative synthesis route. Furthermore, it should be noted that copper catalysts are often synthesized as composites, and, usually, these are either TiO_2 (Andronic *et al*., 2011) or SiO_2 (Tiwari *et al*., 2012) composites. Hence, this synthesis process shows obvious economic

advantages and improved safety, as the sulfide is naturally produced in the growth media by SRB isolated from environmental samples.

In previous work (da Costa *et al*., 2012) we have demonstrated that the production of zinc sulfide nanoparticles (*sphalerite*) using SRB growth media, at room temperature and atmospheric pressure, is possible. Moreover, it has been shown that the use of growth media of different complexities, as well as the filtration or not of these same media, yields nanoparticles (NP's) with no major morphological differences. In the past, bioremediation systems, based on the activity of SRB, have been developed for the treatment of AMD using SRB (Martins *et al*., 2010b). Using this acquired knowledge we set out to, in the present work, synthesize stable copper sulfide nanoparticles and TiO_2 or SiO_2 nanocomposites, and to study their properties when produced from sulfide generated by SRB. We also have determined the potential of such methods of synthesis by using the effluents of a previously developed bioremediation system as the source of dissolved sulfide species, hence providing an integrated environmentally friendly solution for some of the challenges facing the metallurgical and extractive industries.

3.2. Experimental

3.2.1. Bacterial Consortium and Growth Conditions

A SRB consortium enriched from the wetland of the Urgeiriça mine (North of Portugal) and selected from previous studies (Martins *et al*., 2010a), containing mainly species affiliated to *Desulfovibrio desulfuricans*, was used as inoculum. These cultures were grown and maintained in minimum salt medium (MSM) (Sani *et al*., 2001) (1g.L^{-1} NH_4Cl; 0.06g.L^{-1} $CaCl_2.6H_2O$; 0.05g.L^{-1} yeast extract; 1g.L^{-1} $MgSO_4.7H_2O$; 2g.L^{-1} Na_2SO_4, and 5g.L^{-1} $C_3H_5NaO_3$) in anaerobic conditions, at room temperature in 100 mL batches. This SRB culture was able to reduce more than 97% of sulfate in 14 days of incubation in MSM. Anaerobic conditions were achieved by purging the medium with nitrogen gas and by adding ~10 mL of sterile liquid paraffin. Growth parameters, such as sulfate and soluble sulfide, pH and redox potential were measured over time. The cultures were subcultured every three weeks, using 10% (v/v) of SRB inoculum. In the described experiments, only stable cultures (subcultured a minimum of three times) were used.

3.2.2. Bioremediation System and SRB Growth

Having been thoroughly described elsewhere (Barros *et al*., 2009; Martins *et al*., 2010b), a brief description of the bioremediation system ensues. This was designed to be a simple, yet efficient continuous process that uses waste and/or natural cheap materials in order to become an economically and environmentally sustainable bioremediation process. It was composed by two column reactors. In the first, a mixture of calcite tailing and coarse sand (1:2, w/w) was used for the neutralization of the AMD. The second was an anaerobic up-flow packed bed reactor (UAPS) filled with approximately 900 g of coarse sand and 30 mL of inoculum. Modified Postgate medium (da Costa *et al*., 2012) (300 mL) was also added and, in order to allow for the initial bacterial growth, the bioreactor was operated in batch conditions for 2 weeks. Simplified schematics of the bioremediation system can be found in Appendix A.

3.2.3. Copper Sulfide Precipitation

Copper (II) solution with a concentration of ~100 mgL^{-1} was prepared with distilled water using copper sulfate penta-hydrate ($CuSO_4.5H_2O$, >99.5%, Riedel-de Haën). Sonication was used to remove dissolved gases and, after adding the adequate amount of copper sulfate, the pH of the solution was corrected to 2.45±0.01 using a 6M HNO_3 aqueous solution. After, nitrogen was used to purge the prepared solution. Two support materials – TiO_2 and SiO_2 – were used as matrices during the copper sulfide synthesis. A commercial P-25 TiO_2, (Degussa) with a particle size of ~25 nm was used. The SiO_2 particles were prepared using a modified version of the Stöber method (Stober *et al*., 1968). This consisted in adding 1.12 mL of tetraethyl-orthosilicate (Merck KGaA), 24.75 mL of absolute ethanol (Panreac), and 5 mL of ammonia 20% (Panreac) to 8 mL of distilled water. This solution was stirred for 2 hours at room temperature. After filtration, the resulting white particles were dried and submitted to a thermal treatment at 700ºC for 4 hours.

After characterization of the bacterial growth parameters, as previously described, an aliquot of the sulfide containing growth media was added to the copper ion solution above described. The addition was performed when over 90% of the sulfate had been converted to sulfide. The growth culture volume added was calculated based on twice the sulfide content necessary to ensure the complete precipitation of the copper ion present in the solution. This addition, to 50 mL of the metal solution, was carried out in the absence or presence of TiO_2 (0.06 g) or SiO_2 (0.125 g). This operation was done drop-by-drop, using a gas tight syringe with a hypodermic needle, and the metal solution under magnetic stirring at room temperature. The pH of the resulting suspension was measured, as well as the copper ion concentration After the precipitation step, the suspensions were centrifuged and washed twice (Rotofix 32A, Hettich) for 10 minutes at 4000 rpm (~3700 RCF), washed with a mixture of distilled water and ethanol (50:50, v/v) and dried under vacuum at room temperature (APT.Line VD, Binder).

Chemically generated copper sulfide was also obtained by precipitating Cu^{2+} with ~620 $mg.L^{-1}$ (8 mM) aqueous Na_2S solution (Sigma-Aldrich) in similar experimental conditions. For the negative control, distilled water was added to the copper solution. All precipitation assays were carried out in duplicates.

For the experiments using the effluent of the bioremediation system, identical conditions were used; however, the addition of the sulfide-rich solution from the bioreactor was done directly into the metal containing solution, after sampling and measurement of pH and sulfide concentration.

3.2.4. Analytical Methods

Periodically, SRB growth media samples were collected from each batch with a syringe *via* the top of the glass flasks. Sulfide concentration was measured immediately after sampling using a UV-Visible spectrophotometer (DR 2800, Hach-Lange) by the Methylene Blue Method (665 nm, Hach-Lange). Sulfate concentration was also measured by UV/Visible spectroscopy at 450 nm (Hach-Lange) using the sulfaVer4 method (Hach-Lange).

Redox potential and pH of the growth media were measured using a pH/Eh Meter (GLP 21, Crison). Copper ion concentrations, before and after precipitation, were measured by flame atomic absorption spectroscopy using a Varian AA-20 model spectrometer.

The precipitated materials were analyzed by XRD, using a PANalytical X'Pert Pro powder difractommeter operating at 45 kV and 40 mA, with CuKα radiation filtered by Ni. XRD patterns were recorded using an X'Celerator detector, with a step size of 0.016 and a time per step of 100 seconds. The HighScore Plus software, with the ICDD PDF-2 database, was used for peak analysis and crystalline phase identification.

Morphological and analytical characterization of the precipitates was performed by Electron Microscopy. Scanning Electron Microscopy (SEM) using a Field Emission Gun (FEG) - SEM Hitachi SU70 microscope, operated at 15 kV, with an Energy-Dispersive X-ray Spectroscopy (EDX) Bruker detector were used for this purpose. The samples were prepared by deposition of an aliquot of the precipitates directly onto the carbon tape and then coated by carbon evaporation (Emitech K950X). Transmission Electron Microscopy (TEM) coupled to a Bruker EDX analyzer was carried out using a FEG-TEM Hitachi H9000 microscope operated at 300 kV. Samples were prepared by placing a suspension drop, containing the precipitates dispersed in ultra-pure distilled water, on a copper grid coated with an amorphous carbon film.

3.3. Results and Discussion

Figure 3.1 shows the remaining concentration of Cu (II) after CuS precipitation and the corresponding percentage of copper removal from a starting solution containing 104.6 mgL^{-1} in Cu (II) at pH 2.45. The sample description indicates whether the growth media was added in the absence (MSM) or presence of TiO_2 (MSM-T) or SiO_2 (MSM-S). These results were obtained for supernatant solutions from which the precipitates were collected after adding the MSM growth media. High copper removal percentages were obtained for all the samples (>95%) and, in particular for the MSM and MSM-T samples as well as for the direct chemical precipitation method, the removal percentage was higher than 96%. The slightly lower value observed for the MSM-S sample (~90%) may be due to the different final pH, which can be found in Table 3.1, with the pH values of the Cu (II) solutions after precipitation for all samples. However, this result was unexpected as, generally, higher pH values lead to a lower solubility of metal sulfides (Huisman *et al*., 2006). Nonetheless, this may be because amorphous SiO_2 has been shown to decompose hydrogen sulfide into hydrogen (Akamatsu *et al*., 2008). Finally, the final pH of the solution in which Na_2S was added to aqueous Cu (II) was considerably lower than those measured in solutions having growth media. This is a consequence of the buffer action of the growth medium at a pH value of ~7.50. In the experimental conditions used, the remaining copper ions in solution did not exceed a concentration of ~10 $mg.L^{-1}$. Therefore, these results confirm the efficiency of this method to remove copper from contaminated waters, which is in accordance with evidences gathered by other authors (Costa and Duarte, 2005) on the use of SRB in systems for the treatment of acid mine drainage (AMD), with concomitant metal sulfide precipitation.

Figure 3.2 shows the X-ray diffraction patterns obtained for the sample obtained by precipitation using biogenic sulfide; the powder XRD for copper sulfide obtained by chemical precipitation is also shown for comparative purposes (Figure 3.2A). Interestingly, the CuS obtained by adding the biological growth media seems to have yielded *covellite* (ICDD PDF2 #01-078-0876) (Takeuchi *et al*., 1985) without the presence of other crystallites, such as those present in the CuS obtained by adding Na_2S.

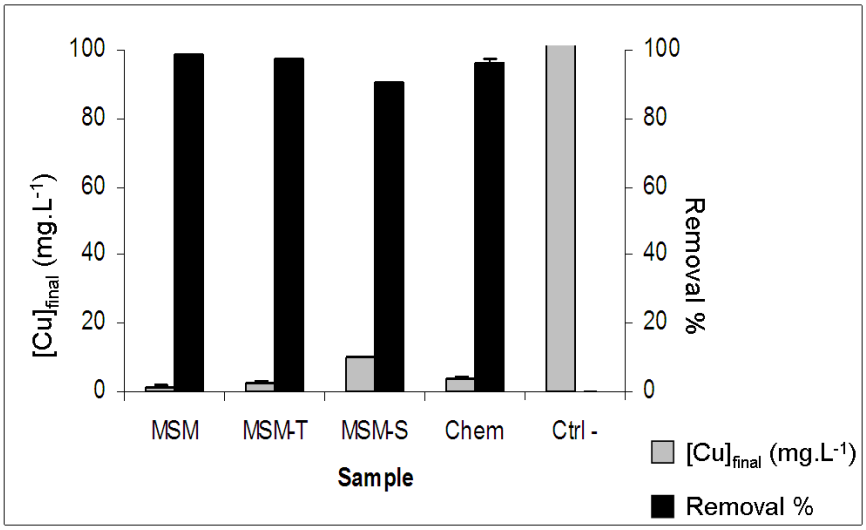

Figure 3.1 – Copper concentration in solution after precipitation and corresponding removal percentage on the different samples tested. Error bars are shown, though not clear. The sample description indicates whether the growth media was added in the absence (MSM) or presence of TiO_2 (MSM-T) or SiO_2 (MSM-S). Results obtained for the chemical precipitation of Cu (II) and of the negative control are also shown. Error bars are shown but may not be visible due to scale.

As Figure 3.2A illustrates, there were some additional peaks to those corresponding to the CuS crystallite, in both cases, which we were unable to identify. These extra peaks may correspond to crystals formed by other contaminants, namely, sodium, present in the sulfide solution added for chemical precipitation, but also present in the composition of the growth media. Note that for samples in which TiO_2 was used as substrate, the intense high reflection of this material obscured the peaks of CuS, which have been detailed in the inset of Figure 3.2B for this sample, evidencing the presence of CuS in the precipitate. For comparative purposes, the TiO_2 diffractogram is shown. Figure 3.2C shows the XRD patterns obtained for both the synthesized SiO_2 and the copper precipitate obtained by adding the sulfide containing growth media in the presence of this substrate. Again, the contribution of the CuS crystallite present in the precipitate containing amorphous SiO_2 is evidenced. The XRD analyses show that crystalline CuS (*covellite*) is present in all the prepared samples.

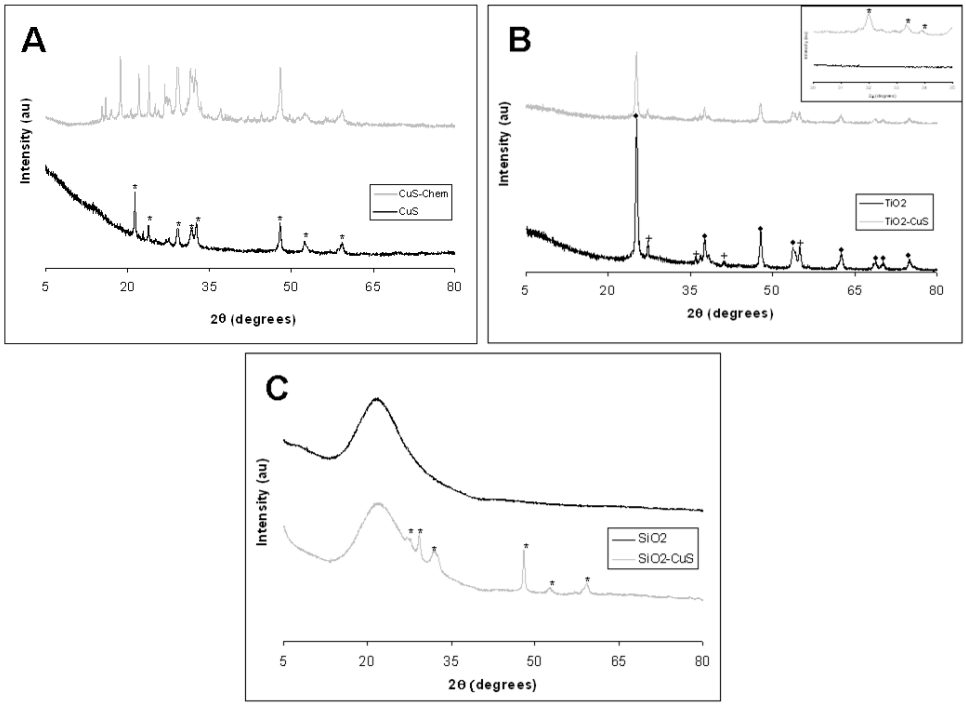

Figure 3.2 – XRD patterns of precipitates obtained in absence of a support and in presence of TiO_2 and SiO_2: (A) chemical precipitation of Cu (II) through the addition of Na_2S (CuS-Chem) and MSM growth media to a copper (II) solution (CuS), without any support; (B) same as CuS in (A), with TiO_2 from Degussa (P25) used as support and (C) with SiO_2 used as support. The "*" symbol refers to the peaks for *covellite* (ICDD PDF2 #01-078-0876), the symbol "♦" refers to the anatase phase (ICDD PDF2 #01-071-1167 and the "+" symbol to the rutile phase (ICDD PDF2 #01-076-1941) of TiO_2. Inset in B shows a section of the XRD pattern evidencing the presence of *covellite* in the TiO_2 composite.

Figure 3.3 shows the SEM images and corresponding EDX analysis for the powders prepared. The particles are predominantly spherical and nanosized. Agglomeration in small clusters of the analyzed sample disabled particle size distribution. EDX analysis confirmed the presence of copper and sulfur in all the samples (Figure 3.3D – 3.3F). As expected, titanium was identified in the precipitate in which TiO_2 was used as substrate (Figure 3.3E). For the sample obtained by adding the MSM medium in the presence of SiO_2, silicon was identified, as well as an additional peak for magnesium. The presence of magnesium may result from vestigial contamination coming from the growth

medium. EDX mapping (Appendix B) revealed the homogeneous distribution of copper sulfide on titanium oxide. On the other hand, the distribution of CuS on silicon dioxide support is of small clustered islands supported on the surface of spherical SiO_2 microparticles (Appendix B).

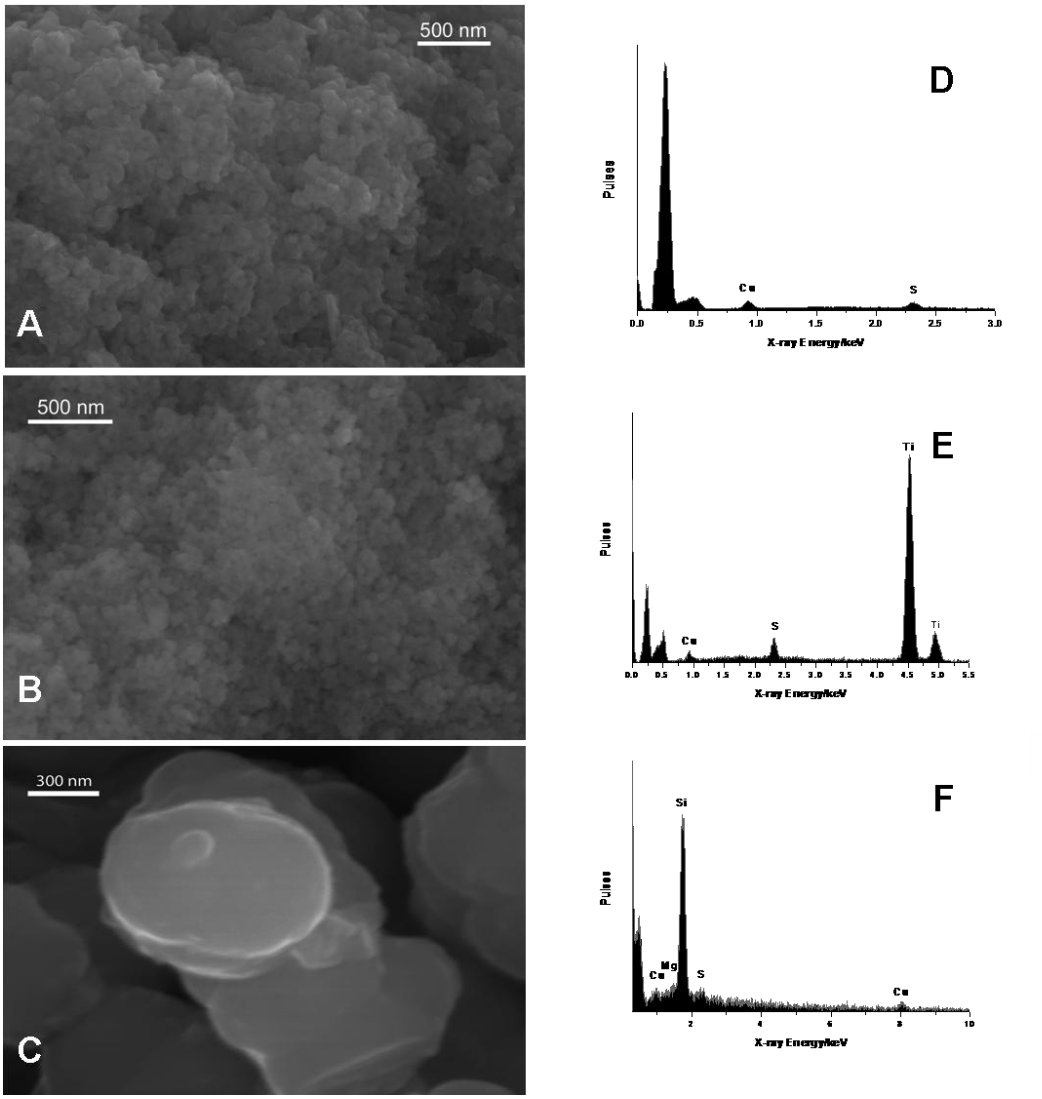

Figure 3.3 – SEM images and corresponding EDX spectra for the nanosized CuS particles, without any support (A, D) in the presence of TiO_2 (B, E) and SiO_2 (C, F).

Figure 3.4A shows the TEM image corresponding to the CuS particles obtained by precipitation of Cu (II) using the biogenic sulfide, with no support present, and the

particle size distribution plot (3.4D). The mean size of the spherical CuS nanoparticles was 3.3 nm ± 0.6 nm. Considering the nanophases obtained in the work of other authors, CuS particles with a hexagonal crystal structure (*covellite*) have been obtained using solvothermal methods (Li *et al*., 2010) and pyrolysis (Nascu *et al*., 1997). These were synthesized resorting to high temperatures with significant morphological differences to ours, consisting of nanoplates, nanorods and nanofilms. However, CuS nanoparticles with similar size (4 – 6 nm) and morphology (spherical) have been obtained using microemulsions at high pressures (Dong *et al*., 2002), but the crystal structure of these nanophases was not reported. Figures 3.4B and 3.4E show the TEM images obtained for the samples prepared in the presence of TiO_2. The particles observed have sizes ranging between 20 – 30 nm. Both size and morphology are in accordance with the information supplied by the manufacturer (Degussa). The homogeneous distribution of CuS on the surface of TiO_2 is evidenced in Figure 3.4E, with the black arrows denoting the titanium dioxide and white arrows the CuS. The particles obtained when CuS was precipitated in the presence of SiO_2, which are approximately 550 – 600 nm in diameter, as expected for the SiO_2 particles (Stober *et al*., 1968) are shown in Figure 3.4C and 4F. Isolated or clustered CuS nanoparticles were not observed, giving us strong evidence that the presence of SiO_2 during the precipitation process results in an uneven distribution of the CuS particles on the substrate's surface. These differences in the deposition of CuS on the surface of TiO_2 and SiO_2 are consistent with the results observed for other metal sulfides (Franco *et al*., 2009). The presence of a distinct deposited phase when using SiO_2 may be due to the more well-defined morphology and larger size of these particles, when compared to that of TiO_2 (da Costa *et al*., 2012).

For the particles obtained when using the UAPB reactor's sulfide-rich effluent, the XRD results showed that *covellite* (ICDD PDF2 #01-078-0876) was obtained (results not shown), which is identical to the results obtained in the batch system (Figure 3.2A). Such assertion is also valid for the synthesis of CuS in the presence of either TiO_2 (Figure 3.2B) or SiO_2 (Figure 3.2C), with the XRD results showing the presence of *covellite* in both samples (results not shown).

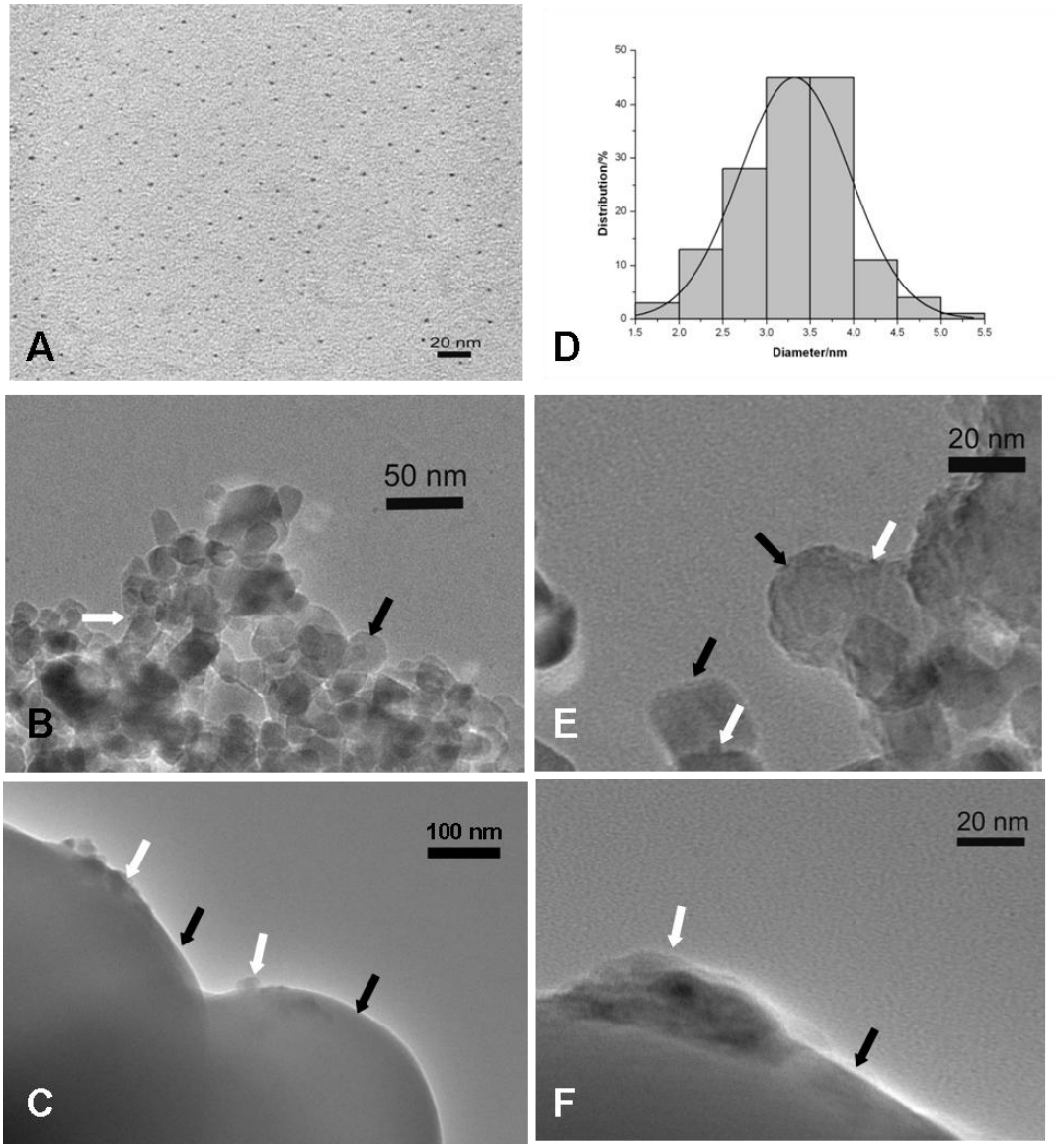

Figure 3.4 – TEM image (A) and corresponding particle size distribution plot (D) for nanosized CuS particles obtained by adding MSM growth media containing biologically generated sulfide to a Cu (II) solution. Also shown are the TEM images obtained for the samples prepared in the presence of TiO_2 (B and E) and SiO_2 (C and F). White arrows point out CuS in the presence of either TiO_2 (black arrows, B and E) or SiO_2 (black arrows, C and F).

In Figure 3.5, TEM, SEM and EDX results for the particles obtained when using the sulfide-rich effluent of the UAPB reactor are shown, either alone (3.5A, 3.5B and 3.5C)

or in the presence of TiO_2 (5D, 5E and 5F) or SiO_2 (5G, 5H and 5I). The CuS particles are spherical and have a mean size slightly smaller (3.2 ± 0.08 nm) than those obtained in the batch system (3.3 ± 0.6 nm), though this difference should not be considered significant. When using TiO_2 (black arrows, Figure 4E), the CuS (white arrows, Figure 3.5E) distribution appears to be homogeneous on the surface of this compound, which is consistent with the results obtained for the batch process (Figure 3.4E). Similarly, the distribution of CuS (white arrows, Figure 3.5H) on the surface of SiO_2 (black arrows, Figure 3.5H) is irregular, as in the case of the composites obtained in the batch method. Hence, the particles and nanocomposites of CuS have proven to be identical to those produced in a batch system, and, to the best of our knowledge, such strategy for the synthesis of CuS nanoparticles resorting to the sulfide-rich effluent from a bioremediation system, without the use of any additional agents, has not yet been reported.

Therefore, CuS nanoparticles can be obtained by this biological route and successfully supported on titanium and silicon dioxides. Moreover, these results confirm the relevance of the method described here to produce materials with potential interest as heterogeneous catalysts by using biologically generated sulfide as the precipitating agent in Cu (II) containing solutions, such as industrial and metallurgical effluents. Furthermore, it constitutes an innovative use for the excess sulfide produced in the bioremediation system.

Considering results previously obtained for ZnS particles (da Costa *et al*., 2012) and the different experimental settings used in the present work, such as pH, it opens up a window for a selective precipitation of either ZnS or CuS particles and their composites. Thus, this constitutes a promising and innovative route for obtaining added value products from wastes, with enormous potential in materials science, catalysis, fuel cells and electronics (Bo *et al*., 2010; Lopes *et al*., 2011; Solanki *et al*., 2010) through the integration of cleaner and sustainable methods in the industrial processes.

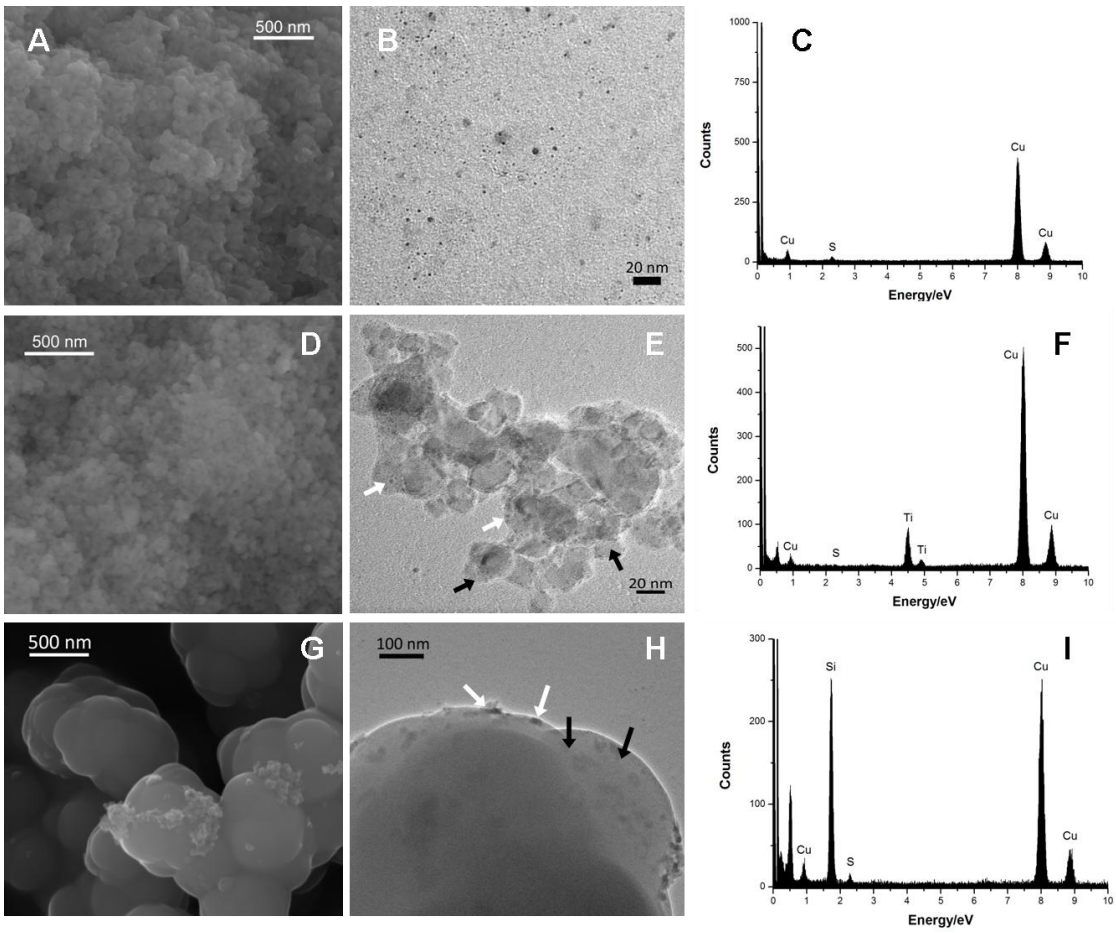

Figure 3.5 – SEM, TEM and EDX results for the nanosized CuS particles obtained by adding sulfide-rich effluent from a bioremediation system based on SRB (A, B and C, respectively). In D – F, the results for the TiO_2 (black arrows in E) and CuS (white arrows in E) composites are shown. Identically, the results for the SiO_2 (black arrows in H) and CuS (white arrows in H) composites (G – I) are also shown.

3.4. Conclusions

We have demonstrated that CuS nanocrystals (*covellite*) with a mean size of ~3.5 nm can be prepared by precipitating copper with biologically produced sulfide. Sulfide was produced by naturally occurring sulfate-reducing bacteria. Besides the economical advantage in the use of a biological source of sulfide, the high percentage of metal removal means an efficient production of nanocrystalline CuS. We also showed that the

use of TiO_2 and SiO_2 as substrates resulted in the respective composite materials. Furthermore, the synthesis method was successfully integrated into an existing bioremediation process, evidencing its potential for an overall "green" synthesis system of nanoparticles with simultaneous wastewater treatment. CuS nanoparticles and composites have been used in processes such as photocatalysis (Li *et al*., 2010; Stroyuk *et al*., 2004) and considering the simplicity of the process presented, this is a convenient route for the biological synthesis of functional materials, with potential applications in bioremediation systems.

Acknowledgements

Funding by Fundação para a Ciência e a Tecnologia (FCT) through a PhD grant (SFRH/BD/43784/2008) is acknowledged. A. V. Girão also thanks FCT for the Post-Doc grant (SFRH/BPD/66407/2009).

References

Akamatsu, K., Nakane, M., Sugawara, T., Hattori, T. and Nakao, S., 2008. Development of a membrane reactor for decomposing hydrogen sulfide into hydrogen using a high-performance amorphous silica membrane. J Membrane Sci, 325(1): 16-19.

Andronic, L., Isac, L. and Duta, A., 2011. Photochemical synthesis of copper sulphide/titanium oxide photocatalyst. J Photoch Photobio A, 221(1): 30-37.

Barros, R.J., Jesus, C., Martins, M. and Costa, M.C., 2009. Marble stone processing powder residue as chemical adjuvant for the biologic treatment of acid mine drainage. Process Biochem, 44(4): 477-480.

Bhagat, M., Burgess, J.E., Antunes, A.P.M., Whiteley, C.G. and Duncan, J.R., 2004. Precipitation of mixed metal residues from wastewater utilising biogenic sulphide. Minerals Engineering, 17(7-8): 925-932.

Bo, X.J., Bai, J., Wang, L.X. and Guo, L.P., 2010. In situ growth of copper sulfide nanoparticles on ordered mesoporous carbon and their application as nonenzymatic amperometric sensor of hydrogen peroxide. Talanta, 81(1-2): 339-345.

Costa, M.C. and Duarte, J.C., 2005. Bioremediation of acid mine drainage using acidic soil and organic wastes for promoting sulphate-reducing bacteria activity on a column reactor. Water Air Soil Poll, 165(1-4): 325-345.

da Costa, J.P., Girao, A.V., Lourenco, J.P., Monteiro, O.C., Trindade, T. and Costa, M.C., 2012. Synthesis of nanocrystalline ZnS using biologically generated sulfide. Hydrometallurgy, 117: 57-63.

Dong, X., Potter, D. and Erkey, C., 2002. Synthesis of CuS nanoparticles in water-in-carbon dioxide microemulsions. Ind Eng Chem Res, 41(18): 4489-4493.

Franco, A., Neves, M.C., Carrott, M.M.L.R., Mendonca, M.H., Pereira, M.I. and Monteiro, O.C., 2009. Photocatalytic decolorization of methylene blue in the presence of TiO(2)/ZnS nanocomposites. Journal of Hazardous Materials, 161(1): 545-550.

Garcia, C., Moreno, D.A., Ballester, A., Blazquez, M.L. and Gonzalez, F., 2001. Bioremediation of an industrial acid mine water by metal-tolerant sulphate-reducing bacteria. Minerals Engineering, 14(9): 997-1008.

Huisman, J.L., Schouten, G. and Schultz, C., 2006. Biologically produced sulphide for purification of process streams, effluent treatment and recovery of metals in the metal and mining industry. Hydrometallurgy, 83(1-4): 106-113.

Kamat, P.V., 2002. Photophysical, photochemical and photocatalytic aspects of metal nanoparticles. Journal of Physical Chemistry B, 106(32): 7729-7744.

Lewis, A. and van Hille, R., 2006. An exploration into the sulphide precipitation method and its effect on metal sulphide removal. Hydrometallurgy, 81(3-4): 197-204.

Lewis, A.E., 2010. Review of metal sulphide precipitation. Hydrometallurgy, 104(2): 222-234.

Li, F., Wu, J.F., Qin, Q.H., Li, Z. and Huang, X.T., 2010. Controllable synthesis, optical and photocatalytic properties of CuS nanomaterials with hierarchical structures. Powder Technol, 198(2): 267-274.

Liz-Marzan, L.M., 2006. Tailoring surface plasmons through the morphology and assembly of metal nanoparticles. Langmuir, 22(1): 32-41.

Lopes, T., Paganin, V.A. and Gonzalez, E.R., 2011. Hydrogen sulfide tolerance of palladium-copper catalysts for PEM fuel cell anode applications. Int J Hydrogen Energ, 36(21): 13703-13707.

Mallick, K., Witcomb, M.J. and Scurrell, M.S., 2007. Self assembly of the metal nanoparticles: Formation of the highly oriented, core-shell type, bimetallic gold-silver film. J Nanopart Res, 9(2): 323-330.

Martins, M., Faleiro, M.L., Chaves, S., Tenreiro, R. and Costa, M.C., 2010a. Effect of uranium (VI) on two sulphate-reducing bacteria cultures from a uranium mine site. Sci Total Environ, 408(12): 2621-2628.

Martins, M., Santos, E.S., Pires, C., Barros, R.J. and Costa, M.C., 2010b. Production of irrigation water from bioremediation of acid mine drainage: comparing the performance of two representative systems. J Clean Prod, 18(3): 248-253.

Nascu, C., Pop, I., Ionescu, V., Indrea, E. and Bratu, I., 1997. Spray pyrolysis deposition of CuS thin films. Mater Lett, 32(2-3): 73-77.

Sani, R.K., Peyton, B.M. and Brown, L.T., 2001. Copper-induced inhibition of growth of *Desulfovibrio desulfuricans* G20: assessment of its toxicity and correlation with those of zinc and lead. Appl Environ Microbiol, 67(10): 4765-72.

Solanki, J.N., Sengupta, R. and Murthy, Z.V.P., 2010. Synthesis of copper sulphide and copper nanoparticles with microemulsion method. Solid State Sci, 12(9): 1560-1566.

Stober, W., Fink, A. and Bohn, E., 1968. Controlled Growth of Monodisperse Silica Spheres in Micron Size Range. J Colloid Interf Sci, 26(1): 62-&.

Stroyuk, A.L., Raevskaya, A.E., Kuchmii, S.Y. and Kryukov, A.I., 2004. Catalytic activity of CuS nanoparticles in hydrosulfide ions air oxidation. J Mol Catal a-Chem, 212(1-2): 259-265.

Takeuchi, Y., Kudoh, Y. and Sato, G., 1985. The Crystal-Structure of Covellite Cus under High-Pressure up to 33-Kbar. Z Kristallogr, 173(1-2): 119-128.

Tiwari, A., Khan, S.A. and Kher, R.S., 2012. Synthesis, structural and optical characterization of nanocrystalline ZnS:Cu embedded in silica matrix. Curr Appl Phys, 12(3): 632-636.

Veeken, A.H.M., de Vries, S., van der Mark, A. and Rulkens, W.H., 2003. Selective precipitation of heavy metals as controlled by a sulfide-selective electrode. Separ Sci Technol, 38(1): 1-19.

Wang, H., Zhang, H.R., Zhao, X.N., Xu, S. and Zhu, J.J., 2002. Preparation of copper monosulfide and nickel monosulfide nanoparticles by sonochemical method. Mater Lett, 55(4): 253-258.

Appendix A

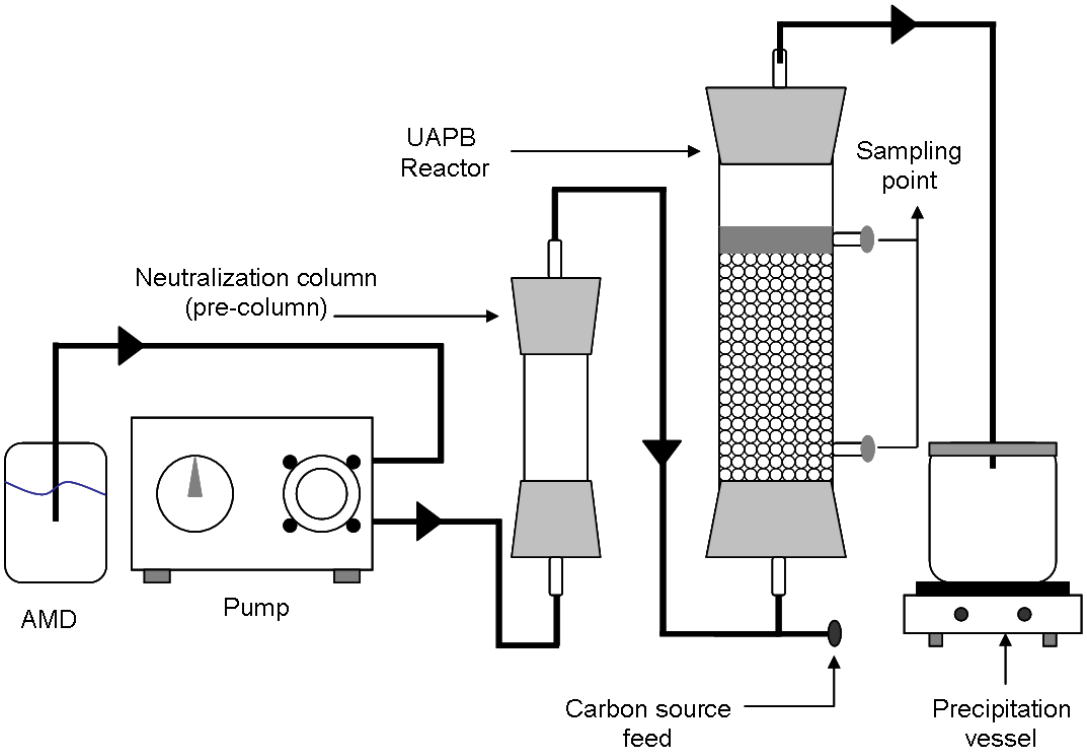

Figure 3.6 – Schematics of the bioremediation system used.

Appendix B

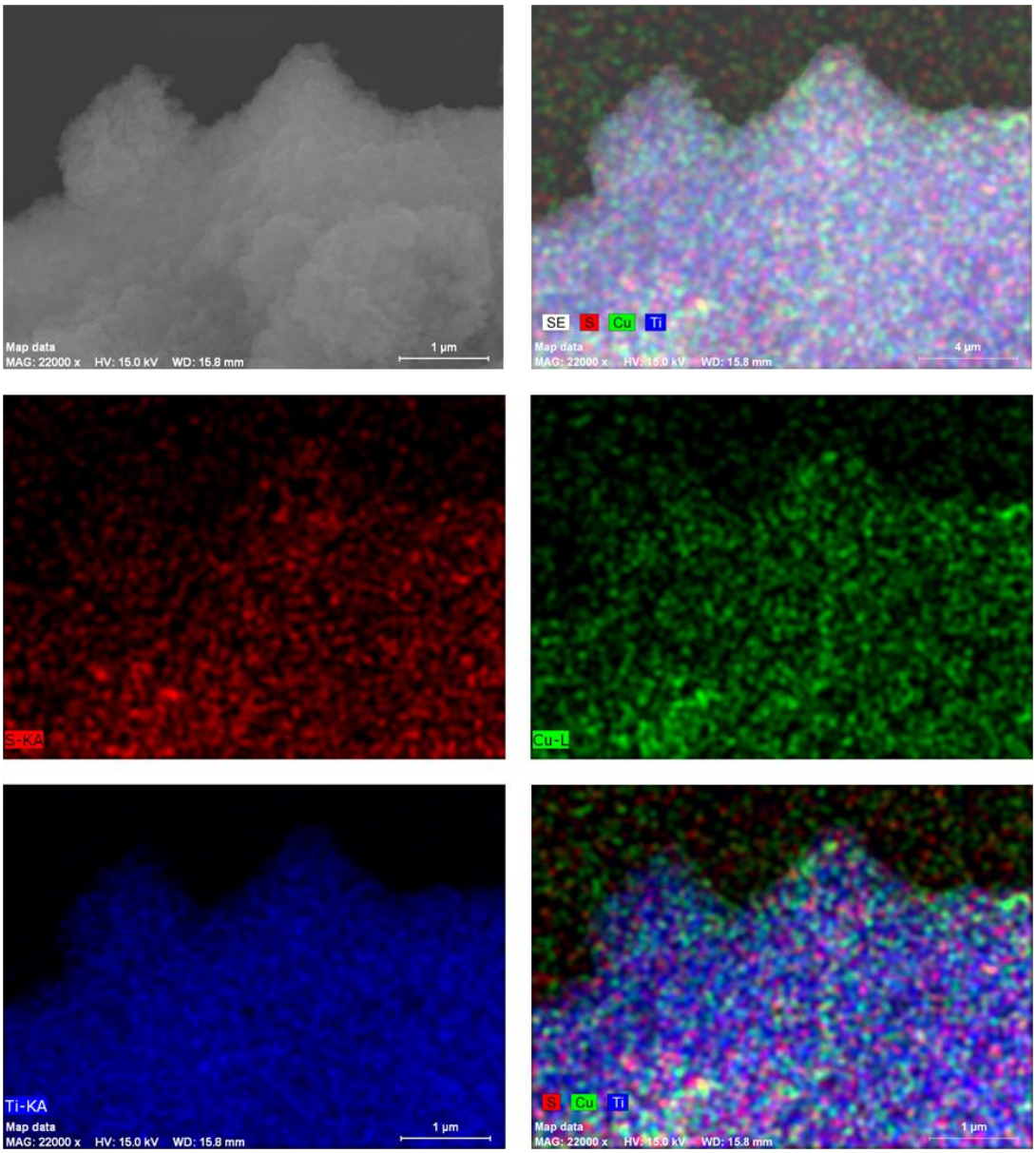

Figure 3.7 – SEM image and EDX mapping for the sample prepared in the presence of TiO_2, obtained by adding MSM growth media containing biologically generated sulfide to a copper (II) solution.

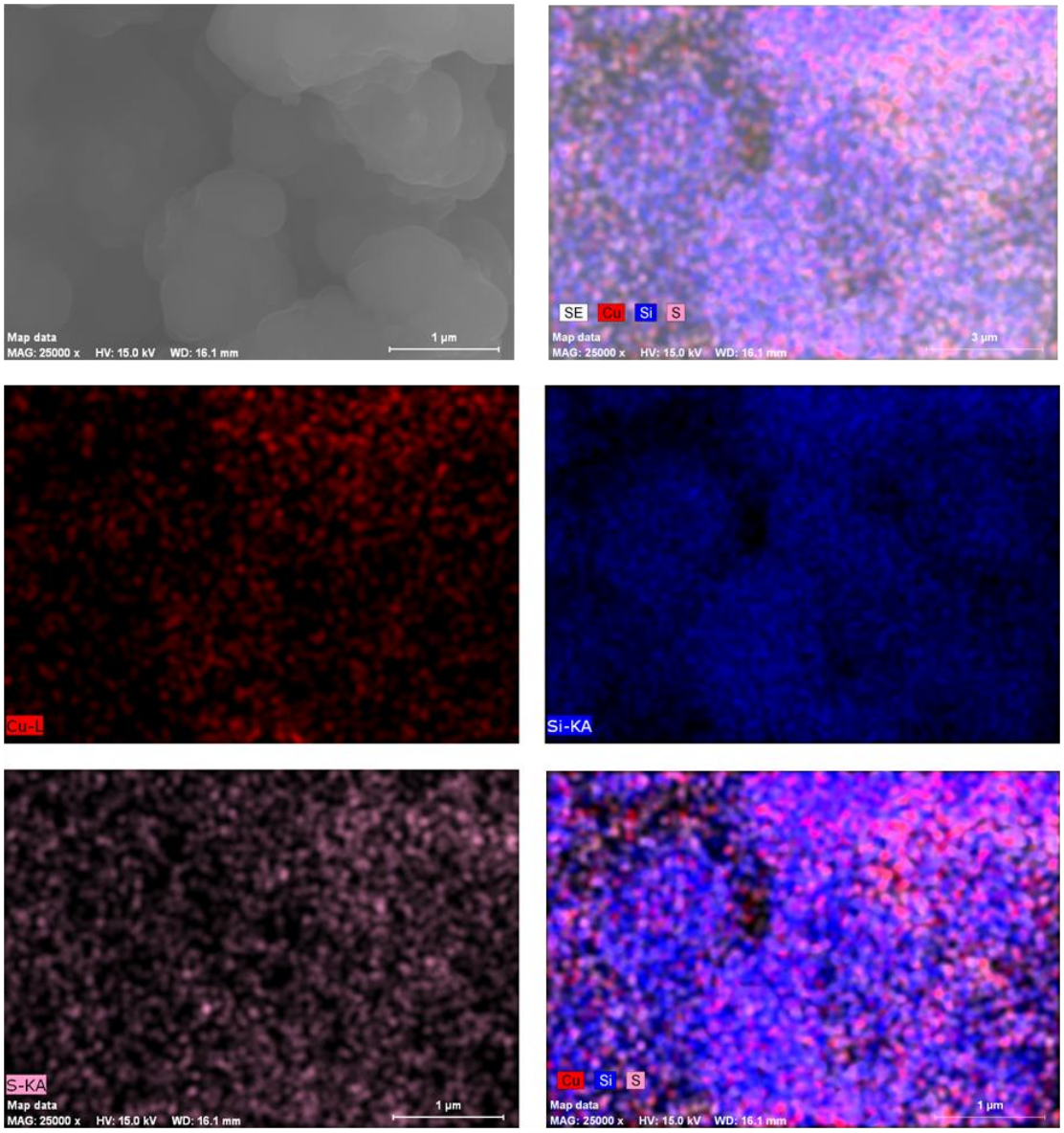

Figure 3.8 – SEM image and EDX mapping for the sample prepared in the presence of SiO2, obtained by adding MSM growth media containing biologically generated sulfide to a copper (II) solution.

Chapter 4 – Selective Precipitation of Biologically Generated Metal Sulfide Nanoparticles Using Artificial and Real Wastewaters

João Pinto da Costa[1], Ana Violeta Girão[2], João P. Lourenço[3], Tito Trindade[2], Maria Clara Costa[1,*]

[1]Universidade do Algarve, CCMar, Campus Gambelas, 8005-139 Faro, Portugal.

[2]Universidade de Aveiro, CICECO, 3810-193 Aveiro, Portugal.

[3]Universidade do Algarve, CIQA, FCT, Ed. 2, Campus Gambelas, 8005-139 Faro, Portugal.

*Corresponding author

Universidade do Algarve, Campus Gambelas

FCT – Edifício 8, Lab. 2.35

8005-139 Faro, Portugal

mcorada@ualg.pt

A modified version of this chapter has been submitted as:

da Costa, J., Girão, A. V., Lourenço, J. P., Trindade, T. and Costa, M. C., (2013), Selective precipitation of biologically generated metal sulfide nanoparticles using artificial and real wastewaters. Hydromet.

A modified section of this chapter has been published as:

da Costa, J., Girão, A. V., Lourenço, J. P., Monteiro, O. C., Trindade, T. and Costa, M. C., (2013), Integrated synthesis of nanosized semiconductors in a bioremediation system for the treatment of AMD using biologically produced sulfide. – In Brown, A., Figueroa, L. and Wolkersdorfer, Ch., Reliable Mine Water Technology, 1:693-699

Abstract

The selective recovery of metals from contaminated wastewaters can be made by precipitation of the corresponding metal sulfides provided that the latter possess very different solubilities. The use of sulfate reducing bacteria (SRB) to precipitate a metal sulfide is potentially advantageous due to *in situ* and on demand sulfide production. In this study, we have evaluated the selective precipitation of Cu(II), Zn(II) and Fe(II) cationic species in the form of nanosized metal sulfides. These metal species are contaminants commonly found in wastewaters of numerous metallurgical and mining industries. The studies have been carried out by using biologically produced sulfide in a continuous bioremediation system applied to both artificial and real wastewaters. We have found that this process allowed for the selective precipitation of copper ions but lower selectivity in the precipitation of zinc and iron ions. This process allowed the removal of over 95% of the metal content in the form of nanosized (4-30 nm) metal sulfide particles. The approach described here was then extended to the precipitation of the metal sulfides in the presence of SiO_2 microparticles, which act as heterogeneous substrates, aiming at their potential reuse in other applications.

Keywords: metal sulfide, nanoparticles, selective precipitation, sulfate-reducing bacteria, biological generated sulfide.

4.1. Introduction

During sulfide-mining operations, sulfidic rock comes into contact with surface or ground water, which, under oxidizing conditions, produces sulfuric acid and diverse iron solutes. The generated acidic water dissolve other metals present in rocks, thus resulting in a low pH, metal-bearing water, often known as acid mine drainage (AMD) or acid rock drainage (ARD) (Doshi, 2006). This problem is of great relevance in Portugal, because extensive sulfide mining activities have played an important role until very recently (Santos Oliveira, 2000). In some Portuguese regions the mine lakes can be very acidic (pH < 3) and high concentration of sulfates (up to 3.5 g/L) and heavy metals can be found, particularly iron, zinc and copper (Martins *et al.*, 2008). Given the potential for adverse environmental effects and burdensome recuperation costs, it is necessary to seek long-term cost-effective treatments for AMD (Doshi, 2006). In this context, bioremediation processes using sulfate-reducing bacteria (SRB) have proven to be a good solution (Garcia *et al.*, 2001; Huisman *et al.*, 2006). In this process, the bacteria use sulfate as the terminal electron acceptor during the metabolism of organic matter, resulting in the production of H_2S (Barnes *et al.*, 1992). Hence, biological sulfide is produced that can be used for metal sulfide precipitation in the presence of cationic species dissolved in water (Bhagat *et al.*, 2004). Such processes have been used in the treatment of both Portuguese (Costa and Duarte, 2005) and Spanish (Garcia *et al.*, 2001) AMD, more specifically, for the precipitation of Fe^{2+}, Zn^{2+} and Cu^{2+}.

The selective precipitation of diverse metal ions from wastewaters and soils has been performed using either chemical sulfide sources or biogenic sulfide (Bhagat *et al.*, 2004; Fang *et al.*, 2012; Fukuta *et al.*, 2004; Sahinkaya *et al.*, 2009; Sampaio *et al.*, 2009; Tokuda *et al.*, 2008; Veeken and Rulkens, 2003). The metal sulfides are obtained in most of the cases as micrometric powders (>1 μm) though our previous work (da Costa *et al.*, 2012; da Costa *et al.*, 2013) described the use of SRB growth media containing biologically produced sulfide to promote the precipitation of zinc and copper in the form of metal sulfide nanoparticles.

Herein, we describe our efforts to implement such methodologies for the selective precipitation of Cu(II), Fe(II) and Zn(II) using both artificial and real (AMD) solutions following a continuous bioremediation system. This system was then evaluated in terms

of obtaining the metal sulfide nanophases coupled to SiO_2 microparticles (Tiwari *et al.*, 2012), aiming at their eventual reuse. Inorganic nanocrystals exhibit size and surface dependent properties, which bestow them with a huge potential in a wide range of applications (Sweeney *et al.*, 2004). The materials obtained here in the form of metal sulfides (ZnS, CuS, FeS) or coupled to amorphous silica might be of special interest in applications such as odor removal (Singh *et al.*, 2010) and environmental remediation processes (Shi *et al.*, 2006).

4.2. Experimental

4.2.1 Bioremediation System and SRB Growth

Having been thoroughly described elsewhere (Martins *et al.*, 2010b), a brief description of the bioremediation system ensues. This was designed to be a simple, yet efficient continuous process that uses waste and/or natural cheap materials in order to become an economically and environmentally sustainable bioremediation process. It was composed of two column reactors and the simplified schematics of this bioremediation system can be found in Appendix A, Figure 4.6. In the first column, a mixture of calcite tailing and coarse sand (1:2, w/w) was used for the neutralization of the AMD. The second was an anaerobic up-flow packed bed reactor (UAPB) filled with approximately 900 g of coarse sand and 30 mL of inoculum. Modified Postgate medium (da Costa *et al.*, 2012) (300 mL) was also added and, in order to allow for the initial bacterial growth, the bioreactor was operated in batch conditions for 2 weeks. A SRB consortium enriched from the wetland of the Urgeiriça mine (North of Portugal) and selected from previous studies (Martins *et al.*, 2010a), containing mainly species affiliated to *Desulfovibrio desulfuricans*, was used as inoculum.

4.2.2 Metal Solutions and Metal Precipitation

It has been shown that the iron present in AMD waters exists, mainly, in the ferrous form (Hubbard *et al.*, 2009). Hence, for the present studies, we have chosen the metallic ions usually present in the Iberian AMD (Cu^{2+}, Zn^{2+} and Fe^{2+}).

After reaching continuous operation, the excess sulfide produced by the SRB in the bioremediation system was used as the sulfide source for the precipitation of the metals in solution, which ensues. The description of the samples is shown in Table 4.1. Schematics shown in Figure 4.1 illustrate the procedures followed.

Table 4.1 – List of used abbreviations and corresponding description for the studied samples.

Abbreviation	Description
SP	Precipitate obtained by adding biogenerated sulfide in a bioremediation system to an artificial metal-containing (Cu, Zn and Fe) solution
P-Si	Precipitate obtained by adding biogenerated sulfide in a bioremediation system to an artificial metal-containing (Cu, Zn and Fe) solution, with SiO_2.
AMD-SP	Precipitate obtained by adding biogenerated sulfide in a bioremediation system to AMD.
AMD-Si	Precipitate obtained by adding biogenerated sulfide in a bioremediation system to AMD., with SiO_2.

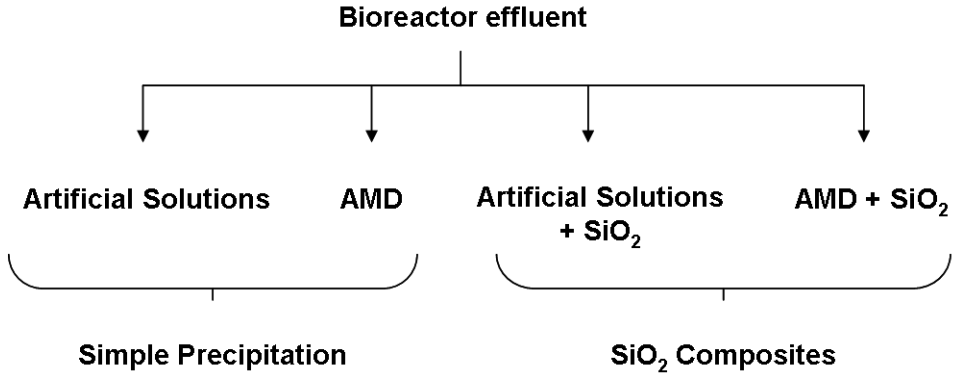

Figure 4.1 – Schematics illustrating the workflow for the selective precipitation of the metal ions using the sulfide-rich effluent from the bioreactor.

4.2.2.1 Artificial Solutions

The metal-containing solutions were prepared using distilled water and a combination of Cu^{2+} ($CuSO_4.5H_2O$, >99%, Riedel-de-Haën), Zn^{2+} ($ZnSO_4.7H_2O$, >99.5%, Panreac) and Fe^{2+} ($FeSO_4.7H_2O$, >99%, Panreac). These salts were added so that an approximate final concentration of 100 $mg.L^{-1}$ of each metal ion was obtained. The initial pH was corrected to 2.1, using a 6 M solution of HNO_3 (Panreac).

The precipitates were obtained by simply adding the sulfide rich media, with and without SiO_2 (P-Si and SP, respectively), which was used as support for the heterogeneous precipitation of the metal sulfides. The SiO_2 particles were prepared using a modified version of the Stöber method (Stober *et al.*, 1968) by mixing 1.12 mL of tetraethyl-orthosilicate (Merck KGaA), 24.75 mL of absolute ethanol (Panreac), and 5 mL of ammonia 20% (Panreac) to 8 mL of distilled water. This solution was stirred during 2 hours at room temperature. After filtration, the resulting white particles were dried and submitted to a thermal treatment at 700ºC for 4 hours The SiO_2 particle size varied between 550 – 600 nm (da Costa *et al.*, 2012).

The volume of growth culture added was calculated based on twice the sulfide content necessary to ensure the complete precipitation of the metal in the solution at each step. This was done in order to compensate for the losses of sulfide during the addition process. These metal solutions (50 mL) were purged with nitrogen and the containing flasks were sealed tight with a rubber cap, in order to avoid oxidation of the metals. The growth media addition was done drop-by-drop, under continuous magnetic stirring (Velp Scientifica), at room temperature. After each precipitation step, the pH of the resulting solution was measured, as well as the metal concentrations (Section 4.2). After precipitation, suspensions were centrifuged (Rotofix 32A, Hettich) for 10 minutes at 4000 rpm (~2900 RCF), washed with distilled water, centrifuged again (4000 rpm, 10 min) and dried under vacuum at room temperature (APT.Line VD, Binder). At each precipitation step, the supernatant was characterized after centrifugation, in terms of pH and metal concentration, and the pH was corrected to the lowest adequate pH value for the precipitation of the corresponding metal sulfide (Huisman *et al.*, 2006), by adding a 1M NaOH solution. This was done in order to minimize the addition of chemicals, such as acids, for the correction of the pH value, as the addition of the sulfide-rich media would result in an increase of the pH solution. Again, the metal solutions were purged with nitrogen and the flasks sealed, before proceeding to the next precipitation step. At each stage, the precipitates were washed with distilled water, centrifuged under the previously described conditions and dried under vacuum at room temperature.

4.2.2.2 AMD

The AMD feeding the UAPB reactor has been previously characterized (Costa *et al.*, 2008) and, briefly, shows a sulfate content of 3.1 $g.L^{-1}$, pH value of 2.1 and a concentration of 49 $mg.L^{-1}$, 107 $mg.L^{-1}$ and 497 $mg.L^{-1}$ for copper, zinc and iron, respectively. This same AMD was used as the source of the metals for their precipitation by adding the sulfide-rich effluent. The procedure followed was identical to that described in the previous section.

4.2.3 Analytical Methods

Sulfide concentration was measured immediately after sampling using a UV-visible spectrophotometer (DR2800 spectrometer, Hach-Lange) by the Methylene Blue Method (665 nm, Hach-Lange). Sulfate concentration was also measured by UV/visible spectroscopy at 450 nm using the SulfaVer4 method (Hach-Lange). The pH values were measured using a pH Meter (GLP 21, Crison). Metal concentrations, before and after precipitation, were determined by flame atomic absorption spectroscopy using a Shimadzu AA-680 model spectrometer. For each sample, three aliquots were considered. In the precipitates, the presence of crystalline phases was assessed by XRD, using the X'Pert Powder (PANalytical, Surrey, UK) with X'Celerator detector, at 45 kV and 40 mA, with a step size of 0.016. The HighScore software was used for peak identification and phase analysis.

The formed precipitates were evaluated by micro-morphology and elemental composition. Scanning Electron Microscopy (SEM) was performed using a Field Emission Gun (FEG) SEM Hitachi SU70 operating at 15 kV. The latter enabled image acquisition in both common SEM and Bright-Field Transmission modes (SEM-STEM mode, copper grid). The samples were prepared by deposition of an aliquot of the samples directly onto the carbon tape and then coated by carbon evaporation (Emitech K950X). Transmission Electron Microscopy (TEM) coupled to EDX was carried out using a FEG-TEM Hitachi H9000 microscope operated at 300 kV. The samples were

prepared by placing a drop, containing the precipitates dispersed in ultra-pure distilled water, on a copper grid coated with amorphous carbon.

4.3. Results and Discussion

4.3.1. Simple Precipitation

4.3.1.1 Artificial Solutions

Figure 4.2 shows the removal percentages of each metal, as well as their concentrations, after each step (4.2A–4.2C) and for the overall process (4.2D). As observed in Figure 4.2A, the first precipitation step seems to be very effective in the removal of copper, resulting also in the precipitation of minor amounts of zinc and iron. In the second step, there was some simultaneous precipitation of both zinc and iron and, at the final precipitation step, iron was almost totally removed. At the end of the process, the solutions (Figure 4.2D) showed trace amounts of metal. Removal percentages ranged from 93% to over 97% (Figure 4.2D), thus attesting to the efficiency of this process in removing the studied metals from water. These results are consistent with those obtained by other authors when using chemical sources of sulfide (Kuchar *et al.*, 2010; Sampaio *et al.*, 2009; Soya *et al.*, 2010; Tokuda *et al.*, 2008) and biogenic sulfide for the selective recovery of metals from other mixed metal systems (Bhagat *et al.*, 2004; Fang *et al.*, 2012; Sahinkaya *et al.*, 2009). These results also indicate the potential of this process for the decontamination of metal-containing waters with concomitant selective synthesis of metal sulfides.

The precipitates obtained at each step were analyzed by powder X-ray diffraction (XRD) and the results are shown in Figures 4.3A – 4.3C. The Bragg reflections corresponding to the *covellite* phase (CuS, JCPD #00-001-1281) are evident in the diffractogram of the precipitate obtained at the first precipitation step (4.3A). Although with lower intensity, such peaks were also identified in the XRD diffractograms of powders obtained at precipitation steps two and three. This indicates that *covellite* is still present in these precipitates but in lower quantities. At the second precipitation step (Figure 4.3A), the most intense observed reflections are consistent to those corresponding to *sphalerite* (ZnS, JCPD #00-003-0579). These also contribute to the diffractogram of the precipitate obtained at the third precipitation step, in which peaks corresponding to iron (III) hydroxide were also identified (JCPD #00-038-0032).

Overall, the results seem to be in accordance with those illustrated in Figure 4.2, further confirming that the sulfide precipitation process herein applied is selective for copper but less selective for zinc and iron. The formation of iron hydroxides can be explained by the side reactions that follow the addition of NaOH for pH correction. Other unidentified phases, which may include nitrates, chlorides and carbonates present and formed in the growth media (Bhagat *et al.*, 2004), are also present in vestigial amounts.

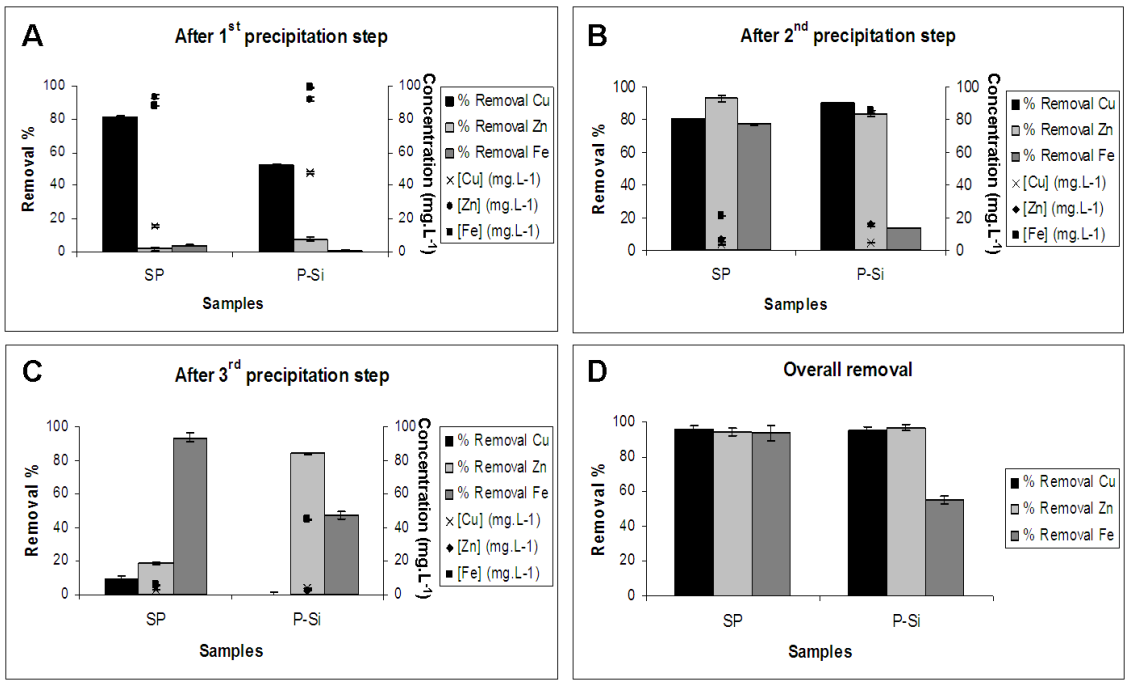

Figure 4.2 - Metal (Cu, Zn and Fe) removal percentage and concentration at the end of the first precipitation step (4.2A), second precipitation step (4.2B) and final (third) precipitation step (4.2C). The overall removal percentage for each metal is shown in 4.2D. Error bars are shown. The used abbreviations describe whether SiO_2 was used (P-Si), or not (SP). Results pertain to the use of artificial solutions as the metal source.

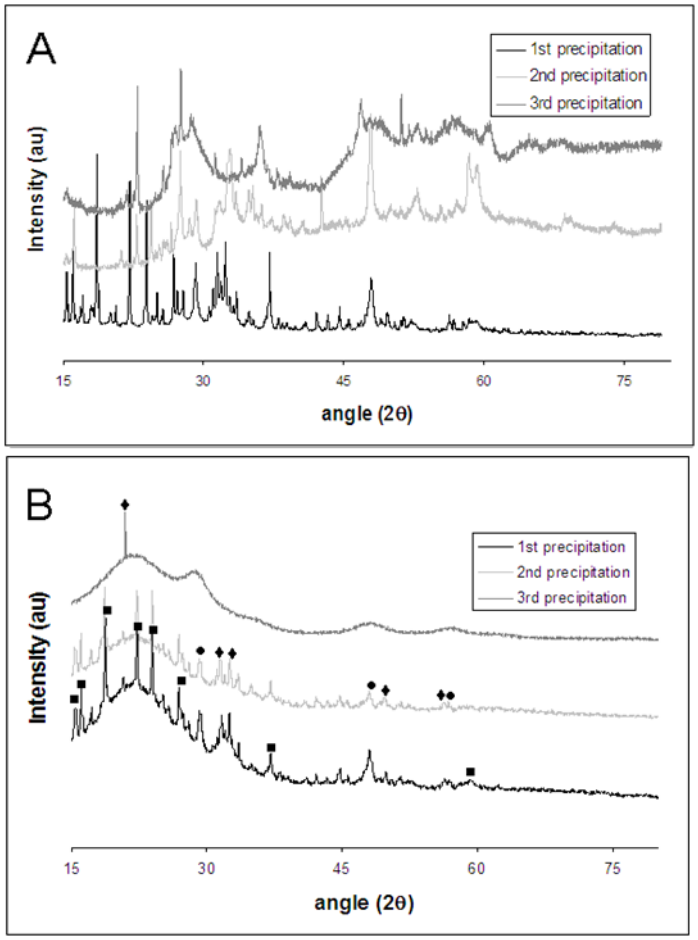

Figure 4.3 – X-ray diffractograms of the precipitates obtained at each step, without any support (4.3A) and in the presence of SiO_2 microparticles (4.3B) when using artificial solutions as the metal source. Symbol "■" refers to *covellite* (JCPD #00-001-1281), "●" to *sphalerite* (JCPD #00-003-0579) and symbol "♦" refers to iron (III) hydroxide (JCPD #00-038-0032).

SEM analyses were also carried out for the precipitates obtained at each step. These are shown in Figure 4.7 (Appendix B). Briefly, all the precipitates showed spheroidal morphology, with sizes ranging between 4 and 30 nm, with smaller particles observed in the precipitate formed at the end of the first step. This is consistent with our previous results (da Costa *et al.*, 2013), in which copper sulfide nanoparticles with average size below 5 nm have been obtained. In the precipitate obtained at the second step, besides spheroidal particles, needle-like particles were also observed (Figure 4.7E, Appendix B). The needle-like particles were approximately 100 nm long and only a few nanometers wide; spheroid particles showed to be 20–30 nm in diameter, which is in

accordance with results previously reported (da Costa *et al.*, 2012). Overall, the results are consistent with the XRD analyses (Figure 4.3), and the EDX analyses confirm these findings (Figure 4.7, Appendix B). In the last obtained precipitate, agglomeration prevented a thorough analysis, though it is possible to verify that spheroid particles seemed to be approximately the same size in diameter as those obtained in the previous precipitation step. EDX studies showed the presence of all the used metals, but also other elements, such as Si, which may result from a cross-contamination due to the fact that the samples were kept in glass vials; P and Cl may be present due to the growth media composition (da Costa *et al.*, 2012).

3.1.2 AMD

Similar experiments to those described above were also performed using real AMD as the source of metals. These results are shown in Figure 4.8 (Appendix B) and are identical to those obtained when using artificial solutions. As such, most of dissolved copper (70 – 80%) is removed at the first precipitation step (Figure 4.8A, Appendix B). At the second precipitation step, over 80% of the remaining zinc is removed, but up to 70% of iron present in solution precipitates simultaneously (Figure 4.8B, Appendix B). In the third and last precipitation step, the remaining iron is removed and all metal ions in solution seem to be present at concentrations lower than 8 $mg.L^{-1}$ (Figure 4.8C, Appendix B).

The crystalline phases present in the precipitates formed in this case have been identified as follows (Figure 4.9, Appendix B). The *covellite* phase (CuS, JCPD #00-001-1281) was identified for precipitates obtained in the first step. At the second and third precipitation steps, the most intense peaks observed are consistent to those corresponding to *sphalerite* (ZnS) (JCPD #00-003-0579) and iron (III) hydroxide (JCPD #00-038-0032), respectively.

Figure 4.10 in Appendix B shows the SEM, TEM and EDX results for the precipitates obtained at each step. TEM results showed that for the first precipitate obtained (Figure 4.10B, Appendix B) very small particles are formed (< 5 nm), consistent with previously obtained results (da Costa *et al.*, 2013). Surprisingly, the particles appear to

be slightly smaller than those obtained using artificial solutions as the source of metals (Figure 4.6B, Appendix B), though this difference in size may be due to some aggregation phenomena in the latter. The presence of titanium can be the result of a minor cross-contamination, though it is also possible that this is the result of Ti being naturally found in Iberian AMD (López-González *et al.*, 2006).

4.3.3 SiO_2-Metal Sulfide Composites

Metal sulfide coated silica particles have been explored in numerous applications (Darbandi *et al.*, 2012; Shi *et al.*, 2006; Singh *et al.*, 2010). Hence, resorting to the previously described method, we attempted the selective precipitation of metal sulfides in the presence of SiO_2.

4.3.3.1 Artificial Solutions

Figure 4.2 shows the removal percentage of each metal, as well as their concentrations, after each step (4.2A–4.2C) and for the overall process (2D). Whenever SiO_2 is used, there seems to be a decrease in metal removal efficiency. When no silica is present, over 80% of copper is removed in the first precipitation step. In the presence of SiO_2, just over 55% of this metal is removed (Figure 4.2). Similarly, at the second precipitation step, zinc is removed to a lower extent when silica is present. At the last precipitation step (Figure 4.2C), the removal of iron is lower than 50% in the presence of SiO_2, markedly lower to that observed when no silica is used (>93%). This lower removal efficiency in the overall process is illustrated in Figure 4.2D: although copper and zinc are removed in the presence of SiO_2, iron is not. This may be due to the fact that amorphous SiO_2 has been shown to decompose hydrogen sulfide (Akamatsu *et al.*, 2008), thus resulting in a lower availability of soluble sulfide species (SSS) involved in the metals precipitation. Consequently, future studies will require that this lower availability of SSS in the presence of SiO_2 is compensated.

In Figure 4.3B, the X-ray diffractograms for the precipitates obtained at each step in the presence of SiO_2 are shown. The results were identical to those obtained when no silica

was used. Briefly, the first precipitate showed, mostly, reflections corresponding to *covellite* (CuS, JCPD #00-001-1281). The most intense observed reflections for the second precipitate obtained are consistent with the presence of *sphalerite* (ZnS, JCPD #00-003-0579). Finally, the precipitate obtained in the last step shows peaks corresponding to iron (III) hydroxide (JCPD #00-038-0032). Again, there are peaks unassigned, which may correspond to nitrates, carbonates and chlorides (Bhagat *et al.*, 2004)

In Figure 4.4, TEM, SEM and EDX results for the obtained precipitates in conditions identical to those described in Figure 4.7 (Appendix B), but synthesized in the presence of SiO_2, are shown. As expected, the silica particles are spheroid and 500 – 600 nm in size. Additionally, the deposition of the precipitates takes place at the surface of the SiO_2, which is consistent with results previously obtained (da Costa *et al.*, 2012), as well as with those reported by other authors (Franco *et al.*, 2009; Stober *et al.*, 1968). Other elements, such as Ca and P, were also identified, and, as previously stated, this presence may be due to the composition of the growth media (da Costa *et al.*, 2012).

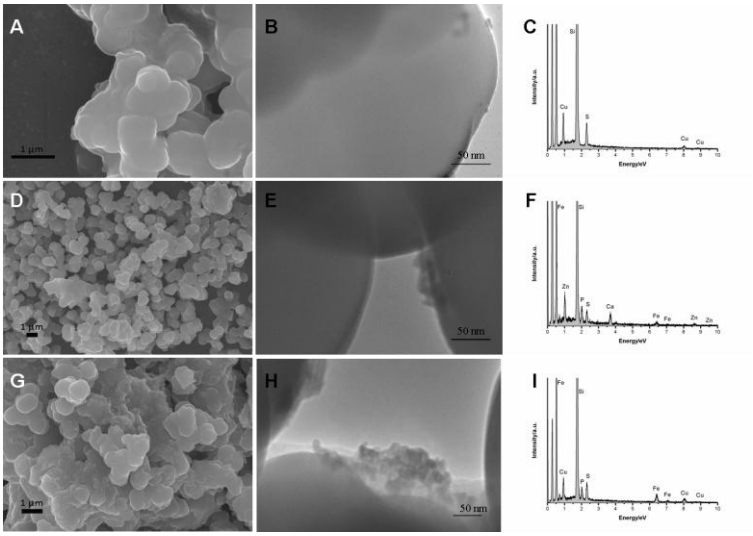

Figure 4.4 – SEM, TEM and EDX results for the precipitates obtained in the presence of SiO_2 microparticles. Figures A through C show the SEM, TEM and EDX results for the precipitate obtained at the end of the first precipitation step. Figures D through F correspond to the same set of analyses for the precipitate obtained at the end of the second precipitation step. Identically, G through I show the equivalent results for the precipitate obtained at the final third step.

4.3.3.2 AMD

Again, results concerning the precipitation efficiency of metals from AMD in the presence of SiO_2 are identical to those previously described. Consistent with the results obtained using artificial solutions, whenever silica is used the removal efficiency seems to be inferior (Figures 4.8A – 4.8D, Appendix B).

When analyzing the XRD results obtained for the precipitates obtained in the presence of silica (Figure 4.9, Appendix B), there seems to be some discrepancy between these and when no SiO_2 is used. Though the peaks with the most intense reflections are consistent with hexagonal covellite, the crystallites identified showed different lattice parameters (CuS, JCPD #03-065-3929). The second precipitate showed intense reflections corresponding to *sphalerite* (ZnS, JCPD #00-003-0579). Finally, the precipitate obtained in the last step showed peaks corresponding to both iron (III) hydroxide (JCPD #00-038-0032) and ZnS (JCPD #00-003-0579). Interestingly, there seems to be a lower complexity of the precipitates formed, though some unidentified peaks are also visible. These may correspond to nitrates, carbonates and chlorides (Bhagat *et al.*, 2004).

SEM and TEM-EDX results are shown in Figure 4.5 and are somewhat identical to those obtained when using artificial solutions. As expected, spheroid particles of silica were observed in all samples, with sizes ranging between 550 and 600 nm. TEM results evidenced that precipitation also occurred at the surface of the SiO_2 particles, which is consistent with results previously attained (da Costa *et al.*, 2012).

Other authors have reported the successful utilization of H_2S in the selective precipitation of metal sulfides but using different multi-metal systems (Fang *et al.*, 2012; Fukuta *et al.*, 2004; Sampaio *et al.*, 2009; Tokuda *et al.*, 2008; Veeken and Rulkens, 2003). The overall removal percentages are quite similar to those obtained in our work, ranging from 86% for zinc to 99% for copper. However, most of these studies versed on the utilization of chemical hydrogen sulfide. When biologically produced sulfide was used, the obtained particles were, at best, at the micrometric range (Fang *et al.*, 2012; Sahinkaya *et al.*, 2009), or unreported (Alvarez *et al.*, 2007; Bhagat *et al.*, 2004). The method herein described allows for the synthesis of nanosized metal sulfides, as well as the corresponding SiO_2 composites. Although a lower selectivity in

the recovery of iron and zinc was observed, such limitation may be overcome by using an online system for the pH measurement and correction. Consequently, this will enable a better control of this parameter (Kalin *et al.*, 2006). Another alternative, suggested by Wang and collaborators (Wang *et al.*, 2013) proposes the control of the pH – redox potential (Eh) system, which may lead to an enhanced selectivity when precipitating iron, copper and zinc as sulfides. Considering the simplicity of the process presented, this is a convenient route for the biological synthesis of functional materials, with potential applications in bioremediation systems.

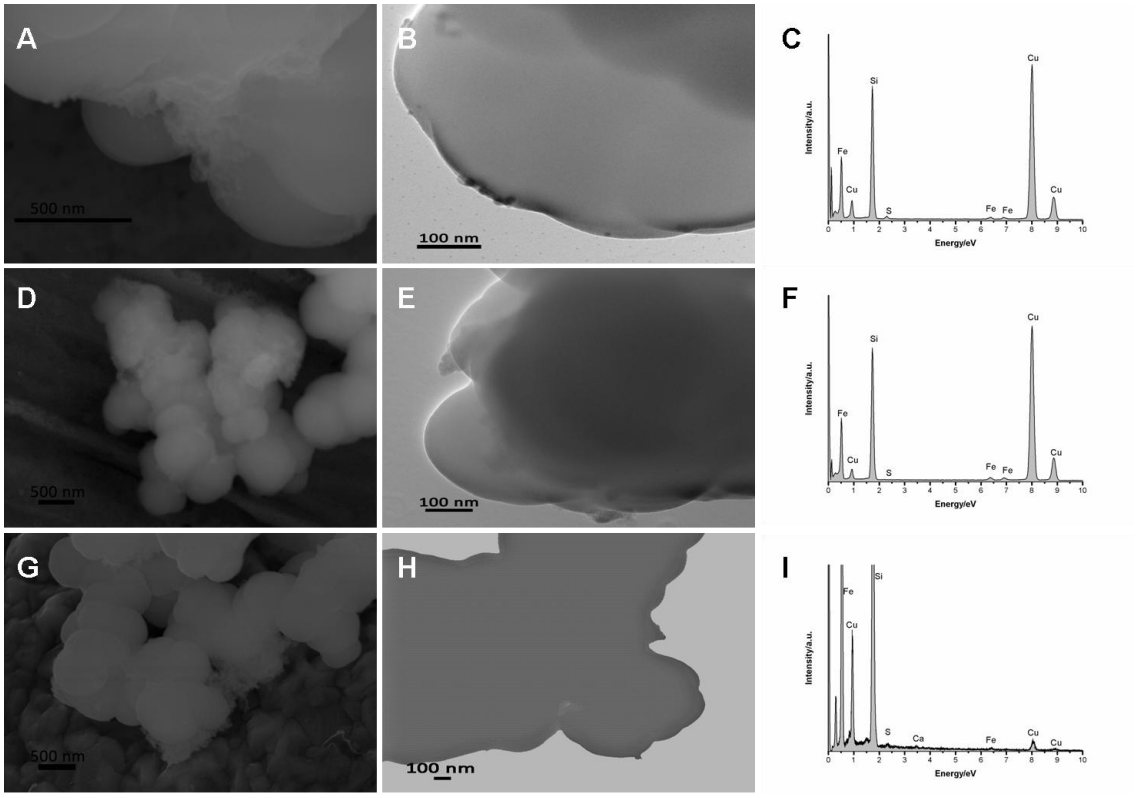

Figure 4.5 – SEM, TEM and EDX results for the precipitates obtained when using AMD and in the presence of SiO_2 microparticles. Figures A through C show the SEM, TEM and EDX results for the precipitate obtained at the end of the first precipitation step. Figures D through F correspond to the same set of analyses for the precipitate obtained at the end of the second precipitation step. Identically, G through I show the equivalent results for the precipitate obtained at the third final step (image H was acquired in the Bright-Field SEM-STEM mode).

4.4. Conclusions

In this work, we have demonstrated that a well established bioremediation system, based on the use of SRB for the production of irrigation water from AMD, can be successfully applied in an integrated system for the selective precipitation of metals as nano-sized semiconductors, resulting in over 95% of metal removal from the analyzed water systems. Selective precipitation and formation of corresponding composites with silica microparticles was also carried out, although it resulted in lower removal efficiency of the metals. The process has shown high selectivity for copper, when using both AMD and artificial metal-containing solutions. The obtained nanoparticles ranged between 4 and 30 nm, mainly presenting spheroid morphology. The observed lower selectivity system used for the precipitation of zinc and iron should be addressed in future studies, which would focus on the feasibility and adequacy in the use of a pH – redox potential system for selectively obtaining these metals as sulfides, also using biologically produced sulfide.

Acknowledgements

Funding by Fundação para a Ciência e a Tecnologia (FCT) through a PhD grant (SFRH/BD/43784/2008) and through project PTDC/AAG-TEC/2721/2012 is acknowledged. A. V. Girão also thanks FCT for the Post-Doc grant (SFRH/BPD/66407/2009).

References

Akamatsu, K., Nakane, M., Sugawara, T., Hattori, T. and Nakao, S., 2008. Development of a membrane reactor for decomposing hydrogen sulfide into hydrogen using a high-performance amorphous silica membrane. J Membrane Sci, 325(1): 16-19.

Alvarez, M.T., Crespo, C. and Mattiasson, B., 2007. Precipitation of Zn(II), Cu(II) and Pb(II) at bench-scale using biogenic hydrogen sulfide from the utilization of volatile fatty acids. Chemosphere, 66(9): 1677-1683.

Barnes, L.J., Janssen, F.J., Scheeren, P.J.H., Versteegh, J.H. and Koch, R.O., 1992. Simultaneous Microbial Removal of Sulfate and Heavy-Metals from Waste-Water. T I Min Metall C, 101: C183-C189.

Bhagat, M., Burgess, J.E., Antunes, A.P.M., Whiteley, C.G. and Duncan, J.R., 2004. Precipitation of mixed metal residues from wastewater utilising biogenic sulphide. Minerals Engineering, 17(7-8): 925-932.

Costa, M.C. and Duarte, J.C., 2005. Bioremediation of acid mine drainage using acidic soil and organic wastes for promoting sulphate-reducing bacteria activity on a column reactor. Water Air Soil Poll, 165(1-4): 325-345.

Costa, M.C., Martins, M., Jesus, C. and Duarte, J.C., 2008. Treatment of acid mine drainage by sulphate-reducing bacteria using low cost matrices. Water Air Soil Poll, 189(1-4): 149-162.

da Costa, J.P., Girao, A.V., Lourenco, J.P., Monteiro, O.C., Trindade, T. and Costa, M.C., 2012. Synthesis of nanocrystalline ZnS using biologically generated sulfide. Hydrometallurgy, 117: 57-63.

da Costa, J.P., Girão, A.V., Lourenço, J.P., Monteiro, O.C., Trindade, T. and Costa, M.C., 2013. Green synthesis of covellite nanocrystals using biologically generated sulfide: Potential for bioremediation systems. J Environ Manage, 128(0): 226-232.

Darbandi, M., Urban, G. and Krüger, M., 2012. Bright luminescent, colloidal stable silica coated CdSe/ZnS nanocomposite by an in situ, one-pot surface functionalization. J Colloid Interf Sci, 365(1): 41-45.

Doshi, S.M., 2006. Bioremediation of Acid Mine Drainage Using Sulfate-Reducing Bacteria. U.S. Environmental Protection Agency.

Fang, D., Zhang, R., Liu, X. and Zhou, L., 2012. Selective recovery of soil-borne metal contaminants through integrated solubilization by biogenic sulfuric acid and precipitation by biogenic sulfide. Journal of Hazardous Materials, 219–220(0): 119-126.

Franco, A., Neves, M.C., Carrott, M.M.L.R., Mendonça, M.H., Pereira, M.I. and Monteiro, O.C., 2009. Photocatalytic decolorization of methylene blue in the presence of TiO2/ZnS nanocomposites. Journal of Hazardous Materials, 161(1): 545-550.

Fukuta, T., Ito, T., Sawada, K., Kojima, Y., Matsuda, H. and Seto, F., 2004. Separation of Cu, Zn and Ni from plating solution by precipitation of metal sulfides. Kagaku Kogaku Ronbun, 30(2): 227-232.

Garcia, C., Moreno, D.A., Ballester, A., Blazquez, M.L. and Gonzalez, F., 2001. Bioremediation of an industrial acid mine water by metal-tolerant sulphate-reducing bacteria. Minerals Engineering, 14(9): 997-1008.

Hubbard, C.G., Black, S. and Coleman, M.L., 2009. Aqueous geochemistry and oxygen isotope compositions of acid mine drainage from the Rio Tinto, SW Spain, highlight inconsistencies in current models. Chem Geol, 265(3-4): 321-334.

Huisman, J.L., Schouten, G. and Schultz, C., 2006. Biologically produced sulphide for purification of process streams, effluent treatment and recovery of metals in the metal and mining industry. Hydrometallurgy, 83(1-4): 106-113.

Kalin, M., Fyson, A. and Wheeler, W.N., 2006. The chemistry of conventional and alternative treatment systems for the neutralization of acid mine drainage. Sci Total Environ, 366(2): 395-408.

Kuchar, D., Fukuta, T., Kubota, M. and Matsuda, H., 2010. Recovery of Cu, Zn, Ni and Cr from plating sludge by combined sulfidation and oxidation treatment. Internatl J Civil Environ Eng, 2: 62-66.

López-González, N., Borrego, J., Ruiz, F., Carro, B., Lozano-Soria, O. and Abad, M., 2006. Geochemical variations in estuarine sediments: Provenance and environmental changes (Southern Spain). Estuarine, Coastal and Shelf Science, 67(1–2): 313-320.

Martins, M., Faleiro, M.L., Chaves, S., Tenreiro, R. and Costa, M.C., 2010a. Effect of uranium (VI) on two sulphate-reducing bacteria cultures from a uranium mine site. Sci Total Environ, 408(12): 2621-2628.

Martins, M., Santos, E.S., Pires, C., Barros, R.J. and Costa, M.C., 2010b. Production of irrigation water from bioremediation of acid mine drainage: comparing the performance of two representative systems. J Clean Prod, 18(3): 248-253.

Martins, M.S.F., Santos, E.S., Barros, R.J.J. and Costa, M.C.S.D., 2008. Treatment of Acid Mine Drainage with Sulphate-reducing Bacteria Using a Two-stage Bioremediation Process. Mine Water and the Environment, Proceedings: 297-300

Sahinkaya, E., Gungor, M., Bayrakdar, A., Yucesoy, Z. and Uyanik, S., 2009. Separate recovery of copper and zinc from acid mine drainage using biogenic sulfide. Journal of Hazardous Materials, 171(1-3): 901-906.

Sampaio, R.M.M., Timmers, R.A., Xu, Y., Keesman, K.J. and Lens, P.N.L., 2009. Selective precipitation of Cu from Zn in a pS controlled continuously stirred tank reactor. Journal of Hazardous Materials, 165(1-3): 256-265.

Santos Oliveira, J.M., Machado Leite, M. R., Canto Machado, M. J., Pedrosa, M. Y., 2000. Auréolas de Dispersão Química Causadas pela Actividade Mineira. Estratégias e uma Metodologia Técnico-científica com Vista à sua Avaliação e Hierarquização. Boletim de Minas, 37.

Shi, X., Sun, K., Balogh, L.P. and Baker Jr, J.R., 2006. Synthesis, characterization, and manipulation of dendrimer-stabilized iron sulfide nanoparticles. Nanotechnology, 17(18): 4554.

Singh, A., Krishna, V., Angerhofer, A., Do, B., MacDonald, G. and Moudgil, B., 2010. Copper Coated Silica Nanoparticles for Odor Removal. Langmuir, 26(20): 15837-15844.

Soya, K., Mihara, N., Kuchar, D., Kubota, M., Matsuda, H. and Fukuta, T., 2010. Selective sulfidation of copper, zinc and nickel in plating wastewater using calcium sulfide. Internat J Civil Environ Eng, 2: 93-97.

Stober, W., Fink, A. and Bohn, E., 1968. Controlled Growth of Monodisperse Silica Spheres in Micron Size Range. J Colloid Interf Sci, 26(1): 62-&.

Sweeney, R.Y., Mao, C.B., Gao, X.X., Burt, J.L., Belcher, A.M., Georgiou, G. and Iverson, B.L., 2004. Bacterial biosynthesis of cadmium sulfide nanocrystals. Chem Biol, 11(11): 1553-1559.

Tiwari, A., Khan, S.A. and Kher, R.S., 2012. Synthesis, structural and optical characterization of nanocrystalline ZnS:Cu embedded in silica matrix. Curr Appl Phys, 12(3): 632-636.

Tokuda, H., Kuchar, D., Mihara, N., Kubota, M., Matsuda, H. and Fukuta, T., 2008. Study on reaction kinetics and selective precipitation of Cu, Zn, Ni and Sn with H(2)S in single-metal and multi-metal systems. Chemosphere, 73(9): 1448-1452.

Veeken, A.H.M. and Rulkens, W.H., 2003. Innovative developments in the selective removal and reuse of heavy metals from wastewaters. Water Science and Technology, 47(10): 9-16.

Wang, L.P., Ponou, J., Matsuo, S., Okaya, K., Dodbiba, G., Nazuka, T. and Fujita, T., 2013. Integrating sulfidization with neutralization treatment for selective recovery of copper and zinc over iron from acid mine drainage. Minerals Engineering, 45(0): 100-107.

Appendix A

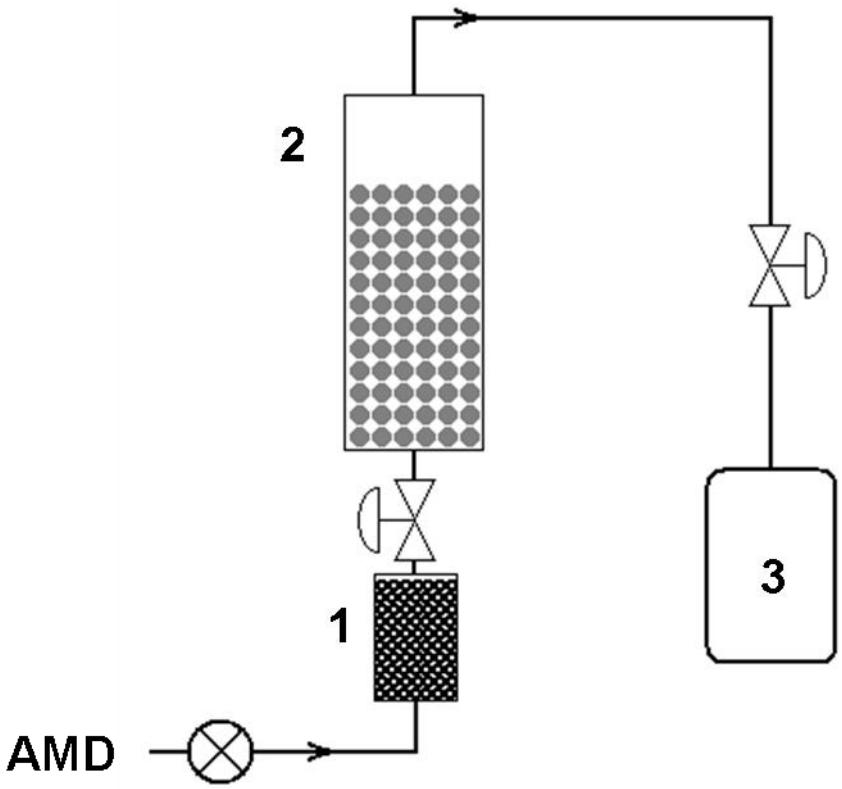

Figure 4.6 – Schematics of the used bioremediation system. 1 – Neutralization column. 2 – Bioreactor. 3 – Precipitation vessel.

Appendix B

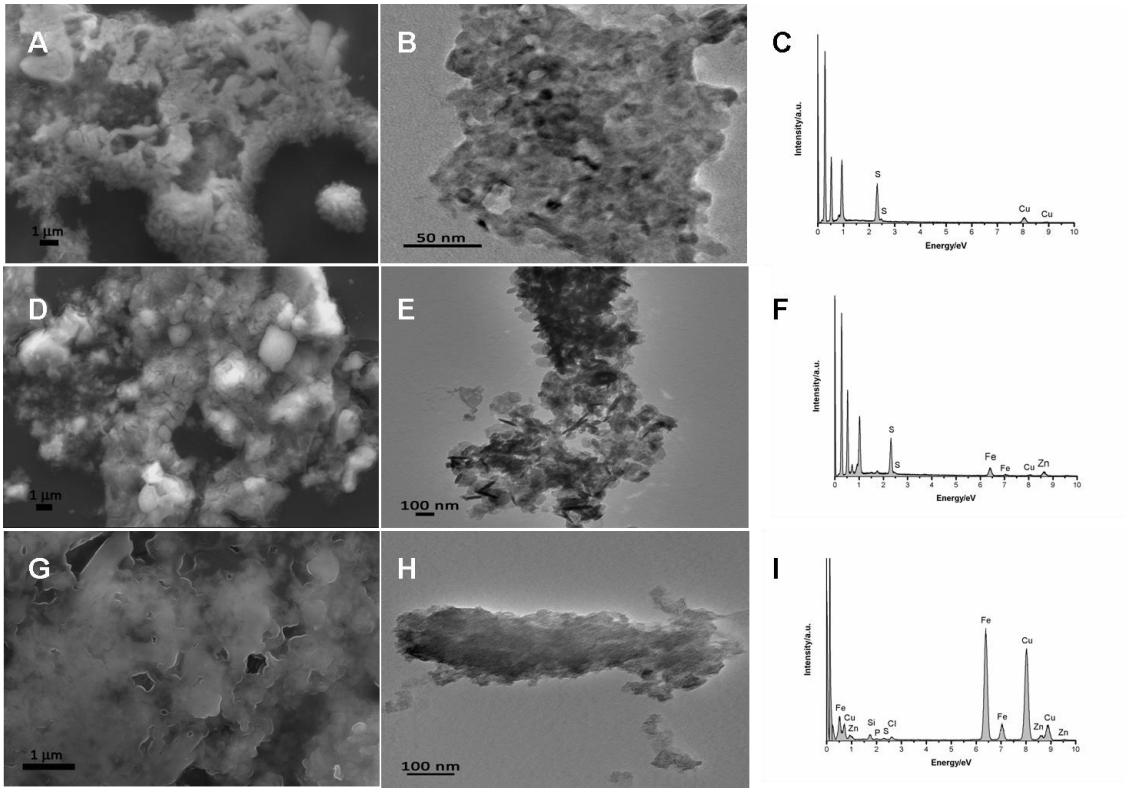

Figure 4.7 –SEM, TEM and EDX results (A, B and C, respectively) for the precipitate obtained at the end of the first precipitation step. Figures D through F correspond to the same set of analyses for the precipitate obtained at the end of the second precipitation step. Similarly, G through I show the equivalent results for the precipitate obtained at the final third step. Results concern the precipitates obtained when using artificial solutions as the metal source.

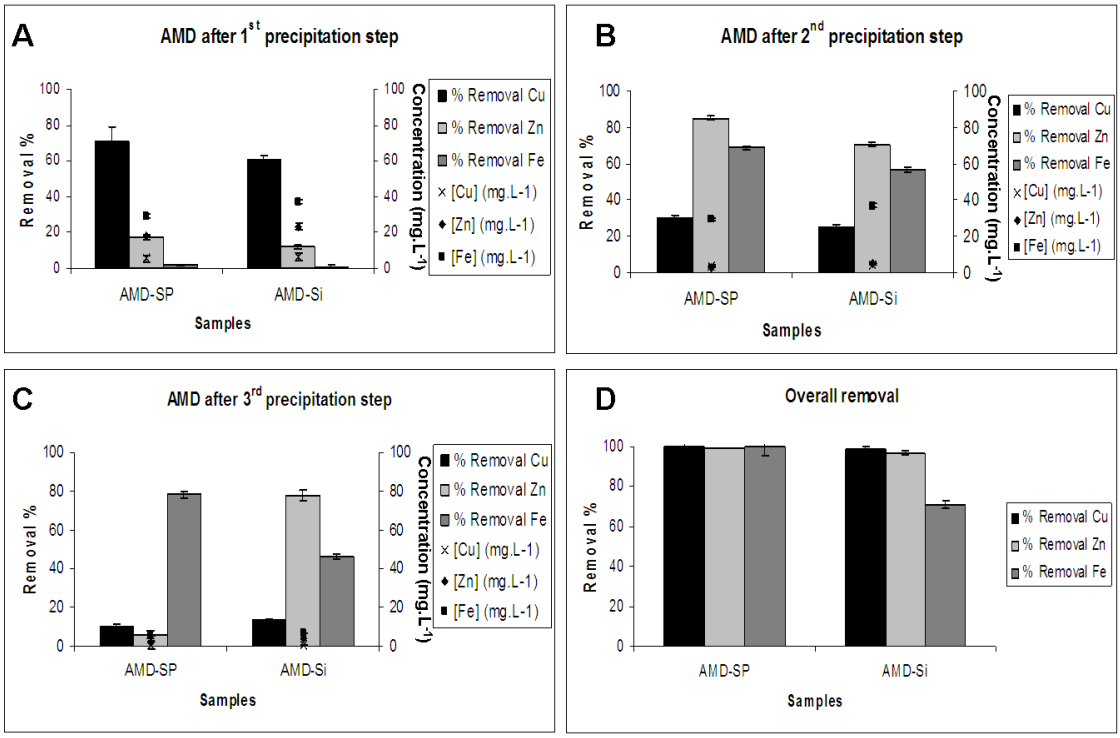

Figure 4.8 – Metal (Cu, Zn and Fe) removal percentage and concentration at the end of the first precipitation step (4.2A), second precipitation step (4.2B) and final precipitation step (4.2C), when using AMD as the metal source. The overall removal percentage for each metal is shown in 4.2D. Error bars are shown. The used abbreviations describe whether SiO_2 was used (AMD-Si), or not (AMD-SP).

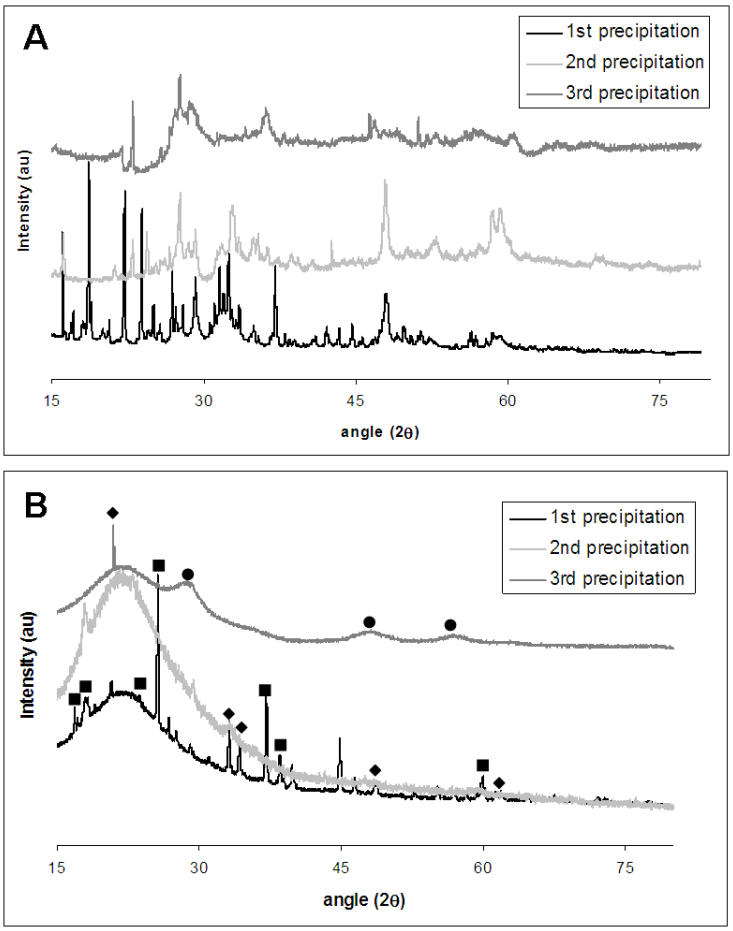

Figure 4.9 – X-ray diffractograms of the precipitates obtained at each step, without any support (4.3A) and in the presence of SiO_2 microparticles (4.3B). Symbol "■" refers to *covellite* (JCPD #03-065-3929), "●" to *sphalerite* (JCPD #00-003-0579) and symbol "♦" refers to iron (III) hydroxide (JCPD #00-038-0032).

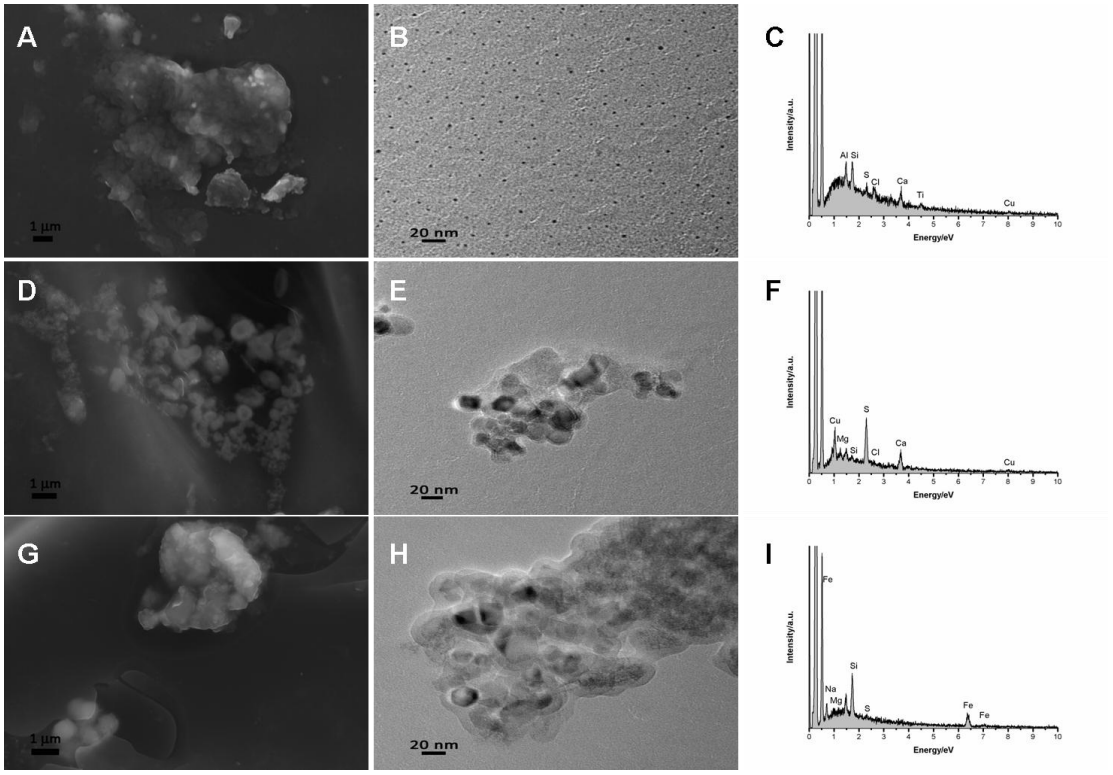

Figure 4.10 –SEM, TEM and EDX results (A, B and C, respectively), for the precipitate obtained at the end of the first precipitation step. Figures D through F correspond to the same set of analyses for the precipitate obtained at the end of the second precipitation step. Similarly, G through I show the equivalent results for the precipitate obtained at the final third step. Results concern the precipitates obtained when using AMD as the metal source

Chapter 5 – Degradation of Safranin-T Using Biologically Produced ZnS-TiO_2 photocatalysts: UV-Visible and Solar Studies

João Pinto da Costa[1*], Ana Violeta Girão[2], O.C. Monteiro[3], Tito Trindade[2], Maria Clara Costa[1]

[1]Universidade do Algarve, CCMar, Campus Gambelas, 8005-139 Faro, Portugal.
[2]Universidade de Aveiro, CICECO, 3810-193 Aveiro, Portugal.
[3]Universidade de Lisboa, FCUL, CQB, Campo Grande, 1749-016 Lisboa, Portugal.

*Corresponding author
Universidade do Algarve, Campus Gambelas
FCT – Edifício 8, Lab. 2.35
8005-139 Faro, Portugal
jcosta@ualg.pt

A modified version of this chapter has been submitted as:
da Costa, J., Girão, A. V., Lourenço, J. P., Monteiro, O. C., Trindade, T. and Costa, M. C., (2013), Degradation of Safranin-T using biologically produced ZnS-TiO_2 photocatalysts: UV-Visible and Solar studies. Biotechnol. Progr.

Abstract

This research demonstrates the potential of ZnS-TiO_2 nanocomposites as catalysts in the photodegradation of an organic pollutant, Safranin-T. The photocatalysts were prepared by modifying the surface of commercial TiO_2 particles with naturally produced ZnS, using sulfide species produced by sulfate-reducing bacteria. Comparative studies using powder XRD and SEM, prior and after photodegradation, were carried out in order to monitor possible structural and morphological changes on the particles. Adsorption properties and specific areas were determined by BET. The final solutions were characterized by UV-Vis and COD content in order to determine Safranin-T concentration as well as their toxicity. The influence of the catalyst amount, initial pH and dye concentration was also evaluated. Finally, the efficiency of the precipitates as catalysts in sunlight mediated photodegradation was investigated, using different volumes of dye-contaminated water (150 mL and 10 L). All tested composites showed potential to be used as photocatalysts for the degradation of Safranin-T, although the ZnS-TiO_2_0.06 composite (0.06 g of TiO_2 per 50 mL of the Zinc solution) has shown to be the most effective. This substantiates the applicability of ZnS-TiO_2 composites obtained by using biologically produced sulfide as photocatalysts for the degradation of Safranin-T, in laboratorial conditions and under direct sunlight.

Keywords: ZnS, TiO_2, nanocomposites, photodegradation, Safranin-T.

5.1. Introduction

Organic dyes are among the major group of pollutants in wastewaters generated by the textile and other industrial processes (Hu and Wang, 1999; Li and Zhang, 1996). In the textile industry, dyes must be highly stable and resistant to washing, light and microbial activity (El-Kemary *et al.*, 2011). Hence, these effluents are not easily degradable and are not removed from water by conventional chemical treatments (Tang and An, 1995). Photocatalytic degradation using semiconductors is an effective technique that results in fast oxidation of the pollutants (Hoffmann *et al.*, 1995; Sobana *et al.*, 2006) and is therefore considered a promising and greener technology for the removal of toxic compounds (Chatterjee and Dasgupta, 2005; Chebli *et al.*, 2011; Janus and Morawski, 2007; Parsons, 2004). Briefly, by exposing a TiO_2 photocatalyst to UV light, the absorption of a photon with an energy superior to the semiconductor band gap causes the promotion of an electron from the valence band to the conduction band (Rauf and Ashraf, 2009) and an electron-hole pair is produced. Commonly, the hole in the valence band (h^+_{vb}) reacts easily with surface-bound H_2O, resulting in the production of hydroxyl radicals ($^{\bullet}OH$), and the electron at the conduction band (e^-_{cb}) reacts with O_2, producing the superoxide radical anion of oxygen (Mahmoodi *et al.*, 2006). Thus, the semiconductor becomes a powerful oxidant, which results in the conversion of the organic pollutant into water and carbon dioxide (Gupta *et al.*, 2007). Equations 5.1 through 5.7 systematize the process.

$$\text{Catalyst} + h\upsilon \rightarrow e^-_{cb} + h^+_{vb} \quad (5.1)$$

$$H_2O + h^+_{vb} \rightarrow {}^{\bullet}OH + H^+ \quad (5.2)$$

$$O_2 + e^-_{cb} \rightarrow O_2^{-\bullet} \quad (5.3)$$

$$O_2^{-\bullet} + 2H_2O \rightarrow 2H_2O_2 \quad (5.4)$$

$$H_2O_2 \rightarrow 2\,{}^{\bullet}OH \quad (5.5)$$

$${}^{\bullet}OH + \text{dye} \rightarrow \text{dye}_{ox} \quad (5.6)$$

$$\text{Dye} + e^-_{cb} \rightarrow \text{dye}_{red} \quad (5.7)$$

Titanium dioxide (TiO_2) has been the most studied material in semiconductor heterogeneous photocatalysis (Hwang *et al.*, 2012; Nakata and Fujishima, 2012; Prieto

et al., 2005). It is a cheap, biologically inactive and photoactive material (Chen and Mao, 2007; Gude *et al.*, 2008). However, it lacks in efficiency under solar irradiation conditions (Franco *et al.*, 2009) due to the large bandgap (*ca.* 3.2 eV for anatase) (Yawalkar *et al.*, 2001), thus absorbing mainly in the UV region (Robert and Malato, 2002). This can be overcome by doping the TiO_2 particles with transition metals (Chen and Mao, 2007; Nunes *et al.*, 2008; Zhang *et al.*, 2006), making the resulting composites visible light responsive photocatalysts. Nonetheless, these metal composites are generally difficult to prepare, often requiring high temperatures and multi-step experimental processes (Franco *et al.*, 2009). Different approaches include the growth of semiconducting nanophases at the surface of TiO_2 (Neves *et al.*, 2008). In this case, the semiconductor with lower bandgap absorbs the photons from visible light and the resulting photogenerated electrons are subsequently transferred to the semiconductor with larger bandgap.

In previous work (da Costa *et al.*, 2012), nanocrystalline ZnS supported on TiO_2 sub-micron particles have been synthesized under ambient conditions and using biogenic sulfide. In order to evaluate the efficiency of such composites, research was carried out using Safranin-T (Figure 5.1A) as a model compound in water decontamination procedures. Safranin-T is a water soluble phenazine dye that has been used as a food dye (Zaghbani *et al.*, 2008) and also in textile and tanneries dyeing processes (Gupta *et al.*, 2007). This dye has been linked to eye irritation and cornea injuries in humans (Gupta *et al.*, 2007) and it has also been reported as a potential carcinogen (Saha *et al.*, 2013). Due to its wide application in numerous industries, the development of efficient and non-costly treatments for its elimination from industrial wastes is of great interest (Gupta *et al.*, 2011).

Photodegradation assays were carried out using a UV-Vis photoreactor for the evaluation of the most suitable experimental conditions. Studies varying the pH, amount of catalyst used and dye concentration were performed. After, solar experiments were performed using the most active catalyst in order to assess the potential of these particles for a practical treatment system implementation.

5.2. Experimental

5.2.1 Chemicals

The cationic dye Safranin-T ($C_{20}H_{19}ClN_4$, M_w=350.85 g.mol^{-1}, λ_{max}=519nm, Figure 5.1A) was provided by Riedal-de-Haën and used without further purification. For the preparation of the solutions, distilled water was used. When necessary, pH values were adjusted using either nitric acid (65%, Panreac) or 1M NaOH solutions. Composites of ZnS-TiO_2 were prepared using different amounts of TiO_2 Degussa (P25) (*ca.* 80% anatase, 20% rutile) per 50 mL of the metal containing solution, at 100 mg.L^{-1}, as described elsewhere (da Costa *et al.*, 2012). Briefly, the sulfide produced by sulfate-reducing bacteria was used to precipitate the dissolved metal in a contaminated solution in the presence of TiO_2. The amounts of TiO_2 per 50 mL of the zinc (II) solution varied between 0.02 g and 0.08 g, with the composites' nomenclature reflecting this (ZnS-TiO_2_0.02, ZnS-TiO_2_0.06 and ZnS-TiO_2_0.08, which correspond to a ratio of 9.31%, 12.4% and 37.3% of ZnS:TiO_2 (w/w), respectively).

5.2.2 Studies in the Absence of Light

Previous to both sets of the photocatalytic experiments (photoreactor and solar), the aqueous suspensions of Safranin-T and nanocomposites were stirred for 30 minutes. After centrifugation (4000 rpm or ~3700 RCF, 5 min), the concentration of Safranin-T was estimated by UV-Vis spectrophotometry.

5.2.3 Photocatalysis

5.2.3.1 Photoreactor Experiments

The photodecolorization experiments were conducted using an Ace Glass photoreactor cooled by water circulation. The reaction vessel, with a volume of 250 mL, was made of borosilicate glass and suitable to accommodate an immersion well. The quartz

immersion well was a double-walled, with inlet and outlet tubes for cooling. The reactor had one angled joint for the sparger tube, one vertical joint for the condenser and one Ace-Thread side arm for the thermometer. The radiation source was a 450 W medium-pressure mercury-vapor lamp (Hanovia). Of the total radiated energy, approximately 40–48% is in the ultraviolet portion of the spectrum and 40–43% in the visible. The radiated watt density was 0.37W/cm^2. Schematic representation of the experimental setup is shown in Figure 5.1B.

The suspensions were prepared by adding 15 mg of the catalyst into 150 mL of 5 ppm Safranin-T aqueous solution. Different catalyst amounts (10 and 20 mg), Safranin-T solution concentration (10, 15, 20 and 50 ppm) and pH value (3, 6.2 and 9) were also used. Prior to irradiation, suspensions were allowed to a 30 minute stirring period, in order to assess any eventual degradation and/or adsorption of the dye (Section 5.2.2). During irradiation, the suspensions were sampled at regular intervals, centrifuged (Rotofix 32A, Hettich) for 5 minutes at 4000 rpm (~3700 RCF) and analyzed by UV-Vis spectrophotometry. After irradiation, powders were collected, dried under vacuum (APT.Line VD, Binder) and characterized by XRD.

5.2.3.2 Solar Experiments

For the solar photocatalytic experiments, 15 mg of the different catalysts were suspended in 150 mL of the Safranin-T solution (5 ppm), and, after allowing for the adsorption-desorption equilibrium to be reached (Section 5.2.2), suspensions were exposed to sunlight under agitation and sampling was done periodically. The experimental set-up is detailed in Figure 5.1C. The glass containers were 115 mm in diameter and 85 mm in height. The water column was approximately 1.5 cm high. The containers were covered with watch-glasses in order to reduce evaporation.

These studies were further extended by using higher volumes of a 5 ppm Safranin-T solution. In these experiments, 10 L were used, maintaining the ratio of catalyst used (15 mg/150 mL of solution). However, considering the results obtained in the photoreactor experiments and in the solar assays when using 150 mL of the dye contaminated solution, the ZnS nanoparticles were not used in these experiments, using

only the best composite (ZnS-TiO_2_0.06) and the commercially available TiO_2. Also, in order to better simulate real-world conditions, the recipients' walls were dark and, during the low solar intensity periods and night time, the recipients were covered with a black plastic, so that the exposure time could be more accurately determined. A simple aquarium pump was used for agitation (NewJet 400). The recipients were 35 cm in diameter and 18 cm in height. The water column was approximately 16 cm high (see supplementary data for the images depicting the set-up).

These studies were carried out during the months of July and August, in the Algarve (Southern Portugal, GPS: N37 02 34, W7 58 20). Mean daily temperatures oscillated between 19.5ºC (min) and 29.7ºC (max). The assays were performed in duplicates and when no clouds were visible. After photocatalytic decolorization, samples were centrifuged (4000 rpm or ~3700 RCF, 5 min) and the concentration of Safranin-T was determined by UV-visible spectrophotometry.

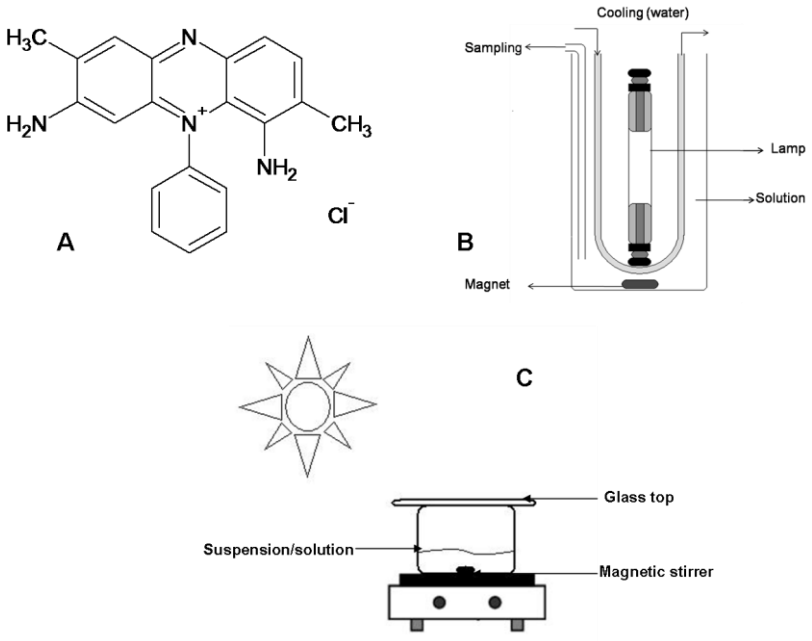

Figure 5.1 – The structure of Safranin-T (5.1A) (Zaghbani *et al.*, 2008) (*adapted*) and schematic representation of the experimental set-up used (5.1B) (Franco *et al.*, 2009) (*adapted*). In 5.1C, the experimental set-up of the small volume solar experiments is detailed.

5.2.4 Analytical Methods

The concentration of Safranin-T was estimated by measuring the absorbance at 519 nm, using a UV-Visible spectrophotometer (DR 2800, Hach-Lange). Chemical Oxygen Demand was determined using the LCK 514 Method, from Hach-Lange.

The pH values of the different solutions/suspensions were measured using a pH/Eh meter (GLP21, Crison).

The catalysts, before and after irradiation, were analyzed by XRD, using a PANalytical X'Pert Pro powder difractommeter operating at 45 kV and 40 mA, with CuKα radiation filtered by Ni. XRD patterns were recorded using an X'Celerator detector, with a step size of 0.016 and a time per step of 500 seconds. The HighScore Plus software, with the ICDD PDF-2 database, was used for peak analysis and crystalline phase identification.

The particle charge was quantified as zeta potential using a Zeta sizer 4 (Malvern Instr., UK). Measurements were performed in distilled water. Morphological and analytical characterization of the powders was performed by electron microscopy. Scanning Electron Microscopy (SEM) using a Field Emission Gun (FEG) - SEM Hitachi S4100 microscope, operated at 25 kV, with an Energy-Dispersive X-ray Spectroscopy (EDX) Rontec detector were used for this purpose, as well as a FEG-SEM Hitach SU70 operating at 15 kV and equipped with an EDX Bruker detector. The samples were prepared by deposition of an aliquot of the samples directly onto the carbon tape and then coated by carbon evaporation (Emitech K950X).

Sorption studies and BET area determination were performed using a Gemini V2 Surface Area Analyzer (Micromeritics), using N_2 as the analysis adsorptive.

FT-IR analyses were carried out using a Mattson 7000 series instrument. Samples were incorporated in KBr pellets for measurements and the reference spectrum (air) was subtracted to each sample spectrum.

5.3. Results and Discussion

5.3.1. Nanocomposites' Characterization

The stability of the aqueous dispersions was assessed by measuring the zeta potential at different pH values. The results obtained are shown in Figure 5.2A. These suggest that the pI of the different composites do not vary in accordance to the amount of TiO_2 used, which has been previously observed (Libanori *et al.*, 2009; Ma *et al.*, 2010) but not explained. However, this may occur in aqueous solutions due to differences in conductivity (MalvernInstruments, 2009). The solutions of Safranin-T prepared without any pH adjustment showed a pH value of ~6.2. Since the zeta potential measured indicated that the particles tend to remain suspended (Riddick, 1968), photocatalytic studies were carried out with no pH correction of the Safranin-T solution, thus contributing to an overall process that requires as little additional chemicals as possible. Among the studied literature, the zeta potential was not reported for the ZnS-TiO_2 composites; nonetheless, the results obtained for TiO_2 are consistent with those previously obtained by other authors (Bullard and Cima, 2006; Suttiponparnit *et al.*, 2011; Svecova *et al.*, 2008).

Sorption studies on the different composites were carried out in order to determine the favorability of the physisorption process. As Figure 5.2B shows, the isotherms obtained are characteristically Type I (Brunauer *et al.*, 1940), which can easily be described using the Langmuir Adsorption isotherm (Czepirski *et al.*, 2000; Khalfaoui *et al.*, 2003; Xu and Langford, 2000). Also, as shown in Figure 5.2B, the different particles appear to have identical behaviors and saturation pressures.

These studies were also used for the determination of the specific surface area (Sharma and Tomar, 2011). For TiO_2 (P25), ZnS-TiO_2_0.02, ZnS-TiO_2_0.06 and ZnS-TiO_2_0.08, the specific surface areas determined by BET isotherms were 71.8, 79.5, 68.5 and 65.9 $m^2.g^{-1}$, respectively. Interestingly, the surface area determined for Degussa's TiO_2 (P25) was different (50+/-15 $m^2.g^{-1}$) of that reported by other authors (Franco *et al.*, 2009; Raj and Viswanathan, 2009; Zhou *et al.*, 2012). This, however, may be due to the inherent differences obtained in different production batches. Also, due to the fact that TiO_2 was analyzed as supplied, small amounts of water present may

have resulted in the deviation observed for this parameter (ISO, 2010; Reisinger, 2013). Although there is some variation on the surface areas of the diverse compounds tested, we would argue that these probably have no final impact on the differences of the photocatalytic activities of the tested composites. In fact, ZnS-TiO_2_0.02 proved to possess a larger specific area than that of the other composites, and, yet, showed lower activity, albeit identical to that of the remaining composites.

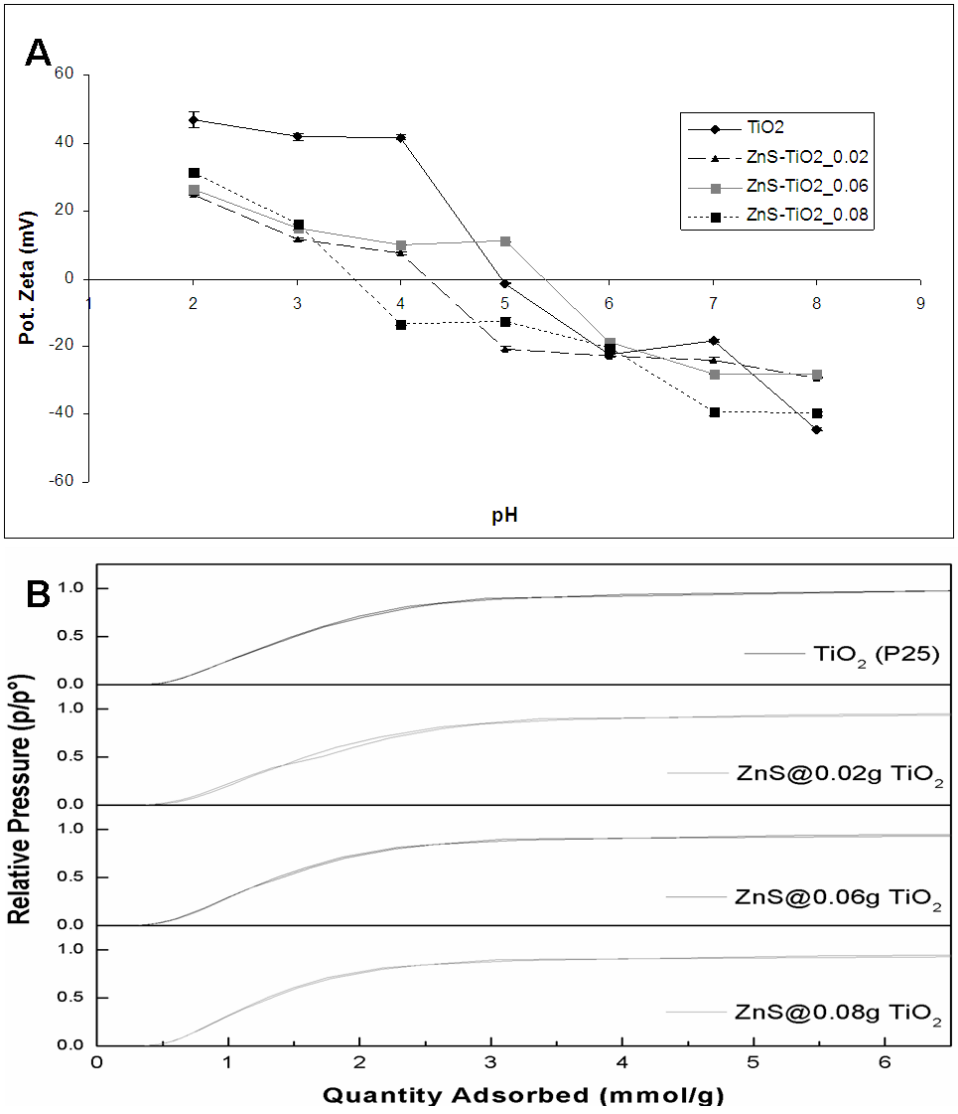

Figure 5.2 – In 5.2A, zeta potential of the different particles in aqueous suspensions as a function of the pH. Error bars are shown. 5.2B – Adsorption isotherm of N_2 on TiO_2 (P25) and of the different ZnS-TiO_2 composites tested.

In order to determine if crystalline changes occurred on the composites when these are subjected to the photocatalytic process, X-ray diffraction (XRD) analyses were carried out. Considering that the results obtained showed no considerable differences to the results previously described (da Costa *et al.*, 2012), these are shown in Appendix A (Figure 5A). There is the appearance of an extra peak just after angle 40º (2θ) in the sample subjected to irradiation for TiO_2 (P25) (Figure 5A.1) and ZnS-TiO_2_0.02 (Figure 5A.2). This extra peak is consistent with that of the rutile phase of TiO_2 and its appearance may be due to the use of the composites in solution, resulting as an additional washing step. Evidence for this is the fact that this peak is visible in the XRD patterns of the remaining ZnS-TiO_2 composites (Figures 5A.3 and 5A.4).

Figure 5.3A shows the diffuse reflectance spectra (converted to absorption by the Kubelka-Munk (KM) function) (Franco *et al.*, 2009; Jia *et al.*, 2007). There is an apparent trend in the absorption onset with an increase in TiO_2 content, which is to be expected (Wu and Chen, 2004; Yang *et al.*, 2010). The bandgap energies for the different synthesized composites were determined using the KM function and are shown in Table 5.1. The estimated Eg value was 3.29 eV for TiO_2, which is in accordance with results obtained in previous work (Franco *et al.*, 2009). For the different composites, the Eg values determined were 3.22, 3.16 and 3.24 eV for the ZnS-TiO_2_0.02, ZnS-TiO_2_0.06 and ZnS-TiO_2_0.08 compounds, respectively. These values suggest that lower energetic requirements would have to be achieved in order to use these materials as photocatalysts on the degradation of Safranin-T. This occurs due to the presence of the ZnS nanophases at the surface of the TiO_2, which results in a faster transfer of electrons (Kim and Kang, 2012).

In Figures 5.3B and 5.3C are shown the SEM images for the ZnS-TiO_2_0.06 prior and after photocatalysis, respectively, with no discernible modifications observed. It should be noted that the observations made are valid for all the composites analyzed (SEM images of the remaining catalysts are not shown, for simplification purposes). The combination of the SEM and XRD analyses (Appendix 5A) suggest that after photodegradation of Safranin-T, the composites do not undergo significant chemical and morphological modifications.

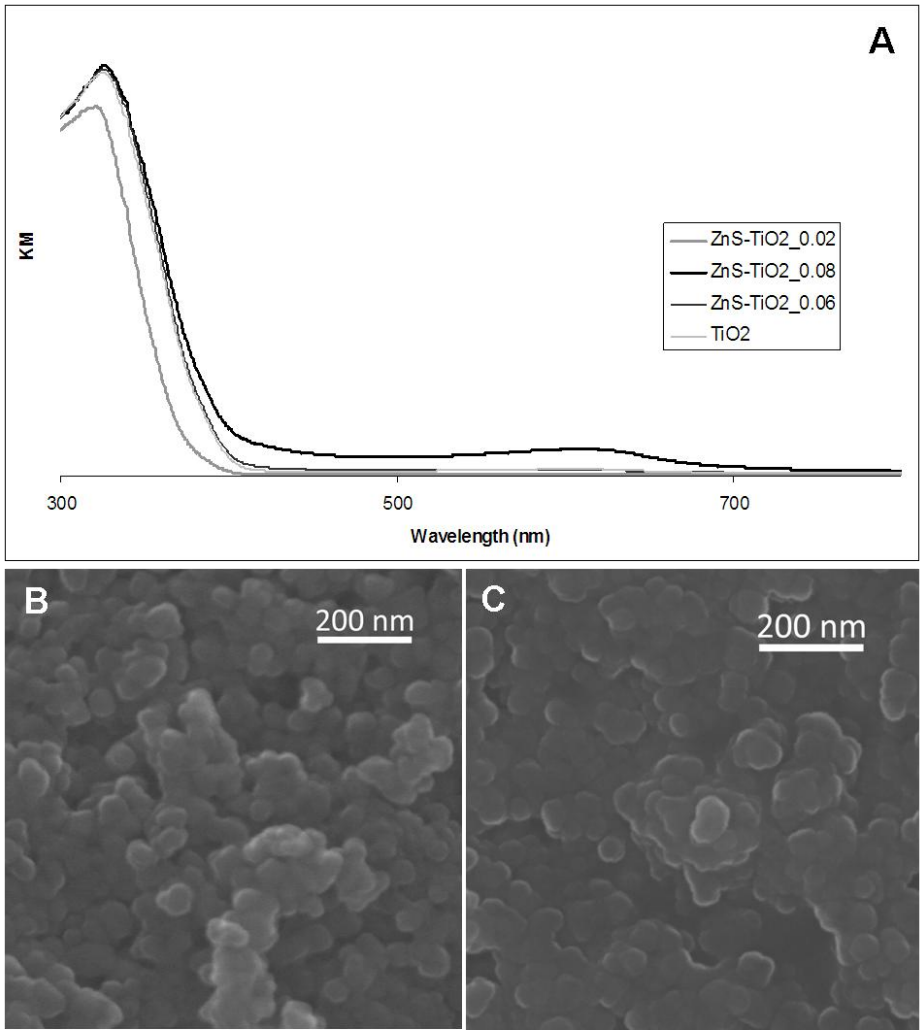

Figure 5.3 – KM vs. wavelength for the different compounds tested (4A). In Figures 5.5B and 5.3C are shown the SEM images of the ZnS-TiO_2_0.06 composite, before and after photodegradation, respectively.

FT-IR analysis was carried out in order to evaluate if, at the end of the photocatalytic process, the used catalysts were modified and if Safranin-T and/or its degradation sub-products were still present at the catalysts surface. The FT-IR spectra (Appendix 5B) display a broad band around 3427 cm^{-1} corresponding to the stretching vibrations of hydrogen-bonded surface adsorbed water molecules and hydroxyl groups. Vibrations of C-H from adventitious carbon on the surface of the surface of the sample were found at around 2922 cm^{-1} and bending vibrations of O-H groups are identified around 1628 cm^{-1} (Ai *et al.*, 2011; Vijayabalan *et al.*, 2009). In general, it can be observed that the spectra corresponding to the used catalysts present the main features of the TiO_2 spectrum and

the vibrations corresponding to the ZnS nanoparticles are not identifiable. Nevertheless, it can be shown that complete degradation of Safranin took place and its degradation sub-products were not – at least significantly – adsorbed at the catalysts' surface (highlighted areas in Figure 5B).

5.3.2 Photoreactor Experiments

5.3.2.1 – Nanocomposites' Activity

The photocatalytic activity of the ZnS-TiO_2 composite samples, expressed as a percentage of the dye over time of irradiation, is shown in Figure 5.4. It is important to evaluate the adsorption characteristics of the system because the process of photo-oxidation takes place at the surface of the particles of the catalyst (Franco *et al.*, 2009). The ability of the catalysts to adsorb Safranin-T at the surface was previously tested in dark conditions. Regardless of the catalyst used, Figure 5.4 shows that there is a slight decrease on the Safranin-T concentration before irradiation took place (Time 0, in Figure 5.4). However, after this period, the adsorption-desorption equilibrium is reached (Franco *et al.*, 2009). It should be noted that the composites ZnS-TiO_2_0.06 and ZnS-TiO_2_0.08 are more effective, as opposed to the ZnS-TiO_2_0.02 composite, which showed lower efficiency (Figure 5.4). On the other hand, nanocrystalline ZnS seems to have little or no photocatalytic activity whatsoever, as results suggest that the initial decrease in the Safranin-T in solution is due to adsorption process and that the degradation rate is identical to the results obtained when no catalyst is used (Figure 5.4). These observations, regarding the lack of photocatalytic activity of ZnS nanoparticles, are consistent with those made by others (Chen *et al.*, 2012; Kim *et al.*, 2007; Sharma *et al.*, 2012; Tsuji and Kudo, 2003), and are to be expected, as, without an appropriate hole scavenger, ZnS can be oxidized (Kohtani *et al.*, 2012; Zhang *et al.*, 2011) a process named photocorrosion (Kisch, 2007).

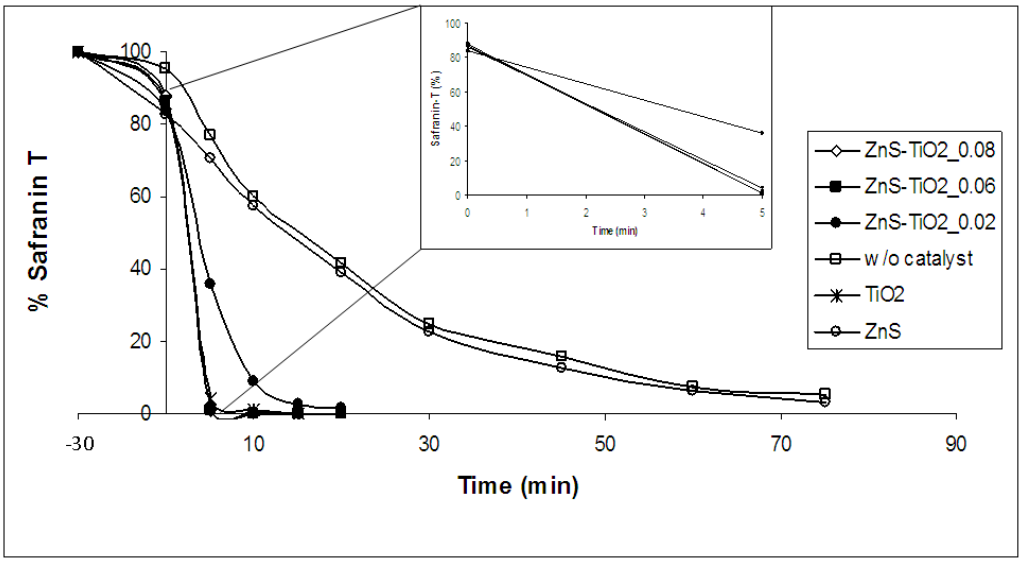

Figure 5.4 – Photocatalytic decolorization of 150 mL of a 5 ppm Safranin-T aqueous solution. When used, the amount of catalyst was 15 mg. Time "0" refers to when the light is turned on. Inset highlights the small differences observed for some catalysts.

The degradation rates, or K*app*, determined as described by Goswami and co-workers (Goswami *et al.*, 2011) were 8.46, 2.53, 7.39, 8.69 and 8.63 min^{-1} for the TiO_2, ZnS, ZnS-TiO_2_0.02, ZnS-TiO_2_0.06 and ZnS-TiO_2_0.08 particles, respectively. The positive effect of the ZnS on the photoactivity of Degussa's P25 may be due to the electronic interaction taking place at the region where the TiO_2 and the metal sulfide come into contact (El-Kemary *et al.*, 2011). This leads to the removal of electrons from TiO_2 to the vicinity of the semiconductor, resulting in an improved charge separation (Herrmann *et al.*, 1986; Zhu *et al.*, 2012). In other words, a more effective electron transfer occurs than in the case of pure TiO_2.

The efficiency of the different composites was also assessed by measuring the Chemical Oxygen Demand (COD), which is also a measure of toxicity (Gupta *et al.*, 2007). Furthermore, the decrease of the COD has been related to the degree of mineralization (Behnajady *et al.*, 2007; Zhao *et al.*, 2010). The COD reduction ratio was determined for each sample and the results obtained are shown in Table 5.1. These indicate that the different solutions have undergone a major decrease in the COD content, with subsequent considerable reduction in their toxicity. Moreover, these results show that the ZnS-TiO_2_0.06 composite is the most effective of the catalysts tested and that Safranin-T seems to have been mineralized to a great extent under these conditions,

which is consistent with the results reported by other authors when using chemically synthesized and commercially available TiO_2 (Gupta *et al.*, 2007; Janaki *et al.*, 2012; Vinu *et al.*, 2010). It should be noted, however, that these results evaluate the COD content at the end of each experiment, which occurred at different time periods.

Table 5.1 – COD reduction percentage in the final solutions of Safranin-T, after photodegradation using the specified catalysts. Results shown are for an average of three measurements[1]. Also shown are the BET areas and the bandgap values determined for the different composites synthesized.

Compound tested	%COD reduction	BET Area ($m^2.g^{-1}$)	Bandgap (eV)
No catalyst	79.96 $\pm$ 3.97	-	-
TiO_2	80.31 $\pm$ 1.15	71.8	3.29
ZnS-TiO_2_0.02	83.08 $\pm$ 1.08	79.5	3.22
ZnS-TiO_2_0.06	84.30 $\pm$ 1.15	68.5	3.16
ZnS-TiO_2_0.08	81.57 $\pm$ 2.12	65.9	3.24

5.3.2.2 Influence of the Amount of Catalyst

The effect of the amount of the catalyst on the photodecolorization process was studied for the ZnS-TiO_2_0.06 sample, which showed the best efficiency for the conditions evaluated. Hence, photocatalysis of a 5 ppm Safranin-T solution with 10, 15 and 20 mg of this catalyst was performed. Results shown in Figure 5.5A indicate that, as expected, during the light-off period, the adsorption increases with the amount of catalyst used. When the photocatalytic process initiates, it takes 30 minutes to be complete using 10 mg of the composite tested. This time is reduced to just 10 minutes when 15 mg of the catalyst are used. This may be explained by the fact that increasing the amount of catalyst will result in an increase of adsorbed dye molecules and of the absorbed photons. As a result of the high density of molecules in the illuminated area, the reaction rate will increase (Franco *et al.*, 2009). However, when the amount of catalyst

[1] Note that the values determined correspond to the final solutions, which were obtained at different durations of the photodegradation process, as illustrated in Figure 5.4

used is 20 mg, the reaction rate decreases, which may be due to the subsequent increase of the suspension's turbidity, resulting in a lower penetration of the light and an enhanced light scattering effect (Senthilkumaar and Porkodi, 2005).

5.3.2.3 Influence of the pH

In aqueous solution, the surface of TiO_2 (P25) is generally positively charged in acidic media and negatively charged in alkaline media (Franco *et al.*, 2009), as evidenced in Figure 5.2A. This means that an increase in the photocatalytic activity is expected to take place with an increase in pH, due to the interactions between the negative composite surface and the Safranin-T cations. Taking these facts into consideration, photodegradation assays using a 5 ppm solution of Safranin-T and 15 mg of the catalyst previously determined as the most efficient (ZnS-TiO_2_0.06) were carried out using different pH values of the initial solution (3, 6.2 and 9).

The results, shown in Figure 5.5B, indicate that, during the light-off period, very low adsorption takes place at pH values of 3 and 6.2, which may be correlated with the cationic behavior of both the catalyst and dye. However, at pH 9, the adsorption is much higher, as the interactions between the negatively charged surface of the composite and the positively charged dye ions increase. During photocatalysis and at pH 6.2, Safranin-T is removed completely after 10 min; after twice that time, ~11% and ~7% are still present for solutions at pH 3 and 9, respectively. Although for the former the initial rate of degradation is higher (Figure 5.5B), it significantly decreases after 5 minutes. This may reflect the difficulties presented by electrostatic interactions, which could prevent the approach of the dye molecules to the catalyst's surface (Franco *et al.*, 2009; Senthilkumaar and Porkodi, 2005). On the other hand, at pH 9, the lower degradation rate may be caused by the high adsorption observed (Figure 5.5B). This could result in a decline of the absorbed light at the catalyst's surface and, consequently, of the efficiency of the photocatalytic process. Hence, the "natural" pH obtained when preparing the Safranin-T solution proved to be the value at which the reaction is more effective.

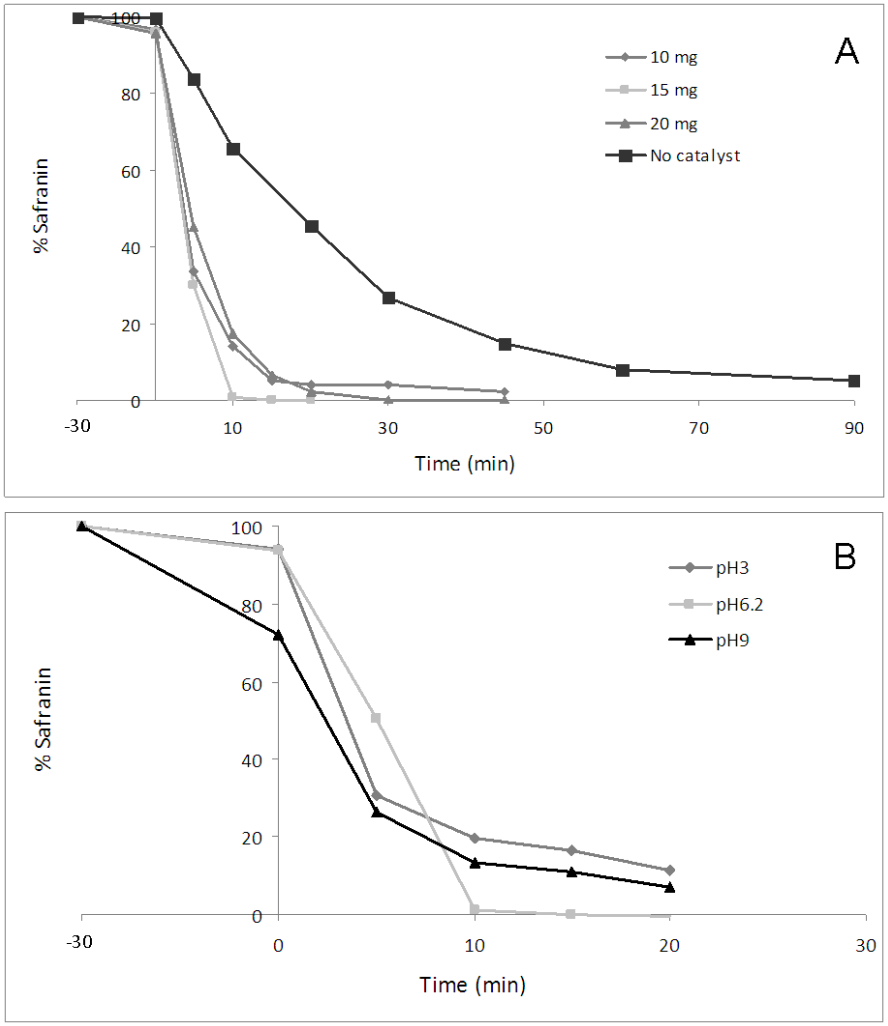

Figure 5.5 – Photocatalytic decolorization of 150 mL of a 5 ppm Safranin-T aqueous solution with different amounts of the ZnS-TiO2_0.06 composite (5.5A). Photocatalytic decolorization of 150 mL of an aqueous solution of Safranin-T at 5 ppm and pH values of 3, 6.2 and 9 using 15 mg of the ZnS-TiO_2_0.06 nanocomposite (5.5B).

5.3.2.4 Influence of the Dye Concentration

Regarding the light-off period, in which the adsorption-desorption process reaches equilibrium, the percentage of adsorbed dye increases with its concentration, which is to be expected. As more dye is available, more dye is adsorbed, until a maximum adsorption level is reached. As seen in Figure 5.6A, for the amount of catalyst used, this threshold seems to exist between 20 ppm and 50 ppm, when no more dye can be adsorbed at the catalyst's surface. After the beginning of the photocatalytic process, the

rates of degradation seem to decrease with the increase of the dye concentration, which is in accordance with observations made by other authors (Neppolian *et al.*, 2002; Toor *et al.*, 2006; Zhu *et al.*, 2009). As the ratio of degradation relates to the probability of formation of hydroxyl free radicals on the catalyst's surface and to the probability of such radicals reacting with the dye molecules, an increase in initial dye concentration will result in a higher probability of reaction (Erdemoglu *et al.*, 2008). However, if the initial dye concentration is further increased, reaction rates may decrease, as the catalyst's active sites are occupied by the dye molecules. Also, if sufficiently high enough, an increased dye concentration will shield the visible light, hence, diminishing the number of light triggered catalyst particles, which will culminate in lower concentration of hydroxyl free radicals (Liu *et al.*, 2006; Zhu *et al.*, 2009).

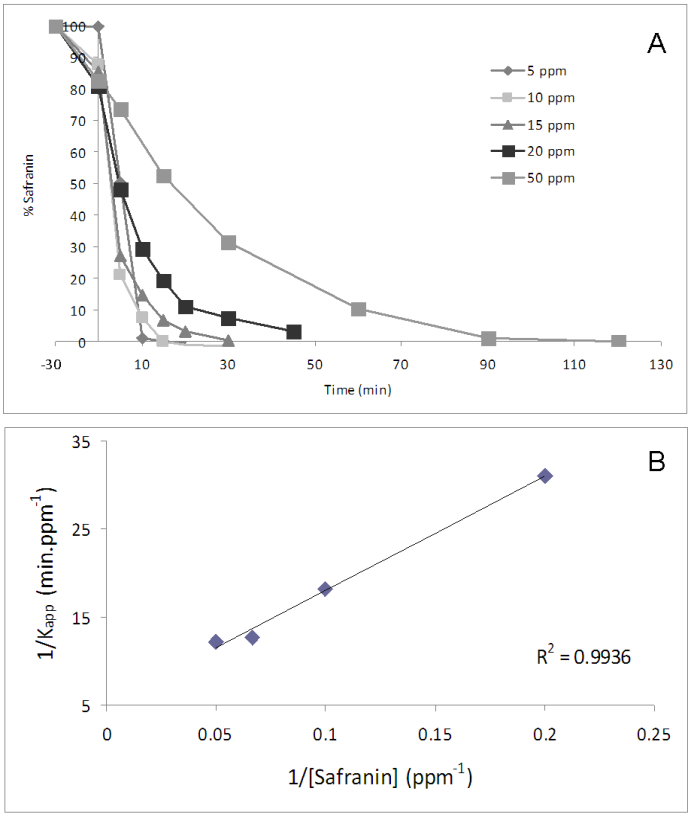

Figure 5.6 – Photocatalytic decolorization of 150 mL of Safranin-T aqueous solutions at different initial concentrations (5, 10, 15, 20 and 50 ppm) using 15 mg of the ZnS-TiO_2_0.06 composites (5.6A). The Langmuir-Hinshelwood model, for the tested conditions, is shown in 6B. The correlation factor (R^2) is also shown. Results obtained for an initial concentration of Safranin-T of 50 ppm were not considered.

Kinetics of the photocatalytic reactions can be expressed by the Langmuir-Hinshelwood (LH) model (Chen *et al.*, 1995; Zhu *et al.*, 2009). This model describes the dependence of the observed reaction rate on the initial dye concentrations (da Silva and Faria, 2003; Sajjad *et al.*, 2010). For low initial dye concentrations, the reaction rate can be expressed by equation 5.8 (Kaur and Singh, 2007; Rauf *et al.*, 2011).

$$\ln (C_i/C_0) = -K_{app}.t \qquad (5.8)$$

where C_0 is the initial dye concentration, C_i is the concentration at time t and K_{app} is the apparent reaction rate constant. Plotting $1/K_{app}$ against $1/C_i$ allows for the determination of the Langmuir adsorption constant (slope, expressed as M^{-1}) (Aarthi *et al.*, 2007; Chong *et al.*, 2010; Rauf and Ashraf, 2009). Considering the results obtained in the degradation experiments using Safranin-T solutions at initial concentrations of 5, 10, 15 and 20 ppm, the LH model seems to adequately fit (Figure 5.6B), with a correlation factor (R^2) >0.99. Results pertaining to an initial concentration of Safranin-T of 50 ppm were neglected, as the LH model is more suited when the initial dye concentrations are low (Kaur and Singh, 2007; Rauf *et al.*, 2011).

5.3.3 Solar Experiments

After establishing which of the tested composites is the most efficient, we set out to determine the photocatalytic activity of this compound under direct sunlight. In order to better mimic the conditions of the experiments carried out using the photoreactor, we used glass recipients, through which the light could pass. Results (Figure 5.7A) were congruent to those obtained in the photoreactor experiments: the ZnS-TiO_2_0.06 composite is more efficient in the degradation of Safranin-T than TiO_2. ZnS alone seems to have no significant photocatalytic activity under solar irradiation. There is an initial decrease (100% to 93%) in the amount of Safranin-T in solution, probably due to the adsorption processes taking place at the surface of the particles. The aspect of the

solutions, prior and after the photocatalytic process, when using the ZnS-TiO2_0.06 composite, is shown in Figures 5C.1 and 5C.2 (Appendix C), respectively.

We further explored the potential of the ZnS-TiO_2_0.06 composite as photocatalyst in real-world conditions by a scale-up of the previously described process, by subjecting a larger volume (10 L) of a 5 ppm Safranin-T solution to solar irradiation and maintaining the particle/volume ratio. The results (Figure 5.7B) showed that, after only 120 minutes, the percentage of Safranin-T in solution is below 10%, when using the ZnS-TiO_2_0.06 composite. For the same time period, when using Degussa's P25, Safranin-T concentration is still at 25%. The images of the solutions prior and after photocatalytic degradation of Safranin T when using the ZnS-TiO_2_0.06 composites as photocatalysts are shown in Appendix 5C (Figures 5C.3 and 5C.4).

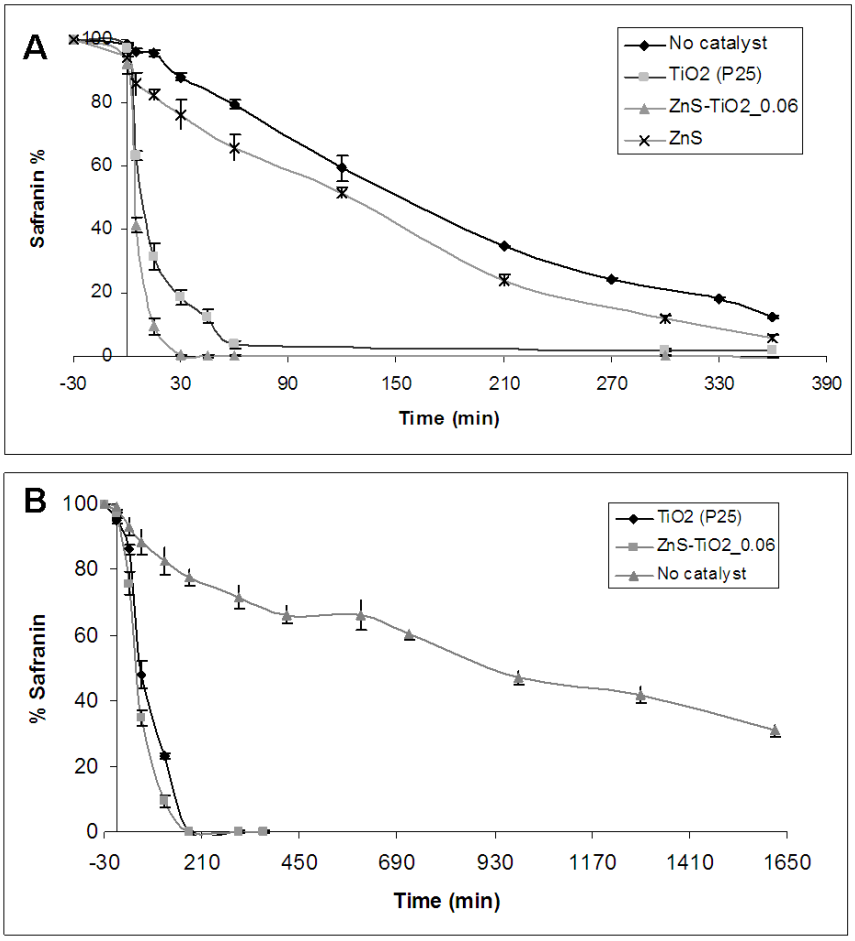

Figure 5.7 – Photocatalytic decolorization of a solution of Safranin-T at 5 ppm using different catalysts at 0.1 $g.L^{-1}$, in a 150 mL (7A) and 10 L of dye solution (7B).

The use of nanostructures in the degradation of dyes has been widely reported (Behnajady *et al.*, 2007; Gude *et al.*, 2008; Zhang *et al.*, 2009; Zhao *et al.*, 2010) and the use of TiO_2-doped particles has been extensively studied (Janaki *et al.*, 2012; Li and Zhang, 1996; Rauf *et al.*, 2007; Zhang *et al.*, 2006; Zhou *et al.*, 2012). However, all these studies report the chemical synthesis of such structures. Having previously described the route for obtaining these nanocomposites as a result of the growth of sulfate-reducing bacteria (da Costa *et al.*, 2012), we set out to demonstrate their applicability. In this work, we have demonstrated that it is possible to use the particles obtained from a simulated remediation process in the photodegradation of a cationic dye. Also, this shows that it is possible to integrate a process in which photocatalytic active particles are produced by using the sub-product of a bioremediation method with a potential practical treatment for hazardous dyes. In other words, this work demonstrates the applicability of these biologically obtained particles.

5.4 Conclusions

In previous work, we have successfully produced ZnS and ZnS-TiO_2 composites, at different ratios of TiO_2, by using a by-product of a bioremediation process. Here, we have tested the photocatalytic activity of these materials over an organic dye (Safranin-T) in both controlled and real-world settings. After characterization of the different ZnS-TiO_2 composites in terms of zeta potential, XRD (before and after photocatalysis), surface area and adsorption, we have concluded that the composites showed an increased efficiency when compared to that of TiO_2 and that they suffer no major changes during the catalytic process. Of these composites, the most efficient photocatalyst was ZnS-TiO_2_0.06 (0.06 g TiO_2 per 50 mL of a 100 $mg.L^{-1}$ solution of Zn). The best results were obtained when using a 5 ppm concentration of Safranin-T, at pH 6.2 and with a catalyst load of 15 mg per 150 mL of dye solution. The Langmuir-Hinshelwood model was used and a good fit to the photodegradation of the dye was achieved. Further analyses (FT-IR) showed that complete degradation of the dye occurs and its degradation products were not adsorbed at the catalysts' surface.

Making use of the advantageous weather conditions of the region, the photodegradation of Safranin-T was studied using direct sunlight in small (150 mL) and large (10 L) dye

solution volumes. The results obtained in both cases were consistent to those obtained using a photoreactor in laboratorial conditions.

This illustrates the potential for integrating a well-documented bioremediation process of contaminated waters with the biologically-mediated production of nanoparticles, which, in turn, we have proven to have applications in environmental remediation processes.

Acknowledgements

Funding by Fundação para a Ciência e a Tecnologia (FCT) through a PhD grant (SFRH/BD/43784/2008) is acknowledged. A. V. Girão also thanks FCT for the Post-Doc grant (SFRH/BPD/66407/2009).

References

Aarthi, T., Narahari, P. and Madras, G., 2007. Photocatalytic degradation of Azure and Sudan dyes using nano TiO2. Journal of Hazardous Materials, 149(3): 725-734.

Ai, Z., Zhu, L., Lee, S. and Zhang, L., 2011. NO treated TiO_2 as an efficient visible light photocatalyst for NO removal. Journal of Hazardous Materials, 192(1): 361-367.

Behnajady, M.A., Modirshahla, N., Daneshvar, N. and Rabbani, M., 2007. Photocatalytic degradation of CI Acid Red 27 by immobilized ZnO on glass plates in continuous-mode. Journal of Hazardous Materials, 140(1-2): 257-263.

Brunauer, S., Deming, L.S., Deming, W.E. and Teller, E., 1940. On a theory of the van der Waals adsorption of gases. Journal of the American Chemical Society, 62: 1723-1732.

Bullard, J.W. and Cima, M.J., 2006. Orientation dependence of the isoelectric point of TiO2 (rutile) surfaces. Langmuir, 22(24): 10264-10271.

Chatterjee, D. and Dasgupta, S., 2005. Visible light induced photocatalytic degradation of organic pollutants. J Photoch Photobio C, 6(2-3): 186-205.

Chebli, D., Fourcade, F., Brosillon, S., Nacef, S. and Amrane, A., 2011. Integration of photocatalysis and biological treatment for azo dye removal - application to AR183. Environ Technol, 32(5): 507-514.

Chen, H.Y., Zahraa, O., Bouchy, M., Thomas, F. and Bottero, J.Y., 1995. Adsorption Properties of TiO_2 Related to the Photocatalytic Degradation of Organic Contaminants in Water. J Photoch Photobio A, 85(1-2): 179-186.

Chen, X. and Mao, S.S., 2007. Titanium dioxide nanomaterials: Synthesis, properties, modifications, and applications. Chemical Reviews, 107(7): 2891-2959.

Chen, Y., Yin, R.H. and Wu, Q.S., 2012. Solvothermal Synthesis of Well-Disperse ZnS Nanorods with Efficient Photocatalytic Properties. J Nanomater.

Chong, M.N., Jin, B., Chow, C.W.K. and Saint, C., 2010. Recent developments in photocatalytic water treatment technology: A review. Water Res, 44(10): 2997-3027.

Czepirski, L., Balys, M.R. and Komorowska-Czepirska, E., 2000. Some generalization of Langmuir adsorption isotherm. Internet J Chem, 3(14): U3-+.

da Costa, J.P., Girao, A.V., Lourenco, J.P., Monteiro, O.C., Trindade, T. and Costa, M.C., 2012. Synthesis of nanocrystalline ZnS using biologically generated sulfide. Hydrometallurgy, 117: 57-63.

da Silva, C.G. and Faria, J.L., 2003. Photochemical and photocatalytic degradation of an azo dye in aqueous solution by UV irradiation. J Photoch Photobio A, 155(1-3): 133-143.

El-Kemary, M., Abdel-Moneam, Y., Madkour, M. and El-Mehasseb, I., 2011. Enhanced photocatalytic degradation of Safranin-O by heterogeneous nanoparticles for environmental applications. J Lumin, 131(4): 570-576.

Erdemoglu, S., Aksu, S.K., Sayilkan, F., Izgi, B., Asilturk, M., Sayilkan, H., Frimmel, F. and Gucer, S., 2008. Photocatalytic degradation of Congo Red by hydrothermally synthesized nanocrystalline TiO_2 and identification of degradation products by LC-MS. Journal of Hazardous Materials, 155(3): 469-476.

Franco, A., Neves, M.C., Carrott, M.M.L.R., Mendonca, M.H., Pereira, M.I. and Monteiro, O.C., 2009. Photocatalytic decolorization of methylene blue in the presence of TiO_2/ZnS nanocomposites. Journal of Hazardous Materials, 161(1): 545-550.

Goswami, N., Saha, R. and Pal, S.K., 2011. Protein-assisted synthesis route of metal nanoparticles: exploration of key chemistry of the biomolecule. J Nanopart Res, 13(10): 5485-5495.

Gude, K., Gun'ko, V.M. and Blitz, J.R., 2008. Adsorption and photocatalytic decomposition of methylene blue on surface modified silica and silica-titania. Colloid Surface A, 325(1-2): 17-20.

Gupta, V.K., Jain, R., Mittal, A., Mathur, M. and Sikarwar, S., 2007. Photochemical degradation of the hazardous dye Safranin-T using TiO2 catalyst. J Colloid Interf Sci, 309(2): 464-469.

Gupta, V.K., Jain, R., Saleh, T.A., Nayak, A., Malathi, S. and Agarwal, S., 2011. Equilibrium and Thermodynamic Studies on the Removal and Recovery of Safranine-T Dye from Industrial Effluents. Separ Sci Technol, 46(5): 839-846.

Herrmann, J.M., Disdier, J. and Pichat, P., 1986. Photoassisted Platinum Deposition on Tio2 Powder Using Various Platinum Complexes. J Phys Chem-Us, 90(22): 6028-6034.

Hoffmann, M.R., Martin, S.T., Choi, W.Y. and Bahnemann, D.W., 1995. Environmental Applications of Semiconductor Photocatalysis. Chemical Reviews, 95(1): 69-96.

Hu, C. and Wang, Y.Z., 1999. Decolorization and biodegradability of photocatalytic treated azo dyes and wool textile wastewater. Chemosphere, 39(12): 2107-2115.

Hwang, K.-J., Lee, J.-W., Shim, W.-G., Jang, H.D., Lee, S.-I. and Yoo, S.-J., 2012. Adsorption and photocatalysis of nanocrystalline TiO_2 particles prepared by sol–gel method for methylene blue degradation. Advanced Powder Technology, 23(3): 414-418.

ISO, 2010. Determination of the specific surface area of solids by gas adsorption — BET method. International Organization for Standardization, pp. 30.

Janaki, V., Oh, B.-T., Shanthi, K., Lee, K.-J., Ramasamy, A.K. and Kamala-Kannan, S., 2012. Efficiency of various semiconductor catalysts for photodegradation of Safranin-T. Research on Chemical Intermediates.

Janus, M. and Morawski, A.W., 2007. New method of improving photocatalytic activity of commercial Degussa P25 for azo dyes, decomposition. Appl Catal B-Environ, 75(1-2): 118-123.

Jia, H.M., Xu, H., Hu, Y., Tang, Y.W. and Zhang, L.Z., 2007. TiO_2@CdS core-shell nanorods films: Fabrication and dramatically enhanced photoelectrochemical properties. Electrochem Commun, 9(3): 354-360.

Kaur, S. and Singh, V., 2007. TiO_2 mediated photocatalytic degradation studies of Reactive Red 198 by UV irradiation. Journal of Hazardous Materials, 141(1): 230-236.

Khalfaoui, M., Knani, S., Hachicha, M.A. and Ben Lamine, A., 2003. New theoretical expressions for the five adsorption type isotherms classified by BET based on statistical physics treatment. J Colloid Interf Sci, 263(2): 350-356.

Kim, C., Doh, S.J., Lee, S.G., Lee, S.J. and Kim, H.Y., 2007. Development of a visible-light sensible ZnS-ZnO photocatalyst and the enhanced photocatalytic activity of

Pt/ZnS-ZnO under visible light irradiation. In: N.A.C. Society (Ed.), NAM - North American Meeting, Houston, Texas.

Kim, J. and Kang, M., 2012. A Newly Designed a TiO_2-Loaded Spherical ZnS Nano/Micro-Composites for High Hydrogen Production from Methanol/Water Solution Photo-Splitting. Bulletin Korean Chemical Society 33(7): 2133-2139.

Kisch, H., 2007. Semiconductor Photocatalysis for Organic Synthesis, Advances in Photochemistry. John Wiley & Sons, Inc., pp. 93-143.

Kohtani, S., Yoshioka, E. and Miyabe, H., 2012. Photocatalytic Hydrogenation on Semiconductor Particles. In: I. Karamé (Ed.), Hydrogenation. Creative Commons.

Li, X.Z. and Zhang, M., 1996. Decolorization and biodegradability of dyeing wastewater treated by a TiO_2-sensitized photo-oxidation process. Water Science and Technology, 34(9): 49-55.

Libanori, R., Giraldi, T.R., Longo, E., Leite, E.R. and Ribeiro, C., 2009. Effect of TiO2 surface modification in Rhodamine B photodegradation. J Sol-Gel Sci Techn, 49(1): 95-100.

Liu, C.C., Hsieh, Y.H., Lai, P.F., Li, C.H. and Kao, C.L., 2006. Photodegradation treatment of azo dye wastewater by UV/TiO_2 process. Dyes Pigments, 68(2-3): 191-195.

Ma, L., Dong, F. and Bian, L., 2010. Enhanced Photocatalytic Degradation of Rutile TiO2 by Analysis of the Surface Potential and Fluorescence, Bioinformatics and Biomedical Engineering (iCBBE), 2010 4th International Conference on, pp. 1-4.

Mahmoodi, N.M., Arami, M., Limaee, N.Y. and Tabrizi, N.S., 2006. Kinetics of heterogeneous photocatalytic degradation of reactive dyes in an immobilized TiO2 photocatalytic reactor. J Colloid Interf Sci, 295(1): 159-164.

MalvernInstruments, 2009. Zeta Potential Characterization of Concentrated Titanium Dioxide Slurries with the ZEN1010 High Concentration Cell.

Nakata, K. and Fujishima, A., 2012. TiO_2 photocatalysis: Design and applications. Journal of Photochemistry and Photobiology C: Photochemistry Reviews, 13(3): 169-189.

Neppolian, B., Shankar, M.V. and Murugesan, V., 2002. Semiconductor assisted photodegradation of textile dye. J Sci Ind Res India, 61(3): 224-230.

Neves, M.C., Monteiro, O.C., Hempelmann, R., Silva, A.M.S. and Trindade, T., 2008. From Single-Molecule Precursors to Coupled Ag_2S/TiO_2 Nanocomposites. Eur J Inorg Chem(28): 4380-4386.

Nunes, M.R., Monteiro, O.C., Castro, A.L., Vasconcelos, D.A. and Silvestre, A.J., 2008. A new chemical route to synthesise TM-doped (TM = Co, Fe) TiO(2) nanoparticles. Eur J Inorg Chem(6): 961-965.

Parsons, S., 2004. Advanced Oxidative Processes for Water and Wastewater Treatment. IWA Publishing, UK, 368 pp.

Prieto, O., Fermoso, J., Nuñez, Y., del Valle, J.L. and Irusta, R., 2005. Decolouration of textile dyes in wastewaters by photocatalysis with TiO_2. Sol Energy, 79(4): 376-383.

Raj, K.J.A. and Viswanathan, B., 2009. Effect of surface area, pore volume and particle size of P25 titania on the phase transformation of anatase to rutile. Indian J Chem A, 48(10): 1378-1382.

Rauf, M.A. and Ashraf, S.S., 2009. Fundamental principles and application of heterogeneous photocatalytic degradation of dyes in solution. Chemical Engineering Journal, 151(1-3): 10-18.

Rauf, M.A., Bukallah, S.B., Hamadi, A., Sulaiman, A. and Hammadi, F., 2007. The effect of operational parameters on the photoinduced decoloration of dyes using a hybrid catalyst V_2O_5/TiO_2. Chemical Engineering Journal, 129(1-3): 167-172.

Rauf, M.A., Meetani, M.A. and Hisaindee, S., 2011. An overview on the photocatalytic degradation of azo dyes in the presence of TiO_2 doped with selective transition metals. Desalination, 276(1-3): 13-27.

Reisinger, M., 2013. Information about AEROXIDE® TiO_2 P 25. In: J.P. da Costa (Ed.), Faro.

Riddick, T.M., 1968. Control of Colloid Stability through Zeta Potential. Zeta-Meter Inc, New York.

Robert, D. and Malato, S., 2002. Solar photocatalysis: a clean process for water detoxification. Sci Total Environ, 291(1-3): 85-97.

Saha, I., Bhattacharyya, J. and Kumar, G.S., 2013. Thermodynamic investigations of ligand–protein interactions: Binding of the phenazinium dyes phenosafranin and safranin O with human serum albumin. The Journal of Chemical Thermodynamics, 56(0): 114-122.

Sajjad, A.K.L., Shamaila, S., Tian, B.Z., Chen, F. and Zhang, J.L., 2010. Comparative studies of operational parameters of degradation of azo dyes in visible light by highly efficient WOx/TiO2 photocatalyst. Journal of Hazardous Materials, 177(1-3): 781-791.

Senthilkumaar, S. and Porkodi, K., 2005. Heterogeneous photocatalytic decomposition of Crystal Violet in UV-illuminated sol-gel derived nanocrystalline TiO2 suspensions. J Colloid Interf Sci, 288(1): 184-189.

Sharma, M., Jain, T., Singh, S. and Pandey, O.P., 2012. Photocatalytic degradation of organic dyes under UV–Visible light using capped ZnS nanoparticles. Sol Energy, 86(1): 626-633.

Sharma, P. and Tomar, R., 2011. Sorption behaviour of nanocrystalline MOR type zeolite for Th(IV) and Eu(III) removal from aqueous waste by batch treatment. J Colloid Interf Sci, 362(1): 144-156.

Sobana, N., Muruganadham, M. and Swaminathan, M., 2006. Nano-Ag particles doped TiO_2 for efficient photodegradation of Direct azo dyes. J Mol Catal a-Chem, 258(1-2): 124-132.

Suttiponparnit, K., Jiang, J.K., Sahu, M., Suvachittanont, S., Charinpanitkul, T. and Biswas, P., 2011. Role of Surface Area, Primary Particle Size, and Crystal Phase on Titanium Dioxide Nanoparticle Dispersion Properties. Nanoscale Res Lett, 6.

Svecova, L., Cremel, S., Sirguey, C., Simonnot, M.O., Sardin, M., Dossot, M. and Mercier-Bion, F., 2008. Comparison between batch and column experiments to determine the surface charge properties of rutile TiO_2 powder. J Colloid Interf Sci, 325(2): 363-370.

Tang, W.Z. and An, H., 1995. Uv/Tio2 Photocatalytic Oxidation of Commercial Dyes in Aqueous-Solutions. Chemosphere, 31(9): 4157-4170.

Toor, A.P., Verma, A., Jotshi, C.K., Bajpai, P.K. and Singh, V., 2006. Photocatalytic degradation of Direct Yellow 12 dye using UV/TiO_2 in a shallow pond slurry reactor. Dyes Pigments, 68(1): 53-60.

Tsuji, I. and Kudo, A., 2003. H_2 evolution from aqueous sulfite solutions under visible-light irradiation over Pb and halogen-codoped ZnS photocatalysts. Journal of Photochemistry and Photobiology A: Chemistry, 156(1–3): 249-252.

Vijayabalan, A., Selvam, K., Velmurugan, R. and Swaminathan, M., 2009. Photocatalytic activity of surface fluorinated TiO_2-P25 in the degradation of Reactive Orange 4. Journal of Hazardous Materials, 172(2–3): 914-921.

Vinu, R., Akki, S.U. and Madras, G., 2010. Investigation of dye functional group on the photocatalytic degradation of dyes by nano-TiO_2. Journal of Hazardous Materials, 176(1-3): 765-773.

Wu, J.C.S. and Chen, C.-H., 2004. A visible-light response vanadium-doped titania nanocatalyst by sol–gel method. Journal of Photochemistry and Photobiology A: Chemistry, 163(3): 509-515.

Xu, Y.M. and Langford, C.H., 2000. Variation of Langmuir adsorption constant determined for TiO(2)-photocatalyzed degradation of acetophenone under different light intensity. J Photoch Photobio A, 133(1-2): 67-71.

Yang, L., Zhang, Y., Ruan, W., Zhao, B., Xu, W. and Lombardi, J.R., 2010. Improved surface-enhanced Raman scattering properties of TiO2 nanoparticles by Zn dopant. Journal of Raman Spectroscopy, 41(7): 721-726.

Yawalkar, A.A., Bhatkhande, D.S., Pangarkar, V.G. and Beenackers, A.A.C.M., 2001. Solar-assisted photochemical and photocatalytic degradation of phenol. J Chem Technol Biot, 76(4): 363-370.

Zaghbani, N., Hafiane, A. and Dhahbi, M., 2008. Removal of Safranin T from wastewater using micellar enhanced ultrafiltration. Desalination, 222(1-3): 348-356.

Zhang, J., Yu, J., Zhang, Y., Li, Q. and Gong, J.R., 2011. Visible Light Photocatalytic H2-Production Activity of CuS/ZnS Porous Nanosheets Based on Photoinduced Interfacial Charge Transfer. Nano Lett, 11(11): 4774-4779.

Zhang, X.W., Zhou, M.H. and Lei, L.C., 2006. Co-deposition of photocatalytic Fe doped TiO2 coatings by MOCVD. Catal Commun, 7(7): 427-431.

Zhang, Y., Li, D.L., Chen, Y., Wang, X.H. and Wang, S.T., 2009. Catalytic wet air oxidation of dye pollutants by polyoxomolybdate nanotubes under room condition. Appl Catal B-Environ, 86(3-4): 182-189.

Zhao, S., Li, J.Z., Wang, L. and Wang, X.H., 2010. Degradation of Rhodamine B and Safranin-T by MoO(3):CeO(2) Nanofibers and Air Using a Continuous Mode. Clean-Soil Air Water, 38(3): 268-274.

Zhou, X.T., Ji, H.B. and Huang, X.J., 2012. Photocatalytic Degradation of Methyl Orange over Metalloporphyrins Supported on TiO_2 Degussa P25. Molecules, 17(2): 1149-1158.

Zhu, H.Y., Jiang, R., Xiao, L., Chang, Y.H., Guan, Y.J., Li, X.D. and Zeng, G.M., 2009. Photocatalytic decolorization and degradation of Congo Red on innovative crosslinked chitosan/nano-CdS composite catalyst under visible light irradiation. Journal of Hazardous Materials, 169(1-3): 933-940.

Zhu, L., Lim, C.S., Meng, Z.D., Choi, J.G., Park, C.Y., Ghost, T., Cho, K.Y. and Oh, W.C., 2012. Hydrothermal synthesis and highly visible light-induced photocatalytic activity of acid functionalized MWCNTs as support for ZnS-photosensitized TiO_2 catalysts. J Ceram Process Res, 13(3): 283-290.

Supplementary Data – Appendix 5A

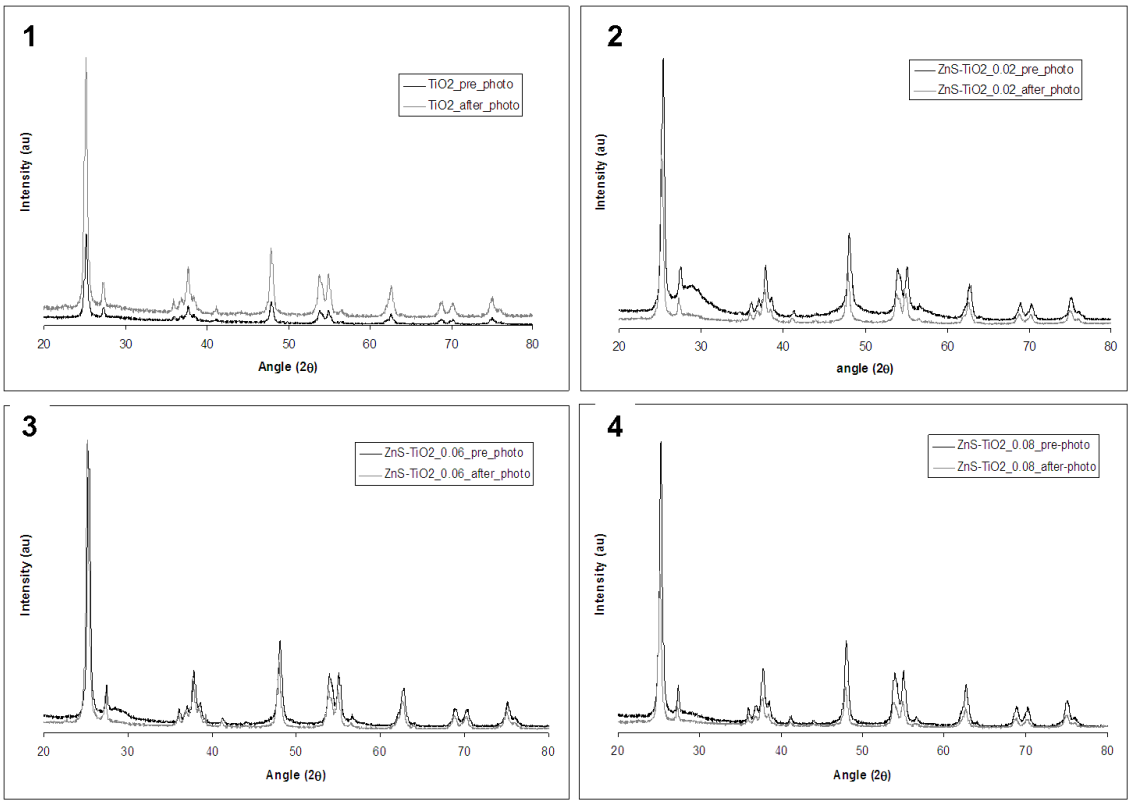

Figure 5.A – XRD patterns for TiO_2 (P25) and the ZnS-TiO_2 composites before (pre-photocatalysis) and after (after photocatalysis) photocatalysis of Safranin-T, for TiO_2 (P25) (1), ZnS-TiO_2_0.02 (2), ZnS-TiO_2_0.06 (3) and ZnS-TiO_2_0.08 (4).

Supplementary Data – Appendix 5B

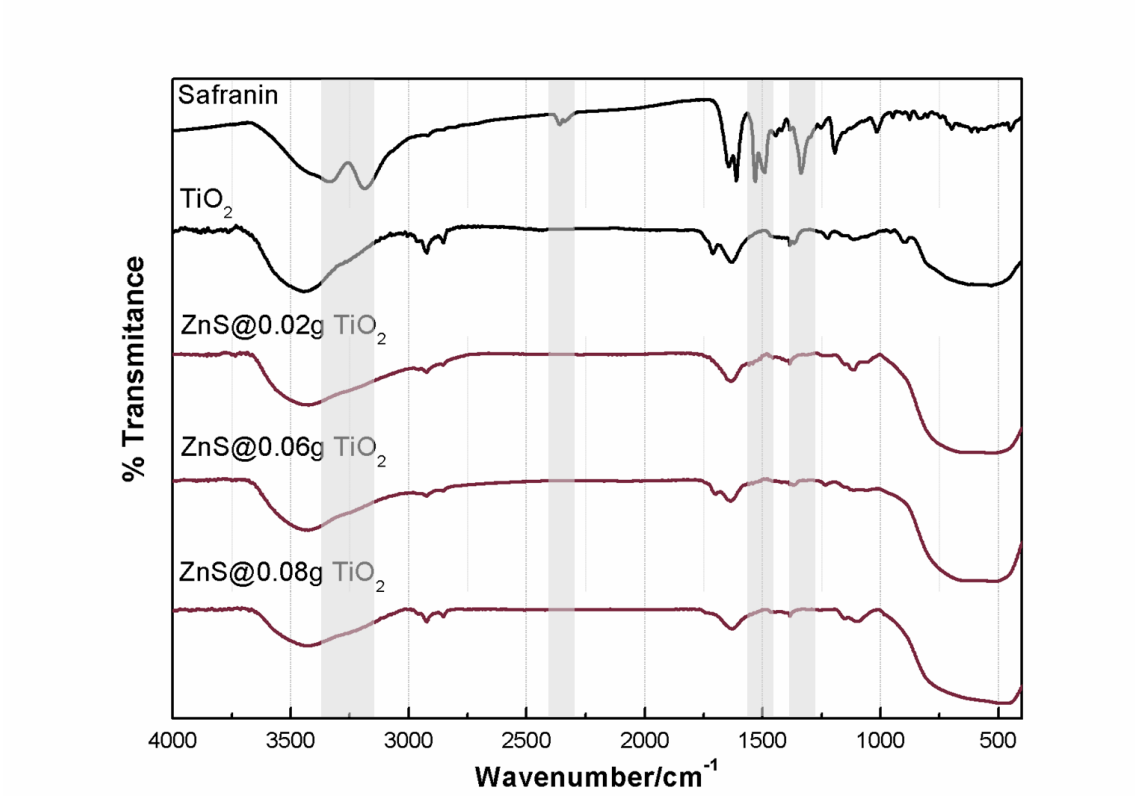

Figure 5.B – FT-IR spectra of the dye Safranin, Degussa's P25 TiO_2 and of the different composites synthesized. For the catalysts, the spectra were obtained after the photocatalysis experiments.

Supplementary Data – Appendix 5C

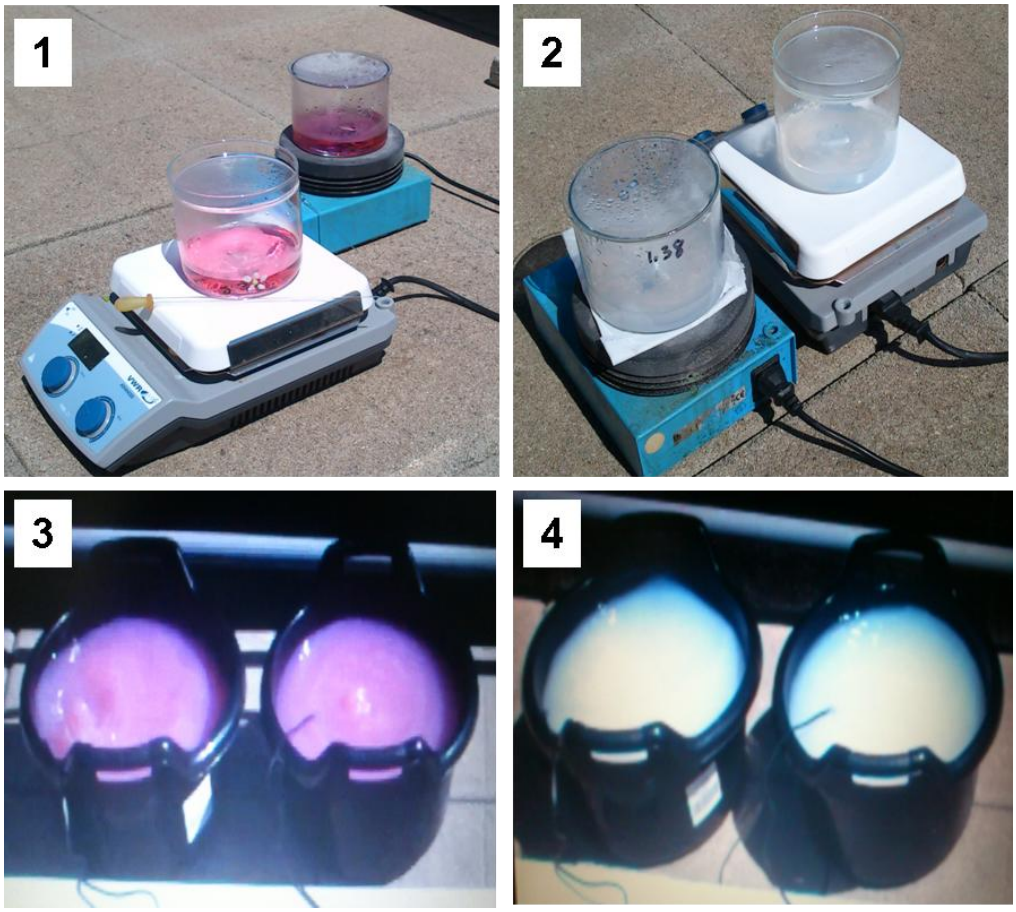

Figure 5C – Photographs prior (1 and 3) and after (2 and 4) the photocatalytic decolorization process of 150 mL (1 and 2) and 10 L (3 and 4) of Safranin-T aqueous solutions at 5 ppm using the 0.1 $g.L^{-1}$ of the ZnS-TiO_2_0.06 composite.

Chapter 6 – Concluding Remarks and Perspectives

The present work provides a broad spectrum of results that highlight the innovative use of sulfate-reducing bacteria for the removal of metals from contaminated waters, be it artificial wastewaters or real ones, such as Acid Mine Drainage, and concomitant synthesis of nano-sized semiconductors and composites. Though most of the work herein described relates, mainly, to the synthesis of said nanostructures using the sulfide produced by SRB in batch systems, studies and considerations using a previously established bioremediation system were also carried out. This substantiates the fact that the underlying principle offers pioneering solutions in a potentially more effective remediation technology accompanied with a synthesis method of added-value products, with prospective applications in areas as diverse as optoelectronics, solar-cells, protein probes or high density batteries.

We have attempted to structure our results by initially demonstrating proof-of-concept, synthesizing nanosized metal sulfides and composites resorting to biologically produced sulfide in a batch system. Afterwards, we integrated such synthesis with an already well established bioremediation system. We then aimed at the selective precipitation of metal sulfides from a mixed-metal system, such as artificial solutions containing more than one dissolved metal and AMD. Finally, we have shown that some of the composites synthesized could act as photocatalysts.

At length, we have demonstrated that monodisperse ZnS and CuS nanocrystals can be prepared by precipitating the corresponding metal with biologically produced sulfide. Moreover, the complexity of the bacterial growth media, as well as the presence of suspended particles showed to have no influence in the morphological characteristics of the produced particles. It was also shown that the use of TiO_2 and SiO_2 as substrates resulted in the synthesis of the corresponding composite materials, thus demonstrating the possibility for the production of composite materials, which possess a wide range of applications. The synthesis of CuS nanoparticles and composites was also successfully integrated into an existing bioremediation process, evidencing its potential for an overall “green” synthesis system of nanoparticles with simultaneous wastewater treatment. Considering the interest of CuS nanoparticles and composites in processes such as photocatalysis and the simplicity of the process presented, this is a convenient route for the biological synthesis of functional materials, with potential applications in bioremediation systems, namely of waste waters.

After the successful synthesis of ZnS-TiO_2 composites using different ratios of both materials, we have tested the photocatalytic activity of these materials over an organic dye (Safranin-T) in both controlled and real-world settings. The different ZnS-TiO_2 composites were characterized in terms of zeta potential, XRD (before and after photocatalysis), surface area and adsorption. Results showed that, generally, the composites showed an increased efficiency when compared to that of "bare" TiO_2 and that they suffer no major changes during the catalytic process. Of the synthesized composites, the most efficient photocatalyst was ZnS-TiO_2_0.06 (0.06 g TiO_2 per 50 mL of a 100 $mg.L^{-1}$ solution of Zn). The best results were obtained when using a 5 ppm concentration of Safranin-T, at pH 6.2 and with a catalyst load of 15 mg per 150 mL of dye solution. The Langmuir-Hinshelwood model was used and a good fit to the photodegradation of the dye was achieved. Complementary chemical oxygen demand (COD) and FT-IR analyses showed that complete degradation of the dye occurs and its degradation products were not adsorbed at the catalysts' surface.

The photodegradation of Safranin-T was also studied using direct sunlight in small (150 mL) and large (10 L) dye solution volumes. The results obtained in both cases were consistent to those obtained using a photoreactor in laboratorial conditions, thus supporting the potential use of these biologically produced nanosized semiconductors in an industrial bioremediation process.

In summary, we have attempted to integrate our research, which, we believe, illustrates the prospective combined use of a well-documented bioremediation process of contaminated waters with the production of metal sulfide nanoparticles and respective nanocomposites. These, in turn, have proven to have applications in environmental remediation processes.

This research, however, does not mark the end and many questions remain to be answered. The established bioremediation process used has shown to be adequate for the removal of sulfate and metals present in the AMD. Could other wastewaters, such as those obtained from the metallurgical or textile/tanning industries be used with the correct modifications to the remediation system? If so, could these effluents also be used as the metal ions source for the synthesis of nanosized metal sulfides?

The described method showed little potential for the fine-tuning of the produced nanoparticles and composites, as this takes place at environmental pressure and temperatures, with minimal changes in the naturally occurring pH of the solutions/suspensions used. Could the use of surfactants, varying dispersing flow-rates

or carefully controlled physical and chemical parameters allow for the production of "designer" nanoparticles? If this is he case, the purely chemical synthesis, with its inherent environmental risks would become but obsolete.

Though the described synthesis process relies in an indirect biological synthesis as well as in the different solubilities of the studied sulfides for selective metal recovery, other authors have reported the use of genetically engineered microorganisms for the deposition of nanosized metal sulfides. Hence, could it be possible to use differently modified organisms for obtaining different metal sulfides, when exposing these organisms to mixed-metal solutions?

The composites obtained (namely, the ZnS-TiO_2 composites) have proven to be efficient catalysts in the degradation of Safranin-T, but it is possible that the degradation of other contaminants, such as emerging pollutants – i. e., chemicals without regulatory status and which impact on environment and human health are poorly understood – is feasible. Moreover, the applications of these compounds are most likely not limited to photocatalytic ones, as previously mentioned, and such potentials should be assessed.

Hence, though a veil has been lifted, many possibilities arise and such questions are intended to be addressed in future research activities.

Appendixes

Selected Publications by the Author

Peer-reviewed Science Periodicals

M. Domingues, C. Simões, J. P. da Costa, A. Reis and P. Domingues; (2009); Identification of 1-palmitoyl-2- linoleoyl-phosphatidylethanolamine modifications under oxidative stress conditions by LC-MS/MS. Biomed. Chrom., 23(6):588-601

João Pinto da Costa, Ana Violeta Girão, João P. Lourenço, Olinda C. Monteiro, Tito Trindade, Maria Clara Costa; (2012); Synthesis of nanocrystalline ZnS using biologically generated sulfide, Hydromet., 117–118:57-63,

João Pinto da Costa, Ana Violeta Girão, João P. Lourenço, O.C. Monteiro, Tito Trindade, Maria Clara Costa; (2013); Green synthesis of covellite nanocrystals using biologically generated sulfide: Potential for bioremediation systems, J. Environ. Manage. 128:226-232

João Pinto da Costa, Ana V. Girão, João P. Lourenço, Olinda C. Monteiro, Tito Trindade and Maria C. Costa; (2013); Integrated synthesis of nanosized semiconductors in a bioremediation system for the treatment of AMD using biologically produced sulfide. – In Brown, A., Figueroa, L. and Wolkersdorfer, Ch., Reliable Mine Water Technology, 1:693-699

Posters and Conferences Proceedings

J. Pinto da Costa, R. W. Lambert and N. Magan; (2008); Effect of weak acid treatments and environmental factors on growth/no growth boundaries for spoilage moulds from beverages. Cranfield MultiStrand Conference, Cranfield, UK. Ref: 138

J. Pinto da Costa, E. S. Santos, O. C. Monteiro, and M. C. Costa; (2009); Biosynthesis of nanosized semiconductors using mine wastes as materials sources. Microbiotec, Vilamoura, Portugal. Ref: 65

J. Pinto da Costa, A. V. Girão, J. P. Lourenço, Tito Trindade and M. C. Costa; (2011); Growth of ZnS nanoparticles using biologically generated sulfide. FEMS, Geneva, Switzerland.

J. Pinto da Costa, A. V. Girão, J. P. Lourenço, Tito Trindade and M. C. Costa; (2012); Use of biogenic sulfide for the synthesis of CuS nanocrystals and nanocomposites. WasteEng'12, Porto, Portugal.